30MW Multi-Rotor Turbine Block Design

Final report

Group 21

Luka Distelbrink	5274400	Mihai Fetecau	5236789
Lorenzo Gonzalez	5242231	Bartosz Jemioł	5275830
Michael Kamal Rizk	5008883	Marco Peralta Tapia	5098955
Ionut Porcescu	5274508	Jānis Pudāns	5307910
Jan Roth	5262054	Mustafa Tuğtekin	5210925

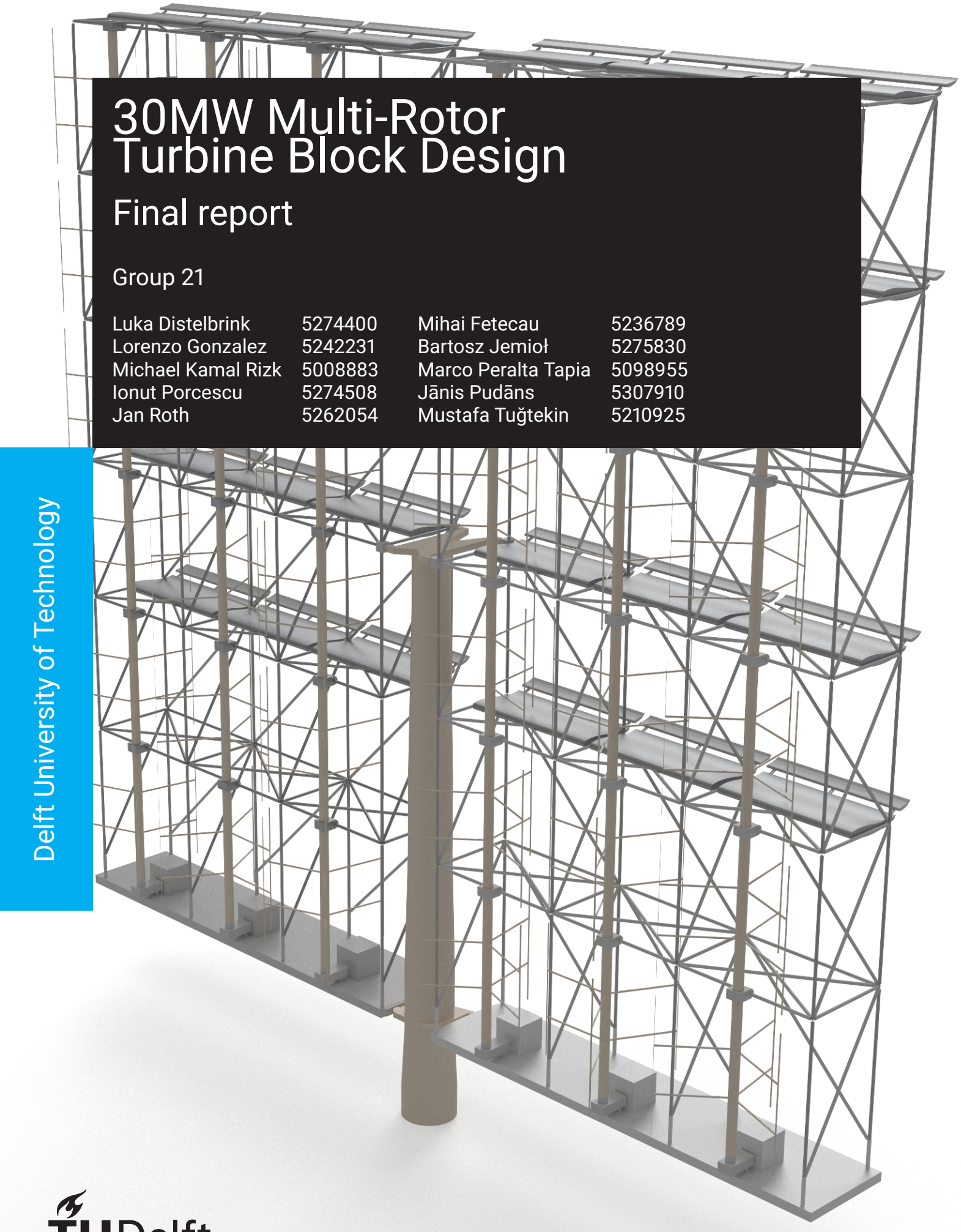

Delft University of Technology

TU Delft

30MW Multi-Rotor Turbine Block Design

Final report

by

Group 21

Luka Distelbrink	5274400	Mihai Fetecau	5236789
Lorenzo Gonzalez	5242231	Bartosz Jemioł	5275830
Michael Kamal Rizk	5008883	Marco Peralta Tapia	5098955
Ionut Porcescu	5274508	Jānis Pudāns	5307910
Jan Roth	5262054	Mustafa Tuğtekin	5210925

Report duration: May 25, 2023 – June 27, 2023
Project tutor: Dr.ir. Carlos Simao Ferreira
Project coaches: Dr. Morgan Li, Stratos Koufis
Course: AE3200 Design Synthesis

TU Delft

Acknowledgements

Over the past ten weeks, we have been working relentlessly to bring the concept of MR-TBD to life. For the large majority of the team, this project represented the first instance of tackling wind energy. Although we were able to use our skills developed during the Bachelor, we initially lacked the necessary understanding to complete such an ambitious task. The success of this project would not have been impossible without the help, expertise and guidance of a few special individuals. We would like to sincerely thank:

Prof. Carlos S. Ferreira, for proposing this incredibly unique and intriguing project and for supervising the development of the design and our development as a team. If not for Prof. Ferreira's attentive and supportive nature, we could not have gotten to the results presented in this report. Thank you for always offering your keen eye to spot our unfeasible estimates, for taking the time to provide feedback and discuss design aspects even outside of planned sessions, and for always reminding us to be positive and excited about this opportunity.

Morgan M. Li and Stratos Koufis, for sharing their experience and knowledge whenever we asked, even if we were inquiring about a different topic than their expertise. Thank you for dropping in during heated working sessions and lending your better judgement to a group of overwhelmed bachelor students.

Prof. Donatella Zapalla, for welcoming our questions and providing us with your valuable expertise in the reliability and maintainability sections. We are very grateful for your attentiveness and interest in our project and for attending and providing your insight during our midterm and final reviews.

Marco Borsotti for help and invaluable advice and help about applying reliability and maintenance analysis.

Thomas Broertjes for this advice and help with designing the high lift device and the rest of the wake control system. We wish him the best of luck with this Master's thesis and a successful future career.

And to the unsung heroes of this story, our families, for their unwavering belief in our capabilities, for their enduring support across the world, and for their investment in our education.

Executive Overview

The goal of this report is to present the conceptual plan of MR-TBD, a proposed wind turbine design of 30 MW with a multi-VAWT rotor configuration. This project was proposed to tackle three main problems facing the industry: the limited amount of favourable offshore wind farm sites, the overwhelming proportion of capital being used for maintenance, and having a handful of giant companies cornering the wind energy market. In turn, MR-TBD offers a more space-efficient design, which can be maintained more easily and produced by smaller OEMs, while also delivering affordable electricity and improving the sustainability of conventional wind turbines.

This executive overview covers the driving requirements and product compliance, a summary of the final technical design, some operational aspects pre- and post-installation, a brief production plan and a financial analysis. The technical design covers the wake and yaw control subsystems, the structural elements that comprise the tower and foundation, the drivetrain configuration and the rotor performance.

Requirements and Compliance

In the preliminary phases of the design process, a number of requirements were imposed by the client of this report, Prof. Carlos S. Ferreira. Out of the initial requirement list, three were identified as driving requirements, as listed in Table 1.

Table 1: *Driving requirement compliance for the system*

ID	Requirement	Value	Status
UR-01	The system shall have a power rating of at least 30 MW	The system has power rating of 31.3 MW	✓
UR-02	The system shall have an energy density of at least 16 $MW km^{-2}$	The system has an energy density close to 20 $MW km^{-2}$	✓
UR-03	The system shall have a 45 % lower levelised cost of energy compared to traditional HAWT	System has 30 % reduced LCoE compared to traditional HAWT	×

After the development of the system, all requirements were checked in order to validate the compliance of the product. All but one of the user requirements were met, namely **UR − 02**. Note that even if the requirement concerning LCoE was not met, the final product is still more affordable than conventional offshore wind turbines. In hindsight, this requirement was unfeasible and should have been re-negotiated during earlier design phases.

Technical design

During the design process of MR-TBD, the system was subdivided into eight subsystems based on their location and functionality. This breakdown was based on the subsystems of conventional wind turbines, with some additions characteristic to the mission at hand. The considered subsystems are as follows:

Tower: The structure above the foundation, which supports the majority of subsystems
Wake control: The aerodynamic surfaces that generate lift and re-energize the wake of the turbine
Rotor: The aerodynamic surfaces and structural components that extract kinetic energy from the wind
Yaw control: The assembly of motors and bearings which rotate the system along the vertical axis
Drivetrain: The mechanical and electrical components that convert kinetic energy into electricity
Foundation: The supporting structure that transfers all tower loads to the seabed
Operation control: The supervisory subsystem that monitors all sensor data during exploitation
Power control: The collection of controllers that define the operational performance of the system

Wake control subsystem design

A common problem that MR-TBD was conceived to alleviate is the low energy density of conventional wind farms. As the energy transition continues and nations distance themselves from polluting and unsustainable sources of energy, the renewable electricity capacity is bound to drastically increase. From the perspective of The Netherlands, an attractive option is using the resource of wind from The North Sea region. Yet, space is a limited commodity, and assuring the nation's energy demand without infringing on shipping lanes, fishing grounds and natural reservations will prove to be difficult. Moreover, the expansion beyond prime wind farm locations would drive up costs and hinder the efforts of switching to renewables. To address this issue, MR-TBD uses aerodynamic surfaces to create large vortices and replenish the wind behind the rotors. This enables packing wind turbines more closely without losing energy production capabilities.

The wake control system of the MR-TBD is comprised of four wings (one per each row of the structure) with a total effective span of 280 m and a chord of 20 m. The design for each wing is to have a two-element cambered airfoil, with both Kruger and triple flaps, which dramatically increase its C_L to the required value. Each of them is divided into six equal sections. The wings themselves have a maximum lift coefficient of $C_L = 3$ when fully deployed. This gives them a drag coefficient of $C_D = 0.256$ and a moment coefficient of at most $C_M = 0.2$.

To determine these values as well as the wake recovery characteristics, an analysis of the effects of lift-generating airfoils was performed by assuming the potential flow and impact of each of the wings could be modelled as a pair of circulation regions. These circulation regions cause upwash, which clears the wake region of slower-moving air behind the rotors and replaces it with clear, fast-moving air, as shown in Figure 1a.

The circulation of the wing is given by its lift coefficient and its chord. Based on the circulation of the wings, the distance needed for the wind to reach the undisturbed velocity can be determined. Using requirement **UR-02** as the energy density target, it was possible to determine the required wing chord and lift coefficient. Results for this analysis can be seen in Figure 1b. The figure shows energy densities achieved for designs with different power ratings, corresponding to different wing configurations.

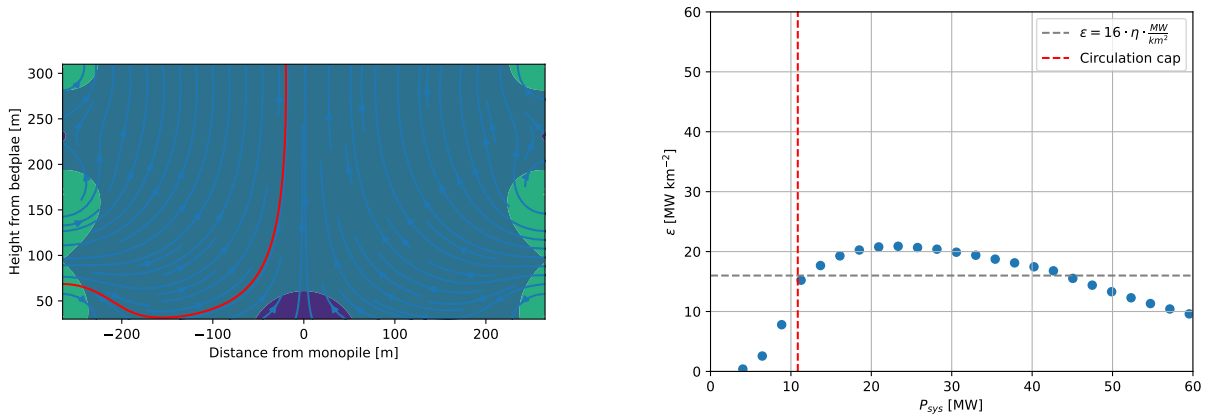

(a) *Velocity profile cross-section aft of the turbine*

(b) *Sizing analysis of the chosen wake control configuration*

Figure 1: *Wake control subsystem performance*

To survive storms, flaps and slats will retract and bring the lift to as low as $C_L \leq 0.074$. The wing sections would be integrated with the structural elements, with the diagonal elements on the bottom of each cell as the base supporting the first and biggest part of the multi-element airfoil. The combined mass of the four

wings is estimated at 648 t, having the mass split halfway between the HLDs and the steel spars, all made from medium carbon steel.

Tower design

The tower structure consists of a large rectangular truss. It was designed using a truss simulation tool that optimises the structure's mass based on its shape and the applied loads by varying the profiles of the hollow cylindrical truss elements. A set of 20 different profiles with associated radii and thicknesses was used. The truss is comprised of smaller rectangular cells that can be tiled together. Seven different cell shapes with varying numbers of braces and brace locations were examined. An entire structure was generated for each, similar to the one displayed in Table 3. The masses of the resulting structures were then compared, and the lightest cell shape was selected. The lightest configuration was 6x6 cells, so this configuration was chosen. A sensitivity analysis was done for the structural mass depending on the depth-to-width ratio of the structure. The ratio associated with the lightest overall structure was 12 %. This leads to a structural depth of 33.6 m.

Because a lower thickness ratio leads to higher moments of inertia, elements with a lower thickness ratio are more resistant to Euler buckling. This leads to lower structural masses, as most elements loaded in compression will fail in Euler buckling. However, sheet buckling needs to be modelled, and once elements become too thin they may become too flexible. In addition to this, a lower thickness ratio leads to higher radii, leading to a higher drag on the structure. As this is a limiting load case, the radii of the elements should be manageable. To balance these factors a thickness-to-radius ratio of 0.01 was chosen.

To select a material, the mass of an optimised design and raw material cost were compared for a few different types of steel. The two most promising options were high- and medium-carbon steel, with high-carbon steel leading to a slightly lighter design. However, medium-carbon steel parts are easier to manufacture as it is softer. It is also more ductile and corrosion-resistant [1]. For these reasons, medium-carbon steel was chosen. In addition to this, multiple layers of white organic solvent-based paint will be applied to the truss structure. This protects the structure from the harsh environment and reduces its capability of absorbing heat from the sun.

To account for the additional mass of connections between the truss elements, a 20 % margin was added to the structural mass, as well as an estimated mass of 312 t for the generator bedplates. The final characteristics of the tower are shown in Table 2.

Table 2: *Tower characteristics*

Cell type	Type 2
Cell count	6 x 6
Total dimensions (w x h x d) [m]	295 x 280 x 33.6
Element thickness ratio [-]	0.01
Material	Medium-alloy steel
Mass [t]	2046
Bedplates [t]	312
Total mass	2767

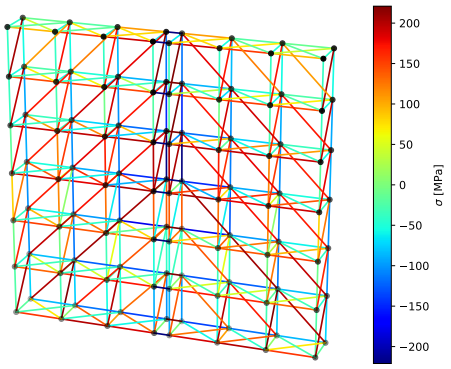

Figure 2: *Stress model of the tower*

Finally, the structure's natural frequencies were analysed, assuming masses of elements were lumped at their nodes. The lowest natural frequency of the structure turned out to be slightly higher than the rotor frequency. As they are very close, this requires special consideration during a more detailed analysis. If the rotor frequency indeed turns out to be a problem, the structure can be made stiffer by increasing the size of

the elements. However, this is not a mass-efficient solution. Another solution would be to design dampers and insert them at the clamps that attach the rotor shafts to the structure to dampen out and remove the problematic excitation frequencies.

Yaw bearings

The yaw control subsystem design consisted of sizing the yaw bearing arrangement to withstand structural and operational loads. It was decided to go with two yaw bearings, a bottom bearing located at the tower's base and a top bearing at the top of the monopile, located at 140 m in height in the tower, to reduce tilting moments. The bearings were sized to withstand axial forces due to weight and radial forces due to maximum produced thrust at the rated wind speed. The dynamic rating C_{dyn} for the bearings was established from the conservative assumption that the tower will have to yaw 180° every 30 minutes to align with the wind. The resulting specifications for both bearings are presented in Table 3.

Table 3: *Top and bottom bearing specifications*

Parameter	Top bearing	Bottom bearing
Inner diameter [m]	10	15
F_a [kN]	68800	11700
F_r [kN]	17200	2920
C_{stat} [kN]	171353.3	29123.8
Lifetime revolution req.	219000	219000
C_{dyn} [kN]	54139.9	9204.8
Estimated mass [kg]	19000	35000

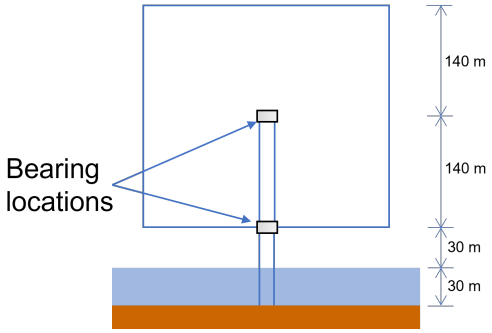

Figure 3: *Bearing locations on the tower*

Furthermore, the bearings will need to include outward-facing gears to be driven by the electrical yaw drives. They will also need corrosion protection to level C5-M (level of corrosion protection required for offshore environments)[1] to prevent the salinity of the water from reducing their service life.

Drive train

Even though wind turbines are portrayed as one of the most sustainable means of energy production, they still employ unsustainable materials and practices, if not directly, then along their respective supply chains. One such material that has negative impacts on the environment and the communities that supply it is neodymium, a Rare Earth Metal (REM) that is used to make the permanent magnets of direct drive generators. The excessive and illegal mining of such materials, mostly performed in countries with loose environmental regulations such as China, is a cost not considered by conventional wind turbine designers. MR-TBD is tackling these issues by avoiding the use of REMs, and nowhere is this decision more evident than in the drivetrain configuration.

The trade-off made in previous design stages concluded that the best generator type to use was a DFIG, a REM-free generator. Furthermore, it was also decided to use brushless DFIGs, since they are more reliable and easier to be maintained. The generators will be placed horizontally, at the bottom part of the truss structure, in order to allow easier accessibility for maintenance and improve labour safety conditions. Because of their strategic placement, all generators could be disconnected and immediately replaced in case of failure. The broken items would be sent onshore to be fixed, while the replacements would assure less downtime.

The torque needed to stop one shaft spinning at a rate of 24 RPM is roughly 6.61 MNm. Currently, no

[1] URL: https://www.liebherr.com/shared/media/components/documents/grosswaelzlager/liebherr-slewing-bearings-product-catalogue-en-metric-web.pdf [cited: 18 June 2023]

commercially available disc brake is able to provide this amount of friction torque without occupying an overwhelming amount of space. Thus, the brake was placed after the gearbox, attached to the high-speed shaft that feeds the generator. In turn, the required moment for braking the shaft becomes 131 kNm.

The gearbox should have a ratio of 43. It is right-angled, translating the rotational axis of the shaft from the vertical plane to the horizontal one. Since gearboxes and generators have the highest probability of failure, they will be placed at the bottom of the tower allowing easier maintenance and reduced downtime.

The induction magnet of the DFIG is fed by a partial converter, rated for 30% of the generator power. The torque control of the rotor is performed using a MPPT controller which manages the voltage of the DC bus within the converter. By doing this, the operating speed of the generator can be varied in order to obtain the desired reaction torque, and in turn, the desired rotor speed. In addition to this 1.5 MW converter, multiple filters are used in order to avoid voltage spikes that could damage components and increase maintenance costs. The final configuration of the drivetrain can be seen in Figure 4

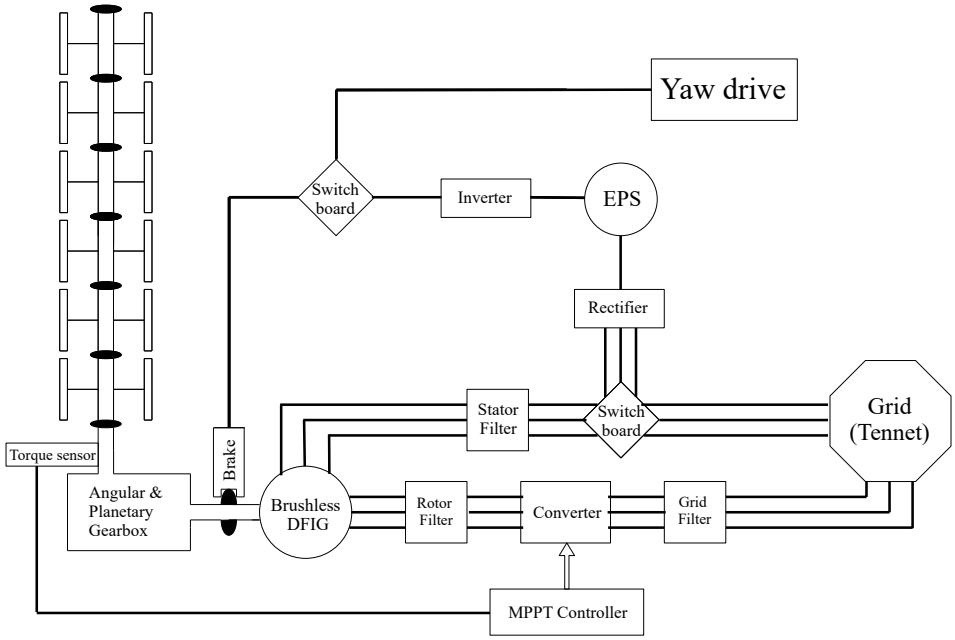

Figure 4: *Conceptual electrical diagram*

Rotors

The rotor airfoil was chosen to be the same as the one used by Jamieson et al. since the performance characteristics of said airfoil were favourable [2]. The choice of the shape required a trade-off, which included V, H, Spiral, Darrieus and Savonius types as possible candidates. Ultimately the H-type rotor was chosen due to its high packing ratio, aerodynamic performance, and easy manufacturability.

The power production strategy influenced both the sizing of the drive train and the sizing of the structural components. The goal of designing a power production strategy is to maximise energy production while keeping the wear and tear on the turbine minimal. For MR-TBD it is best to use a simple power control scheme, capping the production at 30 MW for wind speeds above the rated wind speed. Although this strategy avoids the overloading of power electronics, the shaft will be under extensive loading after the rated wind speed is reached. The relationships between torque, power and wind speed are shown in Figure 5a and Figure 5b.

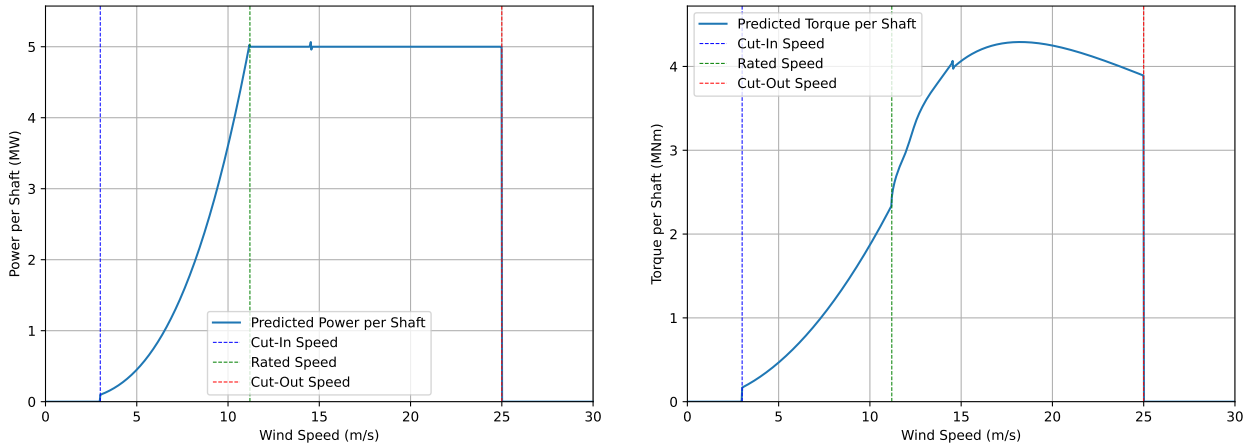

(a) *Power curve*

(b) *Torque curve*

Figure 5: *Operational envelopes of MR-TBD*

The main shaft was sized during the detail design phase. Considering the requirements to withstand the torque of the rotors during the entire operational envelope while also being loaded in compression by its own weight and the weight of the blades and struts, the shaft was sized using fatigue and yielding failure modes. Buckling was not considered as the shaft height is segmented by seven equidistant deep groove ball bearings, which were treated as pin supports. Using the standard of infinite life for the constituent material, low carbon steel, the shaft was designed to have a hollow cylindrical profile, with a diameter of 1.62 m and a thickness of 24.3 mm, spanning 270 m and yielding an individual mass of 260 t. The deflection of the shaft in the most extreme load case considered was evaluated at 3.84 mm at the midway point between each pair of bearings. This was determined to not create connection conflicts with the bearings, which were evaluated based on their reaction loads to weigh 1 t each.

Foundation

The foundation subsystem is required to transfer all loads from the tower to the seabed while also being subjected to aerodynamic and tidal forces. Using trade-off criteria such as structural mass, maintainability, lifetime operations, ecological impact and usable depth, it was decided that a monopile foundation represented the best option.

During the detailed design phase, the yaw subsystem evolved to incorporate two slewing bearings at heights of 30 m and 170 m above sea level, respectively. This forced the monopile design to change to a total height of 200 m from the mudline and aided the gradual transfer of topside loads onto the foundation. At this time, more accurate estimates and models were used to determine the aerodynamic and tidal loading of the system. The monopile was iterated to consider yielding von Mises stress and avoid local and global buckling. Additionally, this enabled the designer to vary the subsystem's diameter and thickness. This resulted in a geometry that varies from a diameter of 17.8 m with a thickness of 100 mm to a diameter of 11 m with a thickness of 60 mm. Due to corrosion and plastic deformation concerns, S355J manganese steel alloy graded for marine conditions is used, leading to a monopile mass of 6200 t.

The possibility of a foundation's collapse due to vibrations due to tidal loads is slight but not impossible. Results show that resonance is not expected during storms or normal conditions when the wind speed varies from 1 m/s to 25 m/s. The problematic scenario is when very exceptional conditions such as hurricanes, cyclones, typhoons, or tornadoes are experienced. Nevertheless, it is desired to equip the monopile with multiple dampers to reduce the risk of failure.

Reliability, Availability, Maintenance, and Safety

Preliminary RAMS analysis was performed, based primarily on research by Carroll et al., who investigated unexpected failures of offshore wind turbines. Assumptions were made based on the changes from the traditional HAWT to the design presented in this report [3]. These were accounted for by changing reliability and material costs for individual components.

The results of these assumptions and scaling factors are shown in Table 4, which shows relative costs of maintenance based on what assumptions are applied; first none, then only the faults are adjusted, next only the material costs, and lastly both. This does not include cost reductions due to lower downtime and ease of access. Assuming this is also mostly scheduled maintenance, this would mean that the assumptions made by the cost model are correct.

Table 4: *Summary of effects of assumptions on relative maintenance costs*

Assumptions Made	Baseline	Adjusted Faults	Adjusted Costs	Adjusted Both
Relative Costs [-]	100.00 %	61.68 %	65.05 %	40.67 %

Based on the adjusted failure rates, the lowered repair time needed for unscheduled maintenance was also found, which was reduced by 18 %. Assuming the same reduction applies to scheduled maintenance, the system's availability would increase to a total of 91.8 % based on [4].

In terms of safety, the system needs no special considerations, given that the system can be operated from a remote control room, only needing maintenance visits; safety rails and guards are installed for safety during maintenance. For ease of access, the frame structure has integrated lifts, catwalks, and stairs, all with safety guards to protect against strong winds.

Control, operations and logistics

The designed wind turbine is equipped with over fifteen types of sensors that continuously measure the atmospheric conditions, the temperature of components, moments and loads experienced. Furthermore, cameras and microphones are used for visual and audio inspection.

Regarding maintenance and logistics, the aspects that must be considered are installation, decommissioning, storing, and repairs. First of all, a number of components will be manufactured mainly in Rotterdam. Multiple manufacturers with plants in the surrounding area have been chosen for the steel components, as well as for the monopile. The more specialised components have been selected via known companies in the Netherlands. For the installation, it was decided to assemble the tower entirely onshore at the Damen Verolme Rotterdam shipping yard and then transport it to the Ijmuiden Ver zone using floaters or dynamically positioned vessels. Regarding the monopile, a vibro-hammer will be used to reduce the negative impact on marine life by reducing driving noise.

One of the most important aspects concerning the design of the wind turbine is the ease of maintenance. Since both the repairing duration and downtime needed to be optimised, placing the higher failure-rated elements, particularly gearboxes, generators and converters, at the bottom of the tower was decided. In case of any malfunctions that cannot be solved in a relatively short time at the location, a spare part will be transported from the depot and immediately replaced by the two cranes mounted on the structure: one on the bedplate and another one at the top of the tower. In this manner, the time period in which the wind turbine does not work at the nominal capacity is significantly diminished. The depot will be placed in the Port of Rotterdam, allowing prompt transportation and accessibility. Once the end-of-life stage is reached after 25 years of service, the wind turbine will be decommissioned. Similarly to the installation, the entire tower, including all components, will be transported back to shore. Removing the monopile from the ground will be made with a lifting tool that also uses a vibro-hammer. In this fashion, the aquatic

habit will be more protected. The companies that have been stated to provide such services are Heerema Marine Contractors, Cape Holland, and Boskalis.

Technical Risk Assessment

The technical risk analysis involved identifying the technical performance, cost, scheduling, sustainability, and programmatic risks. The technical performance risks were further divided into subsystem risks. The most significant identified risks included lightning strikes, harm to surrounding ecosystems through pile driving noise or bird collisions, corrosion of the tower and bearings due to the saline environment, and failures of specific critical components such as the yaw bearing and shaft brakes. On the subsystem level, considerable risks arose from failure with WCT retraction during high wind speeds and YCT instability during windspeeds higher than the rated wind speed.

Mitigation measures were identified for each of these high risks to reduce the likelihood or consequences, resulting in a new post-mitigation risk matrix. Lightning remained a relatively high risk even after the mitigation procedures, so a contingency strategy involving unmanned inspections and maintenance after thunderstorms was proposed.

Sustainability

One of the main pivots of this project is its sustainability aspect. A life cycle analysis was performed to assess the sustainability of the MR-TBD turbine. This study aimed to evaluate the final design's environmental impact throughout all the phases of its life cycle. Initially, a life cycle inventory was performed where all the elements and materials of the final structure were listed. After that, the overall emissions and energy consumption of the following design phases have been considered: extraction of materials, manufacturing, transportation, operations, decommissioning and recycling. To analyse each of these design stages' impact, the MaterialUniverse database of Ansys Granta was used to find all the necessary numbers. The following results were obtained using the EcoAudit tool present in the software. In terms of percentage, the previously mentioned life cycle phases account for 68.5%, 26.5%, 0.5%, 0.00%, and 4%, respectively. After analysing the individual phases, the energy consumed and the CO_2 kg generated per year were estimated. MR-TBD will consume 7.28e6 MJ per year and 5.55e5 kg of CO_2 annually. This leads the MR-TBD turbine to be 37% less polluting than conventional HAWT.

In terms of economic sustainability, the system eliminates the use of rare Earth metals through the use of a DFIG rather than a permanent magnet generator (PMG). This increases the energy safety of the system by reducing the reliance on imported raw materials, leading to a more self-sufficient production process.

The system also has a capacity factor of 56.7%, which is higher than current wind farms. This, combined with a higher power density compared to traditional wind farms, allows for the use of favourable offshore sites with a lower LCoE. The lower power density also enables sea space to be allocated to other economic uses.

Finally, the system promotes affordable and cheap energy as a result of its long life and low maintainability. This reduces the volatility of energy prices through the increase of locally produced renewable energy in accordance with Dutch governmental plans. The reduction in LCoE also leads to more affordable renewable energy for consumers.

Regarding the social sustainability of MR-TBD, there are several aspects considered. In terms of labour rights protection, MR-TBD allows for easier maintenance by lowering maintenance-heavy components and avoiding cramped maintenance conditions. This would increase labour safety regarding maintenance and reduce accidents. Furthermore, by avoiding rare Earth metals, MR-TBD avoids sourcing materials from mines with unsafe and illegal practices that disregard worker rights.

Through the use of smaller components that are more easily manufacturable by original equipment manufacturers (OEMs), MR-TBD also allows for more democratisation in component sourcing by not solely relying on large manufacturers that dominate the market for offshore wind energy.

Finally, through a higher power density, MR-TBD allows for generating more energy with less infringement on fishing and protected grounds.

Budgeting and Cost Analysis

The budgeting and the cost analysis are based on the levelized cost of electricity. The LCoE was chosen as the financial indicator because it incorporates all the performance figures: energy production, power density, and ongoing and upfront costs in one easy-to-compare number. The budget for MR-TBD has been set to an LCoE of 30€/MWh, which is a 45% reduction compared to the projected cost by WindEurope [5]. The design could also replace old farms beyond 2050, which would set the LCoE target at 36€/MWh.

After completing the design, an in-depth cost analysis was performed. The costs were based on modifying costs of a 10 MW wind farm [6]. By comparing the cost of different components to a reference 10MW wind turbine, a good approximation of the LCoE can be achieved. The following changes were made to compute the final LCoE: **(1-2)** Move to a lower LCoE location, **(2-3)** O&M savings for a denser wind farm, **(3-4)** losses due to the wake, **(4-5)** change from conventional HAWT to MR-TBD, **(5-6)** energy recuperation using wake control. The breakdown of how these changes influence the LCoE can be seen in Figure 6. The final LCoE came to 38€/MWh. Additional financial indicators were also computed. The expected time to break even was computed to drop from 13 to 9 years, and the weighted average cost of capital at which the turbine is profitable has risen from 3% to 6.7% (with an energy sale price of 54€/MWh).

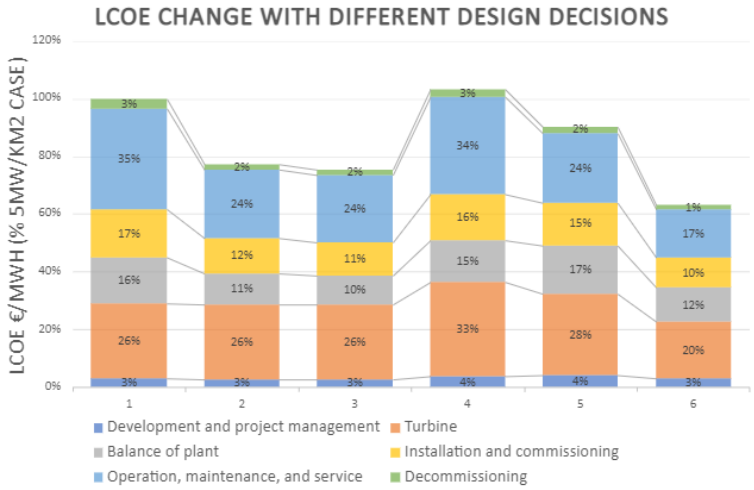

Figure 6: *Cumulation of design choice and their financial impacts*

.

Contents

List of Symbols

ACFM Alternating Current Field Measurement

AEP Annual Energy Production

ASME American Society of Mechanical Engineers

CFD Computation Fluid Dynamic

CTV Crew Transfer Vehicle

DD-PMSG Direct drive with a permanent magnet synchronous generator

DFIG Double Fed induction generator

DP Dynamically positioned

DSE Design Synthesis Exercise

DT digital twin

EESG electrically excited synchronous generator

EPS Emergency Power Source

FKM Forschungskuratorium Maschinenbau

FR functional requirement

GHG Greenhouse Gas

HAWT Horizontal Axis Wind Turbine

HAWT Horizontal axis wind turbine

HLD high lift device

HLV heavy lift vehicle

IEC International Electrotechnical Commission

LCA life-cycle analysis

LCoE Levalized Cost of Electricity

LIDAR light detection and ranging

ML Mudline

MR mission requirement

MR-TBD Multi-Rotor Turbine Block Design

MRS Multi-Rotor System

NEWA New European Wind Atlas project

O&M operations and maintenance

OWT offshore wind turbine

PCB Printed Circuit Board

PID Proportional integral derivative

PMS permanent magnet synchronous

PMSG permanent magnet synchronous generator

RAMS Reliability, Availability, Maintenance, and Safety

REM Rare Earth Metal

RPM rotations per minute

SCADA Supervisory Control and Data Acquisition

SKF Svenska Kullagerfabriken

SR Standard Requirement

SWL Still Water Level

TSR Tip Speed Ratio

TtBE Time to Break Even

UN United Nations

UR User Requirement

VAWT Vertical Axis Wind Turbine

WACC Weighted Average Cost of Capital

WRF Weather, Research and Forecasting

$\bar{\lambda}$	Reduced slenderness	-
β_m	Moment factor	-
ϵ	Power density	$\mathrm{MW\,km^{-2}}$
Γ	Circulation	$\mathrm{m^2\,s^{-1}}$

κ	Flexural buckling	-
ω	Frequency	
ρ	Density	kg/m^3
σ	Normal stress	MPa
σ'	Von Mises stress	MPa
σ'_a	Von Mises alternating stress	MPa
σ'_m	Von Mises mean stress	MPa
τ	Shear stress	MPa
Δn	Slenderness parameter	-
$\eta_L, \eta_R, \eta_{LR}$	Foundation stiffness parameters	-
$\mathbf{K}$	Stiffness matrix	N m^{-1}
$\mathbf{M}$	Mass matrix	kg
τ	Torque	Nm
θ_{rel}	Relative wind angle	rad
$\vec{d}^e$	Direction vector of element e	m
$\vec{F}$	Force vector	N
$\vec{r}$	Position	m
$\vec{u}$	Vector of node displacements	m
$\vec{v}$	Velocity	m s^{-1}
A	Aspect ratio	-
A	Cross-sectional area of a truss element	m^2
A^*	Area per unit length	m
c	Chord of the wing	m
C_τ	Torque coefficient	-
C_D	Drag coefficient	-
C_L	Lift coefficient	-
C_M	Moment coefficient	-
C_n	Inertia coefficient	-
C_P	Power coefficient	-
C_T	Thrust coefficient	-
c_{diam}	Inner to outer diameter ratio	-
c_{diam}	Inner-to-outer diameter ratio	-
C_{dyn}	Dynamic rating	-
C_L, C_R	Foundation flexibility coefficients	-
C_{stat}	Static rating	-
D	Drag force	N
d_o	Outer diameter	m
d_o	Outer diameter	m
D_T	Average outer diameter	m
E	Elasticity modulus	GPa
e	Oswald efficiency factor	-
F	Force	N
f_1	Bearing load factor	-
f_{FB}	Natural frequency of the fixed base	Hz
f_N	Natural frequency of the fixed base-monopile system	Hz
g	Gravitational acceleration	m/s^2
H_s	Significant wave height	m
H_{50yr}	50-year return period wave height	m
j_{load}	Load safety factor	-
$j_{material}$	Material safety factor	-
k	Wave number	m^{-1}
K_{rep}	Bearing load increase factor	-
L	Length of an element	m
L	Lift force	N
L', L^*	Lift per unit span	N m^{-1}

l_{loss}	Lost effective area	m
M_p	Plastic moment resistance	
m_{RNA}	Mass of the rotor-nacelle assembly	kg
m_T	Mass of the tower	kg
N_e	Elastic buckling force	
N_p	Plastic compression resistance	
S_e	Endurance strength	MPa
S_y	Yield strength	MPa
S_0	Static safety factor	-
S_{ult}	Ultimate tensile strength	MPa
T	Torque	N m
t	Time	s
T_s	Significant wave period	s
t_T	Average thickness	m
T_B	Breaking torque	Nm
T_F	Friction torque	Nm
T_J	Inertia torque	Nm
T_L	Load torque	Nm
u_c	Water current speed	$\mathrm{m\,s^{-1}}$
V	Transverse shear load	N
V^*	Volume per unit length	m^2
v_∞	Free-stream velocity	$\mathrm{m\,s^{-1}}$
v_{rated}	Rated windspeed	$\mathrm{m\,s^{-1}}$
v_{rel}	Relative windspeed	$\mathrm{m\,s^{-1}}$
W_p	Plastic resistance capacity	
d	Inner diameter	m
g	Gravitational acceleration	m/s^2
I	Second moment of area	m^4
J	Polar moment of inertia	m^4
m	Mass	kg
Pd	Power density	

1

Introduction

1.1. Introduction

In the last 20 years, the demand for sustainable energy has increased considerably. Wind energy is one of the most sustainable ways of generating electricity, as power is extracted directly by air, and no toxic emissions are produced. Furthermore, both onshore and offshore wind turbines result in being highly cost-effective for generating electricity. To cost-effectively generate power with offshore wind turbines, large turbines are used. The advantage of this is reduced installation and maintenance costs and infrastructure complexity. However, this raises an issue: if the rotor area scales by the square of a size factor, the turbine mass scales by the cube of that very size factor. This can lead to unfeasible structural weights. In addition to this, designing the rotor blades to withstand the required loads and vibrations becomes more complex due to their long slender shape. Consequently, while increasing the size of units is beneficial for less complex infrastructure and lower maintenance costs, it becomes increasingly more difficult to upscale them, and benefits costs benefits due to this size increase are reduced due to the increased complexity of the turbine.

A multi-rotor system has the potential to address several of these issues. Instead of increasing power output by increasing the rotor size, the number of rotors can be increased. This makes them more easily manufacturable but only requires a single foundation and service location compared to using multiple smaller wind turbines. These rotors can be installed in a large truss structure, which can more easily be increased in size. The use of VAWT rotors synergises well with the multi-rotor concept, as their rectangular swept area can be perfectly tiled compared to the circular swept area of HAWTs. In addition to this, there is the potential to couple the vertical shafts together. This would allow the generator to sit at the bottom of the structure, reducing maintenance costs. Another benefit to the multi-rotor is that the truss structure provides the possibility to easily mount a high-lift device to the turbine, which may increase the power density of the system. The smaller individual components of the structure may also increase the democratisation of wind turbine manufacturing, as their smaller size and complexity lowers the barrier of entry.

With this background in mind, the goal of this ten-week project is to produce a conceptual design of a multi-rotor VAWT system. The following report aims to describe the final stages of the design and analysis. The mentioned paper can be seen as a continuation of the Baseline report and the Midterm report [7, 8] in which crucial elements such as subsystem requirements, preliminary design options, and initial design were presented.

The report's structure is as follows: first, the project and its scope are introduced, along with the purpose and the user requirements/constraints. This is followed by Chapter 2, which contains the market analysis performed for the design. Next is Chapter 3, which describes the site selection procedure, as well as what was the final site, which was selected for the turbine. It also presents the wind speeds and distribution at the specified location and its load cases. The last thing in that chapter is the wave model, which comes into play with the under-ocean part of the system.

After that, it follows Chapter 4, which contains some design trade-offs related to design choices which were not yet made in the midterm report [8]. This is followed by Chapter 6 and Chapter 5, the former being a brief summary of the latter. These detail the analysis and results of a more detailed design of the individual subsystems of the system, as well as verification for various models used.

After the design analysis and results presentation, the concepts for its production, operation, and logistics are detailed in Chapter 7. This is followed by cost analysis for the design, presented in Chapter 8. Cost

analysis is followed by Chapter 9, which approaches sustainability of the design, both in a quantitative way and the in a qualitative way.

The report is then continued with Chapter 10, which details the design's technical risks and some mitigation strategies. This is followed by Chapter 11. This chapter shows compliance with the user requirements and other crucial requirements. A brief overview of the future development steps is then provided in Chapter 12. Finally Chapter 13 is a conclusion to the report, along with recommendations for further research.

1.2. Requirements

This section presents the user requirements

This section presents the user requirements the design was subject to. They are the design's primary drivers and must be satisfied. They have been given by the client, then translated into technical requirements, and lastly (re-)negotiated in for some. Compliance of the design with these requirements can be seen in Chapter 11. The requirements are:

UR-01: The system shall have a power rating of at least 30 MW

UR-02: The system shall have a power density of at least 16 $\mathrm{MW\,km^{-2}}$

UR-03: The system shall have a 45 % lower levelized cost of energy compared to traditional horizontal axis offshore wind turbines

UR-04: The system shall have multiple rotors

UR-05: The system shall have lower lifetime emissions than traditional horizontal axis offshore wind turbines

UR-06: The system shall have increased material recyclability than traditional horizontal axis wind turbines

UR-07: The system shall have decreased rare metal use compared to traditional horizontal axis wind turbine

UR-08: The system shall be installable offshore

Subsystem definition

In the previous design phase, the system was broken down into eight subsystems, the scopes of which are presented in Table 1.1. The table has the full name of the subsystem, its identifier, which is used throughout the report, and the scope of it. The last column presents the section in which it is designed.

Table 1.1: *Subsystem definition and location in the report*

Full name	Identifier	Scope	Design section
Tower	TWR	Structure above the foundation, which supports various subsystems. The tower transfers loads from other subsystems to the foundation, to which it is attached to by means of bearings. All the rotors are attached to it through bearings.	Section 5.1
Wake control	WCT	Downforce generating surfaces are used to generate large vortices to move the wake upwards and out of the way of the next turbine. Its function is to allow for higher energy density. It is integrated directly into the TWR structure and can retract during storms to limit the loads.	Section 5.2
Rotor	RTR	Rotor blades, bearings, and breaks, which generate lift and apply torque on the shaft of the drivetrain to extract rotational energy from the wind.	Section 5.3
Yaw control	YCT	Motors and controllers are responsible for yawing the tower in the desired direction. It helps the system achieve higher efficiency by aligning with the wind better. It can also turn the structure away from strong winds during the storm.	Section 5.4
Drive train	DRT	Shaft, gearbox, generator, and supporting components, which focus on transforming the rotational energy of the rotors into electricity.	Section 5.5
Foundation	FND	Part of the supporting structure, which is attached to the ocean floor and extends up to 170 m above the surface. It attaches itself to the tower by means of two bearings. It is the access point for maintenance.	Section 5.6
Operations control	OCT	Collection of systems and components involved in supporting nominal operations and system maintenance. This is quite general and will be further broken down in the following phases of the design.	Section 7.4
Power control	PCT	Systems and controllers involved in controlling the power produced and regulating the loading of the system. It does so by controlling the rotor and drivetrain to maintain the target shaft RPM.	Section 7.3

2

Market analysis

One of the most important factors of any new wind turbine design is its financial feasibility. To determine if MR-TBD is a viable project, the market analysis of it has to be evaluated. This chapter will give an overview of how the market is likely to develop up until 2050. This is presented in Section 2.1. Since the market of offshore wind turbines is concentrated, there are only a few companies that can manufacture large OWTS. Section 2.2 presents how the proposed design addresses this issue.

2.1. Analysis of Competition in the Market

"*LCoE is defined as the revenue required (from whatever source) to earn a rate of return on investment equal to the discount rate (also referred to as the weighted average cost of capital or WACC) over the life of the wind farm. Tax and inflation are not modelled. In other words, it is the lifetime average cost for the energy produced, quoted in today's prices [6].*" To fully capture the advantages of the proposed design, a more holistic view of the pricing is required. WindEurope has presented a plan to expand the production of electricity in the North Sea by 380 GW by 2050 [5]. An expansion of this size with a traditional solution would mean using all of the very low LCoE (under 50€/MWh), as well as all of the low LCoE (between 50€/MWh and 65€/MWh) spots available in the North Sea. There also would be the need to put some wind turbines in the medium LCoE (between 65€/MWh and 80€/MWh) zones. The plan also specifies the amount of power planned per cost bracket. For very low LCoE, the projection is to install 112 GW, for low LCoE 264 GW and 4 GW at medium LCoE locations. With that information, the LCoE of the whole WindEurope project can be calculated. It comes to 54€/MWh. This will be the benchmark for the project and the requirement to lower the LCoE by 45%, meaning the proposed design should achieve an LCoE of around 30€/MWh.

Another way to measure the design performance is to look at what happens after 2050. In 2050 all low-cost areas for offshore wind turbines in the North Sea are expected to be fully developed. That means the only way to increase the power capacity of the North Sea is to develop areas with LCoEs of 65€/MWh or higher. At the same time, turbines built in the 2010s and 2020s will need replacement. All these will have been made in the very low LCoE zones available then. This means that if a design has a higher power density than the wind farms being replaced, power capacity can be increased in the North Sea without building in expensive areas. Therefore, increasing power capacity using conventional wind turbines in 2050 will cost at least 65€/MWh. The proposed design can achieve a similar power increase by replacing old wind farms without increasing the LCoE. In this scenario, the benchmark LCoE will be 65€/MWh. Therefore the design would need to have an LCoE of around 36€/MWh to hit the 45% reduction target.

2.2. Democratising the Offshore Wind Turbine

One glaring issue with the current offshore wind turbine market is a de facto duopoly. Only Siemens and Vestas are currently producing wind turbines of 10 MW and more for the North Sea. Such a small number of manufacturers limits the production throughput, and the lack of competition drives prices up. This situation mainly stems from difficulties in designing and manufacturing the blades for HAWTs. The adverse loading on the blade necessitates the use of composites; the coupled vibration requires advanced computational methods to ensure safe operation and the varying linear velocity long the blades calls for continuously varying airfoils, making manufacturing almost impossible [9–11]. All these challenges make the entry of a new company in the OWT market, unlikely, keeping the duopoly in perpetuity.

One of the goals of the MR-TBD is to enable smaller design firms and local manufacturers to take part in the OWT business. The switch from a single-rotor HAWT to a multi-rotor VAWT should eliminate all the

challenges mentioned before. The nature of the proposed design also lends itself to manufacturing and assembly in facilities made for the marine industry. This eliminates the logistic problems with transporting HAWT components made in specialised plants located far from the shore. Simplifying logistics is another way the design is more approachable for smaller companies. With these changes in mind, it is clear that the proposed design significantly increases the democratisation of OWT and, in theory, could dethrone the duopoly.

3

Site selection

3.1. Turbine Location

Before wind turbines can be installed, a siting study must be undertaken to find the most suitable location in which the farm can be placed. Selecting the correct location for the multi-rotor VAWT considered in this project is crucial to maximising its energy production and overall performance under different conditions. This section of the report presents the results of the location study performed to select the most suitable area in the Dutch North Sea to host the wind turbine in discussion.

The main objective of the siting study is to locate the system such that the energy cost is maximised while minimising its environmental impact. The selection process involves carefully considering various factors to ensure the wind turbine operates safely and efficiently while respecting all the regulations. Firstly, assessing wind resources is essential to determine the energy potential of a specific site. This is needed since the wind of a particular area in the sea determines the wind and wave loads the structure may be subjected to during its operation. Environmental factors, such as protected habitats, bird migration routes, and visual impact, must also be considered. It is crucial, to find an area that is the best compromise between potential harm to the environment and efficiency. Other aspects that must be considered in selecting a site are the site topography, accessibility, grid connection and economic viability.

The Dutch North Sea offers several designated areas where it is possible to build offshore wind farms [1] [2] according to the Dutch Offshore Wind Energy Roadmap. The objective of the Dutch government is to have 11.5 GW of offshore wind in its waters by 2030 [12]. These areas have been identified and allocated by the Dutch government for the development of offshore wind farms based on various factors. These include wind resources, technical feasibility, environmental considerations, and stakeholder engagement. Moreover, the Dutch government has implemented a tendering process to allocate these areas to developers through competitive bidding. Consequently, this allowed limiting the location selection to a few restricted areas in the Dutch North Sea where the grid is already/partially present and all the necessary studies (environmental, geological etc.) have been performed. Figure 3.1 [3] presents all the areas that are under construction (green areas), in development (dotted areas), operational (blue areas), and available (empty areas) for future projects.

[1] https://english.rvo.nl/information/offshore-wind-energy/hollandse-kust-west-wind-farm-zone [cited: 20 June 2023]

[2] https://www.noordzeeloket.nl/en/functions-and-use/offshore-wind-energy/free-passage-shared-use/ijmuiden-ver-wind-farm-zone/ [cited: 20 June 2023]

[3] https://english.rvo.nl/sites/default/files/2023/05/Roadmap-Offshore-Wind-Energy-May-2023_0.pdf [cited: 20 June 2023]

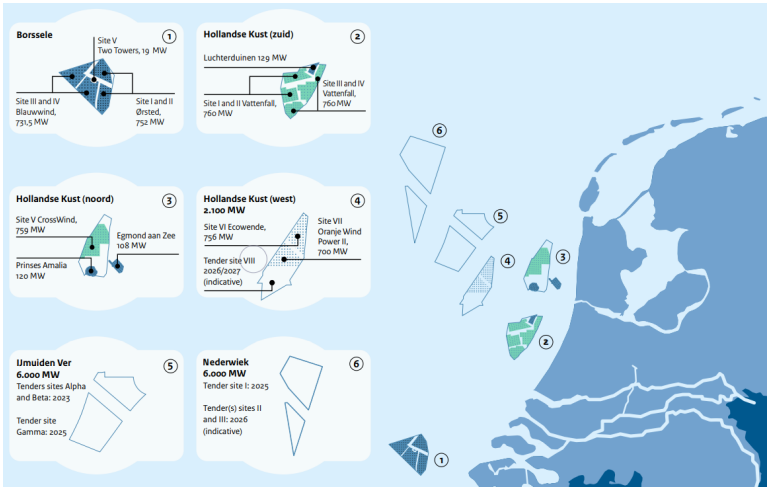

Figure 3.1: *Map of the Dutch wind farm sites, comprising Ijmuiden Ver Wind Farm Zone*

After an availability and feasibility study of the different areas that could host the MR-TBD turbine, three wind farm zones were selected and explored in more detail. The three areas are listed as follows:

- **Hollandse Kust**: located off the coasts of Zuid-Holland and Noord-Holland provinces. It has been divided into several zones, each identified by a specific number. These zones are sequentially numbered from north to south and 18 to 38 km from the coast. While Hollandse Kust Zuid and Noord are already under construction or operational, Hollandse Kust West presents an area which could be feasible for the MR-TBD. Hollandse Kust (west) Wind Farm Zone will accommodate 1400 MW of offshore wind power capacity. Hollandse Kust (west) Wind Farm Zone will accommodate 1.4 GW of offshore wind power capacity and will become operational in 2025 [4].
- **Nederwiek**: this zone is 90 km off the west coast of the Netherlands. Three Wind Farm Sites will be designated in the Wind Farm Zone as NW Wind Farm Sites I, II and III. All these sites are 2 GW in size. The total surface area of the Wind Farm Sites within the zone is approx. 600 km². These Wind Farm Sites will accommodate 6 GW operating from 2030 onwards. [5]
- **IJmuiden Ver**: this wind farm site lies 54 kilometres from the coast to the northwest of the Hollandse Kust (west) wind farm zone. The area comprises four sites, each delivering 1GW from 2027 onwards. The IJmuiden Ver zone will comprise three offshore grid connections and corresponding transformer platforms: Alpha, Beta, and Gamma. These will connect the offshore wind farms at the I & II, III & IV, and the newly planned V & VI sites to the grid [6]. The area is 650 km^2 in size. [7]

After considering these three options' most important advantages and disadvantages, the Ijmuiden Ver wind farm zone was selected. The motivations for this decision are multiple and depend mostly on the characteristics of the individual zones.

Starting from the Hollandse Kust, this option was discarded for three reasons. These are environmental considerations, space considerations, and time considerations. The Hollandse Kust West site is the closest option to the shore. This particularly sensitive environment for marine/flying ecosystems and coastal

[4] https://english.rvo.nl/information/offshore-wind-energy/hollandse-kust-west-wind-farm-zone [cited: 20 June 2023]
[5] https://offshorewind.rvo.nl/cms/view/91063764-5eb7-428e-9c6e-e38fcf3adf22/general-information-nederwiek [cited: 20 June 2023]
[6] https://www.offshorewind.biz/2021/10/26/rvo-talks-6-gw-for-ijmuiden-ver-offshore-wind-zone/ [cited: 20 June 2023]
[7] https://www.noordzeeloket.nl/en/functions-and-use/offshore-wind-energy/free-passage-shared-use/ijmuiden-ver-wind-farm-zone/ [cited: 20 June 2023]

aesthetics represents an issue that cannot be ignored. One of the most important aspects of this project is, in fact, sustainability. Installing and operating such a huge structure relatively close to the shore would be unsustainable, causing several problems for the ecosystems and local stakeholders. Additionally, the shape of the area is not favourable for ship routes compared to the other options. While the other two sites considered present a very wide shipping lane (see Figure 3.1), Hollandse Kust West does not, requiring careful coordination with existing shipping routes and maritime activities to ensure safety and minimise any conflicts or disruptions. Finally, regarding time management, this site option is the least optimal since it requires a final design by 2025. This date is too early for the MR-TBD project, which will probably not be ready at that time.

Moving to the considerations on the Nederwiek site, some issues were encountered as well. Firstly, the area is the furthest from the shore. The main benefit of this is that wind conditions are more favourable, allowing for potentially higher energy production. On the other hand, this may represent a problem since installation, operation, and maintenance procedures may become more of a challenge compared to the other sites that are more accessible. Installing the turbine in such an area will require longer transmission distances and potentially more complex logistic strategies, which can increase costs and operational complexities. This is also a problem for the sustainability of the project. Another issue is dictated by the site development being still at a very initial stage. In fact, the grid connection is not yet present, and the plan for the project still needs to be fully defined. In light of this, this option was also discarded due to the larger downsides of the area compared with the benefits of power production. However, this option may still be considered in case of delays in the MR-TBD project.

Finally, the Ijmuiden Ver wind farm zone is the last option to be considered. This area represents the best compromise between all the previously discussed options. In terms of location, the site is located in a perfect area for multiple reasons. The area has excellent wind conditions because it is far from the coast. The distance from the coast is enough to not be visible to the local stakeholders and not to disturb the wildlife that is more concentrated in that area. In addition, compared to the Hollandse Kust, the IJmuiden Ver zone also offers more space for larger-scale wind farm developments due to its deep waters. This is beneficial for this project due to its extremely large scale. Moreover, as offshore wind technology continues to advance, the IJmuiden Ver area provides the opportunity to implement alternative designs to conventional wind turbines. [8] Regarding time management, the Ijmuiden Ver project results to be the most suitable option that best matches the project's expected duration. A project duration of 4 to 5 years to start operating the turbine in 2027 is reasonable for the duration estimation of the project stipulated by the team. Finally, the already existent DC grid connection and the project's readiness to be started make this option optimal for the placement of the wind turbine discussed in this project.

3.2. Wind Model

It is common knowledge that offshore winds are stronger and less turbulent than onshore ones due to the absence of obstacles that may disturb the airflows [9]. When designing a wind turbine, a wind model plays a crucial role in understanding and predicting the chaotic behaviour of the wind resource at a specific site. Consequently, it is necessary to estimate the possible wind loads as well as assess the wind resource characteristics at the site where the wind turbine will be installed. This section aims to capture the complex and dynamic nature of wind at different heights and present the results obtained by exploring the variations of wind speed, wind directions and power density as a function of time.

The method followed to achieve this uses a broad selection of wind atlas data sets provided by the New European Wind Atlas project (NEWA). The project is the result of a collaboration between multiple Euro-

[8] https://offshorewind.rvo.nl/file/download/c2ae21db-49ba-4bc0-8036-cae87fd087d8/ijv_20230512_psd-alpha-and-beta_draft-version-f.pdf [cited: 20 June 2023]

[9] https://aboutthenetherlands.com/the-reason-why-the-netherlands-is-so-windy/?utm_content=cmp-true[cited: 15 June 2023]

pean technical universities. This model aims to provide the user with atmospheric data covering the entire EU including Turkey, as well as the complete North and Baltic Seas. The data set employed is based on 30 years of mesoscale simulations around all of Europe with the Weather, Research and Forecasting (WRF) model at 3 km × 3 km × 30 min resolution [13].

Using the coordinates of the Ijmuiden Ver site, the corresponding area in Figure 3.2 was selected, and different meteorological data were collected.

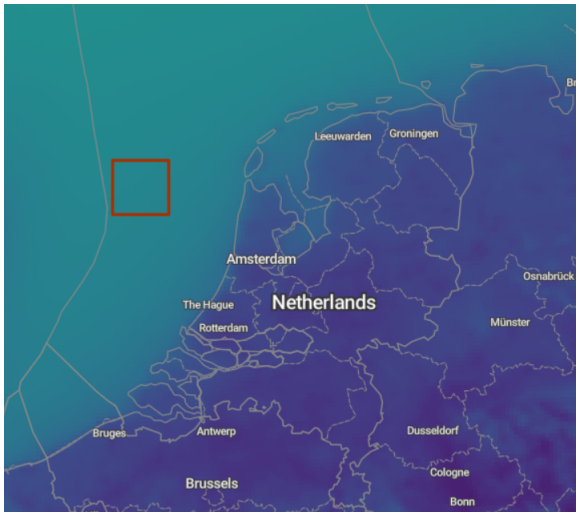

Figure 3.2: *Area corresponding to the Ijmuiden Ver site selected in the Newa website*

Wind speed and wind direction data for the selected area were downloaded from the provided data sets and imported into Python. This process was carried out for various heights (250m, 50m) and three-month intervals spanning a period of three years (2016, 2017, 2018). The choice of dividing the data over periods of three months was due to the larger size of the files for one entire year resulting in errors with the download. After reading the downloaded data in Python, the power density of the area was determined with the following formula:

$$Pd = \frac{1}{2} \cdot \rho \cdot v^3 \cdot \frac{1}{A} \tag{3.1}$$

Everything was then plotted as a function of time, and the following plots of wind speed and power density as a function of time were obtained. Note that for this report, only the wind speed and power density variations of 2018 at 250 m height are presented. This is done to avoid presenting similar graphs that do not add anything to the final report.

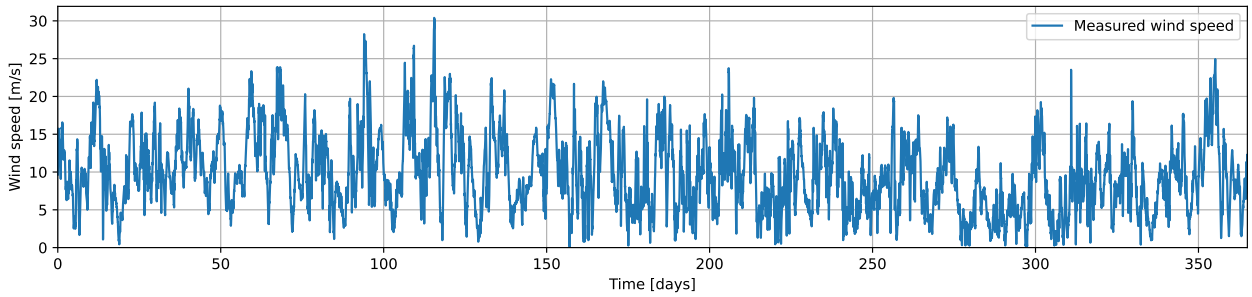

Figure 3.3: *Wind speed variations of the Ijmuiden Ver site at 250m height (2018), from 1st of January to 31st of December*

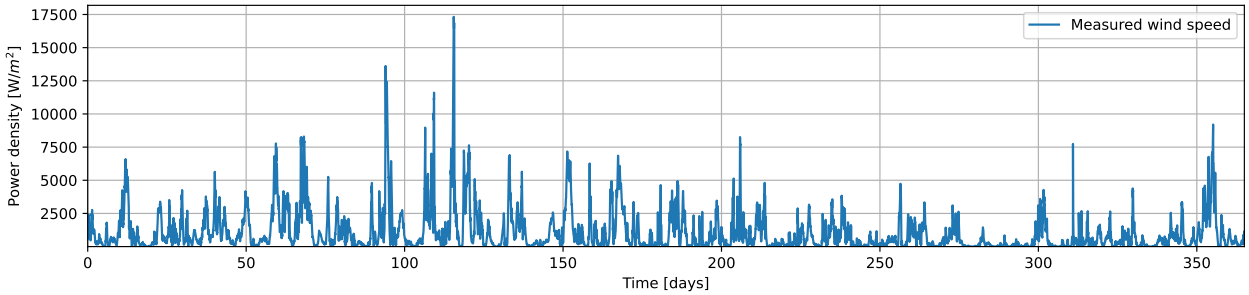

Figure 3.4: *Power density variations of the Ijmuiden Ver site at 250m height (2018), from 1st of January to 31st of December*

As depicted in the graphs, during one year, the changes in windspeed that the MR-TBD turbine may be subjected to are a lot and, at some points, they become very sharp. From Figure 3.3, it is clear that winter is the season of the year in which the highest windspeeds are recorded. On the other hand, from July to October, the minimum windspeeds can be visualised. This is due to the following. In autumn and winter, winds are stronger on average due to the frequent passage of low-pressure systems (storm activity). In fact, in winter, the cold air passes over relatively warm water, resulting in unstable conditions. The latter leads to stronger mixing of momentum downwards. On the other hand, in summer, there is less storm activity, and warmer air passes over relatively cold water. This results in stable conditions with less vertical mixing [14]. Multiple studies have been performed on this topic that presents similar trends to the ones found [15, 16]. Moving to the power density plot, it can be noticed that the location over time of the peaks corresponds to the location of the windspeed ones. This is due to the relationship between power density and wind speed.

The average, maximum and standard deviations of the different windspeed data were recorded and tabulated for all the years and heights considered for this study. These results can be found in the following table 3.1:

Table 3.1: *Windspeed parameters for different heights and years in Ijmuiden Ver site*

WINDSPEED	Average [m/s]	Standard deviation [m/s]	Maximum [m/s]
2016 at 50m	8.97	+/- 4.03	25.52
2017 at 50m	11.05	+/- 4.18	23.50
2018 at 50m	10.10	+/- 3.96	22.14
2016 at 250m	9.49	+/- 4.54	29.39
2017 at 250m	11.94	+/- 4.81	28.014
2018 at 250m	10.95	+/- 4.57	23.87

The same is done for the power density:

Table 3.2: *Power density parameters for different heights and years in Ijmuiden Ver site*

POWER DENSITY	Average [W/m2]	Standard deviation [W/m2]	Maximum [W/m2]
2016 at 50m	739	+/- 993	9870
2017 at 50m	1189	+/- 1161	7912
2018 at 50m	937	+/- 997	6622
2016 at 250m	930	+/- 1358	15070
2017 at 250m	1571	+/- 1716	13145
2018 at 250m	1247	+/- 1411	8301

Wind direction must also be considered to complete the assessment of the wind resources in the Ijmuiden Ver region. The wind direction of an area is a crucial parameter since it provides information on the optimal direction toward which the turbine can be pointed to maximise energy production. Wind direction is measured in degrees with respect to the North direction. A good way of showing the change in wind direction, highlighting the frequency of the direction the wind blows the most, is the wind rose. Wind roses are graphical charts that characterise the speed and direction of winds at a location. Presented in a circular format, the length of each "spoke" around the circle indicates the amount of time that the wind blows from a particular direction. Colours along the spokes indicate magnitudes of windspeeds [10]. The wind roses for the different years considered for this study are presented in figure 3.5. Note that for the sake of brevity, only the plots at 250m height from sea level are presented. This is for the fact that the plots at 50m have exactly the same shape as the ones shown but slightly different colours. This is mainly due to the lower windspeed closer to the sea level.

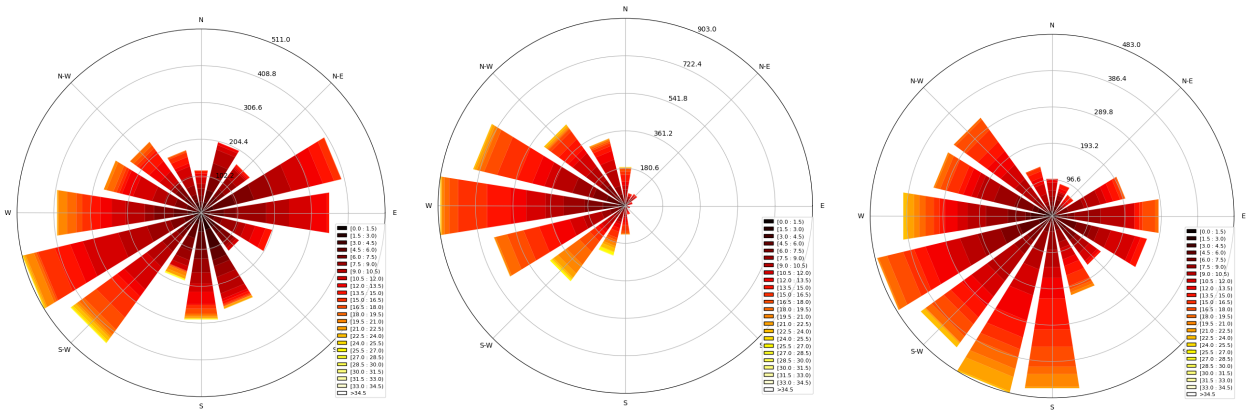

(a) *Wind direction distribution in 2016* **(b)** *Wind direction distribution in 2017* **(c)** *Wind direction distribution in 2018*

Figure 3.5: *Wind roses showing the wind direction changes for three consecutive years at 250m height from sea level. Colours are representative of the wind speed values*

From these plots, several conclusions can be identified. As it is possible to see, the wind has always blown from approximately the same direction for all three years considered. The main difference between the graphs lies in the fact that wind data have an extremely chaotic nature and will never be extremely accurate. In addition, during the years, especially recently, weather conditions have changed severally, mainly due to global warming [17]. This is also a factor to consider while reading the plots presented in this section. Besides this, the similarities in the trends that are presented by these graphs are very positive for the team, also in light of previous studies showing the same results [18]. It is clear that the wind blows the most from

[10] https://english.rvo.nl/information/offshore-wind-energy/hollandse-kust-west-wind-farm-zone [cited: 10 June 2023]

the West/South-West direction. Consequently, this is the ideal direction towards which the wind farm can be oriented to extract the most power.

3.3. Environmental Loading

The system will encounter countless load cases during its lifetime. From a load-inducing perspective only, the environment in which the system operates can be described by four characteristics: wind speed and direction, wave intensity and frequency, wind gusts and wind turbulence. For the purposes of this report, the wind turbulence was not considered, as the correct implementation of an aerodynamic model to evaluate the dynamic turbulence loads would require the extension of the time budget of this exercise.

Based on historical wind data, wind turbines are usually divided into wind classes depending on the wind speeds under which the turbine can be loaded. The pre-defined International Electrotechnical Commission (IEC) classes are presented in Table 3.3 and are defined by four significant wind speeds. The reference wind speed is given as the 50-year return period value for 10-minute average wind speeds, while the annual average is taken as the mean of all 10-minute averaged wind speeds. Gusts, classified as having a duration of over 3 seconds, are broken down into 50-year and 1-year values. All windspeeds were taken at a height of 120 m. As the current design of the systems implies that it will be deployed offshore, with the possibility of expansion beyond the North Sea, it was chosen that the system should belong to Class I, with the highest rated wind speeds.

Table 3.3: *Wind classes as defined by the IEC*

	Wind classes			
	I	II	III	IV
Reference wind speed [m/s]	50	42.5	37.5	30
Annual average wind speed [m/s]	10	8.5	7.5	6
50-year gusts [m/s]	70	59.5	52.5	42
1-year gusts [m/s]	52.5	44.6	39.4	31.5

As mentioned before, the systems will need to operate in offshore conditions, which leads to the consideration of tidal loads. These loads can be mostly estimated using two defining parameters, the significant wave height and the wave period. The significant height is defined as the average of the highest 33% of registered waves [11]. Considering the lack of publicly available historical data regarding wave heights in the North Sea, previously determined values by Fischer et al. have been used [19]. This is a valid assumption, as these measurements were conducted within the UpWind programme at the Ijmuiden K13, a site in the Dutch North Sea with a water depth of 25 m [19]. Thus, all wave calculations that would follow were conducted with the worst-case scenario of having a 50-year return period value of 17.67 m. The significant wave height and period can be computed using Equation 3.2.

$$H_s = 1.1\frac{H_{50yr}}{1.86} = 10.45m \qquad T_s = 11.1\sqrt{\frac{H_s}{g}} = 11.45s \tag{3.2}$$

It is important to note that the system will not behave similarly for all environmental conditions. As presented in Section 5.3, the power production needs to be capped after the rated wind speed is reached. This leads to a sharp decrease in TSR, which conversely will affect the thrust and torque coefficients. As it will be presented in Figure 5.23e, the maximum thrust will be reached at the rated wind speed of 11.2 $\mathrm{m\,s^{-1}}$. Yet, the maximum torque is obtained at the wind speed of 18.2 $\mathrm{m\,s^{-1}}$, as shown in Figure 5.23f. Furthermore, it is assumed that the HLD will impart the highest loads on the tower at this wind speed, as after this peak is

[11] URL: https://www.weather.gov/mfl/waves#:~:text=Significant%20wave%20height%20is%20an,most%20erosion%20on%20a%20beach. [cited: 18 June 2023]

reached, the control system will be able to decrease the aerodynamic coefficients of the wings. Lastly, the system will be strategically parked during storm conditions to limit the loads imparted to the structure. The yaw subsystem will orient the tower along the direction of the wind, while the weathervane stability of the structural elements of the tower will help maintain this position. Furthermore, the HLD will be set to their least effective position and the rotors will be parked using the drivetrain hydraulic brakes.

Concluding, three distinct load cases were considered for the design and analysis of the system. LDC1 refers to rated power production and will yield the largest rotor thrust out of the operational envelope. LDC2 is taken as the point when the largest rotor torque and HLD performance is reached, while LDC3 represents extreme storm conditions with parked rotors. All load cases are illustrated in

Table 3.4: *Load cases considered for the sizing of the system*

	Wind speed [m/s]	C_T	C_t	C_L	C_D	C_M
LDC1	11.2	0.75	0.186	3	0.256	0.3
LDC2	18.1	0.43	0.431	2	0.22	0.2
LDC3	70	0.014	0.015	0.074	0.152	0.1

It is worth mentioning that the aerodynamic coefficients of the rotor were estimated based on the experimental analysis of a parked VAWT performed by Ottermo et al. at Uppsala University [20]. The coefficients were adjusted based on the dimensions of the H-rotor used and the environmental conditions. Yet, the difference in aspect ratio and type of airfoil makes this estimate more conservative.

3.4. Load models

In order to estimate the internal loading and thus size the structural elements of the system, it is imperative to develop a model which can simulate the distribution of external loads acting on the system. This section presents two models: a wind model that can estimate the wind distribution along the system's height and a wave model that can determine the distributed tidal load on the monopile.

Wind model

Due to wind shearing effects between various layers of air and the sea surface, the wind profile will not be constant along the structure's height. This, in turn, will subject the topside structural and aerodynamic elements to a distributed and variable loading. For these purposes, the wind model as presented by Vire within the course of Fundamentals of Wind Energy I [21]. This model employs the sectioning of the wind profile into two distinct parts governed by different equations. Due to the shearing effects with the ground and the vertical turbulence created in the process, the first part of the model is modelled after the log-law presented in Equation 3.3. After reaching the blended height, the model transitions to a power-law as shown in Equation 3.4.

$$V_{(h<h_{blended})} = V_{(h_{ref})} \frac{\log\left(\frac{h}{z_0}\right)}{\log\left(\frac{h_{ref}}{z_0}\right)} \tag{3.3}$$

$$V_{(h>h_{blended})} = V_{(h_{ref})} \left(\frac{h}{h_{ref}}\right)^{\alpha} \tag{3.4}$$

The blended height represents the height where the impact of ground surface patches on vertical wind paths becomes negligible, and the wind is fully horizontally blended. The jump between regions is made by calculating the wind speed at the desired height using as a reference the wind speed at the blended height. The following assumptions were made in order to use this model:

WNM-ASS-01: The initial reference height and wind speed will be taken from the chosen wind class defined by the IEC and presented in Table 3.3 for the storm conditions, namely 70 m/s at 120 m.

WNM-ASS-02: The initial reference height for operation conditions will also be taken at 120 m.

WNM-ASS-03: The blended height for the profile of marine wind is considered equal to 60 m, as assumed by Vire [21].

WNM-ASS-04: The power factor α present in Equation 3.4 is taken as 0.11, as under the guidance of Vire [21].

WNM-ASS-05: The log factor z_0 present in Equation 3.3 is taken to be 0.0002 under sea-interaction conditions, as under the guidance of Vire [21].

Following these relationships, the vertical profile of the wind for LDC1 will look as shown in Figure 3.6.

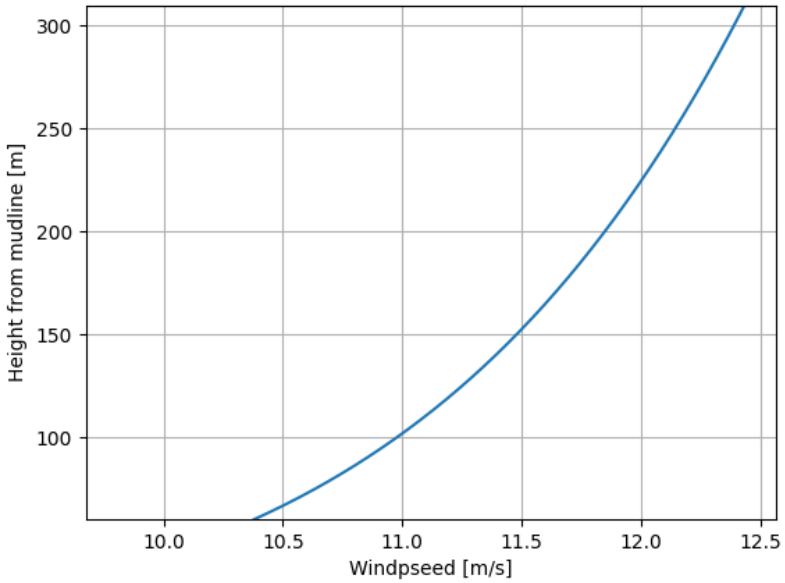

Figure 3.6: *Wind profile for LDC1*

Wave model

Tidal forces can significantly influence the monopile's stability and loading, as storm conditions can create high-impact waves and high dynamic loads. For this report, the tidal loads will be assumed to be static to size the foundation, after which the natural frequency of the monopile will be checked against the wave frequency. The following wave model was obtained from the sizing methodology of XL monopile as published by K.W Hermans [22]. This model employs Airy's wave theory for determining the tidal speed and acceleration and uses Equation 3.5 and Equation 3.6, respectively.

$$u_{(z,t)} = \frac{H_s}{2}\omega\frac{\cosh(kz)}{\sinh(kh)}\sin(\omega t) + u_c(z) \tag{3.5}$$

$$\dot{u}_{(z,t)} = \frac{H_s}{2}\omega^2\frac{\cosh(kz)}{\sinh(kh)}\cos(\omega t) \tag{3.6}$$

It is worth mentioning that the wave number is found iteratively, using Equation 3.7.

$$k = \frac{\omega_n^2}{g h \tanh(k)} \tag{3.7}$$

In order to obtain the loading distribution on the foundation, K.W Hermans uses Morison's equation, which is a semi-empirical relationship to obtain the inline force acting on a body in an oscillatory flow [22]. This force can be broken down into an inertial hydrodynamic component and a drag element, as shown in Equation 3.8. This equation can be applied to the current case, using an inertia coefficient, C_n, of 2, and a water drag coefficient of a cylinder, C_D, of 1. These tidal components are presented in Equation 3.9 and in Equation 3.10, respectively.

$$F_{tidal} = F_I + F_D = \rho_w C_n V^* \dot{u}_{(z,t)} + \frac{1}{2}\rho_w C_D A^* u_{(z,t)} |u_{(z,t)}| \tag{3.8}$$

$$F_{I(z,t)} = z\frac{\pi}{4}\rho_w C_n d_{o(z)}^2 \dot{u}_{(z,t)} \tag{3.9}$$

$$F_{D(z,t)} = z\frac{1}{2}\rho_w C_D d_{o(z)} u_{(z,t)} |u_{(z,t)}| \tag{3.10}$$

As mentioned before, the tidal forces will be considered as worst-case scenario ultimate static loads in this design process. In order to do that, the forces are iterated over a period of the tidal speed and acceleration, and the instance of time which gives the largest total tidal load is taken as the critical time. Thus, the foundation shall carry the tidal loads at the critical time as if they were static. This load profile is then considered in combination with all load cases previously mentioned in Section 3.3. The profile of such a tidal load, taken for a monopile with a constant diameter of 10 m is provided as a visual aid in Figure 3.7

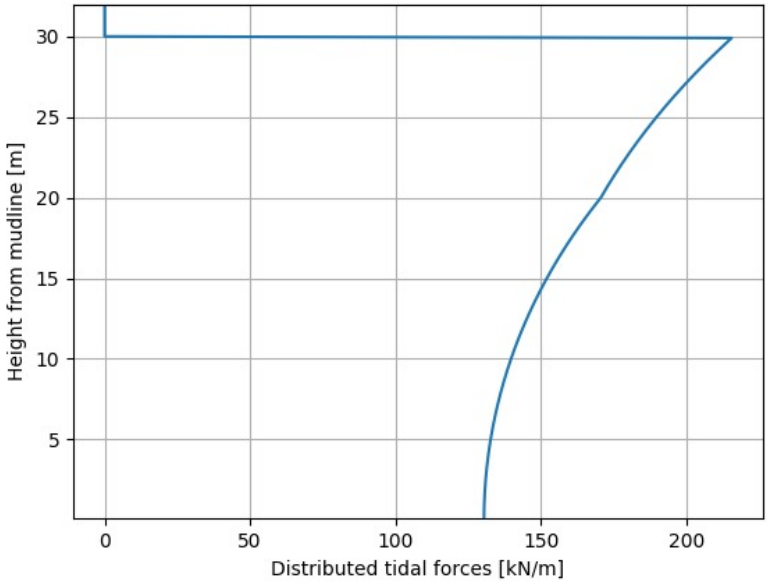

Figure 3.7: *Tidal distributed load along the height of a monopile with a constant diameter of* 10 m

4

Design trade-offs

This chapter covers the identified trade-offs between the available design options. Section 4.1 presents the trade-off for rotor orientation. Section 4.2 trades off the options for the yaw control. Section 4.3 compares the foundation options. Finally, Section 4.4 covers the drive train options. These sections have been shortened as the customer is more familiar with them. Section 4.5 presents different shapes for the structure cell identified. Section 4.6 trades off the main shaft attachment position. Section 4.7 compares different rotor shapes and Section 4.8 covers different individual truss element geometries. Finally, Section 4.9 briefly summarizes the characteristics of the high-level design.

TO score the different options, a consistent colour-scoring scheme was designed. The scheme has a total of four levels presented in Table 4.1. Each criterion was assigned a weight of importance from 1 to 5 and a percentage weight was calculated based on the cumulative weight. The relative weight of importance is also represented by column width in trade-off tables.

Table 4.1: *The explanation of the scoring used for the trade-off of design options*

(R) Unacceptable	(O) Correctable	(L) Acceptable	(G) Exceptional

4.1. Rotor Orientation Trade-off

This section aims to present three design options, HAWT and VAWT, both laid out in a grid with independent drive trains and VAWT grouped on the same drive train. Mass, operations and maintenance, sustainability and other cost-saving options have been evaluated in the section.

Regarding individual VAWTs, for a given power rating, the total generator mass is proportional to one over-the-tip speed ratio times the number of rotors in a row. If rotor mass is kept constant for individual VAWTs, the number of generators is $n \cdot k$. The number of generators for individual HAWTs is $n \cdot k/4$. For grouped VAWT, the number of generators is n.

The trade-off determined that grouped rotor VAWT outperformed other options. To include assumptions made, HAWT are more efficient than VAWT (around +6%) [2, 23]. However, the packing ratio makes the HAWT less space efficient than VAWT (roughly -9%). Also, generator mass is not perfectly linear with torque, as some components of a generator scale with different factors. If the width of the turbine is not approximately equal to the height, then the number of generator scaling changes. More specifically, if the turbine's height is two to four times the rotor diameter, the number of generators becomes comparable between individual rotor HAWT and grouped rotor VAWT.

4.2. Yaw Control Trade-Off

Two types of yawing mechanisms can be identified: passive and active. It was evaluated that no trade-off table is needed for this selection since active yawing control is a project requirement. The active yaw system options considered are electric, hydraulic or aerodynamic. An aerodynamic yaw system stops or slows down the structure's rotors to change the structure's drag non-symmetrically to induce torque and yaw the structure.

The hydraulic yaw system was discounted due to maintenance reasons and cost compared to an electric yaw system. Comparing the electric yaw to the aerodynamic yaw system revealed the main difference between the two to be added mass and the cost of an additional motor as well as the moment arm being larger for the aerodynamic yaw system. The electrical yaw system proved to be too large and expensive

to provide a yaw rate of $1^\circ/s$, so an aerodynamic yaw system became the only choice for primary yaw. An additional benefit of the aerodynamic yaw system is that there is no torque in the monopile.

The aerodynamic control system requires the turbines to function. A backup option may be necessary during a storm or low wind speeds. For this, an electrical yaw system was selected. With this, the system's reliability is higher, allowing some additional yaw without using an aerodynamic yaw system.

4.3. Foundation Trade-Off

The structure can use a monopile, a jacket structure or a floating foundation. A jacket is a truss structure with similar applications as a monopile. A floating foundation is used for deeper water and consists of a pontoon, ballasts and cables attaching it to the sea floor.

Regarding the floating option, the metal mass of the floater was estimated to be 9742 t. This is significantly more than the monopile. The Jacket was found to be the lightest option with a mass estimated around 5400 t when compared to a monopile mass of 7100 t. Installation of fixed foundations is more complicated than the floaters, requiring specialised jack-up vessels. Monopiles and jackets are claimed to be feasible for usage at depths up to 70 m [24] [25]. Floating foundations require minimum depths, which is more relevant at roughly 40m. 70m depth is more than any areas with wind farms planned by the Dutch government[1].

While installation is more difficult for a fixed foundation, it is selected since the depth range better aligns with current North see plans and the mass of a fixed foundation is less.

The jacket structure is a widely underused option for wind farm design, especially because of the maintenance, complexity and lifetime concerns. This caused the jacket not to be chosen. The selected option for the design is thus the monopile. In 2016 80% of all offshore wind turbines employed the monopile for their foundation [26], meaning that the trade-off was in favour of the most commonly employed option.

4.4. Drive Train Trade-Off

Several design options were discovered within the selection of a design for the drive train.

1. Direct drive with a permanent magnet synchronous generator (DD-PMSG) and a full converter
2. Direct drive with an electrically excited synchronous generator (EESG) and a full converter
3. Drive train with a gearbox, a doubly fed induction generator (DFIG) and a partial converter
4. Drive train with a gearbox, a permanent magnet synchronous generator and full converter (PMSG)

The first two design options follow a similar design pattern, having the shaft connected to the rotor directly linked to the generator element. In order to match the frequency of the grid, either 50 Hz or 60 Hz, depending on the installation region, a full converter is included. The other two design options use a gearbox between the rotor and the generator. Usually, a planetary gearbox, comprising either two or three stages, is considered to bring the rotational velocity of the drive shaft within the operational RPM window of the generator. The doubly fed induction generator of design option 3 incorporates a partial converter, which can vary the current frequency to the generator's rotor, making it operable with variable rotational speeds [27].

Li et al. provides an overview of the average amount of rare-earth metals used for different types of generators [28]. DFIGs do not use any rare-earth metals and are, therefore, the most sustainable generator type. DD-EESGs and G-PMSGs use a moderate amount of rare-earth metals, with 30 and 52 tons/GW, respectively. DD-PMSGs are by far the most unsustainable option, with an average rare-earth metal use of 231 tons/GW [28]. According to Pavel et al., 77% of the current global wind energy capacity uses electromagnetic generators, with the remaining 23% using permanent magnet generators [29]. The direct drive

[1] https://north-sea-energy.eu/en/energy-atlas/

generators require the generator to be matched to the specific RPM of the turbine. As the rotors in VAWT are relatively unconventional, direct-drive generators would not be widely available. The use of rare-earth metals is deemed a disadvantage, as the uneven world poses a risk to the supply chain.

Two options, namely the direct drive permanent magnet and the direct drive electrically excited generator, can be easily dismissed based on their performance regarding sustainability and ease of manufacture for small and medium OEMs. Yet, considering the importance of sustainability, especially regarding rare earth metals that go into making the permanent magnets, to the client of this design exercise, it can be argued that the DFIG option is superior. Moreover, considering that 80% of the rare earth metals currently used in the wind energy industry are supplied from China, there lies a critical bottleneck in the supply chain, which can raise the potential risk of supply disruptions and spikes in prices, as seen at the beginning of the Covid-19 pandemic [2] [30]. The 3G DFIG configuration has been selected as the drive train option for these reasons.

A sensitivity analysis was made to analyze if the focus would change from sustainability and democratisation of manufacturing towards better performance, either by giving more importance to availability or power efficiency. In that case, it is clear that a permanent magnet configuration would be the option to choose. If the client opts for eliminating market democratisation requirements and decides to rely on the big drive train manufacturers in the wind industry, then the best configuration would be the direct drive permanent magnet configuration, as common as it is on the market already.

4.5. Triangle vs Rectangle based structure Trade-Off

The structure base cell can be either rectangle-based or triangle based. The trade-off choice shapes are triangles in which a V- shape rotor would fit or a rectangle shape where a H-shape rotor would be mounted seen in Figure 4.1. Other rotors may also be mounted in a rectangle cell. Other shapes are not considered as they have no clear advantage either structurally or concerning rotor shape. This trade-off differentiates between these choices mainly by investigating generator properties for the two cases.

Figure 4.1: *Trade-off choice between the structure cell shape.*

CRIT-STRshape-01 (5/5 Weight - 50%): Generator count
CRIT-STRshape-02 (2/5 Weight - 20%): Structural mass
CRIT-STRshape-03 (3/5 Weight - 30%): Maintenance accessibility

CRIT-STRshape-01: The required generator count refers to the number of shafts required for a set rotor diameter. As the V-shaped rotors are staggered, there will be a shaft in between every rotor radius, while there will be a shaft spaced by diameter for the H-type rotor. This means that for the same rotor diameter, a V-rotor-based turbine will have twice the generator count of an H-rotor-based turbine. If the diameter of the V-rotor is increased, such that the number of generators is the same as for an H-rotor, the torque rating of the drivetrain would have to be doubled. Higher torque drivetrains come with higher purchase prices, worse democratisation and more intensive maintenance.

CRIT-STRshape-02: The required structural mass may be different for a V-rotor based compared to an H-rotor. The v-rotor-based structure allows for diagonal trusses in the front of the structure allowing a more efficient load path. The load path for the V-rotor-based structure is shorter, so the structure may be lighter.

[2] URL: https://strategicmetalsinvest.com/5-year-prices/ [cited 17 May 2023]

CRIT-STRshape-03: The maintenance accessibility refers to how easily the drive train can be maintained based on the shape of the rotor. The access paths can be made similarly; thus the maintenance aspect of the rotors is the same.

Table 4.2: *Rotor type trade-off*

CRIT-RTRshape	**01** Number of Generators	**02** Mass	**03** Maintenance
H-shape	(G)	(L)	(L)
V-shape	(R)	(G)	(L)

Table 4.2 shows that while the structure that accommodates V-shaped-rotors will be lighter, the increase in the number of generators is detrimental, and thus a rectangle is chosen. For a sensitivity analysis, there is not much room for change as the number of generators and the torque in the generators are driving the design.

4.6. Shaft mounting position Trade-Off

The shaft of the rotors can be placed either in the middle of the structure cell or the edge of the structure described in Figure 4.2. The choice is mainly due to the ease of manufacturing and replacing rotors. Additionally, the constraints imposed by the diameter on both design option depth is investigated.

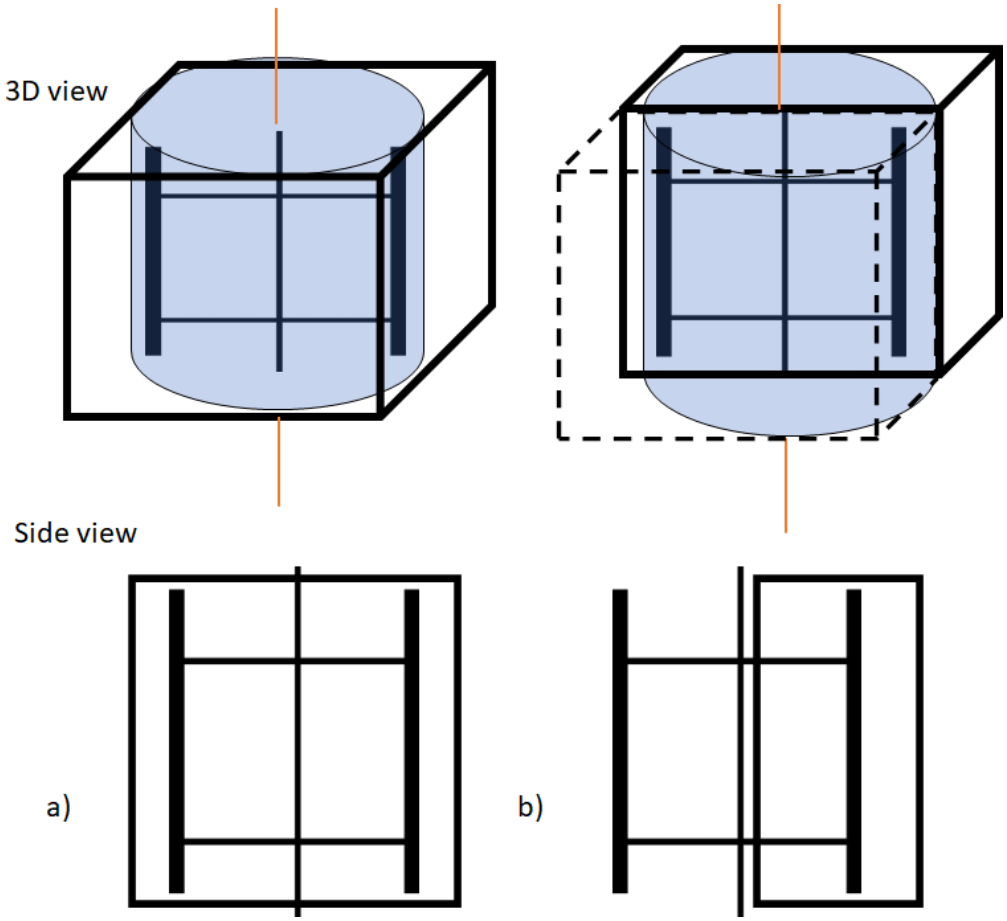

Figure 4.2: *Trade-off choice between the location of the shaft. a) in the middle of the cell and b) on the side of the cell.*

CRIT-AxPos-01 (3/5 Weight - 33%): Minimum structural depth

CRIT-AxPos-02 (3/5 Weight - 33%): Structural mass
CRIT-AxPos-03 (3/5 Weight - 33%): Ease to replace the rotors

CRIT-AxPos-01: The minimum structural refers to how shallow the structure can be without interfering with the rotors depending on their diameter. At this design stage, it is unclear what the optimal structure depth and diameter of the rotors are. This makes mounting at the front advantageous since the range of possible structures and rotor sizes is bigger.

CRIT-AxPos-02: The structural mass refers to how much material is required to support all other subsystems. A comprehensive weight analysis is performed in Section 5.1. In principle, mounting the rotors at the front has benefits for carrying the thrust loads. The load path is less, needing only to travel half the depth. The optimal depth of the structure might be smaller than the diameter; therefore, putting the rotor at the front would make the structure lighter. Additionally, when mounting the rotor at the front of the structure, the centre of gravity is shifted forwards, partially relieving the aerodynamic bending moment, which leads to lower stress on structural members and, therefore, the possibility of making the structure lighter.

CRIT-AxPos-03: The replacement of rotors may be done to extend the system's life. Easy replacement also helps when assembling the system. It helps with maintenance time if a blade needs to be replaced. Having the rotors mounted in front of the structure makes it easily detachable and not entangled in the main structure.

Table 4.3: *Rotor installation location trade-off*

CRIT-AxPos	**01** Minimum depth	**02** Structure mass	**03** Assembly
Front	(G)	(G)	(G)
Middle	(O)	(O)	(O)

From Table 4.3, it is immediately trivial which configuration is best. Mounting the rotors at the front is clearly the better option. It has the potential to be lighter, it is better for maintenance, and it has virtually no drawbacks. Therefore, it has been decided to continue with the front-mounted option for the rest of the design.

4.7. Rotor Selection Trade-Off

This section determines the most efficient and cost-effective option for the shape of the rotor. The possible options can be seen in Figure 4.3. The factors that differentiate are packing ratio and aerodynamic performance, which affects structure mass. Ease of manufacturing impacts initial costs, and different rotor shapes impact power consistency. Sinusoidal or constant loading on the shaft impacts the fatigue life on the drivetrain.

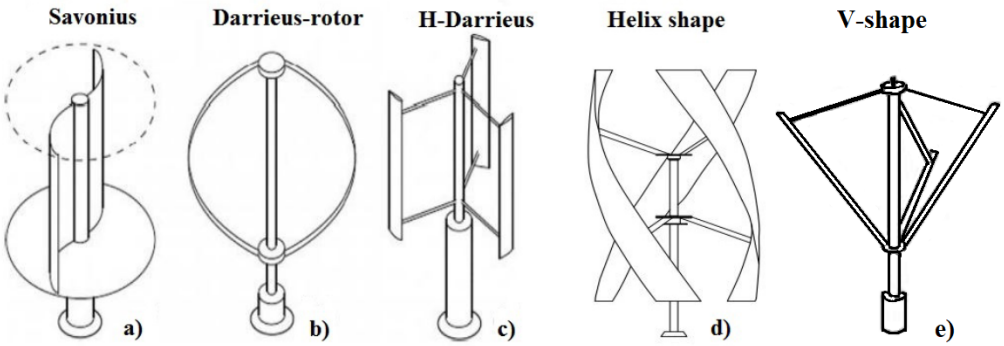

Figure 4.3: *Trade-off choice of the rotor selection. Drag-based Savonius (a). Possible variants of Darrieus VAWT: Troposkien type (b), H-type (c), Gorlov (helical type, d) and V-type (e). [31, 32]*

CRIT-RTRshape-01 (5/5 Weight - 38.5%): Packing ratio
CRIT-RTRshape-02 (2/5 Weight - 15.5%): Aerodynamic performance (C_P, C_T)
CRIT-RTRshape-03 (4/5 Weight - 30.5%): Manufacturability
CRIT-RTRshape-04 (2/5 Weight - 15.5%): Fatigue life

CRIT-RTRshape-01: Packing ratio refers to how well a rotor uses the given space. For the comparison, a rectangle-based structure cell has been used. This makes rotors a), c) and d) perform well in this category. If a triangle-based structure was used, then the V-shaped turbine would perform best. Hence the asterisk in the trade-off table. The Darrieus style rotor will always underperform since truss structures do not synergise with curved shapes.

CRIT-RTRshape-02: The aerodynamic performance is to measure how much power and thrust can be expected to be produced for a given swept area. Drag-based rotors, like the Savonius, have significantly worse parameters than lift-based ones. This makes the Savonius rotor essentially impossible to use in the design. The V-shaped and Darrieus rotors are also not optimal. The fact that different parts of the blades experience different airflow velocities reduces their efficiency compared to the rest of the lift-based rotors.

CRIT-RTRshape-03: Manufacturability is how easy and thus how costly it is to manufacture the rotor. Complex shapes, like in the helical designs, or unfavourable loading paths, like in the V-shape, make these rotor options expensive to manufacture. From this, the H-type and Darrieus-type rotors should be the cheapest lift-based option.

CRIT-RTRshape-04: Helical rotors have a constant torque in the shaft while non-helical rotors with two blades create sinusoidal loading. This effect influences the fatigue on the generators as peak loading is higher. The uneven loading can be mitigated by placing multiple rotors out of phase on the same shaft, creating a more even loading.

Table 4.4: *Rotor shape trade-off*

CRIT-AxPos	**01** Packing ratio	**02** C_P, C_T	**03** Manufacturing	**04** Fatigue life
Savonius	(G)	(R)	(L)	(L)
Darrieus-rotor	(O)	(L)	(G)	(L)
H-shaped	(G)	(L)	(G)	(L)
Helix shaped	(G)	(L)	(R)	(G)
V-shaped	(O)*	(O)	(O)	(L)

To conclude, it can be seen that the H-shaped rotor performs best as it does not have any deficiencies.

There is still the question of the number of blades. Kharade and Jagtap and Battisti et al. determined that 3 blades per rotors have the best performance [31, 33]. As one shaft is likely to contain many blades the issues arising from fatigue should be mitigated.

4.8. Individual element selection Trade-Off

A truss element must be chosen before a design can be proposed. There are many profiles to choose from, but it was decided that four types of elements will be considered, solid cylinders, hollow cylinders/tubes, a truss structure and I beams. The focus of the trade-off is to compare the weight performance of the different sections.

Figure 4.4: *Trade-off choice of individual elements of the structure between a) solid cylinder, b) hallow cylinder, c) truss elements, d) I-beam*

CRIT-IES-01 (5/5 Weight - 50%): Buckling
CRIT-IES-02 (3/5 Weight - 30%): Complexity
CRIT-IES-03 (2/5 Weight - 20%): Torsion resistance

CRIT-IES-01: The buckling performance of a profile is determined by its second moment of area per area of the cross-section. This criterion has been chosen to help minimise the mass of the structure. Since the only buckling mode taken into account is Euler buckling, the section with the highest minimum second moment of the area around any axis is preferred. Therefore sections with an area distributed furthest from the centre are best. From the selection of profiles, only the solid cylinder does not move the material towards the edges, so it underperforms in this category. Analysing the trust option is difficult since the properties will depend on the exact geometry. It has been assumed that it could be optimised for buckling; therefore, it performs well. I beam usually has the best geometry to withstand buckling; however, since the analysis is limited to truss structures (only Euler buckling), the lack of a radial symmetry makes the compression with hollow circular sections (tubes) unfavourable.

CRIT-IES-02: The complexity criteria ensure that the structure remains cheap to build. Making a more complex layout makes every step in the design and life of the structure more difficult, therefore, more expensive. The one profile that is not 'simple' is the trust element. Building trusses from trusses is possible, but it dramatically increases the count of connection points.

CRIT-IES-02: The calculations performed in Section 5.1 are limited due to the truss model used, so no torque values are obtained. However, having a profile that can handle some torque is useful since some internal torques are to be expected.

Table 4.5: *Individual element selection*

CRIT-AxPos	**01** Buckling	**02** Complexity	**03** Torsion
Solid cylinder	(R)	(G)	(O)
Hollow cylinder	(G)	(G)	(G)
Truss elements	(G)	(R)	(L)
I beam	(L)	(G)	(O)

It can be seen that the hollow cylinder outperforms other options. Not only it is highly resistant to buckling, but it is easy to simulate and manufacture, and it is also the most torsion-resistant. For elements where bending has to be considered, an I beam may perform best, and if Euler buckling is very limiting, a truss structure may replace that element.

4.9. General design description

Summarizing the design, to support the multi-rotor system, a large truss structure tower is used. This truss is built up out of tiled cubical cells, made out of hollow cylindrical elements. Each of these cells supports one VAWT rotor, with the rotors vertically connected to a single shaft. Each of these shafts is connected to a DFIG with a partial converter. The truss also supports high-lift devices to create an updraft, blowing out the wake. The rotors are mounted at the front of the structure. This structure is supported by a large monopile. To ensure optimum power production, the system is yawed by differential thrust, with an electric motor as a backup. In Chapter 5 each of the subsystems is designed in more detail.

5

Design analysis

This chapter discusses the detailed analysis performed for six out of eight turbine subsystems. Analysis of the tower subsystem (TWR) is presented in Section 5.1, Section 5.2 contains an analysis of the wake control system (WCT), followed by an analysis of the rotor subsystem (RTR) in Section 5.3. Section 5.4 describes the design of the yaw control system (YCT), followed by the design of the drivetrain (DRT) in Section 4.4. The section is concluded by the design of the foundation (FND) design in Section 5.6.

5.1. TWR analysis

The tower of the MR-TBD design is a large truss structure, consisting of a repeating pattern of smaller cubical cells stacked heightwise and widthwise. To aid the design of this subsystem, a Python program was written that analyses the internal forces in each element, selects an appropriate radius and thickness for this element, and thereby optimises the mass. This section describes the theoretical background for the model, the design decisions made based on the model, and the resulting design. Full source code published under GPL-3 licence can be found at https://github.com/j4nr0th/recTRUSS.

Theoretical Background

The truss model uses the theory of linear elasticity. This employs several assumptions, which are presented below:

TWR-ASS-01: Deformations are linear and obey the relation $\sigma = E\varepsilon$ (which may be rewritten as $F = \frac{EA}{L}L'$)

TWR-ASS-02: Deformations of individual elements are small, hence the change of their relative orientation from the original position is neglected.

TWR-ASS-03: The individual truss elements may only fail under yield (in tension or compression) when $\sigma \geq \sigma_y$ and when loaded with Euler's critical load

TWR-ASS-04: Individual truss elements only carry loads in the direction they are orientated in.

TWR-ASS-05: Trusses behave as if half of their masses are lumped at each of the two nodes to which they connect.

Given these assumptions, the truss structure can be modelled as consisting of a finite number of truss elements. An individual element e is oriented in its reference frame with first node N_0^e at the origin and N_1^e at the location $< L, 0, 0 >^T$. Suppose the vector $\vec{d}^e$ is the vector from node N_0^e to node N_1^e in the global reference frame as $\vec{d}^e =< d_x^e, d_y^e, d_z^e >^T$. In that case, the transformation from the global reference frame to the element's reference frame is defined as per Equation 5.1, with the angles α and β defined as per Equation 5.2 and Equation 5.3.

$$\mathbf{T}_{g\to e} = \begin{bmatrix} \cos\beta & 0 & -\sin\beta \\ 0 & 1 & 0 \\ \sin\beta & 0 & \cos\beta \end{bmatrix} \begin{bmatrix} \cos\alpha & \sin\alpha & 0 \\ \sin\alpha & \cos\alpha & 0 \\ 0 & 0 & 1 \end{bmatrix} \tag{5.1}$$

$$\tan\alpha = \frac{d_y^e}{d_x^e} \tag{5.2}$$

$$\tan\left(\frac{\pi}{2} - \beta\right) = \frac{\sqrt{(d_x^e)^2 + (d_y^e)^2}}{d_z^e} \tag{5.3}$$

By considering a local displacement vector for an element as $\vec{u}^e = < u^e_{0_x}, u^e_{0_y}, u^e_{0_z}, u^e_{1_x}, u^e_{1_y}, u^e_{1_z} >^T$, the forces at nodes N^e_0 and N^e_1 can be expressed in the local reference frame as per Equation 5.4. Using the transformation $\mathbf{T}'_{g\to e}$ per Equation 5.5, this relation can be formulated in the global reference frame as per Equation 5.6 and Equation 5.7. Global stiffness matrix $\mathbf{K}^g$ and force vector $\vec{F}^g$ can be then assembled from the local matrices, which gives the global system as in Equation 5.8. For the global reference frame and system, the superscript g will be dropped. The system can then be reformulated in terms of external loading $\vec{F}_{\text{ext}}$, gravity loading $\vec{F}_g$, and reaction forces $\vec{r}$. This relation is given in Equation 5.9. The external loading $\vec{F}_{\text{ext}}$ is given by the natural boundary conditions at each node, while the weight of each element gives the weight loading $\vec{F}_g$. Assuming a constant cross-section area A and material density ρ, along with constant gravitational acceleration g_0, this gives the load of $\frac{1}{2}\rho AL$ per node, meaning each of the nodes is loaded with half of the weight. In the reference system used by the model, gravity is applied in the direction of the z-axis, downwards. The reaction forces $\vec{r}$ occur due to numerical boundary conditions, which force the nodes to have fixed (usually zero) displacements.

$$\vec{F}^e = \begin{bmatrix} F^e_{0_x} \\ 0 \\ 0 \\ F^e_{1_x} \\ 0 \\ 0 \end{bmatrix} = \frac{EA}{L} \begin{bmatrix} 1 & 0 & 0 & -1 & 0 & 0 \\ 0 & 0 & 0 & 0 & 0 & 0 \\ 0 & 0 & 0 & 0 & 0 & 0 \\ -1 & 0 & 0 & 1 & 0 & 0 \\ 0 & 0 & 0 & 0 & 0 & 0 \\ 0 & 0 & 0 & 0 & 0 & 0 \end{bmatrix} \begin{bmatrix} u^e_{0_x} \\ u^e_{0_y} \\ u^e_{0_z} \\ u^e_{1_x} \\ u^e_{1_y} \\ u^e_{1_z} \end{bmatrix} = \mathbf{K}^e \vec{u}^e \tag{5.4}$$

$$\mathbf{T}'_{g\to e} = \begin{bmatrix} \mathbf{T}_{g\to e} & \mathbf{0} \\ \mathbf{0} & \mathbf{T}_{g\to e} \end{bmatrix} \tag{5.5}$$

$$\mathbf{T}'_{g\to e}\vec{F}^e = \mathbf{T}'_{g\to e}\mathbf{K}^e {\mathbf{T}'_{g\to e}}^T \mathbf{T}'_{g\to e}\vec{u}^e \tag{5.6}$$

$$\vec{F}^{e'} = \mathbf{K}^{e'}\vec{u}^{e'} \tag{5.7}$$

$$\vec{F}^g = \mathbf{K}^g \vec{u}^g \tag{5.8}$$

$$\vec{u} = \mathbf{K}^{-1}\left(\vec{F}_{\text{ext}} + \vec{F}_g + \vec{r}\right) \tag{5.9}$$

By considering only the non-fixed degrees of freedom in Equation 5.9, the matrix $\mathbf{K}_r$ becomes non-singular and hence invertible, provided that the system is either statically determinate or over-determinate. This will also not include reaction forces $\vec{r}$, as they only occur at nodes that have numerical boundary conditions and are hence not free. The system is shown in Equation 5.10. Reaction forces at fixed nodes can be recovered from Equation 5.9.

$$\vec{u}_r = {\mathbf{K}_r}^{-1}\left(\vec{F}_{\text{ext}_r} + \vec{F}_{g_r}\right) \tag{5.10}$$

The structure's mass matrix can be constructed from local matrices, following from **TWR-ASS-05** as per Equation 5.11. This gives a system as Equation 5.12. By applying the Fourier Transform of the system as in Equation 5.13, the solution to which becomes Equation 5.14. The solution becomes indeterminate when the determinant of the matrix ${\mathbf{M}_r}^{-1}\mathbf{K}_r - \omega^2\mathbf{I}$ becomes zero, meaning that the frequency of excitation ω is one of the eigenvalues of matrix ${\mathbf{M}_r}^{-1}\mathbf{K}_r$. Based on that, natural frequencies of the structure can be determined by finding eigenvalues of the matrix ${\mathbf{M}_r}^{-1}\mathbf{K}_r$.

$$\mathbf{M}^e = \frac{\rho AL}{2}\mathbf{I} \tag{5.11}$$

$$\mathbf{M}_r \ddot{\vec{u}}_r + \mathbf{K}_r \vec{u}_r = \vec{F}_r(t) \tag{5.12}$$

$$\left(-\omega^2 \mathbf{M}_r + \mathbf{K}_r\right) \vec{u}_r = \vec{F}_r(\omega) \tag{5.13}$$

$$\vec{u}_r = {\mathbf{M}_r}^{-1} \left({\mathbf{M}_r}^{-1} \mathbf{K}_r - \omega^2 \mathbf{I}\right)^{-1} \vec{F}_r(\omega) \tag{5.14}$$

Verification of the Model

To prove that the simulation implemented the aforementioned mathematics correctly, verification of the model was performed. A statically over-determined problem was used to test if the simulation found the same result as solving the problem analytically.

The problem is illustrated in Figure 5.1, with four nodes A, B, C, and D in the same planes at positions $<0,0,0>^T$, $<4,0,0>^T$, $<0,4,0>^T$, and $<4,4,0>^T$ respectively. The fifth point E is positioned at $<1,1,1>^T$, with a load $P =<0,0,-1000>^T$ applied at the centre. Points A, B, C, and D have numerical boundary conditions applied so that they may not move, meaning they experience reaction forces in all three directions.

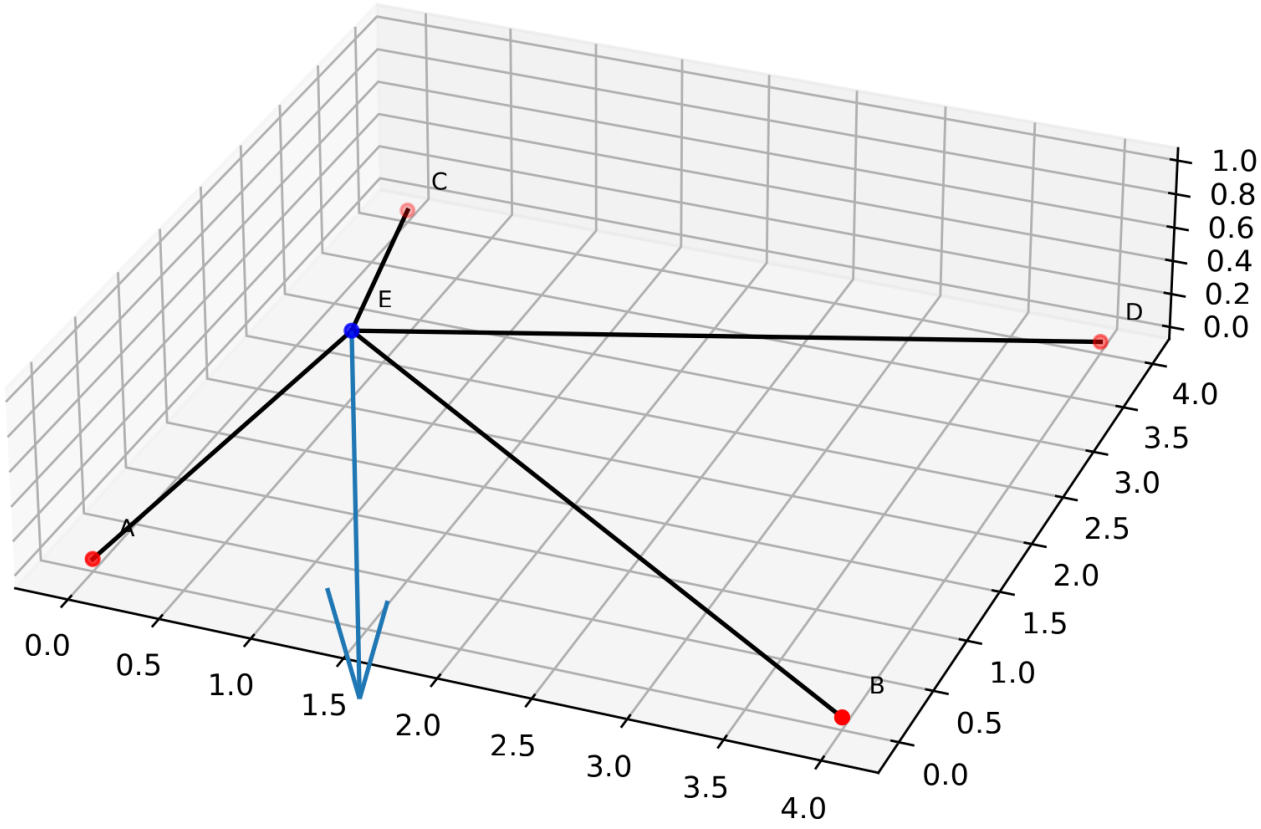

Figure 5.1: *Setup used for verification calculations*

The problem is statically indeterminate, as the equilibrium of forces at point E dictates that the relations Equation 5.15, Equation 5.16, and Equation 5.17 be satisfied. These equations are bound by compatibility

equations Equation 5.18, Equation 5.19, Equation 5.20, and Equation 5.21. These equations use $\vec{r}$ to indicate the position of a point. All elements were considered to have the same profile, a hollow cylinder with an outside radius of 10 mm and a thickness of 1 mm. The used elasticity modulus was 200 GPa

$$+\searrow \sum F_x = -\frac{1}{\sqrt{3}}F_A + \frac{3}{\sqrt{11}}F_B - \frac{1}{\sqrt{11}}F_C + \frac{3}{\sqrt{19}}F_D = 0 \tag{5.15}$$

$$+\nearrow \sum F_y = -\frac{1}{\sqrt{3}}F_A - \frac{1}{\sqrt{11}}F_B + \frac{3}{\sqrt{11}}F_C + \frac{3}{\sqrt{19}}F_D = 0 \tag{5.16}$$

$$+\uparrow \sum F_z = -\frac{1}{\sqrt{3}}F_A - \frac{1}{\sqrt{11}}F_B - \frac{1}{\sqrt{11}}F_C - \frac{1}{\sqrt{19}}F_D = -F \tag{5.17}$$

$$F_A = \frac{E_A A_A}{L_A}\left(||\vec{r}_E - \vec{r}_A|| - L_A\right) \tag{5.18}$$

$$F_B = \frac{E_B A_B}{L_B}\left(||\vec{r}_E - \vec{r}_B|| - L_B\right) \tag{5.19}$$

$$F_C = \frac{E_C A_C}{L_C}\left(||\vec{r}_E - \vec{r}_C|| - L_C\right) \tag{5.20}$$

$$F_D = \frac{E_D A_D}{L_D}\left(||\vec{r}_E - \vec{r}_D|| - L_D\right) \tag{5.21}$$

The solution to the problem was obtained analytically and compared to the values obtained from the simulation. The values and differences between the two are presented in Table 5.1. As can be seen quickly the relative difference (as in difference divided by the analytical value) is in the order between 10^{-5} and 10^{-7}, which can be attributed to errors in rounding and truncation error when computing approximations to the values of inverse square roots. Given the results from Table 5.1, the model is considered validated for solving statically over-determinate problems using linear elasticity.

Table 5.1: *Analytical solution and simulation results for the verification problem along with the differences*

Quantity	Analytical value	Simulation result	Relative difference	Absolute difference
u_{E_x}	2.588861-05	2.588858e-05	1.13e-06	2.92e-11
u_{E_y}	2.588861e-05	2.588858e-05	1.13e-06	2.92e-11
u_{E_z}	-1.81755e-04	-1.81740e-04	7.96e-05	-1.45e-08
F_A	-8664210.99	-8664209.17	2.11e-07	1.82
F_B	-4245768.66	-4245772.15	8.23e-07	3.49
F_C	-4245768.66	-4245772.15	8.23e-07	3.49
F_D	-3548128.79	-3548124.20	1.29e-06	4.59

In addition to verifying these loads, the structural mass calculated by the script was verified to be correct by a hand calculation.

Validation of the model would require a laboratory test with a proper scale model or to use another validated structural simulation software, such as Solidworks, Abaqus, or Ansys. The experimental or software results could then be compared to the model's outputs developed for this design.

Design method

The main structural design tool was a Python implementation of the model described above in Section 5.1. This was used to generate a three-dimensional truss structure as seen in Figure 5.2. As the structure is

symmetric, only half of the structure had to be simulated. A symmetric boundary condition was applied by restricting the movement of nodes on the symmetry line in the left-to-right y-direction. These nodes are yellow in Figure 5.2. To simulate the attachment to the two bearings on the centre column, the two nodes at the bottom left and the two left nodes halfway up the structure are fully constrained. These are shown in red.

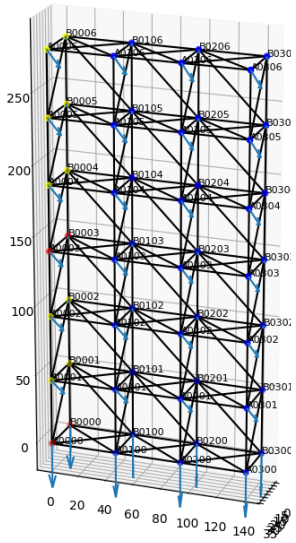

Figure 5.2: *The simulated truss structure. Red nodes are fully constrained, yellow nodes are constrained from moving in the y-direction*

The forces are then applied to the nodes, and the internal loads are simulated. If any element in the truss structure is then loaded above its limit load, its radius and thickness are increased. The program then iterates over these cross-section profiles until all elements are as small as possible but large enough to withstand the internal loading. This way, the mass of the structure is optimised. The structure is a repeating pattern made up of the same cell layout. Still, any structure element can have a different radius and thickness from a predetermined set of radius and thickness profiles.

The failure types considered in the simulation are yield in tension, yield in compression, and Euler buckling. A safety factor of 1.3 was applied to material properties, another safety factor of 1.3 was applied to yielding in compression or tension, and a safety factor of 1.2 was applied to the buckling load. These safety factors follow international standard IEC61400-1 [34].

Applied loads

A range of loads on the structure was considered during the design. As the structure is a truss, these all had to be applied to the nodes. Firstly, the mass of the elements is lumped into the two nodes at their edges. The mass of the drivetrains is distributed over the bottom layer of nodes. The mass of the rotors and shafts is distributed over the nodes at the front face of the structure, except the bottom layer. The mass of these components is summarised in Table 6.2. The forces created by the high lift device and its mass were introduced at the back nodes on the layers where they are present as described in Subsection 5.2.3.

As the nodes at which the yaw torque would be introduced a fully constrained, the torque was modelled by applying a force to every node proportional to its mass, acceleration, and distance to the rotation axis. The acceleration of each node was calculated from the cross-product of the angular acceleration that the torque would induce in the structure and the direction vector from the rotation axis to the node. Using the mass of the node, the acceleration, and Newton's second law, the force required to induce this accelera-

tion is calculated. As this leads to a loop where the applied force on a node depends on the mass, which depends on the minimum profile for the elements connected to it, which in turn again depends on the internal forces, this problem was iterated a few times. The torque ultimately had a very low impact on the structure's mass. The considered torque was 800 kN m as specified in Section 5.4.

Different sources of loads will have different magnitudes depending on the load cases described in Section 3.3. The rotors reach a maximum thrust at the rated wind speed, load case LDC1, while the drag on the structure is the largest during the fifty-year storm scenario, LDC3. To get a set of the most constraining loads on the structure, the worst-case scenario was picked for each individual load source. The drag on the structure and thrust of the rotors were considered as one source, as their load introduction into the structure is exactly the same in the simulation.

The drag on the structure is estimated by projecting the truss onto the plane perpendicular to the wind and multiplying the length of the projected members by the average profile radius. The length of the elements came to around 6200 m, and the average radius of an element came to around 0.45 m. It is important to note that the LDC3 calculated here is larger than the used in the calculations done for the foundation sizing in Subsection 5.6.1. This was done since the increase in weight for the truss for the higher loading was only around 5%. Therefore it was decided that the truss will be sized to withstand the storm conditions with the large side facing the wind. As the drag on the structure in load case LDC3 at 19.1 MN is higher than the rotor thrust for load case LDC1 at 4.51 MN, the structure drag is considered as the limiting thrust. The downforce of the HLDs is the largest during operations at 1245 kN per wing, while the drag is largest during 70 m s^{-1} gusts at 255 kN as calculated in Subsection 5.2.6. While these can not happen at the same time, the structure is conservatively designed by superimposing these two worst-case scenarios.

Scripts were used to distribute the total loads over their respective nodes. To verify that this was done correctly, the forces on the nodes were confirmed to sum up to the total force applied. In addition to this, every time the program is run, there is a visual check in which the user can see at which nodes the loads are applied.

Cell type Selection

For the tower, a modular design was decided as it is both simple to analyse and simple to integrate with other systems. The tower is to be made of cuboid truss cells, which would all have the same dimensions, but with truss elements using different profiles to minimise mass. These different profiles have a range of radii with a constant thickness-to-radius ratio.

The very first thing to be determined was the design of the cell itself. Seven different cell layouts were analyzed. Sketches of these cells are shown below in Figure 5.3 to Figure 5.9.

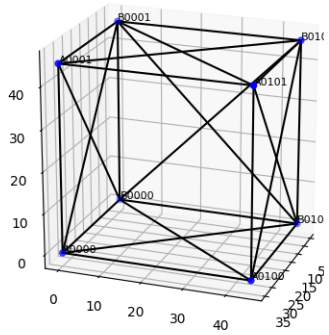

Figure 5.3: *Cell type 1*

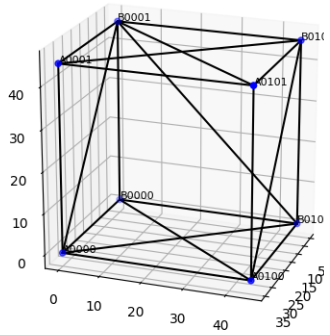

Figure 5.4: *Cell type 2*

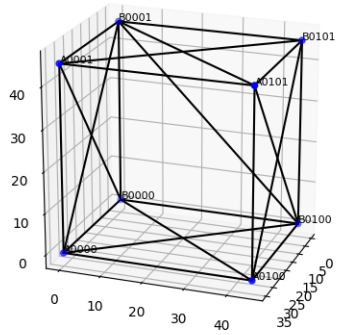

Figure 5.5: *Cell type 3*

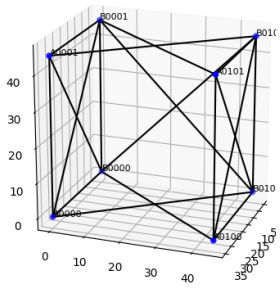

Figure 5.6: *Cell type 4*

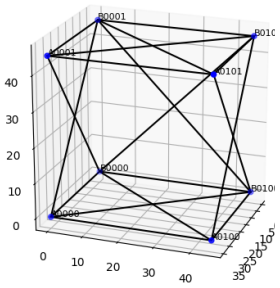

Figure 5.7: *Cell type 5*

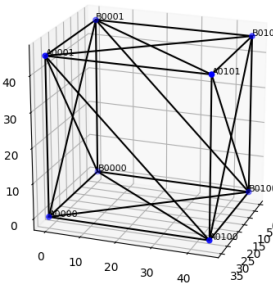

Figure 5.8: *Cell type 6*

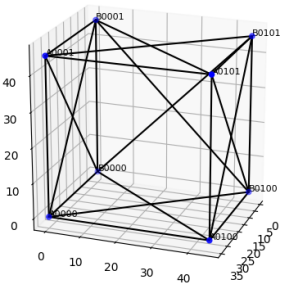

Figure 5.9: *Cell type 7*

A full structure based on these cell types was then generated and optimized for mass. For an accurate comparison, the same forces were applied to each structure, and the same profiles were available to all cell types. The resulting masses are shown below in Table 5.2 note that these masses are not representative of the final mass, but are only used to see how heavy they are relative to each other.

Table 5.2: *A structural mass comparison between the seven cell shapes. Note that these are not representative of a final mass but only compare the relative masses of the cell types.*

Cell type	Cell 1	Cell 2	Cell 3	Cell 4	Cell 5	Cell 6	Cell 7
Mass [tonnes]	5996	5377	6054	4855	6517	5764	5304

Table 5.2 shows that the lightest overall structure was cell type 4. However, this design was later discounted as it provides no location to support the shaft bearings without horizontal members in the front. The next lightest design is cell type 7, closely followed by cell type 2. While cell type 7 was slightly lighter than 2 for the load case in this comparison, it becomes a lot heavier when thrust is increased due to the lack of horizontal braces on the back. For this reason, cell type 2 was chosen.

Cell size selection

Based on the chosen cell shape, the number of cells was then varied for the same overall dimensions of 280 x 280 m. This essentially scales the height and width of each individual cell to find the lightest design. Structure layouts of 4x4 (rows x columns), 6x4, 6x6, 6x10, 6x12, and 8x8 were tested. No layouts with an odd number of columns were considered so that an even number of rotor columns could be used, to allow cancelling out the rotor torque by counter-rotating them. The resulting masses are shown below in Table 5.3.

Table 5.3: *A structural mass comparison between different cell configurations (rows x columns) for the same total structural width and height.*

Cell configuration	4x4	6x4	6x6	6x10	6x12	8x8
Structural mass [tonnes]	4862	4987	4454	5472	6211	4883

Table 5.3 shows that the lightest layout is 6x6, so this was the chosen configuration. The non-square layouts also perform noticeably worse than the square layouts.

Structural depth optimization

Once the cell layout was known, the depth of the structure was optimized. To find the optimal depth, it was varied as a fraction of the structure width between 0.01-0.2. The resulting mass curve is shown in Figure 5.10 below. As the rotors are mounted on the front of the structure instead of the middle, the minimum depth of the structure is the rotor radius. This is a depth ratio of around 8% as indicated by the orange line in Figure 5.10. The mass is minimized for a depth ratio of around 12%, so this is the chosen structure depth. This leads to a depth of 33.6 m.

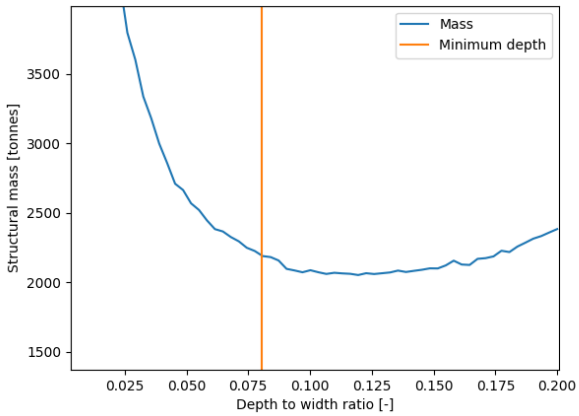

Figure 5.10: *The sensitivity of the structural mass to the depth of the structure*

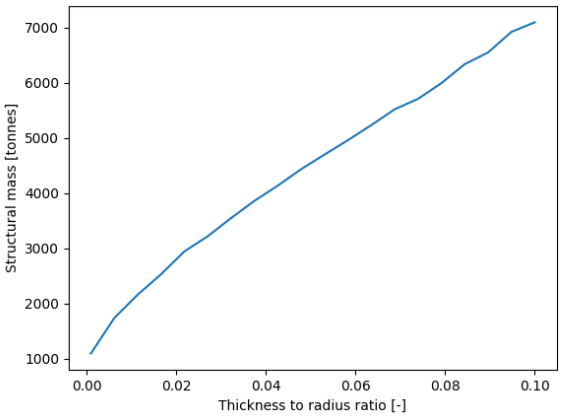

Figure 5.11: *Sensitivity of the structural mass to the thickness to radius ratio*

Profile selection

Finally, the specific profiles of the truss elements have to be chosen. These are a range of hollow cylinders with a constant thickness-to-radius ratio. Only 20 profiles between a minimum and maximum radius are used for manufacturability. In the specific loading case considered, some members are under very little loading and default to the smallest profile. However, they still provide stability to the structure and may be important in unexpected loading conditions. The structural members are approximately 33 m to 65 m long, and they must be stiff enough to such that they do not flex too much under their own mass. For these reasons, a minimum radius 15 cm was chosen. A maximum radius of 2 m was available, but such large members were rarely used. The selection of the thickness-to-radius ratio has a large effect on the mass of the structure, as can be seen in Figure 5.11.

Decreasing the thickness ratio increases the moment of inertia of the cross-section, which increases the resistance to column buckling. This is the failure mode for almost all of the members loaded in compression and therefore has a significant effect on the mass. Out of the total 404 structural elements, 204 are loaded in compression, out of which 180 will fail in column buckling. In addition to this, decreasing the thickness also decreases the mass of members at the minimum radius.

The downside to decreasing the thickness ratio is that the resulting radius increase leads to increased drag on the structure. This is the limiting load case as explained in Figure 5.1. Besides the fact that the total drag on the structure increases, the drag will induce a bending moment on the individual elements, which is not simulated by the truss simulation. In this aspect, using larger, thinner cylinders is undesirable. In addition to this, when the thickness ratio becomes too small, the elements may experience local sheet buckling. This is not simulated, so care must be taken not to pick too small of a ratio. Jamieson et al. uses a thickness to diameter ratio of 1:120, or a thickness to radius ratio of 0.0041 [2]. Using this ratio, 26 structural members have a diameter over 2 m, with two members reaching a diameter of 3.4 m. At a thickness-to-radius ratio of 0.01, only the four largest elements have a diameter of 2 m. To keep down the structural drag and ensure that no sheet buckling will occur but still have a low mass, a thickness ratio of 0.01 was selected.

Material selection

For the truss elements, a few different metals were considered: low-carbon steel, medium-carbon steel, high-carbon steel, low-alloy steel, and stainless steel. Material properties of these steels are shown in Table 5.4 below. To choose the optimal material, an optimised structure was generated for each. First, the raw material costs of these designs are compared. The results are shown in Table 5.5 below.

Table 5.4: *Relavant material properties of the considered types of steel. The data comes from the Ansys Granta Material Universe database*

Material	E [GPa]	σ_y [MPa]	ρ [kg/m3]
High-carbon steel	200	433	7800
Medium-carbon steel	200	376	7800
Low-carbon steel	200	255	7800
Low-alloy steel	200	469	7800
Stainless steel	190	252	7610

Table 5.5: *The mass of the structure for various metal types, and the associated material costs.*

Material	Structural mass [t]	Material cost [M€]
Low-carbon steel	2412	1.51
Medium-carbon steel	2046	1.28
High-carbon steel	1979	1.26
Low alloy steel	1922	1.48
Stainless steel	2422	6.22

Based on these results, medium-carbon steel and high-carbon steel seem like the two best options, with the high-carbon steel design being slightly cheaper than the medium-carbon steel design. However, there are other benefits of using medium-carbon steel over high-carbon steel. As medium-carbon steel is softer, it is generally easier to manufacture parts from or weld. In addition to this, although not as strong as high-carbon steel, low-carbon steel is more ductile. This is a benefit, as it allows for a more damage-tolerant design. Once damage is detected there will be a larger window of time before it has to be repaired. In addition, the corrosion rate of steel increases with carbon content, making medium-carbon steel favourable [1]. For these reasons, medium-carbon steel will be used.

For corrosion protection, multiple layers of white organic solvent-based paint will be applied to the truss structure. This is done to protect the structure from the harsh environment and reduce its capability of absorbing heat from the sun. This process is done for all the above water elements exposed to air. Additionally, a lightning protection system is installed on the structure to protect the turbine from lighting.

Final configuration

The structure's final design is summarised in Table 5.6. With a 6x6 configuration, a depth of 33.6 m, and a thickness-to-radius ratio of 0.01, the optimised structural mass is 2046 t. However, this does not take into account the additional mass of connections between the truss elements. To add a contingency for this, a margin of 20 % is applied to this mass, leading to a mass of 2455 t. This still does not include the mass of the bedplates. The bedplate for the IEA 15-MW offshore wind turbine is 70 t, and the IEA 10-MW offshore wind turbine has a bedplate of 61 t[35][36]. Thus, without going into further loading details, it is possible to roughly estimate the mass of the bedplates for the 5 MW generators to be 52 t per generator. This then leads to the final structural mass of 2767 t. This mass could be reduced by making truss elements thinner, but to safely do so, more detailed buckling analysis should be performed. The final simulated structure is shown below in Figure 5.12, showing the internal stress in the members.

Vibrations

After designing and optimising the structure, the system's natural frequencies were analysed according to the method described in Section 5.1. This mode assumed lumped mass at the nodes, as per **TWR-ASS-05**, which means the analysis is an estimation of the true system. While this will not be completely accurate to the real system, it still provides some insight into the approximate behaviour of the system.

Table 5.6: *A summary of the structure design*

Cell type	Type 2
Cell count	6 x 6
Total dimensions (w x h x d) [m]	295 x 280 x 33.6
Element thickness ratio [-]	0.01
Material	Medium-alloy steel
Mass [t]	2046
Bedplates [t]	312
Total mass including 20% margin and bedplate	2767

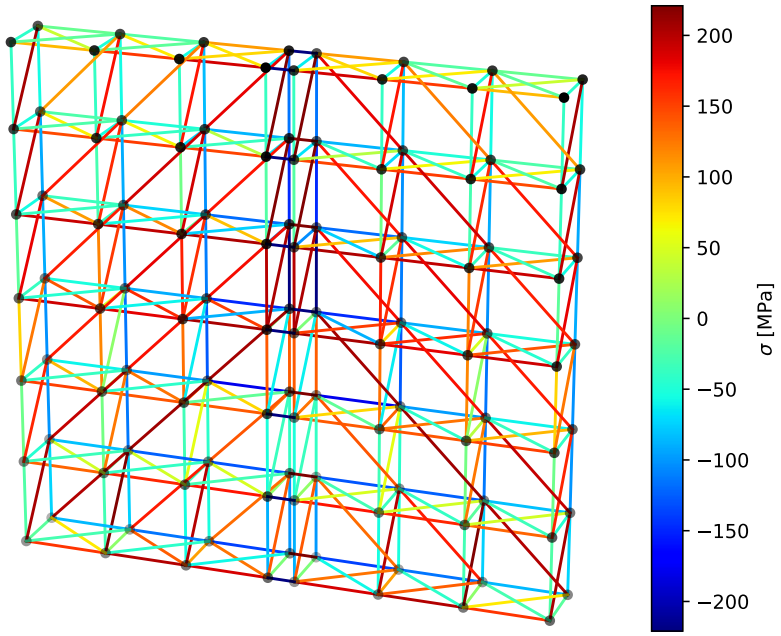

Figure 5.12: *The internal stress in the final structure*

There are two main excitation frequencies in the system, waves hitting the monopile, and the rotation frequency of the rotors. The highest wave frequency considered has a frequency of 0.29 Hz, as shown in Table 5.12. However the larger the period of the waves, the more energy they carry, so the most problematic waves have a lower frequency. The main cause for rotor-induced vibrations is due to the centre of mass of the rotating body not being exactly the centre of rotation. The highest rotor frequency will be obtained at the maximum TSR of 4.5, and the rated wind speed of 11.2 $\mathrm{m\,s^{-1}}$. With the rotor diameter of 45 m, this leads to a rotation frequency of 0.357 Hz. However, the rotation frequency may reduce or completely stop with changes in wind speed. This means any frequency up to 0.357 Hz may be an excitation frequency.

Figure 5.15 shows the excitation frequencies in red and the natural frequencies up to 1 Hz in blue. All frequencies are shown with a bar width of 10% of the frequency. As shown in Figure 5.15, the lowest natural frequency at 0.371 Hz is slightly higher than the rotor frequency. However, as the rotor frequency is very close to the rotor frequency, the excitation frequencies could slightly overlap with this lowest natural frequency, and a more detailed analysis should be performed. If the rotor frequency indeed turns out to be a problematic excitation frequency, a few measures could be taken.

The most apparent solution is to overbuild the structure and make elements larger or thicker than required. This would make the structural members stiffer, increasing the natural frequency. However, the axial stiffness of a rod is only linearly proportional to the cross-sectional area of the element. The mass

of the element is also linearly proportional to the area, which reduces the natural frequency again. While there is a net gain in natural frequency, as only half of the element is lumped at each end, and there are other masses such as the drivetrain components that stay constant, this is not a very mass-efficient way of solving the problem. Another solution could be to isolate the problematic excitation frequencies. The rotor frequency is induced into the structure through the bearings that are mounted to the horizontal truss elements at the front of the structure. A damper could be integrated into the mounting bracket to isolate the vibrations. A sketch of a concept damper system is shown in Figure 5.13 below. The green layer in this sketch represents a layer of damping material. The attachment bolts are shown in red. This could then be modelled as a damper-spring system, as shown in Figure 5.14. This system's damping and spring coefficients then have to be balanced to achieve critical damping.

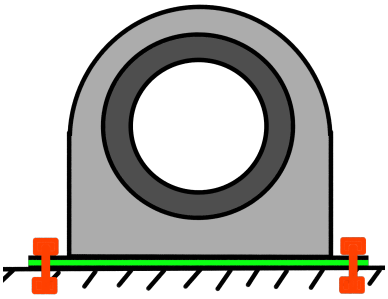

Figure 5.13: *A sketch of a damping mount bracket. Green represents a damping material and the bolts are shown in red.*

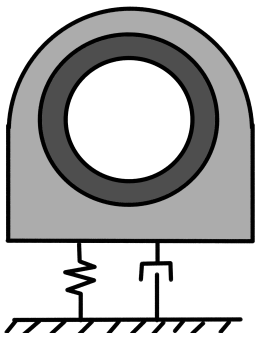

Figure 5.14: *A diagram of the damping mount modelled as a parallel spring and dashpot.*

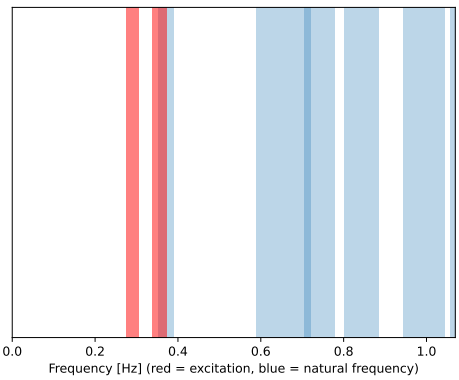

Figure 5.15: *The excitation frequencies and lowest natural frequencies of the system*

5.2. WCT Analysis

This section details the design and analysis of the wake control system (WCT). As the system as a whole strives to be as space efficient as possible, WCT is critical. In order to allow for turbines to be spaced more closely together, the wake must recover fast enough. The idea behind the wake control system is to use the effects of high-lift devices (HLDs) on the flow, namely the trailing tip vortices, which direct the flow in the direction opposite of the lift it creates.

Since the turbine is installed close to the ground, upwards is the best place to move the wake. This means using HLD(s) to generate downforce since the lift is directed downwards. To quantify the effects of HLD on the wake, a simple potential flow model was used.

5.2.1. Theoretical Background

The analysis of the wake behaviour undertook the following assumptions:

WCT-ASS-01: Wake moves with the free-stream velocity
WCT-ASS-02: The effects of viscosity in the wake can be neglected
WCT-ASS-03: The effects of turbulence in the wake can be neglected
WCT-ASS-04: The effects of compressibility in the wake can be neglected
WCT-ASS-05: The flow within the wake is irrotational
WCT-ASS-06: Effects of the individual HLDs, which constitute the WCT can be accounted for by placing constant circulation vortices at the location of their wing tips
WCT-ASS-07: Interactions of the flow in the wake are governed primarily by the velocity components perpendicular to the free-stream velocity.

Assumptions **WCT-ASS-02**, **WCT-ASS-03**, **WCT-ASS-04**, and **WCT-ASS-05** allow for use of potential flow

theory. Along with assumption **WCT-ASS-06**, this allows for modelling effect of the HLDs as simple vortices with constant circulation, the effects of which need to only be considered in two dimensions perpendicular to the free-stream velocity, as per **WCT-ASS-07**. Lastly, with **WCT-ASS-01**, the location of the wake at any point in time in the direction of the free-stream velocity can be determined.

Potential flow is a model used to describe the incompressible, inviscid, irrotational flow. A circulation source (such as a tip vortex) induces a velocity as prescribed by Equation 5.22, where the total circulation of the source is $\vec{\Gamma}$ and the relative position from it is $\vec{r}$.

$$\vec{v} = \frac{\vec{\Gamma}}{2\pi||\vec{r}||^2} \times \vec{r} \tag{5.22}$$

Lift produced by an HLD per unit length is related to the magnitude of circulation by equation Equation 5.23, where L' is lifted per unit length, v_∞ is the free stream velocity, ρ_∞ the free stream density, C_L is the lift coefficient per unit area, and c is the chord length.

$$\left|\left|\vec{\Gamma}\right|\right| = \frac{L'}{v_\infty \rho_\infty} = \frac{1}{2} v_\infty C_L c \tag{5.23}$$

To simulate the effect of multiple vortices on the wake, the domain of the wake was meshed with a grid that had uniform vertical and horizontal spacing. The velocity at a point was computed as a result of the influence of individual vorticity contribution as given by Equation 5.24, where the index n is the index of the individual vortex and 2D flow in the y-z plane was assumed.

$$\vec{v}(\vec{r}) = \sum_{n=1}^{N} \left(\frac{\Gamma_n}{2\pi||\vec{r}_n - \vec{r}||^2} \begin{bmatrix} z - z_n \\ y_n - y \end{bmatrix} \right) \tag{5.24}$$

For each point on the mesh, the instantaneous velocity $\vec{v}$ was computed based on Equation 5.22, which was then used to compute its position at the next time step, according to the explicit Euler method presented in Equation 5.25. This method is unstable but approaches the real solution as the time step Δt approaches zero.

$$\vec{r}(t + \Delta t) = \vec{r}(t) + \Delta t \cdot \vec{v}(\vec{r}(t))) \tag{5.25}$$

After the method was proved to converge for every point which does not start at the centre of a vortex, the method was expanded to every point in the mesh. The simulation was then tweaked to run until every point has left the initial simulated domain. The width of the domain was given a fixed width of 280 m, with a line of symmetry 30 m below the bottom boundary. The symmetry line meant that for every vortex, there was one of equal and opposite strength put on the other side of the symmetry line to simulate the ground effect and condition of tangent flow to the ground.

An initial flow-field for a setup with 6 vortices (and 6 which are placed on the other side of the symmetry plane) is shown in Figure 5.16a. An unrelated example of how a flow field looked at the moment when all points had exited the initial wake region can be seen in Figure 5.16b.

5.2.2. Verification of the Model

For verification of the model, a simple case, with a central vortex was considered. The strength of the vortex was given as $\Gamma = 100\,\mathrm{m^2\,s^{-1}}$, positioned in the middle of simulation domain at point (3,3). A point at a distance of 1 m was placed next to it and the simulation was then started. Calculations were halted once the accumulated errors made the point move outside of the simulation domain of $[3,5] \times [3,5]$, meaning that magnitude of the distance reached at least 100%.

This simulation was repeated for time steps of size $\Delta t = 0.001\,\mathrm{s}$, $0.002\,\mathrm{s}$, $0.004\,\mathrm{s}$, $0.008\,\mathrm{s}$, and $0.016\,\mathrm{s}$. The path taken by the particle can be seen in Figure 5.17. The exact solution is drawn as a blue line, which makes a circle, and the simulated positions are shown as the red line, which quickly starts to deviate away

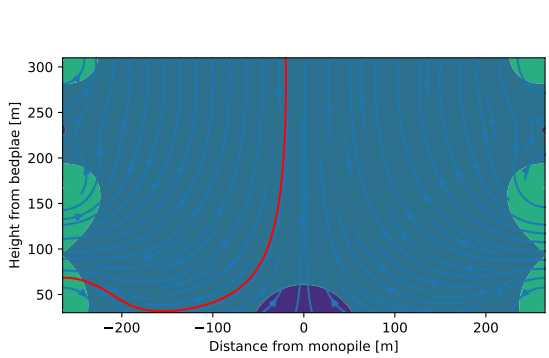

(a) *An example of an initial flow field with a streamline shown in red*

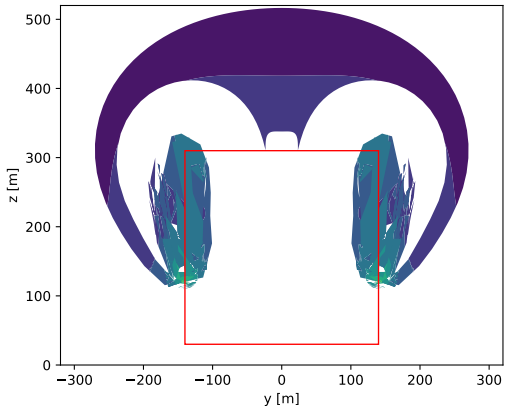

(b) *An example of a final flow field*

Figure 5.16: *Example of a flow field of a simulation and end result of wake propagation*

from the exact solution. The number of steps for the deviation to reach a value of 100% is presented on a double logarithmic plot in Figure 5.18.

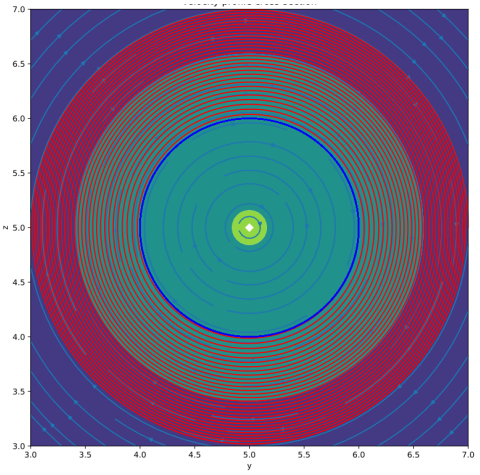

(a) *Propagation of position error with time step of* $\Delta t = 0.001\,\mathrm{s}$

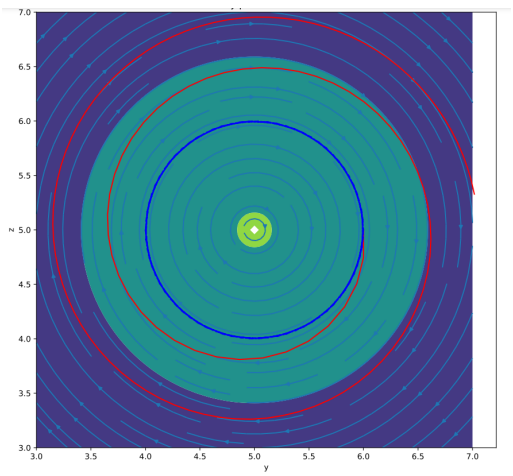

(b) *Propagation of position error with time step of* $\Delta t = 0.016\,\mathrm{s}$

Figure 5.17: *Propagation of positional error with tow different time steps (red) and exact solution (blue)*

The number of time steps taken for the error to exceed 100% was found to be 126, 463, 1851, 7402, and 29609 respectively. As the time step halved, the number of steps increased by a constant factor of $10^{0.6}$. From this, it is concluded that the error approaches zero as the time step Δt approaches zero.

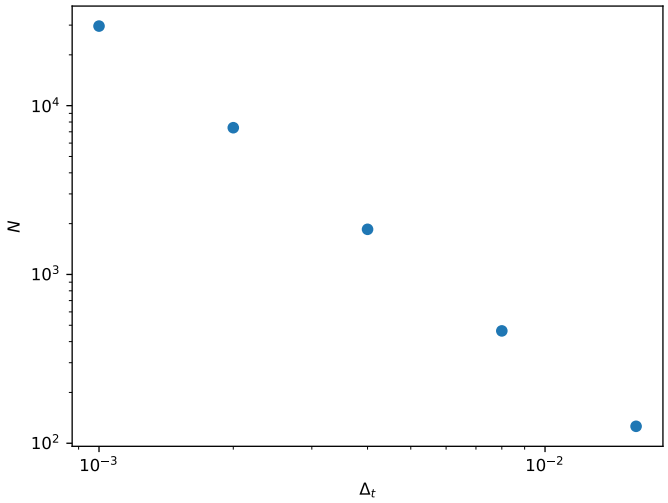

Figure 5.18: *Number of steps for the error to exceed 100% plotted against the size of time step Δt*

The validation plan so far is to compare the model to any test data obtained during the later stages of design, as well as to compare the results to other validated models once they become viable to use (such as ANSYS or OpenFlow).

5.2.3. Analysis of Effects on Energy Density

For the design of the WCT, there are some considerations about the system itself and some which come as a consequence of its interfacing with other subsystems. With regard to the former, the system's main purpose is the re-energization of the wake by means of using circulation produced as a result of lift force generated downwards. This follows based on Equation 5.23.

For analysis of the WCT, circulation Γ had to be determined. According to Equation 5.23, it can be determined based on free stream velocity v_∞, section lift coefficient C_L, and chord c. For the value of the free stream velocity v_∞, the value of the turbine's rated wind speed of $11\,\mathrm{m\,s^{-1}}$ was used when trying to determine energy density.

After talking with an MSc student, Thomas Broertjes, a $C_L = 5$ value was taken as achievable. As justification, it was given that lift coefficients for large commercial planes come to lower values when employing HLDs mainly due to the need to retract them in a single-section airfoil. Since that is not the case for the presented HLD, a cascading airfoil with three or even four sections may be employed.

$$\Gamma = \frac{1}{2} \cdot 11\,\mathrm{m\,s^{-1}} \cdot 5 \cdot c \tag{5.26}$$

For analysis, first of all, a space-filling pattern consisting of diamonds is assumed; then, in order to calculate density total energy of the turbine is divided into the area covered by a single diamond. The diagonal of this diamond is assumed to be the length where the wake is fully recovered so that there is no interference between units. Described setup can be seen better in Figure 5.19.

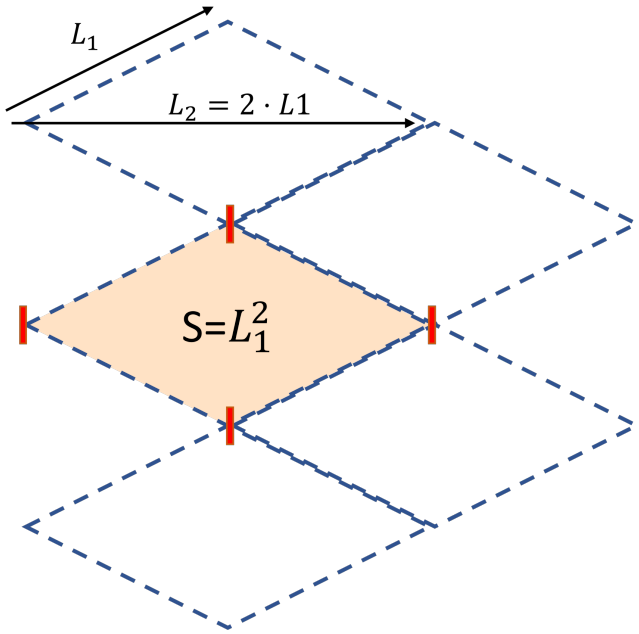

Figure 5.19: *Farm Setup*

Several setups were considered, using different placements of the HLDs, different system/wake widths, and different chord values. The values of chord length were taken to be scaled to 10% of the structural width up to a specified limit. Since the height of the system was kept constant, the metric considered was the maximum possible power produced by the system. Several chord and wing position configurations were considered. It must be noted that for the wake recovery calculations, extra width due to the monopile is considered, and no middle circulation is added to the frame under the assumption of no flow over the monopile. Therefore, it acts like a part of the HLD foil. However, this extra width from the monopile is not considered in aerodynamic loads since it is not a lift-generating surface.

The results for configurations which were considered can be seen in Figure 5.20. These designs included the following configurations for the HLD:

WCT-CFG-1: 4 blades with $c_{\max}$ = 15 m, with blades located at the heights of 310 m, 265 m, 170 m, and 125 m seen in Figure 5.20a

WCT-CFG-2: 4 blades with $c_{\max}$ = 12 m, with blades located at the heights of 310 m, 265 m, 170 m, and 125 m seen in Figure 5.20b

WCT-CFG-3: 4 blades with $c_{\max}$ = 10 m, with blades located at the heights of 310 m, 265 m, 170 m, and 125 m seen in Figure 5.20c

WCT-CFG-4: 4 blades with $c_{\max}$ = 10 m, with blades located at the heights of 310 m, 265 m, 220 m, and 170 m seen in Figure 5.20d

WCT-CFG-5: 6 blades with $c_{\max}$ = 8 m, with blades located at the heights of 310 m, 265 m, 220 m, 170 m, 125 m, and 85 m seen in Figure 5.20e

WCT-CFG-6: 7 blades with $c_{\max}$ = 6.85 m, with blades located at the heights of 310 m, 265 m, 220 m, 170 m, 125 m, 85 m, and 30 m seen in Figure 5.20f

The first three setups are to quantify the effect of the chord length with the position of the HLDs and the number of HLDs as the control variable (fixed). Between setups **WCT-CFG-3** & **WCT-CFG-4**, the number of the HLDs and the location of the HLDs are the control variables, while the locations of the HLDs are changed. **WCT-CFG-5** and **WCT-CFG-6** are the iterations on the number of the blades for fixed generated lift ($n_{blades} \cdot c_{max}$ = const) and positioning.

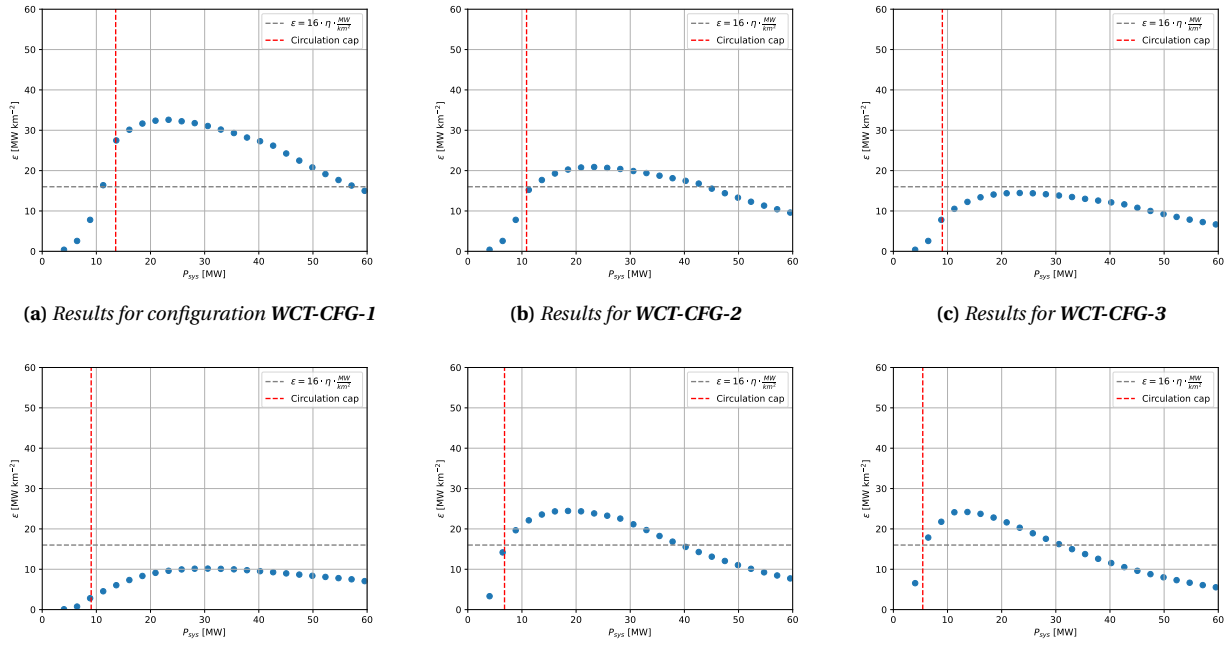

(a) *Results for configuration* ***WCT-CFG-1*** **(b)** *Results for* ***WCT-CFG-2*** **(c)** *Results for* ***WCT-CFG-3***

(d) *Results for* ***WCT-CFG-4*** **(e)** *Results for* ***WCT-CFG-5*** **(f)** *Results for* ***WCT-CFG-6***

Figure 5.20: *Energy density ϵ versus system's maximum available power P_{sys} for several configurations tested with the required minimum power density of $\epsilon = 16\,\text{MW km}^{-2}$ as a horizontal grey dashed line and point where the chord limit indicated as a vertical red line*

Based on results in Figure 5.20, along with the results of the structural and operational maintenance. The structural analysis determined it would be favourable to have a width-to-height ratio of 1:1, which corresponds to the maximum available power of around 31.7 MW in plots shown Figure 5.20. Since a bigger HLD would mean larger loads on the structure and more difficult assembly, the design **WCT-CFG-2** was chosen as the best choice given the constraints.

Considering that analysis results depend only on circulation produced by the WCT, this means that given the current assumptions, it would be possible to change both C_L and c, as long as their product is constant.

5.2.4. Analysis Assumptions, Limitations, and Errors

This section briefly touches on the assumptions made by the rest of the section, and the subsequent limitations and errors which are present in the results and conclusions presented in Subsection 5.2.3.

Assumptions made for the HLDs performance were made for the value of $C_L = 3$, which was made based on the recommendation by T. Broertjes. The choice for the maximum chord of $c = 20\,\text{m}$ is based on the fact that this is not too far off from the root chord of an Airbus A380. This means it is definitely manufacturable. While a larger wing could be produced, it makes retraction of the wing in storm conditions more difficult. Since a multi-section airfoil would be required for desired performance, it was deemed a feasible length for the HLDs chord. However, a much larger value would likely be infeasible to make.

A major assumption on which the wake analysis is based is that when all of the air originally in the area of the original wake is dispersed, a wind turbine placed at that point could operate at or at least very close to full efficiency. This is an assumption which would need to be verified either using CFD simulations or scale models.

The next assumption is that the effects of an airfoil can be modelled well with a pair of stationary vortices of

a set circulation. This is tied to the assumption of potential flow, which is deemed acceptable, considering that low speeds allow for compressibility to be neglected. Viscous effects in the wake should also be rather mild due to the large physical dimensions and consequently low-velocity gradients. On the other hand, the analysis did not take into effect the turbulence of the flow itself and the consequent Reynolds stresses. The effect of these may be significant, however hard to predict, as a very detailed model of wind at the installed location would be required.

Next, since the model used assumes potential flow, This neglects the contribution of viscous forces and dissipative effects. Some of these effects would lower the effectiveness of the WCT, as they would dissipate the energy of the vortices as they travel forward. On the other hand, there would be a positive contribution from the dissipation of momentum into the wake. This would aid re-energization by providing another mechanism of momentum transfer, other than just outside flow coming into the wake.

It is also assumed that the time in which the wake should be removed is the time it takes air to travel the distance between two turbines in a staggered grid, while at the rated wind speed. This assumption is a conservative one, as air in the wake which needs to be replaced would travel at a lower speed.

Lastly, the way in which the effect of tip vortices is modelled also does not include the contribution of the other nearby turbines, which would aid in wake mixing, since the effect of vortices produced by HLDs of other turbines would also generate a contribution to the upwash flow.

5.2.5. Design of WCT

Based on the analysis, using **WCT-CFG-2** would allow having the fewest number of HLDs with the lowest amount of circulation required to still meet the requirement **UR-01**. As such, the WCT was determined to use a design with a total circulation $\Gamma = 330\,\mathrm{m^2\,s^{-1}}$ per blade. As an alternative to the combination of the chord length of $c = 12\,\mathrm{m}$ and lift coefficient of $C_L = 5$, the same circulation may be provided by having a longer chord with $c = 20\,\mathrm{m}$ and lift coefficient of $C_L = 3$.

Based on considerations for the structure in Section 5.1, individual cells have a depth of a bit over 30 m, it would be possible to have the HLDs integrated into the structure. With the larger chord and lower lift coefficient, WCT elements would be less demanding to design and provide additional structural stiffness. As such, the proposed design for WCT is to use four HLDs with maximum values of lift coefficient $C_L = 3$ and chord lengths of $c = 20\,\mathrm{m}$.

Since the value of lift coefficient $C_L = 3$ is still rather high, this could be achieved using a two or three-element airfoil, which would be augmented using slats and flaps in order to increase its lift coefficient C_L to the desired amount.

5.2.6. Integration of WCT

The main effects of WCT on the structure are the loads it will exert on it. With the selected chord of $c = 20\,\mathrm{m}$, operating lift coefficient $C_L = 3$, and rated wind speed of $v = 11\,\mathrm{m\,s^{-1}}$, the operational loads are the downforce L per blade as per Equation 5.27, or a total downforce of about 4.98 MN. For the drag, the force is given by Equation 5.29, resulting in a total structural drag of 425 kN.

$$L = \frac{1}{2} \cdot 1.225\,\mathrm{kg\,m^{-3}} \cdot 280\,\mathrm{m} \cdot 20\,\mathrm{m} \cdot \left(11\,\mathrm{m\,s^{-1}}\right)^2 \cdot 3 = 1245.09\,\mathrm{kN} \tag{5.27}$$

$$C_D \approx \frac{{C_L}^2}{Ae\pi} + C_{D_0} \approx \frac{3^2}{\frac{280}{20} 0.8\pi} + 0.015 = 0.256 \tag{5.28}$$

$$D = \frac{1}{2} \cdot 1.225\,\mathrm{kg\,m^{-3}} \cdot 280\,\mathrm{m} \cdot 20\,\mathrm{m} \cdot \left(11\,\mathrm{m\,s^{-1}}\right)^2 \cdot 0.256 = 106.25\,\mathrm{kN} \tag{5.29}$$

While the forces during operation are very significant, storm safety is the more important case to consider. During the last 50 years, the worst wind conditions had wind gusts with speeds of up to $70\,\mathrm{m\,s^{-1}}$ as per Section 3.3. In order to reduce loading on the structure, the lift would have to be reduced, leading to a consequent reduction in drag. Without this intervention, the total experienced loads would increase by a factor of 40.

Since the proposed design of WCT is to use a multi-element airfoil integrated into the structure, along with some integrated high-lift devices (like slats and flaps), the main idea for reducing loads is to use retraction mechanism to retract HLDs into the individual airfoils, and to move the non-fixed airfoil elements into the same plane as the airflow. This would effectively reduce the lift coefficient to almost zero and the drag coefficient to only a bit more than its profile drag. The required value for the maximum allowed lift coefficient during such a storm would be $C_L = 0.074$ as per Equation 5.30. The drag caused by this would be given as Equation 5.32, meaning that the total loading during the storm would result in 1.02 MN of drag force. This is an optimistic plan, but considering that the forces here are rather small compared to the weight of shafts, rotors, and generators, an increase in the actual values for lift and drag should not be critical.

$$C_L = 3\left(\frac{11\,\mathrm{m\,s^{-1}}}{70\,\mathrm{m\,s^{-1}}}\right)^2 = 0.074 \tag{5.30}$$

$$C_D \approx \frac{{C_L}^2}{Ae\pi} + C_{D_0} \approx \frac{0.074^2}{\frac{280}{20}0.8\pi} + 0.015 = 0.0152 \tag{5.31}$$

$$D = \frac{1}{2}\cdot 1.225\,\mathrm{kg\,m^{-3}}\cdot 280\,\mathrm{m}\cdot 20\,\mathrm{m}\cdot\left(70\,\mathrm{m\,s^{-1}}\right)^2\cdot 0.0152 = 255.45\,\mathrm{kN} \tag{5.32}$$

Since the tower structure would be made six cells wide, as shown in Section 5.1, this offers an opportunity to split each HLD blade into six individual pieces. This would allow for smaller systems which would help in terms of maintenance as well as construction. With the airfoil's chord being 20 m, it would likely be thick enough to allow for the housing of some important components within the airfoil itself. It is decided to have HLD at the bottom of the rotor at each cell; since it has a 20 m chord length, it can be considered a structural element this way.

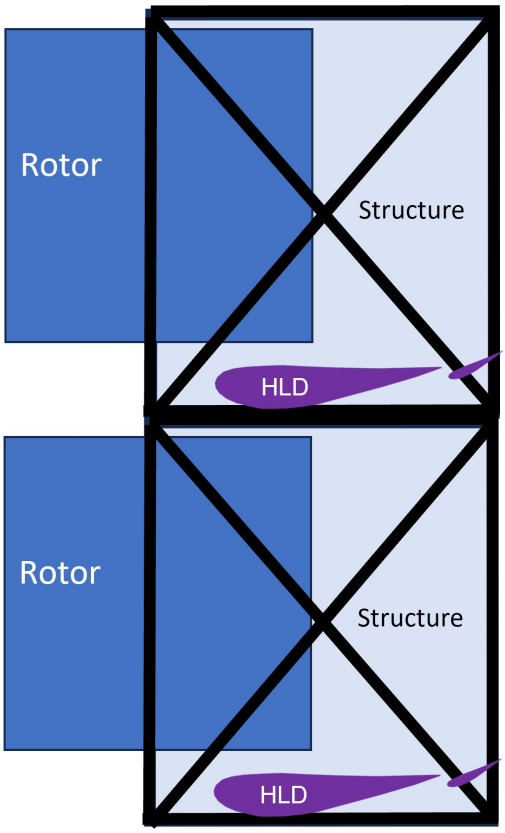

Figure 5.21: *Installation of HLD*

5.2.7. Mass of the WCT

The wings of the WCT subsystem need to withstand the aerodynamic loads while transferring them to the truss structure to which is connected. This adds another functionality apart from the aerodynamic wake performance, namely structural capabilities. With this in mind, it is important to analyse the possible failure modes of the wing and design accordingly. For the purposes of this report, the airfoil thickness will be evaluated against failure by yielding. The following assumptions were taken into consideration:

WCT-ASS-08: The wing is connected to the truss structure at the edges of each truss cell through pin connections

WCT-ASS-09: The loads will be carried exclusively by two spars, located at 25% and 75% of the chord

WCT-ASS-10: Both spars are considered to have a web height equal to half of the airfoil thickness, namely, the spars are 1.5 m high, denoted by the symbol H.

Considering the geometry of the airfoil, the bending stress introduced by the distributed drag is negligible, making the bending stress produced by lift in storm conditions the limiting case factor. Using the wind profile previously described in Section 3.4, it was determined that the maximum loading of the wing is equal to 5.5 kN/m. The maximum stress will be found at the midway point of each truss cell and will be given by Equation 5.33, where t is the thickness of the spars.

$$\sigma = \frac{Mj_{\text{safety}} \cdot y}{I} = \frac{1.7 \frac{L^* w_{\text{cell}}^2}{8} \cdot \frac{H}{2}}{\frac{1}{6} t H^3} = \frac{51}{80} \frac{L^* {w_{\text{cell}}}^2}{t H^2} \tag{5.33}$$

The spars were considered to be made out of the same material as the truss elements of the tower. Applying

the condition that the spars should not yield leads to the spars having a minimum thickness of 12.31 mm and a total spar weight of 81 t. Of course, the WCT subsystem comprises more than the structural spars, as it includes the skin of the airfoil and the HLD assembly. With this in mind, a margin of 100% was applied to the mass of the subsystem, leading to 162 t for each one out of the four wings.

5.3. RTR analysis

The goal of this section is to analyse the performance of the rotors. This will include a closer look at the relations between C_P, C_T and the tip speed ratio, creating power and shaft torque curves and calculating the expected power production. These calculations will provide necessary data for sizing the drivetrain as well as determining the attainable yaw rate.

5.3.1. Obtaining the Thrust and Power Coefficients

The analysis starts with establishing the relation of the power and thrust coefficients with the tip speed ratio (TSR). As a base, the data from a paper by Jamieson et al. is used [2]. In the process of creating power curves, it was discovered that the data does not cover a sufficiently wide TSR range. To maintain a production of 30 MW, with wind speeds exceeding 15 m s^{-1}, the TSR has to drop below 2. The data set only contains C_P and C_T information for TSR values between 2 and 6.5. Therefore, a parabola was fitted to the data. Whenever C_P or C_T information from outside the 2 to 6.5 TSR window is required, the fitted parabola is used to calculate the coefficients. The results of the fusion of the data and the fitted parabola can be seen in Figure 5.22.

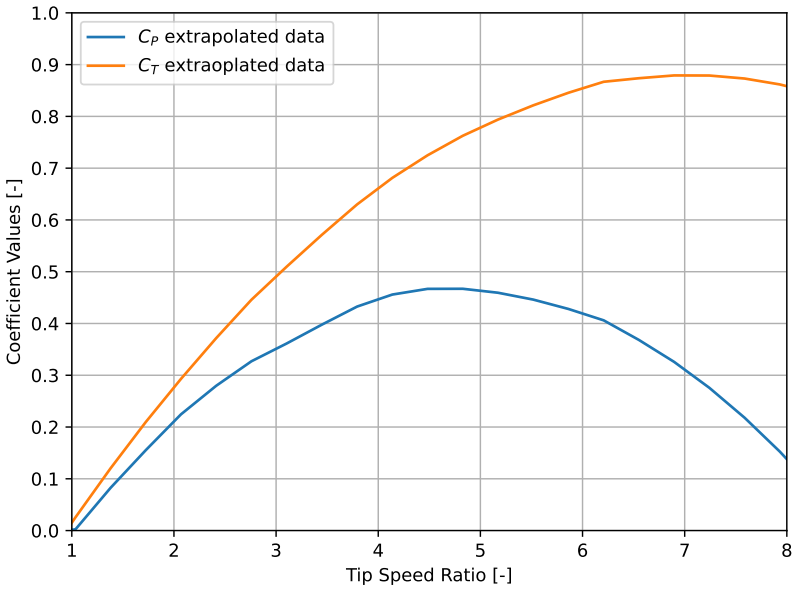

Figure 5.22: *Extrapolated power and thrust coefficients over the tip speed ration*

5.3.2. Power and Shaft Torque Curves

With access to C_P and C_T data at all the necessary TSR values available, a closer look at the turbine operation is possible. The most pertinent information pertaining to operation is the power produced, the torque on the rotor shaft and the thrust of the rotors at a given wind speed. These proprieties will influence the rest of the design and therefore need to be controlled.

In theory, the optimal design would balance out the three values. Creating such a design is beyond the scope of the project, therefore, a simpler approach was taken. The plan of action is to produce as much power as possible while under the rated speed and make the rated power above the rated speed. This is

not the optimal strategy. It causes quite high torques in the rotor shaft and misses out on potential energy production. However, it is also the easiest case to analyse and should provide an underestimate of energy production and an overestimation of shaft torque, leading to conservative performance numbers for the design.

To calculate all of the curves, the following procedure was implemented. First, check if the C_P at TSR equal 4.5 produces more than the 30 MW rated power for a given wind speed. If yes, then the TSR is reduced until rated power is achieved. With the established TSR value, C_T and thrust are calculated. Lastly, the power produced per shaft is divided by the rotational speed of the rotor to get the torque on the shaft.

The power and C_P curves can be seen in Figure 5.23a and Figure 5.23b. It is worth noting that C_P has to drop cubically with wind speed to maintain the rated power production. Such an aggressive change in C_P has a correspondingly quick change of TSR, leading to unforeseen results. The most intriguing of the outcomes is the fact that the thrust produced by the rotors peaks at the rated wind speed and falls from there. The change of TSR, C_T and thrust with wind speed can be seen in Figure 5.23c, Figure 5.23d and Figure 5.23e. The last value that important to the design is the torque on the shaft. The torque curve can be seen in Figure 5.23f. There is an important observation to be made, namely, the torque in the shaft doesn't max out at the rated wind speed, but at a wind speed of around 18.2 $\mathrm{m\,s^{-1}}$. Using the previously mentioned wind profile as depicted in Figure 3.6, the rated power production of the system is evaluated as 31.3 MW. This margin was chosen as contingency considering mechanical and electrical efficiency losses of up to 96%. This evaluation was made assuming that the top 12 m are occupied by the wake control and do not contribute to electricity production. Considering that this top region has the highest winds, this makes the estimate conservative.

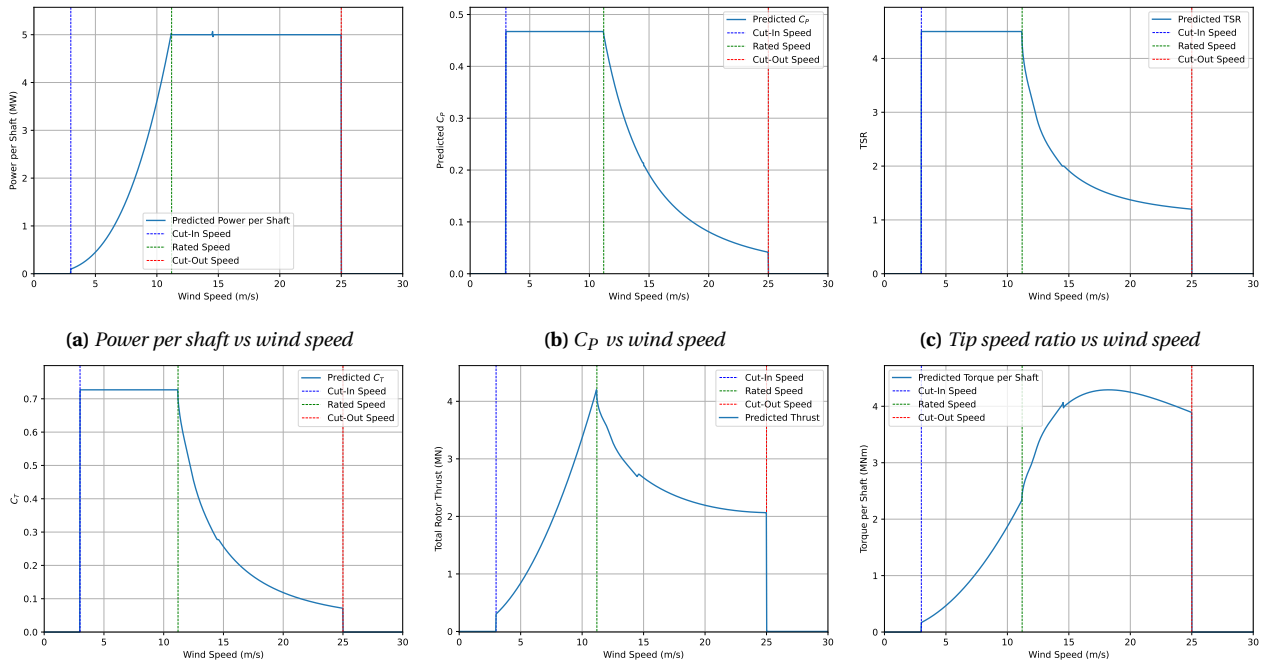

(a) *Power per shaft vs wind speed*

(b) C_P *vs wind speed*

(c) *Tip speed ratio vs wind speed*

(d) C_T *vs wind speed*

(e) *Total rotor thrust vs wind speed*

(f) *Torque per shaft vs wind speed*

5.3.3. Shaft design

The main shaft to which the blades are attached will be connected to the tower using seven equidistant locating bearings, taken as deep groove ball bearings. Through this type of bearing, the shaft will be able to transfer axial and radial loads to the truss structure, effectively fixing and unloading the shaft in the process. A sketch of the shaft, along with the dimensions of the final design, is presented in Figure 5.24a. The shafts are hollow cylinders with a diameter of 1618mm, a thickness of 24.3mm and a length of 270m. All

bearings are modelled as pin supports, restricting translation but allowing for rotation. The shaft will experience aerodynamic lateral loads and torsional loads created by the blades while also carrying the blades and struts' weight. All external and reaction forces and moments considered are presented in Figure 5.24b. The following simplifying assumptions were used:

RTR-ASS-01: All bearings carry the same axial reaction force along the z-axis

RTR-ASS-02: The bearings at the extremities of the shaft carry the same radial reaction force along the x-axis

RTR-ASS-03: The bearings between the first and last bearings carry the same radial reaction force along the x-axis

RTR-ASS-04: All rotors are loaded by the same wind speed

RTR-ASS-05: All rotors are assumed to transfer their entire loads to the shaft through the middle point between consecutive bearings

RTR-ASS-06: The arrangement of the equally phased displaced rotors leads to a constant torque along a full rotation

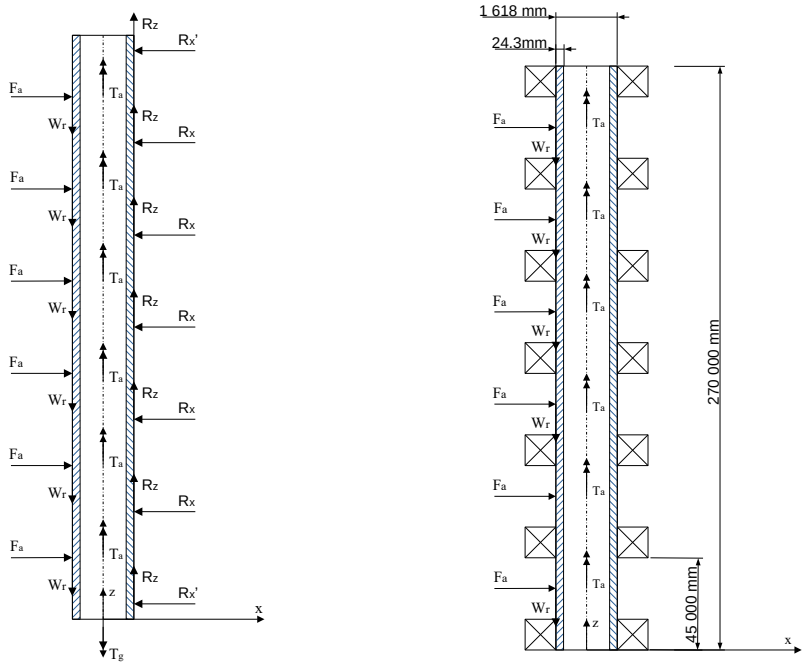

(a) *Sketch of the shaft dimensions and loading* **(b)** *Shaft FBD*

Figure 5.24: *Shaft relevant drawings*

During the shaft sizing, it was determined that the most restrictive load case is LDC2. This was no surprise, as this load case leads to the highest torque the system will experience. By imposing equilibrium of forces and moments, it is possible to determine that the vertical loading of the bearings is equal to 317 kN, while the radial loadings are 63.9 kN and 31.9 kN, respectively. These values will be used further for the sizing of the bearings. The aforementioned loads will determine the internal loading of the shaft as described in Figure 5.25.

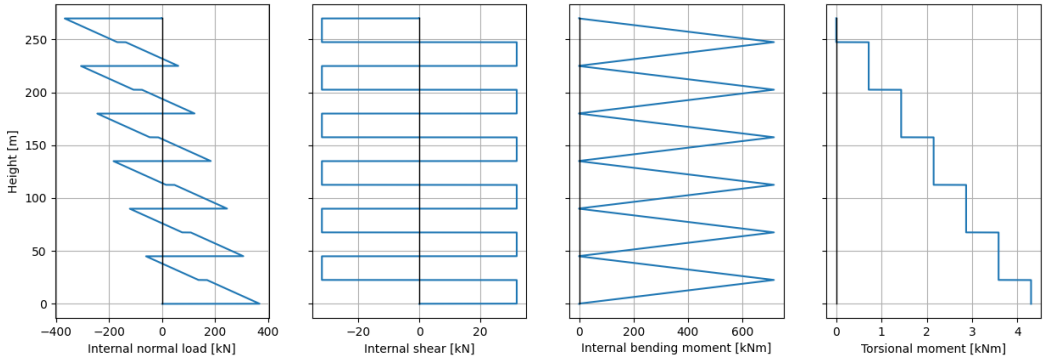

Figure 5.25: *Internal loading of the main shaft*

As the shaft length is set by the necessary rotor swept area, the only dimensions yet to be defined are the diameter and the shaft thickness. These will be accounted for in the following derivation by using the outer diameter, d_o, and the inner-to-outer diameter ratio, c_{diam}. Equation 5.34 and Equation 5.35 were used in order to calculate the normal and shear stresses within the hollow shaft. Note that the transverse shear stress given in Equation 5.35 is given for the maximum found along the shaft's cross-section.

$$\sigma_{axial} = \frac{4P}{\pi d_o^2(1-c_{\text{diam}}^2)} \qquad \sigma_{bending} = \frac{32M_{bending}}{\pi d_o^3(1-c_{\text{diam}}^4)} \tag{5.34}$$

$$\tau_{transverse,max} = \frac{8V_{\text{transverse}}}{\pi d_o^2(1-c_{\text{diam}}^2)} \qquad \tau_{torsion} = \frac{16M_{torsion}}{\pi d_o^3 * (1-c_{\text{diam}}^4)} \tag{5.35}$$

Two distinct failure modes were considered for the shaft: failure through yielding and failure through fatigue. In both cases, a safety factor of 1.3 was considered for both the loads and the performance of the material, yielding a cumulative safety factor of 1.7. For this initial calculations, the material considered was low-carbon steel, with a yield strength of 255 MPa, an ultimate tensile strength of 400 MPa, and an ideal endurance limit of 203 MPa.

Firstly, the yield strength of the material was compared to the von Mises stress of the shaft, as obtained using Equation 5.36. As long as the von Mises stress, multiplied by both safety factors, is lower than the yield stress, the shaft is considered correctly sized

$$\sigma' = \frac{1}{\sqrt{2}}\left[(\sigma_x-\sigma_y)^2+(\sigma_y-\sigma_z)^2+(\sigma_z-\sigma_x)^2+6(\tau_{xy}^2+\tau_{yz}^2+\tau_{xz}^2)\right]^{1/2} \tag{5.36}$$

Secondly, the fatigue life of the shaft must be considered, as the rotor will impart a rotation from 6 RPM to 22 RPM for a lifetime of at least 25 years. In order to account for fatigue, the modified Goodman criterion was employed, which takes into account the impacts of both mean stress and alternating stress on the life of the component. The criterion is presented in Equation 5.37. Note that if this criterion is passed, then the shaft is designed for infinite life.

$$\frac{\sigma'_a}{S_e}+\frac{\sigma'_m}{S_{ult}} \leq \frac{1}{j_{material} * j_{load}} \tag{5.37}$$

Investigating the loading of the rotating shaft, it is easy to conclude that the mean normal and shear stresses are driven only by the axial and torsional shear, respectively, as these stresses are constant across the cross-sectional area of the shaft. In the case of alternating stresses, given that the shaft rotates, each given point on the circumference of the shaft will go from experiencing positive to negative bending and transverse shear stresses. Thus, the expressions of the mean and alternating von Mises stresses are given by Equation 5.38

$$\sigma'_m = \frac{1}{\sqrt{2}}\left[2\sigma^2_{axial} + \tau^2_{torsion}\right]^{1/2} \qquad \sigma'_a = \frac{1}{\sqrt{2}}\left[2\sigma^2_{bending} + \tau^2_{transverse}\right]^{1/2} \tag{5.38}$$

It is worth mentioning that the actual endurance limit of the shaft can greatly differ from the endurance limit of its constituent material, depending on a myriad of factors. In this analysis the following effects were considered:

Surface finish: The roughness of the product's outer layer will affect the propagation of surface cracks, while other finishing processes can introduce residual stresses. Considering rolled steel, the correction factor for surface finish can be considered to be equal to 0.65, as instructed by the guidelines of the FKM [1].

Size: It has been observed that the endurance limit varies with size, possibly due to higher chances of flaws in bigger components. Yet, for thin hollow cylinders made out of steel, with a thickness lower than 40 mm, this factor can be assumed to be equal to 1 [37].

Loading: Loading a member in reverse shear or axial stress has been proven to reduce the endurance limit as more of the cross-section is subjected to full reversed stress, as compared to bending where only the outer layers are fully loaded and the loading factor is equal to 1. As the shaft is under partially reversed shear loading, it was assumed that a load factor of 0.8 would suffice [2].

Reliability: Considering that all S-N curves after which the endurance limit is empirically determined are statistical in nature, this factor accounts for the reliability of the performed fatigue tests. Thus, statistical theory using 8% standard deviation in stress and strength informs us that in order to have a reliability of 0.9999, a reliability factor of 0.702 is needed [3].

Thus, the final fatigue correction factor will be equal to around 0.36. Now, both criteria can be combined while optimising for the lowest mass, with the constraints of having a shaft with an outer diameter smaller than 2 m for ease of manufacturing and a minimum diameter ratio of 0.97 to avoid small thicknesses which can lead to buckling. During the optimisation, it was determined that the critical failure mode is fatigue. The optimised shaft has the dimensions as presented in Figure 5.24b and yielded a single shaft weight of 260 t. Using these dimensions, it was evaluated that the maximum deflection that the shaft will experience will be around 3.84 mm, located in the middle of each shaft section between bearings. This deflection is equivalent to a rotation of 0.01° at the bearings, small enough not to cause additional bearing compatibility issues. Using the SKF bearing catalogues, it is possible to further estimate the mass of each bearing to about 1 tonne per bearing, as inspired by the 618/1700 MB model [4].

[1] URL: https://www.quadco.engineering/en/know-how/material-fatigue-surface-roughness-factor.htm [cited on 18 June 2023]
[2] URL: https://roymech.org/Useful_Tables/Fatigue/FAT_Mod_factors.html [cited on 18 June 2023]
[3] URL: https://roymech.org/Useful_Tables/Fatigue/FAT_Mod_factors.html [cited on 18 June 2023]
[4] https://www.skf.com/sg/products/rolling-bearings/ball-bearings/deep-groove-ball-bearings/productid-618%2F1700%20MB [cited on 18 June 2023]

5.4. YCT Analysis

This section is concerned with the design of the yaw subsystem of the turbine. This consists of sizing the yaw bearings to withstand static and dynamic loads during the system's lifetime.

Since the turbine will have a monopile of diameter larger than 10 meters, there is a need for a yaw bearing that can fit into this arrangement and, similarly to the monopile, be able to withstand both the static loads imparted on it by the external forces and moments from the turbine. Additionally, the service life of the bearing must be sufficiently high to ensure that the yaw motion does not wear out the bearing during the system's lifetime.

A unique problem that this turbine faces is the relatively large moment arm from the centre of thrust to the base of the tower, z_{c_T}. This induces a huge tilting moment on a bearing placed at the bottom of the tower compared to traditional single HAWTs, where the centre of thrust moment arm to the base of the nacelle is only a few meters at most. For this reason, it is challenging to find slew bearings suitable for this application. Thus, two bearings are used to reduce axial and radial loads for each bearing while counteracting the thrust force at the centre of thrust to reduce the tilting moment on the lower yaw bearing. Additionally, some load-bearing capability is maintained if one of the bearings fails. The presence of two bearings rather than one also gives more room to add larger yaw drive pinions, allowing for a higher torque capacity when electrical yaw is used. The bottom bearing will be located at the tower's base, while the top bearing will be on the top of the monopile, 140 m above the bottom bearing.

The static loads considered are the axial force F_a, the radial force F_r and the tilting moment M_k. For this design, F_a is the compression force resulting from the weight of the structure and the downwards-facing lift induced by the WCT. F_r mostly consists of the thrust force resulting from the turbine, while M_k mainly consists of the moment due to this force. The structural truss solver provides loads as seen in Figure 5.26 for the right-hand side of each yaw bearing. Loads on the left-hand side are equivalent in the x and z direction but mirrored in the y direction due to symmetry.

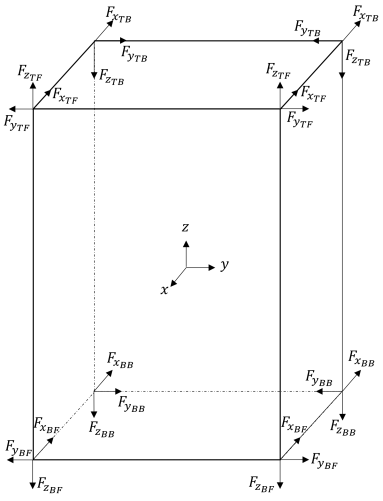

Top bearing

Front: $F_{x_{TF}} = -5.65 \times 10^6\,\text{N}$ $F_{y_{TF}} = 8.41 \times 10^6\,\text{N}$ $F_{z_{TF}} = 4.21 \times 10^6\,\text{N}$

Back: $F_{x_{TB}} = -2.96 \times 10^6\,\text{N}$ $F_{y_{TB}} = 1.01 \times 10^6\,\text{N}$ $F_{z_{TB}} = -2.47 \times 10^7\,\text{N}$

Bottom bearing

Front: $F_{x_{BF}} = -5.13 \times 10^5\,\text{N}$ $F_{y_{BF}} = 2.71 \times 10^6\,\text{N}$ $F_{z_{BF}} = -1.72 \times 10^6\,\text{N}$

Back: $F_{x_{BB}} = -9.47 \times 10^5\,\text{N}$ $F_{y_{BB}} = -7.94 \times 10^6\,\text{N}$ $F_{z_{BB}} = -3.06 \times 10^6\,\text{N}$

Figure 5.26: *Loads transmitted from tower to top and bottom bearings*

Summing these forces results in the following static loads on the top and bottom bearings. It is assumed that the upper bearing lies at the centre of thrust and so tilting moments due to thrust are negligible as they are taken by the upper bearing as radial loads.

Top bearing

$$F_a = 2 \cdot F_{z_{TF}} + 2 \cdot F_{z_{TB}} = -4.01 \times 10^4\,\text{kN} \qquad F_r = 2 \cdot F_{x_{TF}} + 2 \cdot F_{x_{TB}} = -1.72 \times 10^4\,\text{kN}$$

Bottom bearing

$$F_a = 2 \cdot F_{z_{BF}} + 2 \cdot F_{z_{BB}} = -9.56 \times 10^3 \,\text{kN} \qquad F_r = 2 \cdot F_{x_{BF}} + 2 \cdot F_{x_{BB}} = -2.92 \times 10^3 \,\text{kN}$$

Liebherr[5] provides a flowchart for determining the static suitability of a bearing to the loads. This begins with the use of a limiting load diagram which outlines the maximum combination of F_a and M_k that can be withstood. If the loading point fits within the diagram, the loading ratio F_a/F_r is checked to ensure it is above 4 for a four-point contact ball bearing. In both bearings, it can be seen that F_a is less than 4 times larger than F_r, so the bearings will have to be oversized to withstand $F_a = 4 \cdot F_r$. This is $F_a = -6.88 \times 10^4$ kN for the top bearing and $F_a = -1.17 \times 10^4$ kN for the bottom bearing.

After this step, the static load stability is checked using Equation 5.39 which compares the equivalent axial load P_0 to the static load rating C_{stat}.

$$S_0 = \frac{C_{\text{stat}}}{P_0} \qquad P_0 = K_{\text{rep}} \cdot f_1 \left(F_A + 1.93 \cdot F_R + \frac{4 \cdot M_k}{D_L} \right) \tag{5.39}$$

Where K_{rep} is the load increase factor, equal to 1.2 for wind turbine yaw bearings, f_1 is the load factor, 1.0 for a single row bearing and 1.4 for a double-row ball bearing. For these calculations, the bearing will be assumed to be double row as they can handle more loads. The static safety factor S_0 for slew bearings must be higher than 1.0. If all of these conditions are met, the bearing can be considered suitable for static loads.

The bearing must also be ensured to have a sufficient dynamic life. This is especially true for the yaw bearings as they cannot be easily replaced during the turbine's service life since they transmit all the tower forces to the monopile. Therefore it must be ensured that their longevity exceeds that of the turbine's lifetime. The dynamic analysis, also provided by Liebherr[6], is performed through the use of the Miner rule to calculate the estimated 10% probability of failure bearing service life L_{10}. For this, load levels need to be established. This specifies the number of rotations that will need to be done by the system at each load situation. For this turbine, different wind speeds result in different F_r values. F_a and M_k will remain constant in all cases. To come up with a conservative estimate, it can be assumed that the wind turbine consistently generates the largest thrust possible and therefore largest F_r which happens at the rated wind speed. Making this assumption allows the use of only one load level.

After determining the load cases, the dynamic equivalent axial loads can be calculated, assuming the use of ball bearings, using Equation 5.40.

$$P_a = {K_{rep}}^{0.66} \cdot \left(F_a + 0.63 \cdot F_r + \frac{2 \cdot M_k}{D_L} \right) \tag{5.40}$$

Since only one load level is considered, the equivalent dynamic bearing load is simply the dynamic equivalent axial load. Lastly, to calculate the bearing service life, expressed in the number of rotations, Equation 5.41 is used.

$$L_{10} = 10^6 \cdot \left(\frac{C_{dyn}}{P_a} \right)^p \tag{5.41}$$

[5] URL: https://www.liebherr.com/shared/media/components/documents/grosswaelzlager/liebherr-slewing-bearings-product-catalogue-en-metric-web.pdf [cited: 05 June 2023]

[6] URL: https://www.liebherr.com/shared/media/components/documents/grosswaelzlager/liebherr-slewing-bearings-product-catalogue-en-metric-web.pdf [cited: 05 June 2023]

Where p is the service life exponent, $p = 3$ for ball bearings. Wind changes direction by a few degrees every 30 minutes. Using a conservative assumption that the bearings will have to make a 180° rotation to align with the wind every 30 minutes implies 219000 full rotations over the lifetime, which can comfortably assure that the bearing has sufficient life.

Performing the static and dynamic loading analysis leads to the following specifications for each bearing as seen in Table 5.7. Due to the large diameter of the bearings, they will probably have to be segmented bearings. These are usually custom-made per request, and therefore, static and dynamic load ratings are not provided for them. The equations for calculating the equivalent loads might also differ for larger-diameter bearings. Therefore, a consultation with the bearing manufacturer and an analysis performed by them for the suitability of the bearings is required. Due to insufficient data about the masses of yaw bearings with such diameters and specifications, a preliminary mass estimation was made by extrapolating the mass to outer diameter relation of the Liebherr ROD-50-DA bearing lineup[7]. This leads to a combined mass of 54 tonnes for both bearings. To account for other smaller components of the yaw system, such as brakes, yaw drives, etc. a mass of 100 tonnes is budgeted for the yaw system.

Table 5.7: *Top and bottom bearing specifications*

Parameter	Top bearing	Bottom bearing
Inner diameter [m]	10	15
F_a [kN]	68800	11700
F_r [kN]	17200	2920
C_{stat} [kN]	171353.3	29123.8
Lifetime revolution req.	219000	219000
C_{dyn} [kN]	54139.9	9204.8
Estimated mass [kg]	19000	35000

Furthermore, the bearings will need to include outward-facing gears in order to be driven by the electrical yaw drives. They will also need corrosion protection to level C5-M (level of corrosion protection required for offshore environments)[8] to prevent the salinity of the water from reducing their service life.

5.5. DRT Analysis

This chapter aims to present the wind turbine's drive train design. The drive train is the mechanical system responsible for transferring power from the rotor blades to the generator. The generator transforms the mechanical power into an electrical one. The most important components of the assembly that will be presented are the brake, gearbox and generator.

Generators

The conclusion drawn in the Midterm Report was the starting point in choosing the most appropriate generators. It has been decided that a drive train with a gearbox, a doubly fed induction generator (DFIG), and a partial converter will be used.

The power required for each generator depends on several design considerations. The most important one was the reduction of the power produced from the 60 MW to 30 MW. Secondly, it was assumed that having a generator per shaft would be the most optimal solution in terms of simplicity and maintenance. It is important to keep in mind how many segments will produce the total power required for the wind turbine

[7] URL: https://www.liebherr.com/shared/media/components/documents/grosswaelzlager/liebherr-slewing-bearings-product-catalogue-en-metric-web.pdf [cited: 05 June 2023]
[8] URL: https://www.liebherr.com/shared/media/components/documents/grosswaelzlager/liebherr-slewing-bearings-product-catalogue-en-metric-web.pdf [cited: 18 June 2023]

in order to comply with the imposed requirement. As six shafts have been selected in Subsection 5.3.3, the wind turbine will be equipped with six generators, each being able to deliver roughly 5 MW each.

Brushless DFIGs can be considered the best in terms of sustainability and ease of maintenance. They have three two-phase windings which are used for handling the electrical power. The current frequency to the generator's rotor can be varied and thus, making it operable for variable rotational speeds. Brushless generators do not have sliding rings or brush arrangements. They include a separate exciter. Such devices use magnetic induction between the exciter stator, exciter rotor winding, and the rectifier assembly to supply the current to the main rotor winding[9]. Multiple advantages of using such generators can be identified. The first one is that they necessitate less maintenance. Since there are no moving parts, in particular, sliding rings and carbon brushes, there is no wear or tear. Additionally, they are less noisy due to the lack of friction. However, noise pollution was not considered an issue as the wind turbine is offshore and TSR is lower than the conventional horizontal ones. Aside from that, they are more expensive as a result of higher reliability. Moreover, they do weigh more and take up more space as they have a primary rotor and an exciter rotor. [10]

The closest version of the required generator was found in the paper of the American Society of Mechanical Engineers (ASME) [38]. It has a rated power of around 5.56 MW However, it is a direct drive one that is directly connected to the turbine shaft, which is not the case for the designed wind turbine. After further consideration, the decision is to have a generator that is part of the AMK series, provided by ABB. [11]. Nevertheless, the largest ever-built brushless generator can produce a maximal power of 500 kW [39]. Therefore, further research is advised for developing such a device that will be rated at such power.

Due to having a unique product, the wind turbine should have customised components according to the desired specifications. Nevertheless, they should be reasonably in accordance with what is available on the market. The most important characteristics of the generator are presented in Table 5.8.

Table 5.8: *DFIG characteristics [40]*

Power [MW]	5.56
Rated Speed [rpm]	1750
Voltage [V]	690-1000
Locked rotor voltage [V]	1800
Total mass [t]	16

Figure 5.27: *Double fed induction generator model*

As previously stated, six generators will be needed, one for each shaft. Each will be placed underneath the vertical structure of the turbine. They will be mounted horizontally in order to avoid any uncontrolled movement by virtue of the rotation of the shafts. This arrangement will further facilitate the maintenance work since the generators will be easily disconnected from the assembly and then transported for the onshore maintenance service. They will also be accessible via catwalks, tower stairways, or even elevators.

[9] URL: https://www.promsnab.info/catalogues/rotheerde/rothe_erde_gwl_en_13.08_v05w.pdf [cited: 04 June 2023]
[10] URL: https://yourpowerguide.com/brushless-generator/ [cited: 04 June 2023]
[11] URL: https://new.abb.com/docs/default-source/ewea-doc/generators-for-wind-turbines-standard-slip-ring-generator-series-for-doubly-fed-concept.pdf [cited: 04 June 2023]

Brake system

The brake system is another essential element of the drive train. The main use of this system is for safety, over-speed protection, and maintenance during extreme weather conditions or emergencies. This is usually the case when the wind speed exceeds safe levels and the wind turbine should be slowed down to operate within the specified wind speed range. Furthermore, the brakes can also completely stop the rotors and keep them in a stationary position while proceeding with maintenance and service activities. The torque needed for stopping a single shaft can be calculated with Equation 5.42[12]:

$$T_B = T_J + T_L - T_F \tag{5.42}$$

where T_B represents the total breaking torque, T_J - inertia torque, T_L- load torque and T_F- friction torque. T_J describes the dynamic braking, which depends on the polar moment of inertia of the entire shaft, $J = \pi \cdot \rho \cdot l \cdot \frac{d_0^4 - d^4}{32}$ and the angular acceleration of both shaft and blades. Additionally, T_L is the torque each shaft produces. The braking system must overcome this load before it can start slowing down the structure. For a conservative estimation, a safety factor of 1.3 will be assumed for this load. Friction torque stands for the friction between the breaking mechanism in the shaft. This can be assumed to be 0 since it is significantly lower than the other two terms. In order to calculate the angular acceleration of the shaft a breaking time of 10 min was considered to be reasonable [13], while the ω was taken as an input from the shaft sizing section Subsection 5.3.3. In order to calculate the polar moment of inertia of one shaft together with the blades Equation 5.43 was used.

$$J = \pi \cdot \rho \cdot l \cdot \frac{d_0^4 - d^4}{32} + m\frac{d_0^2}{4} \tag{5.43}$$

where l=280 m- total length of the shaft, d_0=1.57 m- outer diameter of the shaft, d=1.47 m- inner diameter of the shaft, m=1 t- mass of a single blade. Moreover, to simplify the calculations, it was considered that all blades are point masses at a distance $\frac{d_0}{2}$ from the rotational axis. All necessary values for picking a model for the brake are showcased in Table 5.9.

Table 5.9: *Brake system characteristics*

Mass [kg]	610
Reaction time [s]	0.2
Breaking time [s]	600
T_J [kNm]	33.24
T_L [kNm]	5577
T_F [kNm]	0
T_B [kNm]	5610.24
Rated torque [kNm]	207

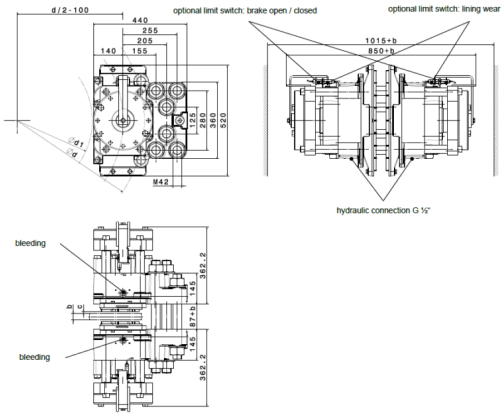

Figure 5.28: *Brake system model*

As displayed in Table 5.9, the total moment for breaking is approximately 6.61 MNm. This value is beyond the capacity of any brake on the market, and for this reason, it was decided to place the brake after the gearbox, as the gearbox can reduce the torque required for stopping the mechanism. In this matter, the breaking assembly will act on the high-speed shaft of the transmission and not on the low-speed one.

[12] URL: https://www.altraliterature.com/-/media/Files/Literature/Brand/twiflex-limited/Catalogs/p-1648-tf-a4-sections/p-1648-tf-a4_braking_calculations.ashx?fbclid=IwAR3s8CZGSesCItDDjXGUXM_PUGm7ocSEBrmm9pUMfoneN2prGVJnVh7FgBw [cited: 13 June 2023]

[13] URL: https://www.bbc.com/news/blogs-magazine-monitor-24706238 [cited: 17 June 2023]

Gearbox

The gearbox is the wind turbine element that transmits and converts the power between the driving source and the driven load. Usually, gearboxes are used for speed conversion, load distribution, mechanical isolation, and torque or directional changes. Three main reasons exist for choosing to equip the wind turbine with a gearbox. The first one is that it is not realistic to halt the main shafts considering the current technology of the braking systems. Since the torque experienced by each shaft is about 4.29 MNm and the total moment needed for stopping each sub-assembly is approximately 5.61 MNm, those values should be lowered in order to be able to be dealt with. Secondly, as the designed product is a vertical wind turbine, the rotational axis of the rotors is vertical, and the generators are placed horizontally. The consequence of this is that the rotational axis should be altered by 90 deg, which can only be achieved by a bevel gear. Lastly, this type of transmission is well-developed and is almost at its maximum efficiency point. [14] Even if the failure of a gearbox for a wind turbine is more probable than other's components, removing it improves the reliability of the entire turbine. However, the lack of such a device is reflected in a direct drive and, thus, a direct drive generator which is costly and heavier than a DFIG.

As stated, each shaft will be connected with a right-angle gear, including multiple planetary stage bearings and a bevel. The bearings are used for reducing the torque and increasing the angular velocity of the shaft, respectively. The assembly is rated to have an efficiency between 93% and 97%. [15]. Since the shafts spin at a rated speed of 28 RPM and the rated at 120 RPM, a gearbox ratio of about 43 will be needed. A single-stage planetary bearing can have a ratio that ranges from 3 : 1 to 10 : 1, but it is considered that the best combination of pinion and planet-gear size leads to ratios between 4 : 1 and 8 : 1. [16] In this matter, it was decided to include a double-stage gearhead for aiming to a ratio of 43. A reasonable product that has been found available is the ABXU 535 or ABXU 555 right-angle gearbox models provided by Rexton. Figure 5.29 depicts the technical drawing of them. [17]

Table 5.10: *Gearbox characteristics*

Low-speed shaft velocity [RPM]	28
High-speed shaft velocity [RPM]	1200
Low-speed shaft torque [kNm]	5611
High-speed shaft torque [kNm]	131
Gear ratio [-]	43
Mass [t]	4

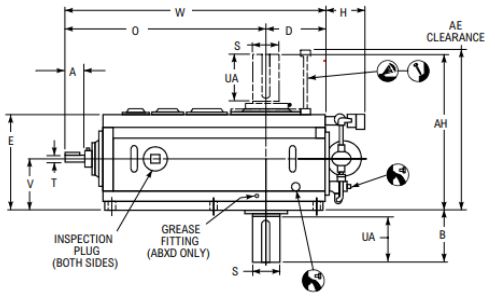

Figure 5.29: *Gearbox model*

As illustrated in Table 5.10, the gearbox should have a ratio of about 43. The component has not been found in the Rexton catalogue and that is why an existing model was updated with the required specifications, which were also dependent on other elements of the drive train. In addition, concerning the gearbox's ratio, the torque the braking system needs to counteract was lowered from 5611 kNm to only 131 kNm. In this context, the SHI 251 1750 mm brake model, provided by Hindon, was chosen for the designed wind turbine. It is a hydraulic disc brake used for holding and emergency stop applications, which is installed and developed for breaking on the output shaft of the right-angle transmission. A technical drawing of it is pictured in Figure 5.28. [18] If necessary, the connection between several parts of the drive train will be

[14] URL: https://www.engineering.com/story/the-future-of-wind-turbines-comparing-direct-drive-and-gearbox [cited: 18 June 2023]
[15] URL: https://www.meadinfo.org/2008/11/gear-efficiency-spur-helical-bevel-worm.html [cited: 18 June 2023]
[16] URL: https://www.machinedesign.com/motors-drives/article/21834575/planetary-gears-a-review-of-basic-design-criteria-and-new-options-for-sizing [cited: 18 June 2023]
[17] URL: https://www.rexnord.com [cited: 18 June 2023]
[18] URL: https://www.hindon.com/product/industrial-brakes/disc/shi-251-1750-mm/ [cited: 18 June 2023]

made via couplings.

5.6. FND Analysis

The system's foundation has the function of carrying all gravitational, aerodynamic, and tidal loads experienced by the system and transferring them into the sea bed. In previous reports, it has been decided that the best design option for the foundation is an XXL monopile. Currently, extra-large monopiles are used in water depths exceeding 30 m, having diameters that can reach 11 m at mudline and wall thicknesses of around 150 mm [19]. As of the date of this report, the heaviest ever installed monopiles lay in the Baltic Sea at Parkwind's Arcadis Ost 1 and weigh more than 2000 t. In this section, the sizing of such a monopile is performed using the design guidelines and methodology laid out in [22].

5.6.1. Monopile sizing

The monopile is supposed to carry all loads experienced by the tower. These loads are introduced through the yawing bearings, and they are of three types: transverse loads, normal loads and bending moments. Additionally, the foundation will experience a loading driven by waves for the submerged section, and driven by wind, for the afloat section. The models described in Section 3.4 will be used for these purposes. For the current design sizing process, the monopile will be considered to be capped at the mudline so that the driving length of the monopile can be evaluated independently. One unusual characteristic of the monopile to be designed is the height. Due to the large overturning moment of the turbines, a second yaw bearing has to be placed halfway up the truss structure at a height of 170 m above the water. To achieve this, a central tower will be located on top of the monopile that supports this bearing, analogous to the tower of a conventional wind turbine. This central tower is considered part of the foundation. The following assumptions have been used:

FND-ASS-01: Half of the weight of the topside mass is introduced through each bearing

FND-ASS-02: The monopile is assumed to be clamped to the seabed

FND-ASS-03: The drag coefficient under wind loading of the afloat portion of the monopile is equal to 1.2

FND-ASS-04: The drag coefficient under wave loading of the submerged portion of the monopile is equal to 1

FND-ASS-05: The inertial coefficient under wave loading of the submerged portion of the monopile is equal to 2

FND-ASS-06: The tidal loading is assumed to be applied between the SWL and the ML

FND-ASS-07: The torque created by one pair of counter-rotating rotors is assumed to be zero, leading to no torque loading of the monopile

The bearing loading can be further broken down into its constituent elements as shown in Equation 5.44 to Equation 5.49.

$$V_{B1} = D_{HLD,top} + D_{HLD,top-middle} + T_{upper-tower} \tag{5.44}$$

$$V_{B2} = D_{HLD,bottom} + D_{HLD,bottom-middle} + T_{lower-tower} \tag{5.45}$$

$$N_{B1} = L_{HLD,top} + L_{HLD,top-middle} + \frac{1}{2} mass_{topside} * g \tag{5.46}$$

$$N_{B2} = L_{HLD,bottom} + L_{HLD,bottom-middle} + \frac{1}{2} mass_{topside} * g \tag{5.47}$$

[19] URL: https://www.offshorewind.biz/2020/05/11/beyond-xxl-slim-monopiles-for-deep-water-wind-farms/ [cited on 19 June 2023]

$$M_{B1} = D_{HLD,top} * (z_{HLD,top} - z_{B1}) + D_{HLD,top-middle} * (z_{HLD,top-middle} - z_{B1}) + M_{HLD,top} + M_{HLD,top-middle} + \int_{z_{B1}}^{z_{top}} T^*_{(z)} * z\,dz \tag{5.48}$$

$$M_{B2} = D_{HLD,bottom} * (z_{HLD,bottom} - z_{B1}) + D_{HLD,bottom-middle} * (z_{HLD,bottom-middle} - z_{B1}) + M_{HLD,top} + M_{HLD,bottom-middle} + \int_{z_{B1}}^{z_{bottom}} T^*_{(z)} * z\,dz \tag{5.49}$$

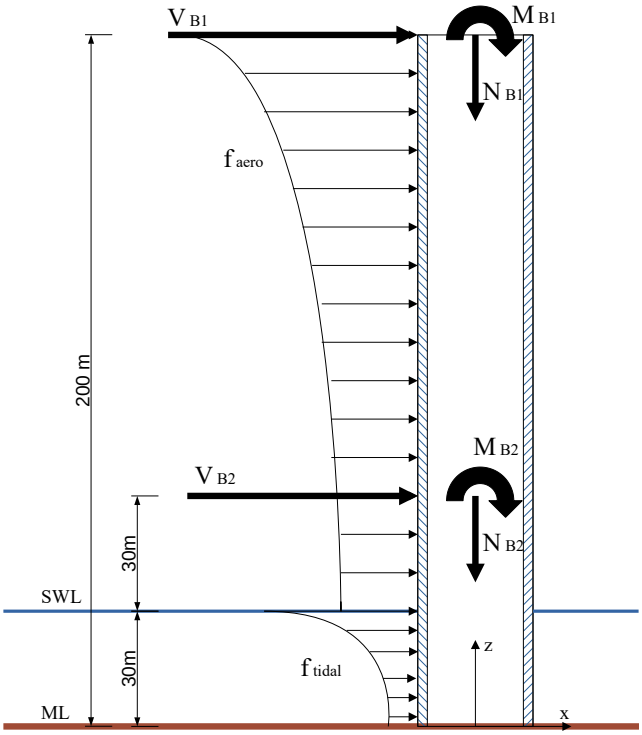

Figure 5.30: *Drawing of the loading of the monopile*

Using the previous loading, it is possible to solve for the seabed reaction forces and determine the monopile loading diagram. The loading diagram for operation at rated conditions, namely LDC1, is provided in Figure 5.31.

The stresses throughout the monopile can be calculated using the above-mentioned loading together with the stress equations described by Equation 5.34, andEquation 5.35. Moreover, Equation 5.36 can be used in order to obtain the von Mises stress.

The foundation was tested against three failure modes: failure by yielding, local buckling, and global buckling. The yielding criterion is applied in the same way it was used in Section 5.3, again using the von Mises stress with a cumulative safety factor of 1.7. The two buckling failure modes were investigated using the methodology described by K.W Hermans [22]. The local buckling criterion is described by Equation 5.50.

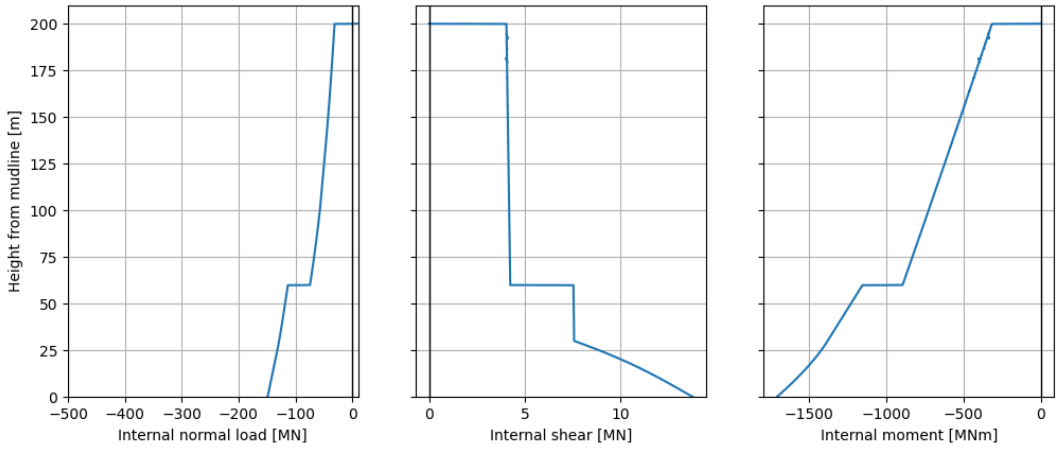

Figure 5.31: *NVM loading diagram of the monopile under LDC1*

$$\frac{N j_{\text{load}} j_{\text{material}}}{N_e} \leq 1 \qquad N_e = \frac{\pi^2 EI}{4.8L^2} \tag{5.50}$$

The global buckling criterion, also called the DNVGL standard, was developed by Det Norske Veritas and the Germanischer Lloyd [41]. This standard is a global buckling check and takes into account both normal and bending moment loading. The unity check follows Equation 5.51.

$$\frac{N j_{\text{load}}}{\kappa N_p} + \frac{\beta_m M j_{\text{load}}}{M_p} + \Delta n \leq 1 \tag{5.51}$$

The plastic resistances present in Equation 5.51 are determined using Equation 5.52

$$N_p = \frac{A_{\text{cross}} S_{\text{yield}}}{j_{\text{material}}} \qquad M_p = \frac{1}{6} d_o^3 \left[1 - \left(1 - \frac{2t}{d_o}\right)^3\right] \frac{S_{\text{yield}}}{j_{\text{material}}} \tag{5.52}$$

In addition to these elements, a third term evaluates the impact of the slenderness of the structure on global buckling. First, the reduced slenderness is calculated using the following equations:

$$\bar{\lambda} = \sqrt{\frac{N_p j_{\text{material}}}{N_e}} \qquad \phi = \frac{1}{2}[1 + 0.2(\bar{\lambda} - 0.2) + \bar{\lambda}^2] \qquad \kappa = \begin{cases} \frac{1}{\phi + \sqrt{\phi^2 - \bar{\lambda}^2}} & \text{if } \bar{\lambda} > 0.2 \\ 1 & \text{if } \bar{\lambda} \leq 0.2 \end{cases}$$

Lastly, the slenderness parameter can be calculated using

$$\Delta n = \min(0.25\kappa\bar{\lambda}, 0.1) \tag{5.53}$$

Using all three structural integrity checks, it is possible to size the monopile. As with the design of the main shaft, two design parameters are considered: the outer diameter, d_o, and the inner-to-outer diameter rato c_{diam}. The sizing of the monopile was performed with the goal of optimising for the lowest mass, keeping in

Table 5.11: *Mechanical properties of S355J alloy steel based on nominal thickness*

Thickness [mm]	3-15	16-40	40-63	63-80	80-100	100-150	150-200	200-250
Yield strength [MPa]	355	345	335	325	315	295	285	275
Tensile strength [MPa]	550	550	550	550	550	525	525	—

mind that the yield strength of the element would depend on the wall thickness, as shown in Table 5.11[20]. Note that the low-carbon manganese alloy steel S355J was chosen for the monopile as it is graded for use in marine conditions and is widespread among current monopile materials.

During the sizing of the monopile, it was discovered that the drag of the tower in storm conditions would create too high of a bending moment, leading to early global buckling. This would happen only if the tower was oriented perpendicular to the direction of the wind. In order to mitigate this, the yaw subsystem was given the additional function of yawing the structure parallel to the direction of the wind during extreme storm conditions.

During the hand optimisation procedure, it was also noticed that the best geometry for the monopile would be a cone with a varying slope and thickness. Due to manufacturing reasons though, this was deemed unfeasible, so only three steps in diameter between 11 m to 17.8 m were considered. This optimisation resulted in the following geometry, as shown in Figure 5.32. The final design will weigh 6200 t.

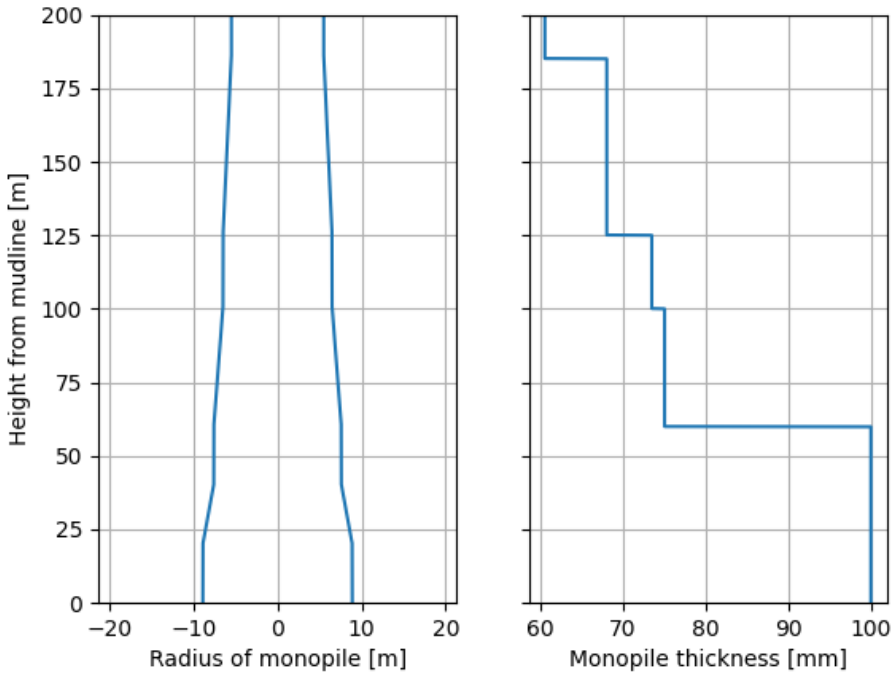

Figure 5.32: *Profile of the chosen design of the monopile*

The buckling and yielding criteria for all load cases of the chosen monopile design are presented in Figure 5.33.

[20] URL: https://www.joostdevree.nl/bouwkunde2/jpgs/staal_23_standaarden_s355_european_standard_steel.pdf [cited on 18 June 2023]

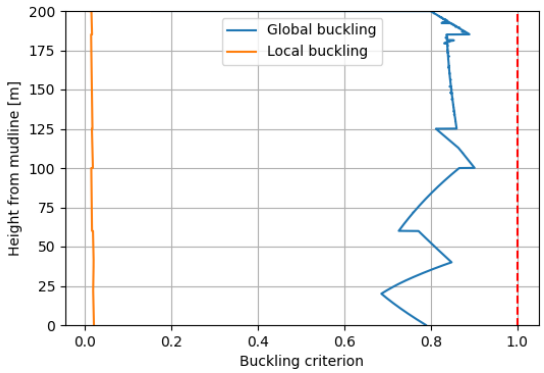

(a) *Buckling criteria for LDC1*

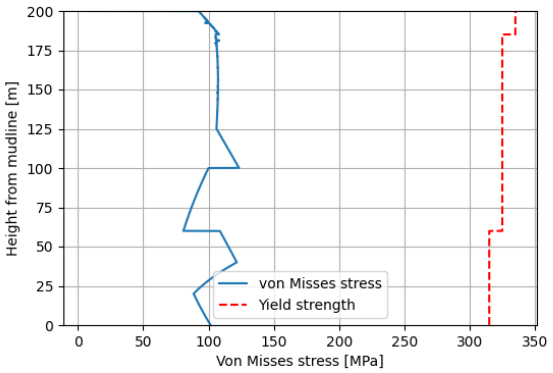

(b) *Yielding criterion for LDC1*

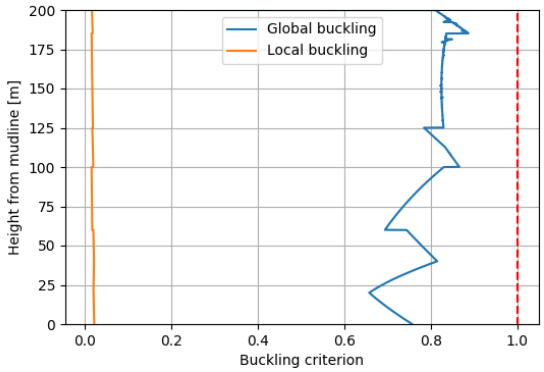

(c) *Buckling criteria for LDC2*

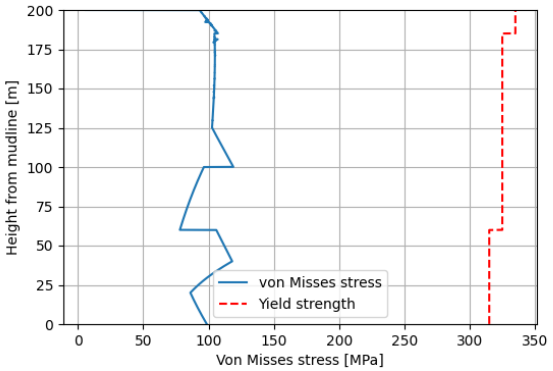

(d) *Yielding criterion for LDC2*

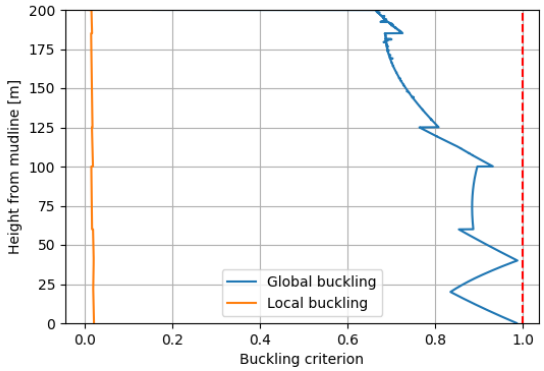

(e) *Buckling criteria for LDC3*

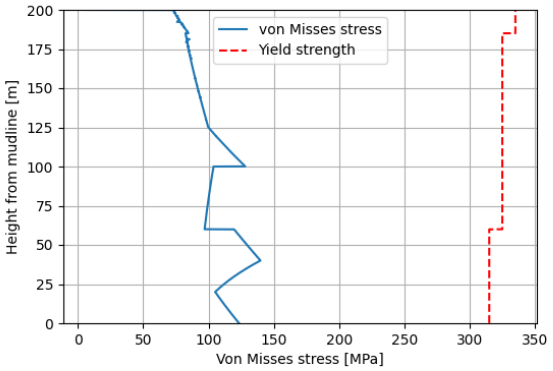

(f) *Yielding criterion for LDC3*

Figure 5.33: *Failure modes criteria of the final monopile design*

It is important to note here that the design of the driving section of the monopile, which lies under the mudline and it transfers the loads into the sea bed, was not sized in this design phase. This is because using historical data and interpolating about these points will not yield a valid value for the driving length, as the only available data was addressing small monopiles with base diameters lower than 7, most definitely yielding inaccurate results [26]. After consultations with an external expert on the topic of underground monopile foundations, Ir. Jeroen Donkers of Huisman Equipment B.V., it was determined that more information on the sea bed composition and a more advanced FEM model which can analyse dynamic loading would be required to size the driving portion of the monopile correctly. Thus, it was decided that the sizing of the driving length of the monopile will be conducted during post-DSE activities.

5.6.2. Vibrations analysis for the monopile

As predicted, the wind turbine's foundation experiences vibrations that could lead to catastrophic failures. Even though it was assumed that the vibrations from the tower are fully damped, the monopile is exposed to several loading conditions. The most important one considered is the vibrations from the tidal loads. In this subsection, the frequencies of the waves and foundation will be analysed and afterwards compared. To avoid the failure of the structure, the resonance should not be achieved, which happens when the natural frequencies of the two are equal.

Firstly, the natural frequency of the foundation will be calculated. Bakhti et al. propose a finite element investigation of offshore wind turbine's harmonics with a monopile base [42]. It particularly studies the interaction of the geometry of the basis with the soil. However, this analysis is beyond the scope of this design exercise. The core formulas will be used to obtain the desired data. The paper uses f_{FB} to define the first eigenfrequency of the fixed base, which can be calculated based on geometric characteristics. Equation 5.54 presents how the f_{FB} can be calculated [42].

$$f_{FB} = \frac{1}{2\pi} \cdot \sqrt{\frac{3 \cdot E \cdot I}{L^3 \cdot (m_{RNA} + \frac{33}{144} m_T)}} \tag{5.54}$$

where E- Young Modulus of the material from which the monopile is made, L-total monopile length, I -second moment of inertia of a hollow cylinder, which can be calculated in terms of the diameter and thickness of the body by $I = \frac{1}{8} \cdot (D_T - t_T)^3 \cdot t_T \cdot \pi$. As presented in Subsection 5.6.1, the pile has both varying thickness and diameter and not necessarily the same D/t ratio along its length. Since the diameter changes reasonably in a linear manner, D_T can be estimated by $D_T = \frac{D_{top} + D_{base}}{2}$. In contrast, t_T can be approximated by averaging the values for the different thicknesses by taking in account the right proportions. In addition, m_{RNA} is the total mass of the rotor-nacelle assembly, which can be assumed to be equal to the mass of the entire structure above the foundation, whereas the m_T represents the mass of the monopile.

The next step in the analysis is to investigate how the sea bed interacts with the steel structure of the foundation. Apart from the length above the mud line, the base should be mounted into the ground so that it does not deflect due to the several loading scenarios. The first natural frequency of the system, which includes the pile and the soil, can be computed with Equation 5.6.2 [42].

$$f_N = C_L \cdot C_R \cdot f_{FB} \tag{5.55}$$

where C_R and C_R stand for the foundation flexibility coefficients. They depend mainly on the soil's characteristics and possibly the metocean conditions, particularly winds and rains that can slightly influence the submarine land. They can be expressed by Equation 5.57 and Equation 5.56 [43].

$$C_R = 1 - \frac{1}{1 + 0.6 \cdot (\eta_R - \frac{\eta_{LR}^2}{\eta_L})} \tag{5.56}$$

$$C_L = 1 - \frac{1}{1 + 0.5 \cdot (\eta_L - \frac{\eta_{LR}^2}{\eta_R})} \tag{5.57}$$

η_L, η_R, and η_{LR} can be further determined with formulas for the stiffness of monopiles exhibiting rigid behaviour. For these calculations, it was assumed that the solid stiffness profile is a parabolic one since it is the most regular one according to Figure A.1. They can be computed with the formulas displayed in Table A.1, which can be found in Appendix A. E constitutes the Young Modules of the soil which was

approximated with 147.65 MPa considering the values and ratios from Figure A.2. Furthermore, the f_{vs} suggests the effect of the water movement on the sea bed, which, regardless, does not have a major influence on the frequency of the system combining the soil and foundation. Assuming that the diameter of the monopile ranges from 17.8 m to 11 m and thickness is between 0.1 m and 0.06 m, $f_N = 0.148 Hz$.

Lastly, the natural frequencies of the tides need to be estimated. Since waves' propagation is principally dependent on the wind spee,d which acts as an exciting force, it can be accepted that waves have a periodic motion which can be defined by amplitude, periodicity, frequency, wavelength, and phase. Schløer et al. proposed a method in which the significant wave height can be related with respect to the wind speed [44]. The approach is particularly advantageous due to the fact that a reference wind turbine of 10 MW, suggested by the Technical University of Denmark, was chosen. Presumably, it is located in the North Sea. Two different scenarios were investigated. The first one implies normal weather conditions, when all load cases are within the normal parameters, while the second one entails the ultimate limit state when extreme weather conditions are assumed. Table A.2 and Table A.3, which can are presented in Appendix A, indicate the values of wind speed and the corresponding wave height for both cases. Two expressions have been found by interpolating the values where v is the wind speed. Both Equation 5.59 and Equation 5.58 have a coefficient of determination for the regression of 0.99.

$$H_S = 0.0032\,v^2 + 0.0227\,v + 0.9242 \tag{5.58}$$

$$H_S = 0.0071\,v^2 - 0.1074\,v + 6.1445 \tag{5.59}$$

Based on the wind speed from Section 3.2, the probability of occurrence of each wind velocity has been computed. The most recent information, from 2018, has been used for a level of 50 m above sea level since it could reproduce the conditions at water level better than the data from a height of 250 m. Equation 5.60 was used in order to compute the period tides starting from their significant height [44].

$$T_S = 11.1 \cdot \sqrt{\frac{H_S}{g}} \tag{5.60}$$

where g- gravitational acceleration. Table 5.12 showcases the recorded wind speeds together with their calculated probabilities of occurrence. The speeds are rounded to the nearest integer to simplify the calculations. The period, height, and first natural frequency of waves are presented for the normal and extreme weather scenarios which have been calculated starting from Equation 5.59 and 5.58.

Table 5.12: *Recorded and probability of occurrence of each wind speed, and the height, period, and first natural frequency of the waves in IJmuiden Ver zone*

Wind speed[m/s]	Probability[%]	H_{normal}[m]	T_{normal}[s]	f_{normal}[Hz]	$H_{extreme}$[m]	$T_{extreme}$[s]	$f_{extreme}$[Hz]
1	1.85	0.95	3.45	0.29	6.04	8.71	0.11
2	3.22	0.98	3.51	0.28	5.96	8.65	0.12
3	5.14	1.02	3.58	0.28	5.89	8.60	0.12
4	5.61	1.07	3.66	0.27	5.83	8.56	0.12
5	6.90	1.12	3.75	0.27	5.79	8.52	0.12
6	7.19	1.18	3.84	0.26	5.76	8.50	0.12
7	9.17	1.24	3.95	0.25	5.74	8.49	0.12
8	9.54	1.31	4.06	0.25	5.74	8.49	0.12
9	9.89	1.39	4.17	0.24	5.75	8.50	0.12
10	8.32	1.47	4.30	0.23	5.78	8.52	0.12
11	8.07	1.56	4.43	0.23	5.82	8.55	0.12
12	5.77	1.66	4.56	0.22	5.88	8.59	0.12
13	4.73	1.76	4.70	0.21	5.95	8.64	0.12
14	4.10	1.87	4.85	0.21	6.03	8.70	0.11
15	3.29	1.98	4.99	0.20	6.13	8.78	0.11
16	2.48	2.11	5.14	0.19	6.24	8.86	0.11
17	1.50	2.23	5.30	0.19	6.37	8.94	0.11
18	1.15	2.37	5.46	0.18	6.51	9.04	0.11
19	0.78	2.51	5.62	0.18	6.67	9.15	0.11
20	0.65	2.66	5.78	0.17	6.84	9.27	0.11
21	0.35	2.81	5.94	0.17	7.02	9.39	0.11
22	0.17	2.97	6.11	0.16	7.22	9.52	0.11
23	0.10	3.14	6.28	0.16	7.43	9.66	0.10
24	0.03	3.31	6.45	0.16	7.66	9.81	0.10
25	0.02	3.49	6.62	0.15	7.90	9.96	0.10

As depicted in Table 5.12, the fundamental frequencies of the waves created for each wind velocity are presented. For the ordinary case, the natural frequencies vary from 0.29 Hz, when the wind speed is roughly 1 m/s, to 0.15 Hz when a wind of 25 m/s is experienced. Furthermore, frequencies oscillate between 0.10 Hz and 0.12 Hz in the ultimate limit case. Since the first harmonic of the fixed foundation and soil is near 0.148 Hz, it can be accepted that it is not likely for the system, including the base and waves, to achieve the resonance below 24 m/s wind speed in terms of the first eigenfrequencies. There are no data recording a higher wind speed than 24 m/s according to Section 3.2. However, the resonance is plausible only if $f_{monopile} = f_{waves} = f_{N_{nat}}$, where $f_{N_{nat}}$ is the N^{th} eigenfrequency of waves.

To conclude, the possibility of failure as a consequence of vibrations due to tidal loads is small, but not impossible. Results show that resonance is not expected during storms or normal conditions when the wind speed varies from 1 m/s to 25 m/s. The more problematic scenario is when the wind exceeds this upper limit. In general, there was no recorded value in this sense in the reference year, 2018. However, in case of very exceptional conditions such as hurricanes, cyclones, typhoons or tornadoes, the collapse of the foundation is likely. Nevertheless, the wind turbine's foundation was not designed with the primary scope of resisting vibrations but withstanding the loads. One solution that was already introduced in this design exercise for the tower of the entire assembly was to equip the wind turbine with several dampers that will reduce vibrations. In this manner, they will be dampened out and not further propagated to the structure's foundation. Therefore, various dampers will be placed along the monopile to minimise the failure risk due to the water's oscillation.

6

Final design

This chapter presents the results of previous chapters, calculations, and trade-offs. It gives an overview of relevant numbers and dimensions. The design consists of multiple cubical cells. The cells are supported by a monopile. Inside the cell are vertical-axis wind turbines with H-shaped rotors. The shafts of the rotors are attached in front of the structure. The Drive train has a gearbox with a doubly fed induction generator (DFIG) and a partial converter. The yaw system uses differential thrust or aerodynamic effects to yaw. An electrical yaw system is used as a backup. A scaled drawing can be seen in Figure 6.1. Design parameters are summarised in Table 6.1 and Table 6.2

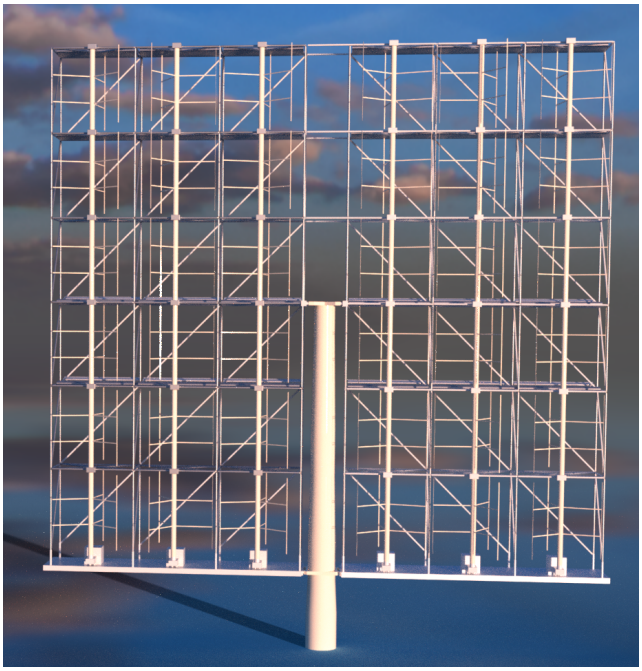

Figure 6.1: *Render of Final Design*

TWR Design

The tower is a large truss structure, consisting of repeating cubes. The truss structure is 140 m wide on each side of the central monopile, leading to a total width of 290 m. The height and depth of the truss are 280 m and 33.6 m respectively. The mass of the truss structure, including bedplates for the generator is 2767 t. The truss elements are made out of medium-carbon steel, and optimized for structural mass. The elements are all between 0.3 m to 2 m in diameter. To protect the structure from corrosion, multiple layers of white organic solvent-based paint will be applied to the truss structure. This is done to protect the structure from the harsh environment and reduce its capability of absorbing heat from the sun. To protect the turbine from lightning, a lightning protection system is installed on the structure.

WCT Design

The wake control system consists of four wing blades, which are each split into six equal sections, integrated into individual tower cells. Individual sections are two-element airfoils, which can move the second segment in order to drop their lift coefficient below $C_L \leq 0.074$ in case of storms but can reach a lift coefficient of up to $C_L = 3$ when fully deployed during operation. When operating, their drag coefficient is almost $C_D = 0.256$, which drops to $C_D = 0.0152$ when retracted. To allow for large changes in C_L and C_D,

Kruger slats and triple-slotted flaps would be installed in one or both airfoil elements.

Wake control systems can fully recover the wake of a turbine over 2.5 km. On a staggered grid, this gives a power density of almost 20 MW km^{-2}. WCTs of subsequent turbines are expected to interfere in a constructive way and improve wake recovery even further. Most parts of the WCT are to be made of medium-carbon steel.

RTR Design
The rotor subsystem consists of six vertically oriented shafts of 270 m connected to the drivetrain at the lower extremity. The profile of the low carbon steel shaft is of a hollow cylinder with a diameter of 1.6 m and a wall thickness of 24.3 m. All shafts are supported by the tower through seven equidistant deep groove ball bearings. Attached to each shaft are six H-type rotors of height 45 m and a diameter of 46.7 m. All rotors attached to the same shaft are equally phased displaced in order to smooth the torque fluctuations. The blades are supported by simple circular profile struts. All blades have the airfoil profile of the DU17DBD25.

YCT Design
The yaw control subsystem consists of two slewing bearings of diameter 10 and 15 meters attached to the monopile and tower at 170 m and 30 m above sea level respectively. The yawing mechanism uses an on-off differential thrust controller to yaw during operational conditions. Yaw breaks are included to fix the tower during the non-yawing time. Additionally, the subsystem includes an electrical yawing system with yaw drives at a rated torque of 800 kNm for yawing during storms, wind speeds below cut-in speed, and cable disentanglement.

DRT Design
The drive train is a standard one including a generator, gearbox, brake, and several couplings. Since there will be six shafts in total and the power requirement is set to 30 MW, each segment needs to produce 5 MW. The chosen brushless generator is part of the AMK series, provided by ABB. It should have a rated power of around 5.56 MW and a total mass of 16 t. The gearbox, manufactured by Rexton, is right-angled. It should have a conversion ratio of 43 weighting roughly 4 t. The 610 kg break is placed after the gearbox. It is produced by Hindon and produces a break torque of 207 kNm.

FND Design
The foundation consists of a variable diameter and thickness monopile that spans to 170 m above sea level and is 200 m long from the mud line. Due to corrosion risks, the monopile has been manufactured using S355J marine-grade steel and primed with anti-corrosive paint. The tower is connected to the monopile using two slewed bearings, through which all topside loads are transferred. Due to this reason, the monopile starts from a diameter of 11 m and thickness of 60 mm and gets to a diameter of 17.8 m and a thickness of 100 mm.

OCT Design
Fifteen different sensors are installed on the structure to collect data to develop models and synchronize the digital twin of the structure for predictive maintenance. The most prominent of these sensors are an anemometer, wind vane, and wind gust sensor to measure wind characteristics during the operations, which will be placed per cell (midpoint of edges) of the structure to provide enough spatial resolution. Accelerometers and strain gauges are utilized mostly to pair the data from the wind and system response to improve the prediction algorithm and pair weather conditions with possible failures. This way, shortly after operations start, exact loadings of the truss elements due to extreme weather conditions will be determined. They have been placed on the connectors of the HLD and truss structure. Also, they have been installed on the other moving systems, such as RTR, to detect any misalignments of the shafts from the

frequency spectrum change. Also, sensors such as acoustic sensors and ACFM will be utilised for error detection due to the working principle of these sensors as they can detect surface-level cracks in structures. Additionally, oil sensors will be placed on the bearings and generators to detect oil conditions such that the condition of these parts will be monitored. All the data generated by these sensors will be collected by SCADA.

PCT Design

The rotor airfoil was chosen so that the turbine will be stall regulated, meaning that the maximum rotation rate can be enforced through dynamic stall at a certain wind speed. This assures that the rotor does not go over its rotation limit and that the power electronics are not overcharged by the excess produced power. Torque control is used in order to obtain maximum efficiency before reaching the rated wind speed. This is done by varying the synchronous speed of the generator through the interface of the DC-DC bus within the partial converter. An Optimum Torque Controller was chosen together with a Maximum Power Point Tracking algorithm. Hydraulic brakes were employed in case of sudden power halting during operations.

Table 6.1: *Key parameters for the MR-TBD design*

Parameter	Unit	Value
Power rating	MW	31.3
Power density	$W m^{-2}$	20
Turbine class	—	IEC class I
Control		Variable speed
Cut-in wind speed	$m s^{-1}$	3
Rated wind speed	$m s^{-1}$	11.2
Cut-out wind speed	$m s^{-1}$	25
Design TSR	—	4.5
Rotor diameter	m	46.7
Rotor height	m	45
Airfoil series	—	DU17DBD25
Number of rotors	—	36
Number of shafts	—	6
Turbine height	m	310
Turbine width	m	295
Cell dimensions	m	46.67 X 46.67 X 33.6
truss thickness ratio	-	0.01
Drivetrain	—	Geared
Gearbox	—	Angular & Planetary
Generator	—	Brushless DFIG
Wake control	—	Adjustable HLD
Wing chord	m	20
Wing span	m	280

Table 6.2: *Weights of all sized subsystems*

Element	Mass [tn]
Rotor	1717
Main shaft	260 X6
Blades	3.2 X6
Bearings	1 X42
Tower	2767
Truss	2455
Bedplate	52 X6
Yaw control	100
Bearings	54
Drivetrain	46
Wake control	648
Wing	81 X4
HLD	81 X4
Drivetrain	150
Gearbox	4 X6
Break	0.6 X6
Generator	16 X6
Converter	4 X6
Miscellaneous	0.4 X6
Monopile	6200
Total	11582

7

Production, operation and logistics

7.1. Production plan

Now that the design has been chosen and the materials for the various components have been decided, the production can take shape. As the project will be deployed in the North Sea next to the Netherlands, the location of where components are manufactured is an important parameter to keep in mind. This section is divided into a description of the production and manufacturing of all the components of MR-TBD, followed by a description of the assembly process.

Monopile

The monopile consists of 3 main structures: a large hollow cylinder made of low carbon steel, the yaw bearings/transition pieces through which loads are transferred to the monopile and an underground foundation made from concrete. It is broken up by the lowest yaw bearing, and the bearings themselves as part of the yaw control subsystem (YCT).

The monopile itself must thus be manufactured as two separate cylinders of varying thickness and diameter, following Figure 5.32. As described by Anandavijayan and Brennan, monopiles in the offshore wind industry are constructed by bending metal sheets into cylindrical 'cans', usually by three-point or roll bending, followed by welding them into place before tack welding and circumferential welding the cans together [45]. This same process will be used to create the monopiles for the MR TBD design, as it is a mature and trusted technology in the industry. The processing time depends on the size of the monopile (as well as the production interval decided by the manufacturer).

Monopiles require large factories to be manufactured. However, the Netherlands is home to various companies that have the capabilities to produce them. Of particular interest is Sif offshore foundations, who possess a monopile manufacturing plant in Roermond and are also building a site in Rotterdam [1]. This is beneficial for the construction as Rotterdam possesses large dry docks and is near the proposed implementation site of the project.

The bearings in the monopile must allow for free yaw rotation, support and transport the complete loading from the rest of the tower into the monopile, and be connected to the electrical yawing system. For this, the bearings must be manufactured accurately, as any imperfections or decrease in quality may cause significant load transfer or vibration issues. The bearings will be mainly made from low alloy steel for their casing in combination with various other materials and lubricants as they are complex parts. They will also be sensitive to corrosion, so corrosion prevention methods (mainly to reach c5m protection level Section 5.4) will be used to keep them clean, as well as keeping them as far from the saltwater environment as possible i.e. protective outer layers.

Due to how crucial the bearings are to load transfer and how they will constantly be under gravitational loading of the rest of the tower, the maintenance required must be minimal, as the replacement of the bearings would require the entire tower section to be removed or propped up in order to operate on it. The production will be handed off to wind turbine and crane-bearing manufacturing companies in order to assure the quality of the product. Of particular interest of these are Liebherr [2], SKF [3], and Huisman [4] as they produce products of similar size and strength to those required for the project.

[1] URL:https://windpowernl.com/2023/02/14/sif-gives-green-light-for-worlds-largest-monopile-manufacturing-plant/ [cited on 19 June 2023]
[2] URL: https://home.liebherr.com/nl/nld/home/homepage.html [cited: 20 June 2023]
[3] URL: https://www.skf.com/nl [cited: 20 June 2023]
[4] URL: https://www.huismanequipment.com/en/ [cited: 20 June 2023]

Rotor and wake control system

Both the rotors of the turbines and the wake control system mainly feature long airfoils that do not vary in profile along their lengths. However, the differences in size for both require different methods of production.

Given that the rotor blade chord and thickness are smaller than a meter, and that they are made purely from steel, they are small enough to be produced via extrusion. This method can produce constant profiles of metal but becomes more difficult for larger parts, requiring larger machinery. Thus the HLD airfoils will instead be made by metal forming processes. Similar to the monopile, the forming of the HLD profiles can be done by bending and rolling large metal sheets and welding them into the right shapes.

It is necessary for both these processes to find companies that have the correct machinery and experience for metal forming. For steel components, there are various manufacturers in the Netherlands that have manufacturing plants capable of creating the airfoils necessary. The most advantageous of these are ThyssenKrupp [5] and Tata Steel [6] for their manufacturing plant locations near Rotterdam.

Finally, the rotors also require bearings and shafts as part of the turbines. The shafts will be planned for in the subsection discussing the truss structure while the bearings are a more complex design. As mentioned in Figure 5.1, there may be vibration issues in the truss structure. One of the potential solutions is integrating dampers into the mounting brackets and combining these with the bearings of each rotor shaft. This would result in a more complex design that would require more development and more complex manufacturing. However, for basic bearings, there are various companies that specialise in their production, in particular SKF and Huisman and Liebherr.

Drivetrain

The drivetrain has been analyzed and broken down into a series of components. The following table summarises the most likely manufacturers based on their manufacturing abilities and specialisations for each of the component categories (except for the rotor shafts which will be explained in the truss section)

Table 7.1: *Drivetrain manufacturing*

Component	Possible Manufacturers
Generator	ABB ltd
Gearbox	Rexnord
Brake	Hindon

Complex components

Given that the project encompasses a large and complex system, there are many parts that have complex sub-components and require specialised knowledge and tools to produce, beyond the processes listed earlier. Of particular importance are the electrical connections, electrical yaw motor, and specialised sensors that cover the structure. Each of these components is complex enough that describing their manufacturing is not relevant to this project. Instead, the relevant manufacturers are listed in Table 7.2 below.

Table 7.2: *Component manufacturing*

Component	Possible Manufacturers
Electrical connections/cabling	Tennet (also handles the connection to the electrical grid)
Electrical yaw motor	Liebherr
Sensors	Industry specialists

[5] URL: https://www.thyssenkrupp-steel.com/en/ [cited: 20 June 2023]
[6] URL: https://www.tatasteeleurope.com/nl/home [cited: 20 June 2023]

It must be noted that there are various types of sensors so no single manufacturer was chosen.

Truss and tower structure
The truss structure as well as the rotor shafts are made from medium alloy carbon steel specifically AISI 1040 and are both series of metal hollow cylinders that are sized for the loading that they must withstand. They comprise a variety of thicknesses and radii. The truss beams all have radii between 150mm and 1m, thicknesses ranging from 15mm to 100mm, and a length between 34m and 70m while the shafts all have a radius of 809mm thickness of 24.3mm and a length of 270m. Given that all of these components have simple circular cross sections and are structural components, hot rolling the components is the chosen method of manufacturing.

The tower contains one final structural component: the base plate on which the drivetrain rests. This is a large plate that must transfer the loads to the appropriate beams and the tower. Due to its multiple points of loading, as well as the differences in geometry, it has different material requirements. High-carbon steel is used as its material.

Due to the large size of the members, the cylinders and the baseplate will all be manufactured from multiple smaller members joined together during assembly. This benefits the shafts by making them easier and cheaper to replace in case of faults. The same effect applies to the beams and the baseplate, although more care must be taken due to their structural importance. The manufacturing of such large shafts requires the machinery and experience of large steel manufacturers. Again, the most advantageous of these are ThyssenKrupp and Tata Steel.

Assembly
Traditional wind turbines are tall with a small base. Transporting them upright in one piece is difficult. In contrast, the truss structure of the MR-TBD design has a wide and deep base, which is capable of carrying all exerted loads. It is therefore well suited to be transported in a single piece, which then only has to be lifted and installed onto the monopile. This saves money by avoiding the high cost of assembling the turbine at sea with little infrastructure, and unstable and dangerous conditions. It also minimizes the amount of time at sea as well as the vessels needed for the process since the structure can simply be towed and connected to the foundation.

Thus the assembly of the structure should be completed onshore. The most suitable location to assemble it is a shipyard or drydock.

The shipyard must be large enough to fit the whole structure, so it must be at least 280m long and 40m wide. In addition to this, it must be near the Ijmuiden installation site and must provide easy access to it without obstructions along the way to the site. Also, the transportation of materials and components must be facilitated and the travel distance minimized for both time and emissions from transport.

Thus the Damen Verolme Rotterdam shipping yard was chosen. It possesses multiple berths and a drydock more than 300m long that can be utilized to construct the turbine and is less than 10km from the city of Rotterdam itself as well as most of the manufacturing plants in the area. The Yard is also under 100km from the installation leading to rapid transport of the construction to be possible. Finally, it has multiple berths that can be used for assembly, meaning that multiple structures can be built at once, hastening the installation time of wind farms as a whole as well as individual systems.

7.2. Reliability, Availability, Maintainability, and Safety
This section discusses the reliability, availability, maintainability, and safety of the system. This analysis is mainly based on data collected in reports by Carroll et al. [3]. The data in these reports concert traditional HAWTs. This data is then modified based on the changes made by the system's design. Data on offshore wind turbines are seldom available and often onshore wind turbine data must be adapted for use in these

data sets.

Reliability

The reliability of the system is first examined on a subsystem and component level. The failure rates for different components with regard to unscheduled maintenance are presented in Table 7.3. The failure rates are based on data for events requiring a major replacement, major repair, minor repair, or cases where no cost data was available. The adjusted rates are presented in Table 7.4, which includes changes explained in the following paragraphs.

Major replacement means that a heavy lift vessel (HLV) was needed to carry out the repair. Using HLVs means large expenses and they are not always available immediately, meaning more downtime. For both major and minor repairs, a crew transfer vessel (CTV) was considered. These vessels nowadays have a carrying capacity of between 1 t and up to 30 t [7].

Table 7.3: *Base failure rates from [3]*

Component	Major Replacement	Major Repair	Minor Repair	Unknown	Total
Pitch/Hydraulic	0.001	0.179	0.824	0.072	1.076
Others	0.001	0.042	0.812	0.150	1.005
Generator	0.095	0.321	0.485	0.098	0.999
Gearbox	0.154	0.038	0.395	0.046	0.633
Blades	0.001	0.010	0.456	0.053	0.520
Oil and Coolant	0.000	0.006	0.407	0.058	0.471
Electrical components	0.002	0.016	0.358	0.059	0.435
Circuit breaker	0.002	0.054	0.326	0.048	0.430
Control	0.001	0.054	0.355	0.018	0.428
Safety	0.000	0.004	0.373	0.015	0.392
Sensors	0.000	0.070	0.247	0.029	0.346
Pumps and motors	0.000	0.043	0.278	0.025	0.346
Shaft hub	0.001	0.038	0.182	0.014	0.235
Heaters/coolers	0.000	0.007	0.190	0.016	0.213
Yaw system	0.001	0.006	0.162	0.020	0.189
Tower and foundation	0.000	0.089	0.092	0.004	0.185
Power supply and converter	0.005	0.081	0.076	0.018	0.180
Service items	0.000	0.001	0.108	0.016	0.125
Transformer	0.001	0.003	0.052	0.009	0.065
Total	0.265	1.062	6.178	0.768	8.273

The system aims to reduce maintenance by reducing both the rate at which components fail, as well as the material and transport costs of maintenance. The system uses DFIGs with 3-stage gearboxes. These two components commonly become the main sources of downtime [4].

In the case of unscheduled maintenance, the most common cause of failure of DFIGs is the failure of the slip ring, which is responsible in 31.1 % of cases [3]. Because the MR-TBD system proposes the use of a brushless DFIG, this source of failure would be eliminated due to the lack of slip rings. In brushed generators, the repair of the slip rings is a very labor-intensive process due to their location, and the general size of the generator. For this reason, it is assumed that the aforementioned 31.1 % failure rate reduction affects the major replacement and major repair categories. The failure rate for these categories is reduced such that the total failure rate of the generator is reduced by 31.1 %.

For the case of the gearbox, one of the main reasons for the need for unscheduled maintenance requiring

[7] https://www.4coffshore.com/support/an-introduction-to-crew-transfer-vessels-aid2.html [cited: 20 June 2023]

HLVs rather than CTVs is the fact that in traditional HAWTs the gearboxes are heavy and located at the top of the tower. The design of the proposed system avoids this by having a strong base plate at the height of 30 m above sea level with a built-in crane, meaning that HLVs would not be needed and CTVs could carry out these replacements. This results in quicker response times and lower transport costs.

Another thing to consider for the gearboxes used by the system is that they would experience loads that would cause much less fatigue. With six rotors per shaft, with three blades each, the torque loading would be almost constant, barring gusts. This would mean that the lifetime of gearboxes would be much longer, and the probability of mechanical failure would be much lower compared to the traditional turbines. With that in mind, the assumed reduction in overall unscheduled maintenance for gearboxes is 10 %, in the categories of major replacements and major repairs.

Another major difference between a traditional OWT and the proposed system design is the size of the tower structure. With a large truss, it can be assumed that the number of repairs and unscheduled maintenance events will be greater. To account for this, the occurrence of maintenance events was set to 200 % for the tower. The same goes for the number of sensors and consequently their failure/repair rate.

For turbine blades, the main cause for blade repair comes from corrosion of the blades due to leading edge erosion, which occurs on HAWTs when blades are moving close to the sea surface, where they hit droplets with high relative velocity. For the proposed design, this will not happen at comparable impact velocity. The main reason for this, is that the tip speed ratio of the VAWTs is 4.5, compared to typical ratios around 9.0. Since the velocity is halved, the kinetic energy of droplets hitting the blades is one-fourth the kinetic energy for an impact on a traditional HAWT. In addition to this, the blades always move parallel to the water surface. The blades stay at the same level, meaning that the higher the blades are placed, the less they will suffer from leading-edge erosion. As such, it is asserted that the number of replacements and unscheduled maintenance events will be reduced by 50 %.

Other failures in Table 7.3 come mainly from failures of hatches and doors, as well as covers and lifts. Issues with hatches and doors typically aren't a problem and do not have an impact on actual performance. Still, by not requiring a compact design of subsystems compared to traditional ones which must fit into a tight nacelle, it is asserted that the number of maintenance events in this category will be reduced by 25 %.

Since the yaw system primarily uses aerodynamic forces during its normal operation and seldom employs the use of its electric motor, it is expected that less stress will be placed on the electric motor. Combined with the large and bulky design, this means that the system would likely fail less often. As such, it is asserted that the number of failures will reduce by 30 %.

Since the system's rotors are stall-regulated machines, they will not be using a pitch system. As such, the failure rates in the Pitch/Hydraulics category are expected to decrease. The reduction in major repair rate and minor repair rate of 20 % and 10 % respectively are asserted.

Table 7.4: *Adjusted failure rates*

Component	Major Replacement	Major Repair	Minor Repair	Unknown	Total
Pitch/Hydraulic	0.001	0.179	0.824	0.072	1.076
Others	0.001	0.042	0.812	0.150	1.005
Generator	0.047	0.158	0.485	0.098	0.788
Gearbox	0.091	0.038	0.395	0.046	0.570
Blades	0.001	0.010	0.456	0.053	0.520
Oil and Coolant	0.000	0.006	0.407	0.058	0.471
Electrical components	0.002	0.016	0.358	0.059	0.435
Circuit breaker	0.002	0.054	0.326	0.048	0.430
Control	0.001	0.054	0.355	0.018	0.428
Safety	0.000	0.004	0.373	0.015	0.392
Sensors	0.000	0.140	0.494	0.029	0.663
Pumps and motors	0.000	0.043	0.278	0.025	0.346
Shaft hub	0.001	0.038	0.182	0.014	0.235
Heaters/coolers	0.000	0.007	0.190	0.016	0.213
Yaw system	0.000	0.002	0.054	0.020	0.076
Tower and foundation	0.000	0.178	0.184	0.004	0.366
Power supply and converter	0.005	0.081	0.076	0.018	0.180
Service items	0.000	0.001	0.108	0.016	0.125
Transformer	0.001	0.003	0.052	0.009	0.065
Total	0.153	1.054	6.409	0.768	8.384

Availability

For unscheduled repairs, the time required per component was computed using the scaling factors from Table 7.5, Table 7.6, Table 7.7 and repair times presented by Carroll et al. along with failure rates from Table 7.3 and Table 7.4 [3]. The results for that are presented in Table 7.8 and Table 7.9 respectively.

Table 7.5: *Weight factors to account for size and number of subsystems (first table)*

Component	Pitch/Hydraulic	Others	Generator	Gearbox	Blades	Oil and Coolant	Electrical components
Relative to VAWT	0.3	1	6	6	36	6	6

Table 7.6: *Weight factors to account for size and number of subsystems (second table)*

Component	Circuit breaker	Control	Safety	Sensors	Pumps and motors	Shaft hub	Heaters/ coolers	Yaw system
Relative to VAWT	1	3	1	10	1	6	2	5

Table 7.7: *Weight factors to account for size and number of subsystems (third table)*

Component	Tower and foundation	Power supply and converter	Service items	Transformer
Relative to VAWT	4	3	1	1

Table 7.8: *Base component repair times*

Component	Major Replacement	Major Repair	Minor Repair	Unknown	Total
Pitch/Hydraulic	0.025	3.401	7.416	1.224	12.066
Others	0.036	0.882	4.060	1.200	6.178
Generator	7.695	7.704	3.395	1.274	20.068
Gearbox	35.574	0.836	3.160	0.322	39.892
Blades	0.288	0.210	4.104	1.484	6.086
Oil and Coolant	0.000	0.108	1.628	0.174	1.910
Electrical components	0.036	0.224	1.790	0.413	2.463
Circuit breaker	0.300	1.026	1.304	0.240	2.870
Control	0.012	0.756	2.840	0.306	3.914
Safety	0.000	0.028	0.746	0.030	0.804
Sensors	0.000	0.420	1.976	0.232	2.628
Pumps and motors	0.000	0.430	1.112	0.175	1.717
Shaft hub	0.298	1.520	1.820	0.112	3.750
Heaters/coolers	0.000	0.126	0.760	0.048	0.934
Yaw system	0.049	0.120	0.810	0.180	1.159
Tower and foundation	0.000	0.178	0.460	0.024	0.662
Power supply and converter	0.285	1.134	0.532	0.180	2.131
Service items	0.000	0.000	0.756	0.144	0.900
Transformer	0.001	0.078	0.364	0.171	0.614
Total	44.599	19.181	39.033	7.933	110.746

Table 7.9: *Adjusted repair times*

Component	Major Replacement	Major Repair	Minor Repair	Unknown	Total
Pitch/Hydraulic	0.025	3.401	7.416	1.224	12.066
Others	0.036	0.882	4.060	1.200	6.178
Generator	3.807	3.792	3.395	1.274	12.268
Gearbox	21.021	0.836	3.160	0.322	25.339
Blades	0.288	0.210	4.104	1.484	6.086
Oil and Coolant	0.000	0.108	1.628	0.174	1.910
Electrical components	0.036	0.224	1.790	0.413	2.463
Circuit breaker	0.300	1.026	1.304	0.240	2.870
Control	0.012	0.756	2.840	0.306	3.914
Safety	0.000	0.028	0.746	0.030	0.804
Sensors	0.000	0.840	3.952	0.232	5.024
Pumps and motors	0.000	0.430	1.112	0.175	1.717
Shaft hub	0.298	1.520	1.820	0.112	3.750
Heaters/coolers	0.000	0.126	0.760	0.048	0.934
Yaw system	0.000	0.040	0.270	0.180	0.490
Tower and foundation	0.000	0.356	0.920	0.024	1.300
Power supply and converter	0.285	1.134	0.532	0.180	2.131
Service items	0.000	0.000	0.756	0.144	0.900
Transformer	0.001	0.078	0.364	0.171	0.614
Total	26.109	15.787	40.929	7.933	90.758

As a result of all the aforementioned modifications, the total repair time per year is reduced by 20.00 hours or 18.0 % per year. Assuming the same would follow for the scheduled maintenance, this would imply a significant increase in availability. This is not considering the fact that a failure on a single shaft would cause a 33 % reduction in power, rather than 100 % of a traditional HAWT.

Based on an article by Carroll et al., for a wind farm which is 50 km to 60 km from shore, the expected availability of a system with a DFIG would be at about 90 %. Considering the reduction in unscheduled maintenance time and assuming it carries over to scheduled as well, this would give an estimate of wind farm availability of 91.8 %.

Maintenance

Material costs were derived based on failure rates and component costs. Costs for individual component materials and transport from an article by Carroll et al. were adjusted in a manner similar to the failure rates [3]. Outcomes of this are presented in Table 7.10. The changes included:

- Generator material cost for major replacement was reduced by 30 % on account of it being a less complicated machine, as it does not need to be as compact as possible
- Gearbox material costs for all cases were reduced by 50 % on account of not requiring an external crane and not needing to be as compact as possible
- Blade costs were reduced by 70 % since the production and material costs would be lower due to the use of steel instead of composites, as well as being installable with smaller machinery.
- Yaw system costs were raised by 200 % due to the larger system scale

Table 7.10: *Adjusted component cost adapted from [3]*

Component	Major Replacement	Major Repair	Minor Repair
Pitch/Hydraulic	€ 14 000.00	€ 1 900.00	€ 210.00
Others	€ 10 000.00	€ 2 400.00	€ 110.00
Generator	€ 42 000.00	€ 3 500.00	€ 160.00
Gearbox	€ 115 000.00	€ 1 250.00	€ 62.50
Blades	€ 27 000.00	€ 450.00	€ 51.00
Oil and Coolant	€ -	€ 2 000.00	€ 160.00
Electrical components	€ 12 000.00	€ 2 000.00	€ 100.00
Circuit breaker	€ 13 500.00	€ 2 300.00	€ 260.00
Control	€ 13 000.00	€ 2 000.00	€ 200.00
Safety	€ -	€ -	€ -
Sensors	€ -	€ 2 500.00	€ 150.00
Pumps and motors	€ -	€ 2 000.00	€ 330.00
Shaft hub	€ 95 000.00	€ 1 500.00	€ 160.00
Heaters/coolers	€ -	€ 1 300.00	€ 465.00
Yaw system	€ 37 500.00	€ 9 000.00	€ 420.00
Tower and foundation	€ 1 100.00	€ 140.00	€ -
Power supply and converter	€ 13 000.00	€ 5 300.00	€ 240.00
Service items	€ -	€ 1 200.00	€ 80.00
Transformer	€ 70 000.00	€ 2 300.00	€ 95.00

Based on costs in an article by Carroll et al., costs expected due to materials are presented in Table 7.11 [3]. These are sorted from the most expensive base costs (not based on values adjusted for the proposed design). The costs of transport were not changed from the reference article by Carroll et al. [3]. Since not all systems are the same size or are installed the same number of times per turbine, scaling factors from Table 7.5, Table 7.6, and Table 7.7 were used.

Table 7.11: *Unscheduled Maintenance Costs*

Component	Base	Adjusted Faults	Adjusted Costs	Adjusted Both
Pitch/Hydraulic	€ 158.14	€ 158.14	€ 158.14	€ 158.14
Others	€ 200.12	€ 200.12	€ 200.12	€ 200.12
Generator	€ 41 406.60	€ 20 703.60	€ 31 146.60	€ 15 627.60
Gearbox	€ 213 386.25	€ 126 446.25	€ 106 693.13	€ 63 223.13
Blades	€ 6 570.72	€ 6 570.72	€ 1 971.22	€ 1 971.22
Oil and Coolant	€ 462.72	€ 462.72	€ 462.72	€ 462.72
Electrical components	€ 550.80	€ 550.80	€ 550.80	€ 550.80
Circuit breaker	€ 235.96	€ 235.96	€ 235.96	€ 235.96
Control	€ 576.00	€ 576.00	€ 576.00	€ 576.00
Safety	€ -	€ -	€ -	€ -
Sensors	€ 2 120.50	€ 4 241.00	€ 2 120.50	€ 4 241.00
Pumps and motors	€ 177.74	€ 177.74	€ 177.74	€ 177.74
Shaft hub	€ 1 086.72	€ 1 086.72	€ 1 086.72	€ 1 086.72
Heaters/coolers	€ 194.90	€ 194.90	€ 194.90	€ 194.90
Yaw system	€ 265.90	€ 67.80	€ 797.70	€ 203.40
Tower and foundation	€ 49.84	€ 99.68	€ 49.84	€ 99.68
Power supply and converter	€ 1 537.62	€ 1 537.62	€ 1 537.62	€ 1 537.62
Service items	€ 9.84	€ 9.84	€ 9.84	€ 9.84
Transformer	€ 81.84	€ 81.84	€ 81.84	€ 81.84
Total Materials	€ 269 072.21	€ 163 401.45	€ 148 051.38	€ 90 638.42
Total Transport	€ 77 229.11	€ 50 203.01	€ 77 229.11	€ 50 203.01
Total	€ 346 301.32	€ 213 604.47	€ 225 280.50	€ 140 841.44
LCoE	€ 2.32	€ 1.43	€ 1.51	€ 0.95
Change	100.00%	61.68%	65.05%	40.67%

Based on effects on LCoE in Table 7.11 the reduction in maintenance costs is between 35 % and 60 %, depending on what assumptions hold. Assuming that actual maintenance costs scale the same way as the unscheduled maintenance costs, the expected reductions show results reflective of changes to the previously used cost model, where the maintenance cost reduction for the LCoE was estimated between 40 % and 50 %.

In offshore wind turbines, a key issue for maintenance is that a site may not be accessible at all times, which may lead to long downtimes. Combined with the need for specialized maintenance vessels, this leads to lower availability than their onshore counterparts. Combined with the harsh marine operating conditions, and consequently higher failure rates, O&M becomes even more critical.

The simplest maintenance strategy would be corrective maintenance for components with longer lifetimes, such as generators, gearboxes, and shaft hubs. For other components with shorter lifetimes, such as dampers, and converters, a preventative maintenance strategy with a fixed schedule based on weather and site accessibility would be sufficient. However, with the use of sensors and a novel maintenance strategy, availability and maintenance costs could be improved.

Based on research by Xia et al., wind turbine blade maintenance costs may be reduced by as much as 18 % by employing a condition-based maintenance strategy [46]. Condition-based maintenance may also be applied to other subsystems using the Digital Twin technique as Zhong et al. [47]. This technique is based on creating a digital simulation of the system which is continuously updated using sensor data and then used to predict the remaining useful life of individual components. This technique necessitates the

use of appropriate sensors to ensure that the digital twin is actually representative of the real system. The approach to maintenance for the overall system and subsystems is further discussed in Section 7.3.

Safety

The system itself is not manned but still needs to be safe to operate and safe to fail. It also has to be safe for and during maintenance. The most safety-critical components are:

- The shaft brakes, which must prevent shafts from rotating. These may be deployed due to failure on the related systems, maintenance, or the need to park the system during storms
- Yaw system brake, which should hold the system in place during maintenance to allow safe operation and prevent the system motion during storms
- The monopile because it supports the entire turbine.
- The lightning protection system, is essential for a large steel structure. Without a proper lightning protection system, there is a large risk of damage to components due to lightning strikes, which can not be avoided.

For the case of shaft brakes, it would be wise to include one or more additional redundant systems, since maintenance of shaft bearings is expected to be among the most common types of maintenance which will be needed. In addition, their performance should be monitored by the use of strain gauges and hydraulic oil sensors.

For the yaw system brake, the bearing and the brake should be monitored with strain gauges, cameras, and potentially accelerometers to check for abnormal vibrations. There may also be a need for an additional emergency brake, which should be fail-safe and lock the system in place with respect to the monopile in case of failure.

The monopile itself can not be fail-safe or redundant and as such requires constant monitoring, which could be done visually via remote underwater drones and mounted cameras. Additionally, the status of the ocean floor would also need to be monitored.

For the lightning protection system, redundancy seems like the best option, as a failure of this system could to the failure of other critical components. The system is also easily replaceable and does not incur a large cost for installation.

7.3. Operations

Control strategy

Controlling and operating the wind turbine was another aspect that needed to be analyzed in this design stage. The wind turbine can only operate in a set range of wind speeds. It was assumed that the cut-in and cut-out wind velocities are 3 to $4 m/s$ and 25 m/s, respectively [8]. Within this interval, the wind turbine should be able to produce usable power and safely run. Three control techniques will be implemented in order to ensure that the maintenance required is minimized and the energy produced is maximized. According to Mwaniki et al., the designed product should have a supervisory, control and safety system.

The supervisory system aims to continuously monitor the entire assembly to facilitate preventive maintenance and planned system service. It is also capable of shutting down the system in case of extreme wind scenarios and other catastrophic failures.

Secondly, a control system will be needed to control the actuators and adjust the rates of individual elements for producing the required power in different conditions. This system will deal with regulating the

[8] https://theroundup.org/wind-turbine-power-curve/ [cited: 20 June 2023]

torque on the drivetrain through the DFIG settings, provide the proper orientation for the high lift device, command generator inputs, for converting the power mechanical into electrical power and vice-versa, and turn on the yawing system when the structure needs to orientate itself with the wind direction.

Lastly, the wind turbine should have a second redundant control system for safety. This should be independent of the main control system. In case of serious issues, it should halt the required operations and engage brakes. Usually, it aims to halt any activity in order to prevent additional damage.

Control of WCT

The wake control system should be controlled to provide the required wake recovery, but not produce loads of unacceptable magnitude. The control system concept is outlined in Figure 7.1. The main idea behind it is that the target value of circulation Γ_{ref} would be given as input, which would change the deflection of slats, flaps, and other sections of the airfoil in order to produce this desired circulation. The lift and drag produced would in turn have an effect on the structure, which should be integrated into another, bigger control loop.

At this stage, it is not possible to give a more detailed control block diagram, as many more details about the actual implementation of the WCT concept would be required. As more information becomes available at later design stages, the control block diagram in Figure 7.1 should be updated.

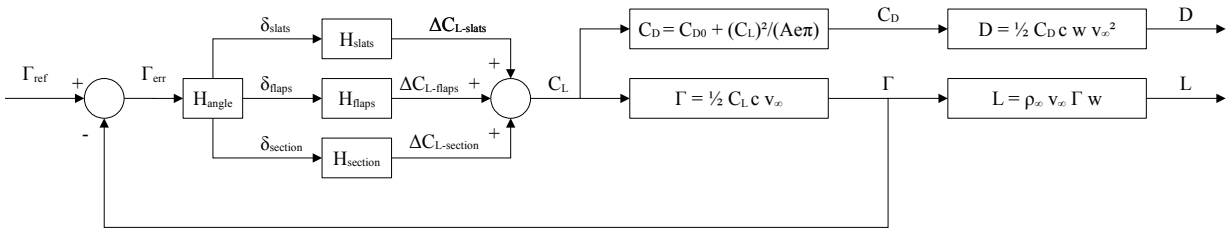

Figure 7.1: *Concept for control of WCT*

Torque control

In order to obtain maximum power production in the operating regime limited bu the cut-in and rated wind speeds, it is required to regulate the TSR of the rotors. As the introduction of a pitching system will introduce costly maintenance aspects in this purposely low-maintenance design, it was decided that the appropriate method for rotor control is through the generator. As discussed in the previous report, the DFIG requires a feeding connection from a power source in order to generate the variable magnetic field used in electricity production. By connecting a PI controller to the inverter and DC bus within the rotor-side converter, both the voltage and phase slip of the rotor can be modified. Changing these parameters leads to different values of generator synchronous speed, allowing the controller to set the slip setting of the DFIG. The slip of the generator is defined as the percentage difference between the rotor speed and the synchronous speed. For a DFIG the synchronous speed depends on the voltage fed into the generator rotor and the number of magnetic poles within.

The relationship between the slip of the generator and the produced torque is presented in Figure 7.2 [9].

[9] URL: https://www.elprocus.com/what-is-slip-in-an-induction-motor-importance-its-formula/ [cited: 16 June 2023]

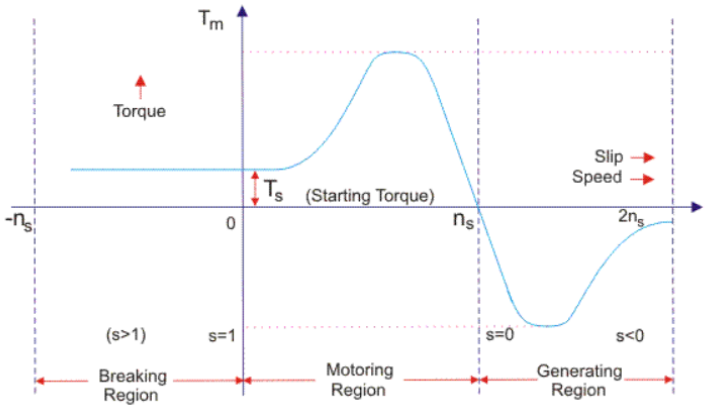

Figure 7.2: *Relationship between generator slip and torque for a generic induction generator, with positive torque relating to torque delivered by the generator.*

By either increasing or decreasing the synchronous speed of the generator it is possible to influence the shaft torque, and thus the speed of the rotors. By doing so, the turbine TSR can be modified to approach the optimum value for the given airfoil, thus maximizing the total power production. Multiple controller designs can be considered to regulate the TSR of the system, such as Tip Speed Ratio Control (TSRC), Optimal Torque Control (OTC), Power Signal Feedback Control (PSFC), and Perturbation and Observation Control (POC). From literature, it was determined that OCT is able to deliver maximum power while maintaining low response and recovery times compared to the other three [49]. Moreover, using OTC would also be beneficial when encountering turbulent gusts, as the low response time would make the controller more adaptable to these changes in wind speeds. This method can be combined with the implementation of a Maximum Power Point Tracking controller for the DC-to-DC converter connected to the DFIG in order to keep power transfer at maximum efficiency.

Control of YCT

Next, the yaw control system is designed. This consists of yaw control during operating conditions with differential thrust and yaw control using electric motors during low wind and storms. Finally, verification and validation are performed for the simulations developed.

Unforced yaw system response

Firstly, a wind velocity vector that is incident at an angle θ_v would cause the thrust generated by the left-most rotor as seen in Figure 7.3 to have a larger effective area, and thereby a higher thrust, than the other rotors. This is because part of the wake of each rotor, presented as the dotted lines in Figure 7.3, overlaps with the next rotor, causing it to lose efficiency. Assuming that there is no space between the rotors, the lost effective width of each rotor, l_{loss}, can be calculated by $l_{loss} = D(1 - \cos\theta_v)$ where D is the diameter the rotor. The only rotor which does not experience this effect is the first rotor and therefore provides a slightly higher thrust which exerts a torque on the system. The wind velocity in the wake of each rotor can be found using the c_t relation to the induction coefficient in Equation 7.1 [50].

Using a c_t of 0.75 results in an induction coefficient of 0.25 which leads to a wind velocity that is 75% of the freestream velocity, thus the shading effect can be assumed to lead to a 75% of freestream speed at the wake.

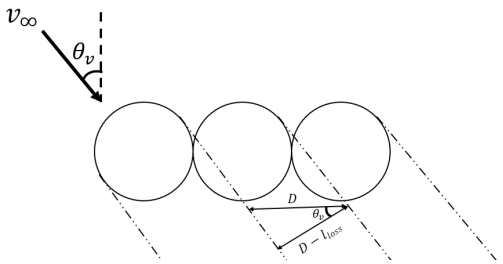

Figure 7.3: *Shielding effect*

$$c_t = 4a(1-a) \qquad a = 1 - \frac{v_{wake}}{v_\infty} \tag{7.1}$$

The resultant torque (anticlockwise positive) induced by this effect is described by Equation 7.2.

$$\tau_{shield} = \frac{1}{2}\rho c_t(0.25 l_{loss}) H\left(v_\infty^2 + 2\frac{W-D}{2}\omega v_\infty \cos(\theta_v - \theta_{sys}) + \omega^2\left(\frac{W-D}{2}\right)^2\right)\cos\theta_{rel}\cdot\frac{W-D}{2} \tag{7.2}$$

In the case where wind speeds are below the rated wind speed v_{rated}, if a torque is applied that causes the structure to rotate at an angular velocity ω, a dampening torque is induced. This is due to the increase in relative wind speed, and thereby thrust, in the rotors moving into the wind, and a complementary decrease in those moving away from the wind. This is because the thrust-to-wind-speed gradient is positive below v_{rated}.

Simulating this, the natural response of the system due to a change in the angle of wind velocity θ_v is to re-align to be perpendicular to the wind velocity, therefore the system is stable with regards to wind direction changes. However, this motion is overdamped, leading to a correction time of hours. Thus, an additional torque needs to be applied to decrease the time of angle correction.

Yaw control with differential thrust

The use of differential thrust to yaw the turbine relies on reducing the thrust generated by one or more rotors which in turn reduces the torque generated on that side of the turbine, causing it to yaw in the desired direction. This method is able to achieve high torques, and therefore a faster correction rate, without having to use large motors.

A Python script simulates the application of this by setting an initial angular displacement, velocity, and acceleration of zero for the system, with a wind velocity vector aligned at θ_v counterclockwise. The simulation follows a turbine-fixed frame of reference and so the wind speed vector changes relative to the rotor as it moves. Thus the effective wind speed angle is $\theta_v - \theta_{sys}$. The relative velocity V_{rel} and angle of relative velocity θ_{rel} experienced by each rotor are calculated iteratively as ω changes.

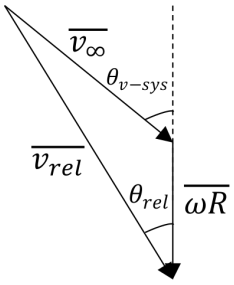

Figure 7.4: *Relative velocity for a rotor moving into the wind*

$$v_{rel} = \sqrt{v_\infty^2 + 2v_\infty \omega R\cos(\theta_v - \theta_{sys}) + \omega^2 R^2} \tag{7.3}$$

$$\theta_{rel} = \arctan2\left(\frac{v_\infty \cdot \sin(\theta_v - \theta_{sys})}{v_\infty \cdot \cos(\theta_v - \theta_{sys}) + \omega R}\right) \tag{7.4}$$

The relative velocity is used in the calculation of the thrust vector in the direction of relative velocity for each rotor. The perpendicular component of each thrust vector is calculated and multiplied by its moment arm to calculate the torque induced by each rotor. Finally, the torques are added, resulting in the total applied torque on the turbine system. This iteratively leads to a new α through $\alpha = \tau / I$, and thereby ω and θ are updated.

The controller used for differential thrust is a simple on-off switch to turn the outermost rotors depending on the sign of the angle error. The controller accounts for overshooting the target angle by reversing the side on which the rotors are switched off, until the system angle θ_{sys} is within 10% of the desired angle θ_v, where all rotors are switched back on and the system is allowed to self-stabilize. A block diagram of the controller can be seen in Figure 7.5. The on-off controls are displayed as Heaviside step functions denoted by U.

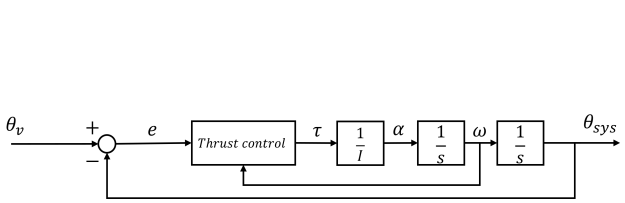

(a) *Torque control diagram*

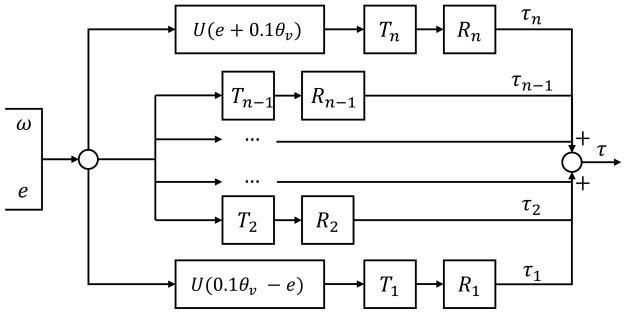

(b) *Thrust Controller*

Figure 7.5: *Block diagram of yaw control*

Simulating system response to the thrust controller results in yaw error correction times as shown in Figure 7.6 for a mass moment of inertia $2.75 \times 10^{10}\,\mathrm{kg\,m^2}$, and a wind speed of $10\,\mathrm{m\,s^{-1}}$.

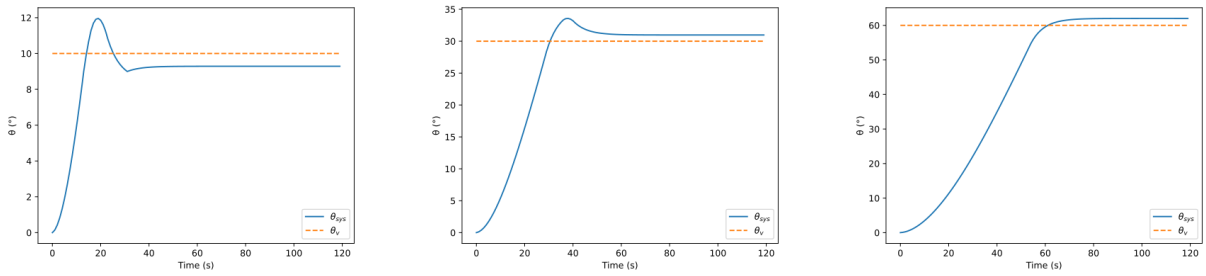

(a) $\theta_v = 10°$ **(b)** $\theta_v = 30°$ **(c)** $\theta_v = 60°$

Figure 7.6: *System response to varying changes in* θ_v *at* $10\,\mathrm{m\,s^{-1}}$

Limitations

One of the limitations of this yaw control mechanism is that it does not optimize for power production while yawing. Rather it serves as a simple mechanism that can perform yaw quickly, and therefore allow for more non-yawing time where all the rotors can give maximum performance. The use of other more complex yaw controllers can be designed to minimize power loss while yawing as well.

Additionally, the simulation assumes a wind speed below v_{rated}, so c_t remains 0.75, this is the case most of the time. In reality, the system will also need to yaw at or above v_{rated}. Above v_{rated}, thrust decreases with

wind speed, which causes the system to become unstable with changes in θ_v as the direction of the dampening torque reverses. This can be overcome by applying yaw brakes when the wind speed approaches v_{rated} to avoid an unstable free movement. When disengaging the brakes and yawing the system, the thrust generated by the rotors can be artificially lowered to keep a positive thrust to wind speed gradient, keeping the system yaw stable even during $v_\infty > v_{rated}$.

Using differential thrust is slightly less effective during lower wind speeds, as it takes longer to yaw. However, the time to yaw is still very small compared to changes in wind direction, so it could still be used. When there is virtually no wind, the use of an electrical yaw system becomes more effective.

Yaw control with electric motor

The use of electric motor drives connected by a set of planetary gearboxes to the yaw slewing bearings to induce a torque and therefore yaw the system is also possible. This can be useful, for example, during storms, when the differential thrust cannot be used as all rotors are put on standby. Another use case would be below cut-in speed when the wind speed is too low to use differential thrust.

This section will size the electric yaw system-based dampening torque that is induced by the rotational speed. The main assumptions will be that there is no shielding effect and that the system inertia is small and reaches terminal velocity quickly. The calculations boil down to the thrust force of the structure times the moment arm integrated over the domain. The critical case will be in 70 $\mathrm{m\,s^{-1}}$ storm conditions rotating at 90°/30min.

Previous simulations showed that the system is highly damped, so damping dominates over inertia. It is assumed the system will spend most of the time at terminal velocity while yawing. During this time, the Torque produced by the electric motors will be equal to this damping torque. Damping torque is due to different relative wind speeds on opposite sides of the structure due to the rotation of the structure. Assuming the worst-case scenario when the structure is 90° to the wind, the relative wind speed distribution will be linear to the distance along the width of the structure $v_{rel} = v_\infty + \omega R$ Equation 7.5. Figure 7.7 and the following equations help to understand the reasoning. Drag force is proportional to v^2, so the Drag force distribution will be a parabola.The combined drag force comes from the drag of the rotors described in Equation 7.7 and from the wings described in Equation 7.8. The wings' drag must be multiplied by the number of wings. The derivation assumes one wing.To get the torque distribution acting on the structure the force distribution needs to be multiplied by the distance from the rotational axis described in Equation 7.6. Torque distribution will be a 3rd-order polynomial and which needs to be integrated over the domain of the structure to get the total torque. So the torque has up to fourth-order dependencies on the radius. To do this in integral form, it is advantageous to notice that these variables are not dependent on the height of the structure, so it is possible to only integrate along one dimension along the width to get the resultant torque. This integration is performed in Equation 7.9,Equation 7.10 and Equation 7.11. Since the structure is symmetric and the integration is carried from -R to +R, even order terms cancel out, and we are left to only consider odd-numbered terms. The equation is valid for $v > 3m/s$.

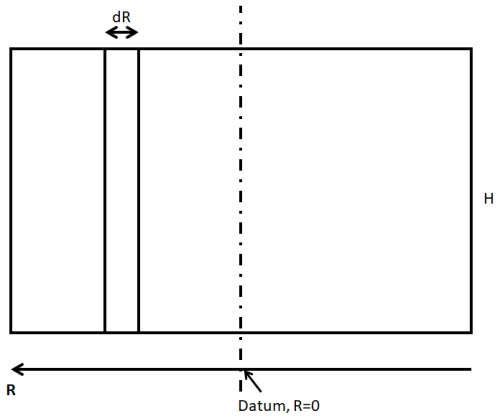

Figure 7.7: *Drawing for the derivation*

- $\rho = 1.225 kg/m^3$ - air density
- $C_T = 0.014$ - thrust coefficient when stationary
- $C_D = 0.0152$ - drag coefficient when stationary
- $H = 280m$ - height of the structure without clearance
- $c = 20m$ - cord of the wing
- $R = 145m$ - half of the width of the structure
- v - free stream velocity velocity
- ω - rotational velocity of the system
- τ - Torque

$$v_{rel} = v_\infty + \omega R \tag{7.5}$$

$$\tau = (F_{flow} + F_{wing}) \cdot R \tag{7.6}$$

$$F_{flow} = C_T \frac{1}{2} \rho v^2 H dR \tag{7.7}$$

$$F_{wing} = C_D \frac{1}{2} \rho v^2 c dR \tag{7.8}$$

$$\tau_{storm} = \int_{-R}^{R} C_T \frac{1}{2} \rho (v + \omega R)^2 HR + C_D \frac{1}{2} \rho (v + \omega R)^2 cR \, dR = \frac{1}{2} \rho (C_T H + C_D c) \int_{-R}^{R} (v + \omega R)^2 R \, dR \tag{7.9}$$

$$\int_{-R}^{R} (v + \omega R)^2 R \, dR = \int_{-R}^{R} v^2 R + 2vR^2\omega + R^3\omega^2 \, dR = \frac{1}{2} v^2 R^2 + \frac{2}{3} vR^3\omega + \frac{1}{4} R^4\omega^2 \Big|_{-R}^{R} = \frac{4}{3} vR^3\omega \tag{7.10}$$

$$\tau_{storm} = \frac{1}{2} \rho (C_T H + C_D c) \frac{4}{3} vR^3\omega \tag{7.11}$$

It can be seen that Equation 7.11 requires zero torque to yaw the structure at any rotational speed, which is not true. This is because it was assumed that the relative speed always acts in one direction. When in Equation 7.7 and Equation 7.8, the velocity is squared, and the direction of the wind is lost. This is a good assumption as long as v>wR; however, at $v = 0$ m/s, the sign changes direction in the middle of the structure. Therefore Equation 7.12 accounts for this change in direction. Another inaccuracy is that this equation assumes only one wing to get the result for four wings $C_d c$ should be multiplied by 4. The results Table 7.12 are with four wings.

$$\tau_{v=0} = \int_{-R}^{0} (F_{flow} + F_{wing}) \cdot R \, dR - \int_{0}^{R} (F_{flow} + F_{wing}) \cdot R \, dR = \frac{1}{2} \rho (C_T H + C_D c) (\frac{1}{4} R^4\omega^2 \Big|_{-R}^{0} - \frac{1}{4} R^4\omega^2 \Big|_{0}^{R}) =$$

$$= \frac{1}{2} \rho (C_T H + C_D c) (-\frac{1}{4} R^4\omega^2 - \frac{1}{4} R^4\omega^2) = \frac{1}{4} \rho (C_T H + C_D c) (-R^4\omega^2) \tag{7.12}$$

For a torque rating, wind speed and yaw rate are needed. To size the electrical yaw system, the yaw rate requirement should be found. Several conditions will be considered. Wind speed calculations will be presented for 70m/s, 50m/s 30m/s and 0m/s. These speeds are between 50-year maximum and 0m/s while not considering operating conditions. To determine the yaw rate required during storm conditions and during low wind speed conditions, historical wind data is considered. Wind data presents the wind speed and wind direction in 2016, 2017 and 2018 for every 30 minutes [13]. Wind data indicated that within 30 minutes the wind can change the direction by 180° however this change was rare [13]. The 75 percentile is a change of 4.5° and the 95 percentile is a change of 11.5°. To compare, for a typical yaw system for operating conditions, the yaw rate is 1°/s [51]. The results are presented in Table 7.12

Table 7.12: *Torque in MNm required to yaw the system depending on wind speed and rotational speed.*

	0 m/s	30 m/s	50 m/s	70 m/s
4.5° / 30 min	<0.01	0.02	0.03	0.04
11.5°/30 min	<0.01	0.04	0.07	0.10
90° / 30 min	<0.01	0.33	0.56	0.78
180°/30 min	<0.01	0.67	1.12	1.56
1°/s	0.21	6.70	11.16	15.62

Table 7.13: *Time required to accelerate the structure*

	t[s]	t[min]
4.5° / 30 min	2	0.1
11.5°/30 min	6	0.1
90° / 30 min	49	0.8
180°/30 min	98	1.6
1°/s	980	16.3

Based on the table, we can see that the limiting case is yaw during storm conditions. It is very unlikely that a rare storm event will happen at the same time as a rare wind change happens, so the red cells (> 1.2MNm) of Table 7.12 are not design requirements. Considering this, an electric yaw system capable of providing 800 kNm is selected. To check if the assumption of a damping-dominated system was correct it is required to calculate the time it would take to accelerate the system to the given yaw rate calculated in Table 7.13. It can be seen that for anything less than 180°/ 30min acceleration time is at least 20 times smaller than 30 minutes.

Verification of yaw simulation

The yaw simulation is verified to ensure that it performs the calculations correctly. For this, the simulation is restricted to only the $0 < \theta < \frac{\pi}{2}$ quadrant of the wind directions, as the reaction of the system to wind vectors from any of the other quadrants is symmetric.

The verification consists of checking that the program performs as expected for each step of the analysis by comparing output from the program to calculations done manually. This is performed for an iteration for the leftmost rotor where $v_\infty = 10\,\mathrm{m\,s^{-1}}$, $\theta_v = 30°$, $\Delta t = 1\,\mathrm{s}$, $t = 4\,\mathrm{s}$, $\alpha = 0.001\,660\,506\,869\,86\,\mathrm{rad\,s^{-2}}$, $\omega = 0.007\,749\,071\,214\,34\,\mathrm{rad\,s^{-1}}$, $\theta_{sys} = 0.020\,453\,453\,970\,14\,\mathrm{rad}$, and Total torque = 45 675 014 N m.

Table 7.14: *Verification using hand calculation at t = 4 iteration for a single rotor*

Step	Output from code	Hand Calculation	Absolute Error	Relative Error
R	-116.66666667	-116.66666667	0	0
ωR	-0.90405831	-0.904058308	1.63E-09	-1.8E-09
v_{rel}	9.21829427	9.218294267	-3E-09	-3.3E-10
θ_{rel}	0.55045175	0.55045175	3.66E-10	6.65E-10
T	510074.1375302	510074.1375	-2.4E-06	-4.8E-12
$T_\perp$	434730.22512485	434730.2251	-2.5E-06	-5.7E-12
τ	50718526.26456571	50718526.27	0.001161	2.29E-11

The results show that the code performs as expected based on the given equations. The maximum relative error found in this case is in the order of 1×10^{-9}, which can be considered negligible. Furthermore, the

simulation is convergent with a reduction in time step.

Validation of yaw simulation

The physical equations used in the simulation must be validated to ensure that they accurately reflect the dynamics that would occur in real-life. The assumptions made in the initial simulation need to be validated to be true. This can be done either through the comparison of results with literature or by building a prototype and collecting real-life data and comparing results. Since this is a novel concept, it would be difficult to find literature in which such type of system is addressed. MacMahon et al. provides such a simulation for yaw with differential thrust for an MRS, however, this is provided for an MRS of HAWTs so cannot be directly used to validate this model [52]. Therefore it is better to collect real-life data from a prototype instead.

Sensors

Sensors are devices that detect and respond to physical input or changes in the environment. It is imperative for the designed wind turbine to be equipped with several sensors in order to detect potential issues and prevent the failure of the structure. Multiple types of sensors have been identified that will be installed on the wind turbine. They are presented and briefly described below:

1. Anemometer. The anemometer measures the wind speed and it will be placed in various locations.
2. Wind vane. It measures the wind direction and it will be placed in multiple locations.
3. Wind gust sensor. The wind gust sensors detect the sudden changes in wind speed. It will be located on the top of the structure.
4. Torque sensor. The torque sensor measures the magnitude of the torque exerted on the shaft. It should be located on each rotor and generator.
5. Accelerometer. This device is used for monitoring the vibrations inside the wind turbine. Vibrations could constitute an issue, especially for the tower while operating and in extreme weather conditions.
6. Thermometers. They will be placed in several locations in order to check the temperature of multiple components. Typically, the elements that experience the most overheating are the power electronics, generator windings, gearboxes, and bearings. [10]
7. Yaw position sensor. Since the wind turbine is equipped with two bearings that will facilitate the yawing movement, such devices will be presumably placed near the motors.
8. Generator voltage and current sensors. Each generator will include this type of equipment.
9. Rotor speed sensors. Six instruments will be needed in total, one for each shaft.
10. Ice detection sensors. Since the wind turbine is located in the Ijmuiden Ver zone, a harsh climate can be experienced during winter. Having the blades covered with ice can damage their structure of them and also affect the power production efficiency.
11. Rain sensors and Light Detection and Ranging (LIDAR) scanner. LIDAR scanners are capable of mapping the wind's and rain's characteristics in advance. They sent laser pulses into the atmosphere which are further reflected by particles from the air.[11]

[10] https://www.ediweekly.com/overheated-bearings-gearboxes-among-causes-wind-turbine-fires/ [cited: 13 June 2023]

[11] https://www.vaisala.com/sites/default/files/documents/WEA-LEO-ScanningLidar-eBook-B212128EN-A.pdf 18 June 2023

12. Cameras. Cameras will be used mostly for monitoring the external cracks and damage to the wind turbine. Since there is a lot of free space in the truss structure, they can be mounted in several locations on the struts and transmit up-to-date information consciously.
13. Strain gauges. This equipment is meant to measure the strain in different turbine members. They will be located in different spots.
14. Oil condition sensors. Six such sensors will be needed for each gearbox.
15. Humidity and pressure sensor. These instruments will be used to measure the atmospheric conditions.
16. GPS. The GPS is particularly important in the case of maintenance work when a specific wind turbine is damaged inside a wind farm.
17. Lighting sensors. They should be located in several parts of the structure.
18. Acoustic sensors and microphones, which will be used for noise monitoring. Noise pollution should not be an issue as a lower TSR, except for the installation phase of the wind turbine, but they should be present to detect, when possible, to detect different types of mechanical malfunctions.
19. ACFM sensors, is a probe sensor to detect surface level cracks on the conductive surfaces of the structure. It is mainly utilized for the truss structure and blades of the rotor, as they are hollow metal cylinders.

The most important data to be collected by SCADA for predictive maintenance were decided. They are presented for the individual subsystems level (FND, TWR, YCT, PCT, WCT, DRT, RTR). The list is not exhaustive, only including the most relevant sensors.

FND: Foundation health would require sensors to determine the progress of corrosion and any structural damage. FND will be installed with strain gauges to measure the strain induced on the monopile as a function of the wind speed. In addition, it will have acoustic sensors to inspect the interference pattern of sent signals and analyze crack formations.

TWR: Since it has a significant number of truss elements, the TWR system will be the closest inspected. Furthermore, every load induced in the system goes through the truss structure to the monopile. Therefore, analysis of the vibrational characteristics of this structure is essential for cutting operational expenses. The TWR will be equipped with multiple accelerometers and strain gauges to send the frequency spectrum and amplitude of vibrations due to wind characteristic changes to the SCADA. These devices will also be used to detect rotor-induced vibrations and to determine interference between aerodynamic loads induced by the HLD and rotors. To inspect partial failures and cracks of the truss structures, both acoustic and ACFM (Alternating current field measurement) sensors will be used. Moreover, the cameras and microphones will be placed on this structure for visual and noise inspection of both itself and the rotors.

RTR: The RTR structure will also be monitored, given relatively high and fluctuating loading. Both ACFM(since blades are entirely metallic) and acoustic sensors will be used for operational and non-operational inspections, respectively, for crack formations. Also, RTR RPM will be measured with the vibrations on the RTR.

DRT: DRT failures are catastrophic for the operations. Oil sensors for the gearboxes will be installed for oil pressure, temperature, granularity, and leakage. Also, vibrations on the gearboxes and shafts will be collected as functions of generator RPM and capacity to predict failures before they happen.

YCT: Attitude and yaw rate of the structure during the yaw movements will be collected as well as the vibrations with yaw position sensor and accelerometers on the truss structure, respectively.

WCT: WCT induces high loads on the structure that supports it and itself. These loadings are heavily influenced by wind characteristics and are unstable. Therefore, accelerometers and strain gauges will be utilized.

Interrelations between the collected data and sensors can be observed better in Figure 7.8.

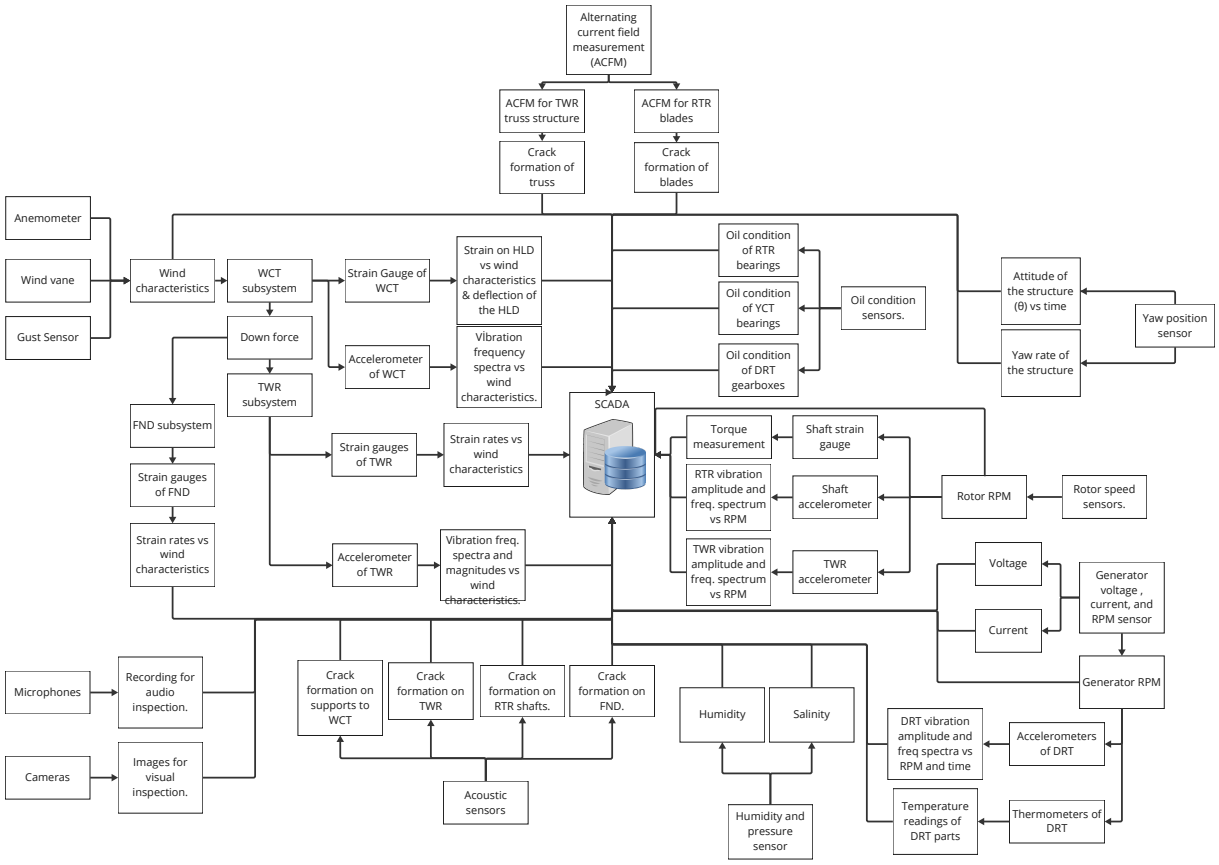

Figure 7.8: *SCADA data acquisition and sensor connection diagram*

Electrical layout

It is important to evaluate, at least at the conceptual level, the components of the electrical department that enable the system to send and receive power to and from the grid. Usually, offshore wind parks are connected to the grid through a transformer platform that converts the AC current from the wind turbines to HVDC current. This is done in order to minimize cable losses over the tens of kilometers between the wind park and the landing point. As the scope of the MR-TBD project did not include the transformer platform, it was assumed that will be covered by Tennet, the Dutch national grid operator.

The main electrical elements that can be found on the turbine are the generator, the partial converter that provides a load to the generator's induction rotor, and various filters that prevent the overloading of other components. Due to safety reasons, the system also includes an Emergency Power Source (EPS) that can operate independently of the generator and the grid connection. This EPS is designed to power both the hydraulic brake and the yaw drive to operate in emergency conditions. The sizing of this additional power bank will be considered in the next design iterations post-DSE. A conceptual diagram is provided in Figure 7.9.

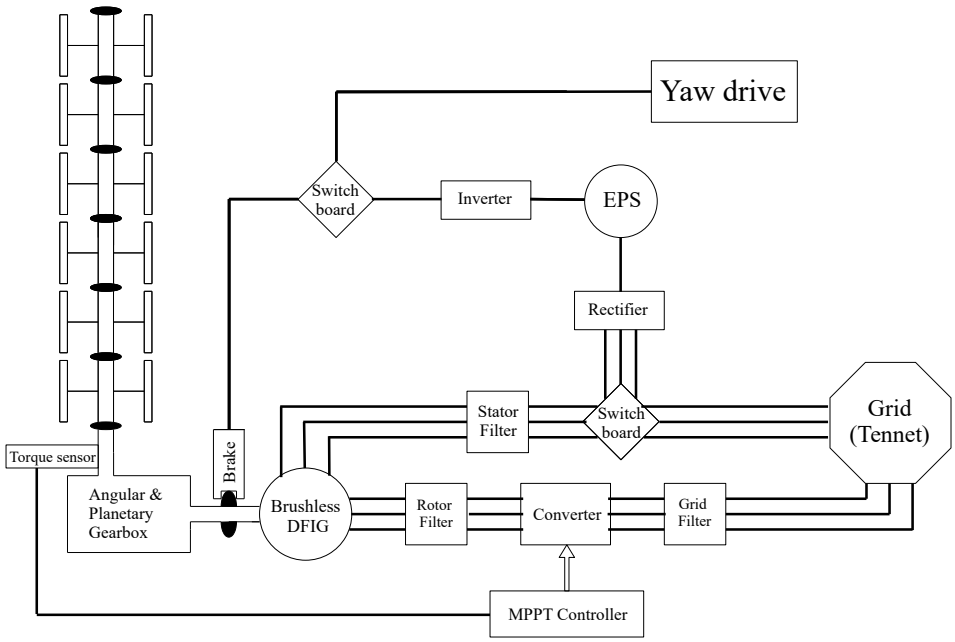

Figure 7.9: *Conceptual electrical diagram*

System Operation

The system's function flow diagram (FFD) and function breakdown structure (FBS) have been updated from their initial version presented in the baseline report [7]. Some functions in both have been changed, namely, all the functions related to the pitching of the blades. Functions were also made more specific and all but one were now broken down into three levels.

For the FFD, the diagram was remade to show the nesting of the tasks within each other more clearly. The previous version of the diagram did not show the hierarchy quite as clearly.


Start-up system
Receive power from grid
Receive AC from the grid
Convert AC to generator frequency
Convert AC to DC for other systems
Start-up power system
Start-up control system
Start-up main controller
Start-up HLD controller
Start-up YCT controller
Start-up RPM control system
Establish communications link
Send signal to comms equipment
Send message to power station
Await response
OR
Receive response
Connection timed out
Send power to other subsystems
Send power to sensors
Send power to YCT actuators
Send power to rotors
Send power to operation support systems
1
Communicate with control station
Check status of the system
Start system health monitoring
Check status of rotors
Check status of YCT
Check status of tower
Check generator and drive train status
Check hydraulic system
Check electrical components
Check functioning of all subsystems
Check vibrations of the structure
Check environmental conditions
Measure wind direction
Measure wind speed
Measure air temperature
Measure system temperature
Measure humidity
Measure air density
Compare with forecast data
Send data to main computer
Send system status to control station
Send generator status
Send rotor status
Send tower status
Send shaft status
Synchronize measurements with digital twin
Send system attitude
Send hydraulic system status
Send environment data to control station
Send wind speed
Send wind direction
Send density
Send temperature
Receive response from control station
Await response
OR
Receive response
Connection timed out
Respond to feedback
Update system and environment status regularly
OR
2
(Re-)Start operation
Start-up generators
Activate safety and monitoring
Release shaft break
Spin up rotors
Power up electro-magnets
Send system status to control station
Check generator state
Check power train status
Check rotors' bearings
Activate safety systems
Release rotors
Monitor rotor vibrations and RPM
Deploy HLD
Unlock actuators
Angle up the second section
Extend flaps
Extend slats
3
Determine operation parameters
Find wind velocity vector
Measure wind direction
Measure wind speed
Measure wind gusts
Measure turbulence
Compare wind to attitude
Check attitude of the system
Compare wind direction
Determine gust direction
Check if wind velocity is within operating range
Send wind data to controller
Determine if velocity is high enough
Determine if velocity is low enough
OR
Send diagnostic data to other main computer
Perform subsystem checks
Send results to main control station
Check all status data and response
OR
Request repairs
4
Orient in the correct direction
Determine required attitude
Check wind measurement data
Check the target power level
Use power needed to maintain needed attitude
Determine required rotor RPM
Compute needed rotational torque
Compute what shafts to slow down
Determine target RPM
Verify orientation
Check current attitude
Chack current power production
Verify attitude with wind measurements
OR
Adjust rotor RPM
Check current error in RPM
Determine required control signal
OR
Engage shaft breaks
OR
Change generator loading
Yaw the structure
Check yaw error
Determine electric motor input needed
Apply motor torque
OR
5
Generate Electricity
Convert wind energy to kinetic energy
Generate lift from relative airspeed
Spin up the rotors
Transfer torque to the shaft
Adjust shaft speed
Measure shaft speed
Determine optimal RPM
OR
Apply shaft break
Convert rotational energy into electricity
Transfer torque from shaft to gearbox
Use gearbox to achieve required RPM
Produce electrical power
6
Send power to substation
Connect to substation
Measure generated voltage
Measure generated current
Communicate power produced to substation
Increase voltage
Determine optimum voltage
Transform voltage to correct value
Send electrical power to substation
Send electrical power to substation
OR
7
Halt operations
Stop the rotors
Check rotor RPM
Apply shaft breaks
Wait for rotors to stop
Retract HLD
Retract slats
Retract flaps
Angle down the second section
Lock the actuators
Power down subsystems
Power down generators
Power down control system
Power down sensors
Cut connection with grid
Inform main station about sucessful shutdown
Inform main station about powering off
Wait for further orders
OR
8
Facilitate maintenance
Check status of subsystems
Check communication system
Check status of rotors
Check status of YCT
Check status of tower
Check generator and drive train status
Check hydraulic system
Check electrical components
Check the status of coating
Determine which parts need replacement
Review diagnostic data
Compare diagnostic data with benchmark
Identify malfunctions
Test critical parts for fatigue
Identify fatigued parts
Determine what parts are scheduled for replacement
Compare results with digital twin
Record parts to be replaced
Maintain the system
Provide evidence of damage
Apply new coating where needed
Inspect parts in question
Replace parts in question
Check if maintenance was successful
Run system diagnostics
Compare measurements to expected values
9
End operations
Check the structural integrity
Check structural damage
Check fatigue status
Check coating status
Check corrosion
Check the subsystem status
Check generators and drivetrains
Check electrical component status
Check actuators
Check sensors
Disassemble the system and decommission
Determine which parts may be salvaged
Salvage parts which can still be salvaged
Disconnect main tower and monopile
Tow the tower back to shore for recycling
10

Functional Breakdown

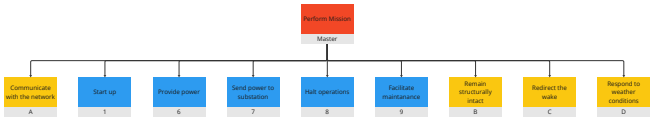

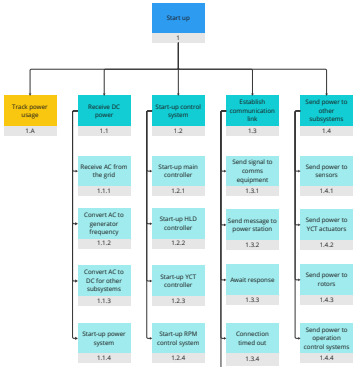

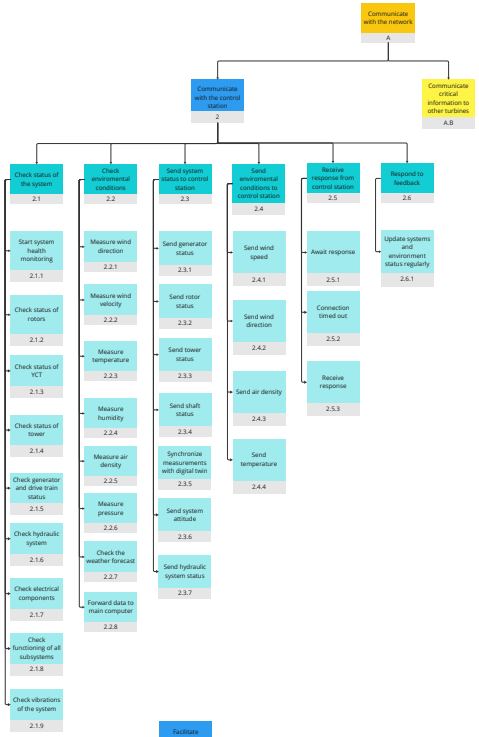

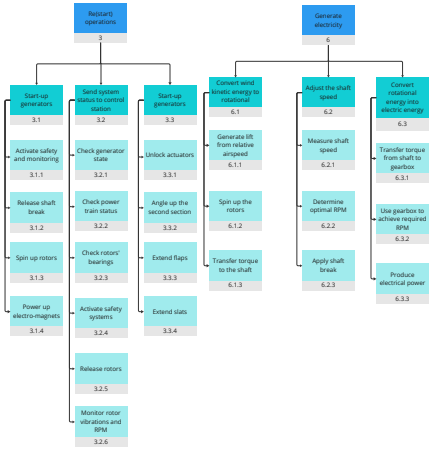

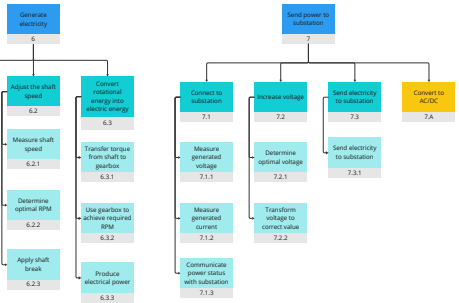

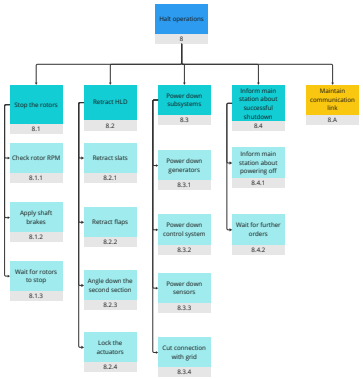

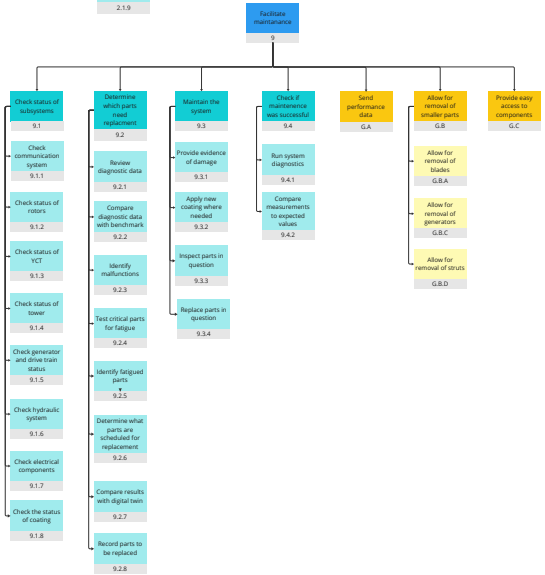

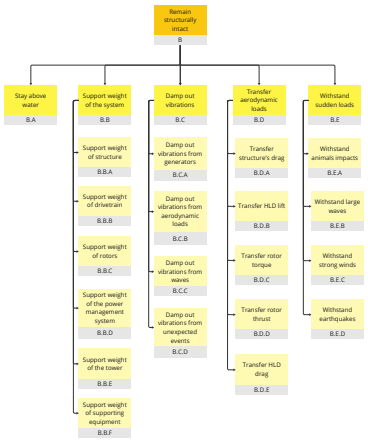

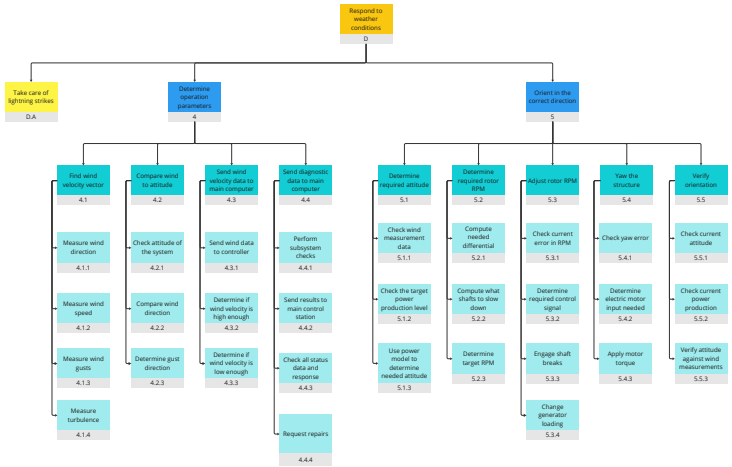

Expected Annual Energy Production

The main goal of any wind turbine is to produce electrical energy. With all the data presented before it is possible to estimate the energy production of the design. The calculation was straightforward, the power production for a given wind speed was given in Section 5.3 and the wind speed data was given in Section 3.2. To obtain the yearly energy production, for every data point in the wind model, the power produced is calculated. Since the wind data points are spaced 30 minutes apart, it is assumed that the wind conditions are stable, so the power produced can be multiplied with time separation of the data points to get the energy produced. Using this approach, the annual energy production (AEP) was calculated to be around 149 GWh. This is roughly in line with the values predicted by the Catapult data, which were 134 GWh [6]. The energy production calculated here is most likely an overestimation, since stops for maintenance or other disruption are not taken into account. However, it still shows that the proposed design has an energy production close to expectations.

7.4. Maintenance and logistics

This section describes the operations plan for the designed wind turbine. It focuses on the installation, decommissioning and maintenance of the system. Its operations are not expected to be much different from the offshore ones of the current wind turbines. This would mean that an onshore control center is used for most of the operations, with a small support crew on the wind farm site to allow for quick repair.

Installation and offshore transportation

A few aspects of the installation and decommissioning of the wind turbine will closely follow the procedures currently in place for traditional designs. For example, the installation of the foundation and connection to the grid will remain the same, just on a larger scale. What will be different is the transportation of the structure to the IJmuiden Ver zone and the installation of the structure.

The design of the tower will be built onshore and then towed to the location where it should be placed. The monopile will be installed on the ocean floor up to a few meters below the surface of the ocean. The structural frame will be built and equipped with all components inland. There are multiple ways in which the tower, including all elements, and the monopile can be transported to the desired location. The most common methods are to use a crane that will ferry the assembly, pile drive the foundation and afterwards mount the tower. An alternative would be to employ dynamically positioned (DP)/anchor handling/floating vessels in combination with floaters to transport and connect the two components of the wind turbine. With regard to big floaters nominated, they would be filled with more water to sink further down, allowing for the monopile to be joined to the structure. For inserting the monopile into the ground, the typical hydraulic hammering could be adequate. The big disadvantage of the impact driving method is the generation of underwater noise that can affect marine life [53]. However, there is an additional technique that uses hamming by vibrations. Simulations and calculations prove that this will save up to 40 % reduction in installation time and installation cost. [12] Installation and transportation services are provided by several companies from the Netherlands, namely, Heerema Marine Contractors [13], Cape Holland [14]and Boskalis [15], respectively.

Before proceeding with the installation of the foundation, there are preliminary measures and preparations that need to be taken into account. The most important ones are protecting the seabed and preventing it from further deepening while driving the foundation and parking the necessary vessels [16]. Fur-

[12] URL: https://ocean-energyresources.com/2021/07/30/introduction-of-safe-installation-process-for-ultra-long-xxl-monopiles/ [cited: 20 June 2023]
[13] URL: https://www.heerema.com/heerema-marine-contractors [cited: 26 June 2023]
[14] URL: https://capeholland.com [cited: 26 June 2023]
[15] URL: https://boskalis.com/ [cited: 26 June 2023]
[16] URL: https://boskalis.com/ [cited: 26 June 2023]

thermore, seabed rock installation is required to establish the connection with the onshore grid. The three companies mentioned above do have facilities for performing all preparatory operations.

Storing and Repairing Parts

There are four different maintenance strategies that can be adopted to ensure that the wind turbine operates within the normal parameters: corrective maintenance, preventive, condition-based and predictive maintenance. From previous work, it has been decided that predictive maintenance allows for both the lowest operational costs and downtime. However, in practice, a combination of all four needs to be employed.

An essential advantage of the MR-TBD design is the ease of pursuing the maintenance work. Since the wind turbine has six shafts, when a component from one of the shafts is ruined, the repair can be done, by only turning off the shaft from the opposite side. For this scenario, the yawing movement will be avoided and power will still be produced, but at a lower capacity. As presented in Table 7.3, elements from the electrical/power sector and drive train are more likely to fail, in particular, the gearbox, generator, power supply and converters. For this reason, it was decided to place them at the bottom part of the tower. They will be accessible via stairs, catwalks and a central elevator located along the symmetry line of the wind turbine. The maintenance of the damaged parts will be done relatively fast and efficiently. For changing and handling the elements located on the bedplate of the tower, a crane will be placed there, while for dealing with the compromised rotors of HLDs, the crane situated on the last level of the truss structure, will be employed. For instance, if a gearbox or a generator is broken, it will be immediately changed in an effective way. After disconnecting it from the entire assembly, it will be transferred to the underneath vessel and thereafter fixed at the onshore depot. The affected unit will be changed to a newer one right away after it is disjointed. In this fashion, the downtime is minimised since the maintenance work is not performed offshore and the replacement is effective. The only period when the wind turbine will experience a loss in energy production will be while travelling to the location and shifting the parts. Table 7.8 and Table 7.9 showcase a replacement time for the generator of about eight and four hours, respectively, which is reasonable. The gearbox replacement times can be assumed to be almost the same since the procedure of fixing it is similar.

In order to have an efficient and safe maintenance service, personnel performing maintenance to the wind turbines needs to have easy access to spare parts. If possible, spare parts are often stored in specific warehouses close to the wind turbine site, known as depots [54]. For the design presented in this paper, only one depot will be considered due to the potentially limited extent of the wind farm and the limitations in the project's cost. Inside this facility, both repairable and discardable parts may be stored, and the quantity of each item will be formally known as the stock level of the storage [54]. Warehouses make up the entire skeleton of the support aspect of the project, assembly components, and can also allow for repairs of certain components. Apart from not severe repairs done at the depot, most broken items are sent to a workshop/provider for repair. Most of the time, workshops are in small designated areas close to the depot, where each turbine component's repair facilities are provided. Especially for advanced equipment, the workshop can often be the property of the part manufacturer. In some cases, operators get a new item from the manufacturer in exchange for sending a broken item obtaining a deduction on the component's price. The time it takes for an item to be repaired and returned to the depot is called turn-around time (TAT). This is a very important parameter when optimising stocks for repairable items [54]. Finally, every item needs to be properly collected inside the depot and an inventory of all the elements needs to be performed. This is done to keep track of and identify all the stored items.

Onshore Transportation

Onshore transportation is one of the biggest challenges in designing and building a wind farm. The large size and weight of most components make the design extremely hard to transport, even for small distances. Due to the increased number of elements, the logistics cost is expected to be high for regular wind

turbines. However, this will not be the case for the designed product since most of the manufacturers and providers are located close to the Port of Rotterdam, where the central depot of the wind turbine will be situated, as stated in Section 7.1. They will be able to transport all the components via ships and when necessary, via trains or trucks. The only elements that might not be available on the domestic market are the elements from the drive train and sensors. In this sense, one option would be to be delivered by freighters to Amsterdam Schiphol Airport and then further transported by vessels or trains to the final destination. The second option would be to directly deliver them by cargo ships to Rotterdam.

Onshore transportation is not considered an issue on account of the location chosen for the depot of the wind turbine. It will facilitate a reliable method of ferrying goods with a low risk of delay.

Decomissioning

Although life extension is a valuable tool for increasing the EROI of the asset and making the system more sustainable, it is only a prolonging of the inevitable decommissioning. According to decision 98/3 of the OSPAR convention, ratified by all Western European countries, all offshore structures above 4000 t are required to be disassembled by parts once they reach the end of their useful lives [17] Thus, it is important to prepare for this event from the inception of the project. Otherwise, future wind farms will have to deal with the left-behind structures and develop their own decommissioning plan. Moreover, planning and designing for the decommissioning phase would make the disposal of the asset go smoother and would mitigate the costs, emissions, and impact on the environment.

Nevertheless the decision from the OSPAR convection, the plan for decommissioning is similar to the one for the installation. The tower, including all elements, will be placed on a floater or dynamically positioned (DP)/anchor handling/floating vessels and transported back to the shore. The companies that have been stated for installing the designed wind turbine, Heerema Marine Contractors [18], Cape Holland [19], and Boskalis [20] are able to provide such services.

The only potential issue with the wind turbine's last stage of life that can be encountered while disassembling the structure is the removal of the foundation. Since the monopile has a massive size and a large embedded length, it will be difficult to extract all of it. Any excavation work should be avoided as much as possible due to the marine environment created around its underwater part [53]. Besides the standard procedure of digging below the mud line, there are two other methods for decommissioning the foundation of a wind turbine. According to Cape Holland, it is proposed to apply pressure on the inside of the monopile which pushes the cylinder upwards in the same manner as with the extraction of the suction bucket. Secondly, a lifting tool and a vibro-hammer in one can be used in order to minimise the impact on the aquatic habitat. Moreover, especially using a hammer that can also provide small vibrations will contribute to significant cost savings. [21]

[17] URL: https://www.ospar.org/news/scm-21 [cited 06 June 2023]
[18] URL: https://www.heerema.com/heerema-marine-contractors [cited: 26 June 2023]
[19] URL: https://capeholland.com [cited: 26 June 2023]
[20] URL: https://boskalis.com/ [cited: 26 June 2023]
[21] URL: https://www.offshorewind.biz/2016/12/07/cape-holland-tests-decommissioning-tool/ [cited: 20 June 2023]

8

Cost analysis

In order for the MR-TBD design to be economically viable, the cost of the system has to be analysed. The main metric by which this is evaluated is LCoE. This analysis is performed based on data from Catapult [6]. This data is then modified in steps, based on the estimated effect of the differences between the MR-TBD design, and the reference 10 MW turbine used in the Catapult model [6]. Section 8.1 explains the cost model. The differences between the reference turbine and MR-MRS, and the resulting impact on cost are further described in Section 8.2. Section 8.3 then goes over the weight average cost of capital. The time to break even is discussed in Section 8.4. Finally, conclusions are drawn based on the analysis in Section 8.5.

8.1. Description of the Budget Model

In order to estimate the system's initial budget, the average cost breakdown of a traditional HAWT wind farm from the Offshore Renewable Energy Catapult was used [6]. The individual components of the cost breakdown were then modified based on various estimations of how the designed system differs from the HAWT wind farm. These assumptions are discussed in Section 8.2. Each stage of assumptions leads to a new LCoE (see Section 8.2). The costs provided by Catapult are broken down into the cost of the turbine, the balance of the plant, development and project management, installation and commissioning, maintenance and service, and operations and decommissioning. The Catapult offshore wind farm model uses a 1 GW wind farm consisting of 100 10 MW wind turbines located 60 km from shore at a 30 m water depth. Thus, the differences between the Catapult wind farm concept and the proposed wind farm concept significantly affect the costs of individual components of the model. The costs are normalised to €/MWh allowing the costs to be compared. The annual electricity production of around 4471 GWh per year (E_t) used in the LCoE calculation has also been taken from the Catapult breakdown. The equation for LCoE, adjusted for inflation, is given in Equation 8.1 [6].

- LCoE - levelized cost of electricity
- t - time in years
- I_t -Investment expenditure in year t
- M_t - Operations maintenance and service expenditure in year t
- E_t - Net energy generation in year t
- $n = 27$ years - Lifetime of the project in years
- $r = 3\%$ - Discount rate or WACC
- WACC - the weighted average cost of capital
- CapEx - The capital expenditure (including development expenditure)
- OpEx - The operational expenditure
- DecEx - The decommissioning expenditure
- O&M - Operations and Maintenance

$$\mathrm{LCoE} = \frac{\sum_{t=-5}^{n+1} \frac{I_t + M_t}{(1+r)^t}}{\sum_{t=-5}^{n+1} \frac{E_t}{(1+r)^t}} \tag{8.1}$$

CapEx is the turbine's plant balance, installation, and decommissioning capital expenditure. These are costs that are only incurred once. In contrast, OpEx is the operational expenditure that is mostly concerned with the operations and maintenance of the system. These are continuous expenses during operation. In light of this, the yearly OpEx can be multiplied by the system's lifetime to determine its effect on the final LCoE. The wind farm's lifetime was assumed to be 27 years, the same as the Catapult model. The discount rate heavily influences the LCoE. The Catapult model used a discount rate of 6%,E.C.M. Ruijgrok used 3%, and Freeman et al. didn't mention a discount rate [6, 55–57]. A dilemma arises, since the lack of a discount

rate for the WindEurope study, means a direct comparison with it is problematic [5]. It has been decided that a discount rate of 3% should be used since the study validated the "move" of the Catapult wind farm to a lower LCoE area using 3% as the discount rate [55].

8.2. Budget of the Proposed Design

Having established the model used and the performance goals (see Chapter 2), the modifications that will be applied, and the feasibility of achieving the goals will be assessed. It is important to note that, for the sake of conciseness, only changes to the original Catapult data will be shown in the tables.

There are five cost-driving differences between the proposed design and the conventional option. The key differentiators are shown below and will be further explained throughout this section.

1-2 Moving to lower LCoE areas (see Table 8.1)

2-3 Increasing power density from 5 MW/km^2 to 16 MW/km^2 (see Table 8.2)

3-4 Introduction of wake losses due to the increase of power density (see Table 8.3)

4-5 Switching from a conventional HAWT to a multi-rotor VAWT (see Table 8.5)

5-6 Recovering the production lost with a wake control system (see Table 8.6)

The power density increase will allow the planned capacity of 380 GW to fit into the very low LCoE area. This area is generally cheaper due to a shorter distance to shore and shallower water depth. The cost benefits associated with this are shown in Table 8.1.

Table 8.1: *Table showing the changes to the Catapult model to account for benefits of a lower LCoE location **(1-2)***

Name	LCoE Before	Change	LCoE After	Reason
Export cable	€ 1,91	-50,00%	€ 0,95	Closer to shore, less cable required
Foundation cost	€ 2,20	-66,00%	€ 0,75	Shallower water, smaller foundation
Offshore substation structure	€ 0,88	-33,00%	€ 0,59	Shallower water, less structure needed
Development and consenting services	€ 0,73	-33,00%	€ 0,49	Better understood regions, easier development
Offshore substation installation	€ 0,51	-50,00%	€ 0,26	Closer to shore, less rent time on equipment
Cable burial	€ 0,29	-50,00%	€ 0,15	Closer to shore
Cable pull-in	€ 0,11	-50,00%	€ 0,06	Smaller area of operation less rent time on equipment
Other (cable-laying vessel, survey works, route clearnace cable protection)	€ 2,73	-50,00%	€ 1,37	Closer to shore, less rent time on equipment
Turbine installation	€ 0,73	-25,00%	€ 0,55	Shallower water, easier and quicker installation
Sea-based support	€ 0,04	-40,00%	€ 0,02	Closer to shore
Maintenance of turbine	€ 8,56	-50,00%	€ 4,28	Closer to shore less time spent traveling
Maintenance of balance of plant	€ 4,67	-40,00%	€ 2,80	Closer to shore, less time spent traveling
Offshore logistics	€ 0,42	-30,00%	€ 0,29	Closer to shore
Turbine decommissioning	€ 0,27	-30,00%	€ 0,19	Closer to shore
Foundation decommissioning	€ 0,45	-33,00%	€ 0,30	Closer to shore
Cable decommissioning	€ 0,85	-50,00%	€ 0,42	Less cable to decommission
Substation decommissioning	€ 0,39	-30,00%	€ 0,27	Closer to shore
Total LCoE [EUR/MWh]	**€ 56,61**		**€ 43,82**	

Increasing the power density and therefore decreasing the turbine spacing in a wind farm has additional benefits. As turbines are closer to each other, the travel time between individual turbines shortens, and the length of the cabling connecting them is decreased. It also lessens the impact on the environment. The LCoE benefits of these changes are summarised in Table 8.2.

Table 8.2: *Table showing the changes to the Catapult model to account for the benefits of a higher density wind farm* ***(2-3)***

Name	LCoE before	Change	LCoE after	Reason
Array cable	€ 0,51	-50,00%	€ 0,26	Less area covered
Electrical system	€ 0,66	-15,00%	€ 0,56	Smaller system simpler to monitor
Facilities	€ 0,29	-15,00%	€ 0,25	Smaller area requires less facilities
Environmental surveys	€ 0,06	-20,00%	€ 0,05	Less area covered
Resource and metocean assessment	€ 0,06	-20,00%	€ 0,05	Less area covered
Cable burial	€ 0,15	-20,00%	€ 0,12	Less cable to bury
Cable pull-in	€ 0,06	-20,00%	€ 0,04	Less traveling, shorter rent periods
Electrical testing and termination	€ 0,10	-20,00%	€ 0,08	Less traveling, shorter rent periods
Other (cable-laying vessel route clearance cable protection)	€ 1,37	-20,00%	€ 1,09	Less traveling, shorter rent periods
Turbine installation	€ 0,55	-15,00%	€ 0,47	Less traveling, shorter rent periods
Sea-based support	€ 0,02	-20,00%	€ 0,02	Less area covered
Onshore logistics	€ 0,12	-15,00%	€ 0,10	Less area covered
Offshore logistics	€ 0,29	-15,00%	€ 0,25	Less area covered
Turbine decommissioning	€ 0,19	-15,00%	€ 0,16	Less traveling, shorter rent periods
Foundation decommissioning	€ 0,30	-15,00%	€ 0,26	Less traveling, shorter rent periods
Cable decommissioning	€ 0,42	-20,00%	€ 0,34	Less cable
LCoE [EUR/MWh]	**€ 43,82**		**€ 42,76**	

Unfortunately, the change in the power density will also have a negative performance impact. According to analysis performed by Ferreira, a traditional wind farm would lose about 30% of its electricity production due to wake losses [58]. The impact of lost production can be seen in Table 8.3

Table 8.3: *Effects of the wake on energy production and their impact on LCoE for a traditional HAWT* ***3-4***

Name	LCoE before [EUR/MWh]	Change	LCoE after [EUR/MWh]
Production lost due to wake	€ 42,76	42,00%	€ 61,03

The next step is to change the configuration of the wind farm from conventional single-rotor HAWTs to multi-rotor VAWTs. Changing the turbine design has large implications for costs. A big change stems from the multi-rotor VAWT allowing the use of components less optimised for weight. In addition to this, the design is more accommodating to maintenance, making it significantly cheaper. The design's influence on costs can be seen in Table 8.4 and Table 8.5. Table 8.4 shows part of the costs that could be evaluated based on data from the Chapter 5. In that table, a value that describes the size of the subsystem is compared between a reference 10MW HAWT and the MR-TBD. For subsystems that have not been sized yet, Table 8.5 shows the anticipated price changes.

Table 8.4: *A data-driven cost analysis based on the approximate sizing*

Component	Reference data	MR-TBD data	Change	New LCoE
Bedplate	8.24 t/MW [59]	10.40 t/MW	26%	€ 0.53
Main shaft	5.9 t/MW (3.2 EUR/kg) [60]	48.6 t/MW (0.5 EUR/kg)	28%	€ 0.54
Yaw system	30 KNm/MW	26.7 KNm/MW	-11%	€ 0.32
Yaw bearing	0.3t/MW	1.8 t/MW	500%	€ 0.21
Blades	151 000 EUR/MW [6]	10 000 EUR/MW	-96%	€ 0.03
Steel for the tower (including HLDs)	62.9 t/MW [61]	111 t/MW	76%	€ 0.67
Foundation cost	207 t/MW [61]	205 t/MW	-1%	€ 1.06
Turbine maintenance	Based on RAMS	Based on RAMS	-60%	€ 2.45
Gearbox	198m diameter TSR 9 [61]	45m diameter TSR 4.5	-55%	€ 0.67
Generators	198m diameter TSR 9 [61]	45m diameter TSR 4.5	-55%	€ 0.95

Table 8.5: *Table showing the changes to the Catapult model to account for benefits of a multi-rotor VAWT* ***(4-5)***

Name	LCoE before [EUR/MWh]	Change	LCoE after [EUR/MWh]
Main bearing	€ 0,42	-50,00%	€ 0,21
Power take-off	€ 2,10	-10,00%	€ 1,32
Nacelle auxiliary systems	€ 0,15	-50,00%	€ 0,07
Nacelle cover	€ 0,21	-50,00%	€ 0,10
Small engineering components	€ 0,52	10,00%	€ 0,58
Structural fasteners	€ 0,15	50,00%	€ 0,22
Hub casting	€ 0,31	-75,00%	€ 0,08
Blade bearings	€ 0,42	-100,00%	€ -
Pitch system	€ 0,21	-100,00%	€ -
Fabricated steel components	€ 0,11	-33,00%	€ 0,08
Tower internals	€ 0,15	20,00%	€ 0,18
Other (includes assembly, wind turbine supplier aspects of installation and commissioning profit and warranty)	€ 7,13	20,00%	€ 8,56
Array cable	€ 0,37	-25,00%	€ 0,28
Transition piece	€ 2,10	50,00%	€ 3,15
Corrosion protection	€ 0,42	25,00%	€ 0,52
Development and consenting services	€ 0,70	25,00%	€ 0,88
Engineering and consultancy	€ 0,08	25,00%	€ 0,10
Foundation Installation	€ 1,05	-33,00%	€ 0,70
Cable burial	€ 0,17	-15,00%	€ 0,14
Cable pull-in	€ 0,06	-30,00%	€ 0,04
Other (cable-laying vessel seruvey works, route clearnace cable protection)	€ 1,56	-15,00%	€ 1,33
Turbine installation	€ 0,67	-20,00%	€ 0,53
LCoE [EUR/MWh]	**€ 61,03**		**€ 54,29**

The final LCoE is obtained by applying the effects of wake re-energization. The MRS-VAWT layout is conducive to placing large high-lift devices producing upwash. This should recover the energy production to levels comparable with conventional wind farms [58]. The final LCoE value can be seen in Table 8.9

Table 8.6: *Impact of wake control on LCoE in a VAWT design **(5-6)***

Name	LCoE before [EUR/MWh]	Change	LCoE after [EUR/MWh]
Production gained due to wake control	€ 53,29	-30,00%	€ 38,01

It is important to recognise that the cost analysis performed has some limitations. Regarding error accumulation, wake loss calculations are investigated. Wake losses influence energy generated. In steps 2-4, wake losses are introduced, which are removed in steps 5-6 due to the wing on the structure. If errors were made using estimating these wake losses, they should destructively annihilate since the energy efficiency at 1 is the same as in 6.

8.3. Weight Average Cost of Capital

The weight average cost of capital (WACC) is an important metric for any investment. It dictates which projects are built and which are never considered. The easiest way to see if the MR-TBD is a better investment than traditional HAWTs is to see what WACC can be achieved for both configurations. There were two targets set in Chapter 2. One for expanding the production in the North Sea up until 2050 and one for expanding production past 2050. The first assumes that wind turbines can still be placed in relatively cost-attractive areas, while the other assumes that these spots were already used, so the MR-TBD is used to increase the energy density in already existing or just decommissioned farms. Both targets assumed that the traditional designs achieve WACCs of around 3%. In Table 8.7 the WACCs achievable by MR-TBD are shown.

Table 8.7: *WACC comparison between conventional HAWT and MR-TBD*

Sale price of energy	54€/MWh	65€/MWh
Traditional design return on investment	3%	3%
MR TBD	6.7%	8.7%

From the analysis, it is clear that MR-TBD can achieve ROIs much higher than conventional HAWT designs and could remain profitable for longer, despite adverse market forces.

8.4. Time to Break Even

The last financial factor to calculate is the time to break even (TtBE). This metric shows how much time needs to pass for an investment to recoup the upfront costs. With a lower initial cost to install and with lower maintenance costs, it is easy to foresee that the proposed design should have a shorter TtBE. This is confirmed with calculations, the results of which can be seen in Table 8.8.

Table 8.8: *Years of operation to break even*

Sale price of energy	54€ /MWH	65€ /MWh
Traditional design return on investment	13.4 years	11 years
MR TBD	9 years	7.3 years

8.5. Conclusion and Final Budgeting

There are a few takeaways from the cost analysis. A concise visualization of the budgeting of the wind turbine can be seen in Figure 8.1 and Figure 8.2. The most crucial takeaway from the analysis is that, depending on the target selected, building wind energy in the North Sea now or replacing old wind farms beyond 2050, the design slightly underachieves or overachieves. If the goal is to lower the LCoE by 45% for the development of the North Sea now, then the design is not economical enough. The LCoE estimate is 8€/MWh over the target value. However, E.C.M. Ruijgrok indicates that there are many locations with an LCoE under 40€/MWh, which suggests that the analysis in steps (1-2) is on the conservative side [55]. This means that an LCoE of 36€/MWh is plausible, although hard to achieve. If the goal is to provide an excellent alternative to increasing the power capacity in the North Sea beyond 2050, the design would be a great candidate. This means the proposed design would be a good replacement for ageing turbines in the future.

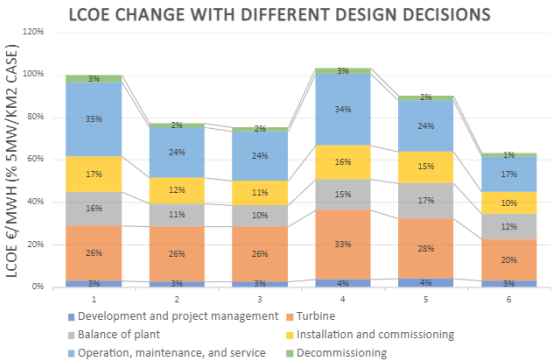

Figure 8.1: *LCoE change as a percentage of 5MW/km^2 case with different design changes*

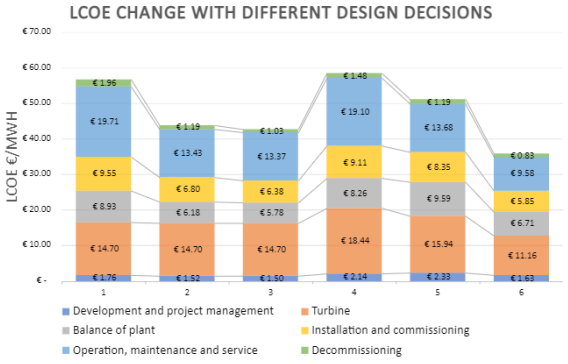

Figure 8.2: *LCoE change as absolute with different design changes*

Table 8.9: *Comparison of the final LCoE for MR-TBD and a conventional HAWT*

	LCoE [EUR/MWh]
Conventional HAWT	58
MR-TBD	38

9

Sustainability

In this chapter, the sustainability strategy is presented. The scope of this chapter addresses both the way sustainability is taken into account in the design and the way the product or system contributes to sustainability. Impacts have been broken down into environmental, economic and social sustainability aspects.

9.1. Environmental sustainability

One of the main pivots of this project is its sustainability aspect. The project's mission objective itself states that to have a successful design, it is crucial to improve the system's sustainability under different factors, including materials, energy, and emissions. To achieve this, a life cycle study needs to be performed, and the environmental impact of the final design needs to be assessed. This is what this section is going to focus on.

A life cycle analysis (LCA) is a systematic study used to assess the environmental impacts of a product, process, or service throughout its entire life cycle. For this project, this study aims to evaluate the ecological impact of the MR-TBD turbine throughout its whole life cycle phases, from the extraction of materials to decommissioning. This analysis helps identify areas where improvements can be made to minimize environmental harm and promote sustainable practices.

Multiple LCAs were performed in recent years about different conventional wind turbines [62, 63]. Depending on the level of detail of the study, various factors can be considered, including resource consumption, energy use, emissions to air, water, and soil, and potential impacts on human health and ecosystems. Since the MR-TBD is still in the early phase of the design, the only two factors that are considered in this study are the energy consumed and the CO_2 emissions generated during its life cycle.

To perform a complete LCA, it is crucial to define all the life cycle phases of the turbine as well as define all the components that make up the structure with their respective materials. The MR-TBD consists of many components with different electrical and mechanical parts; hence, gathering information on all the parts composing it is challenging. Consequently, the team has used the Ansys Granta MaterialUniverse database to collect all the necessary information about materials and production methods and to perform the detailed LCA analysis. Ansys Granta aims to provide the user with an easy-to-use database of materials properties as well as analysis tools for environmental, production, and cost estimations. After obtaining the necessary information on the weight and the materials of all the individual subsystems, the following life cycle inventory was defined:

Table 9.1: *Final design inventory table*

Subsystem	Elements	Percentage of total [%]	Weight [ton]	Material	Manufacturing process
Truss structure	Structure	58.11	2455.00	AISI1040 medium carbon steel	Welding
	Shafts	34.51	1458.00	Medium carbon steel	Fine, coarse machining
	Base plate	7.38	312.00	High carbon steel	Rolling
	Total		4225.00		
Rotors	Blades	73.25	115.00	Low carbon steel	Forming, welding (extrusion)
	Bearings	26.75	42.00	AISI5046 low alloy steel	Fine machining, grinding
	Total		**157.00**		
Foundation	Monopile		6140.00	S355 low carbon steel	Welding, rolling
Wake management	HLD		1088.00	medium carbon steel	Forming, welding
Yaw system	Bearings		100.00	AISI5046, silicon nitride	Coarse machining, grinding
Electrical subsystem	Generator	54.69	84.00	Copper, cast iron, low carbon steel	Assembly components
	Cables	11.72	18.00	Copper	Wire drawing
	Gearbox	15.63	24.00	Low alloy/medium carbon steel	Fine machining, grinding/low pressure die casting
	Converters	15.63	24.00	Resin, copper, fibre glass	Outsourcing
	Brake	2.34	3.60	Low alloy steel	Casting
	Total		**153.60**		
		Total weight	11863.60		

In addition to showing the number of elements per subsystem, Table 9.1 presents all their respective materials as well as their manufacturing processes. These last have been described in detail in Section 7.1. For simplicity, only the main elements of the overall design that account for the most environmental impact have been considered. It is important to notice that some structural elements have not been included in this analysis, although their environmental impact is considerable. An example of this is the concrete used to fix the foundation underwater. This choice has been made due to the fact that in the entire design process, the sizing of this part of the foundation has never been considered. Taking it into account is one of the Post DSE activities Section 12.1.

The overall emissions and energy consumption of the following design phases have been considered:

- Extraction of materials
- Production and assembly of components
- Transportation
- Installation
- Operations
- Decommissioning and recycling

9.1.1. Extraction of materials impact

Materials are made from naturally occurring ores or feedstocks. Making them requires energy and releases emissions on a very large scale. The main parameter considered for this section of the LCA is the so-called embodied energy of the material. This is a crucial parameter since it represents the energy required to create 1kg of usable stock. As the MR-TBD is almost entirely steel-made, multiple aspects of this material must be considered to assess the environmental impact of its extraction and processing. Extracting steel often involves large-scale mining operations, which can have an adverse environmental footprint. Its extraction and processing for wind turbine applications require high energy inputs due to high energy-intensive processes like mining and refining. These contribute to greenhouse gas emissions and the consumption of non-renewable energy sources. Supply chains for wind turbines are also very complex, leading to high transportation emissions. For this project, the material extraction and processing accounts for almost 70% of the overall emissions. Specifically, the energy consumed amounts to 68.5% of the overall energy consumed, while the CO_2 footprint account for 69.4%. Consequently, the total energy consumed for this phase of the MR-TBD's life cycle is 120 TJ. On the other hand, the t of CO2 generated are 9600. This is a very reasonable result, also considering the amount of materials the MR-TBD will need to produce. A more detailed table of this life cycle phase is shown in Appendix A.

9.1.2. Production and assembly of components impact

The manufacturing of the MR-TBD is also a critical stage of its life cycle. This phase, in fact, can be considered the second most polluting aspect of the design, accounting for 25% of the overall emissions. The variable characterizing it is the processing energy, the total energy used to shape, join and finish 1kg of material to create a component or product. The overall CO_2 emissions and energy consumption of this life cycle phase are caused by multiple things and are highly dependent on the material and manufacturing process. Manufacturing wind turbine components requires a significant amount of energy, mainly sourced from power plants. These rely on fossil fuels and emit greenhouse gases and other pollutants during electricity generation. Secondly, manufacturing processes involved in producing the MR-TBD, such as steel fabrication, casting, forging, machining, and assembly, generate a considerable amount of CO_2. In addition to this, especially for some specific material processing, chemicals may be used. Inadequate handling, storage, or disposal of these chemicals can lead to environmental pollution, including soil and water contamination. For this phase of the LCA, the material processes considered in Section 7.1 are considered. As can be seen in Appendix B in Table B.2, some manufacturing processes slightly differ from the ones considered in Section 7.1. This is due to the fact that for a few processes, data was not present in the Ansys database. To fix this, similar manufacturing processes, both in terms of emissions and final products, have been selected for the LCA. In light of this, the emissions related to this life cycle phase are presented: 48 TJ of energy consumed and 3600 t of CO_2.

9.1.3. Transportation impact

For transportation, the environmental impact has been assessed according to the logistics plan presented in Section 7.3. The impact on the environment of this design phase mainly comes from the routes that the MR-TBD elements need to follow before finalizing the construction at the wind farm site. It is important to note that the transportation related to raw materials extraction and processing is not considered. Instead, they are considered in the extraction of materials subsection. Specifically, the ecological impact of two main routes has been evaluated. Assuming that all the steel needed to build the structure is already in the Netherlands, it will need to be transported from the different steel companies to the Damen Verolme drydock in Rotterdam. These companies are a few and spread over the Netherlands. Consequently, an indicative route of 113km by train is considered due to the small size of the country and the efficient transportation network. The second transportation route consists of moving the assembled structure from the drydock to the Ijmuiden Ver site. This will be performed by medium size coastal freights that will tug the entire structure for 115 km. This being said, the overall transportation ecological impact results to be extremely small compared to the other phases (0.5%). This is mainly due to the fact that the entire structure will be manufactured in the Netherlands and will use accessible materials. The energy consumed for transportation is 828 GJ, while the CO_2 footprint is 59.6 t.

9.1.4. Operations impact

The impact of wind turbine operations is mainly related to maintenance. During most of its life, the MR-TBD will not produce a lot of emissions. Most of them come from the transportation of crew members and repairing materials. Since the complete maintenance strategy has not yet been defined at this stage of the design process, assumptions were made regarding the most likely route. As a consequence, an average of 5 visits per year per 25 years has been assumed to assess the environmental impact of this design phase. This number is based on the results obtained in the RAMS Section 7.2. The vehicles used to maintain the structure are small-size coastal freights operating at maximum power. The route's starting point is assumed to be 65km far from the wind turbine site, which is the average distance of the turbine from the coast. In light of this, 130km routes need to be followed to perform maintenance 5 times a year per 25 years. This being said the operation phase of the MR-TBD turbine accounts for less than 1% of the overall emissions for both energy consumed and CO_2 emissions. Therefore, this contribution to the system's ecological impact can be neglected.

9.1.5. Decommissioning and recycling impact

The last two phases of the life cycle of the MR-TBD wind turbine to be assessed consist of decommissioning and recycling. The decommissioning and recycling phases of the MR-TBD turbine involve its removal from the site location at the end of its operational life and the subsequent recycling or disposal of its components. Due to the fact that the time to decommission a wind turbine is pretty low, compared to the installation one, this phase of the design will have an almost negligible impact on the overall emissions of the turbine itself. This, in fact, contributes to 4.25% of the total environmental impact. On the other hand, the recycling aspect of the turbine life cycle cannot be ignored. This is, in fact, one of the most important aspects that designers need to consider in order to have a final product being as sustainable as possible. Being mostly made of different types of steel, the recyclability potential of the turbine is pretty high. The main reason is that there is a strong and consistent demand for recycled steel in various industries. The market for it is well-established and economically viable and could represent an additional source of income for the project. Based on the percentage of steel reused, it is possible to reduce the overall impact of the wind turbine up to 10/15%. For the MR-TBD turbine, the percentage of recycled material has been chosen to be 90%. This leads to the following result: a reduction of -27 TJ of energy and -2000 t of CO_2 emissions reduction to the overall project's environmental impact. This is an incredible result since it corresponds to a reduction of 15% of the consumed energy and CO_2 emissions for recycling 90% of the entire structure

9.1.6. Summary of the results

In light of all these results obtained previously, Figure 9.1, Table 9.2, Figure 9.2, and Figure 9.3 presents a summary of the overall environmental impact of the turbine:

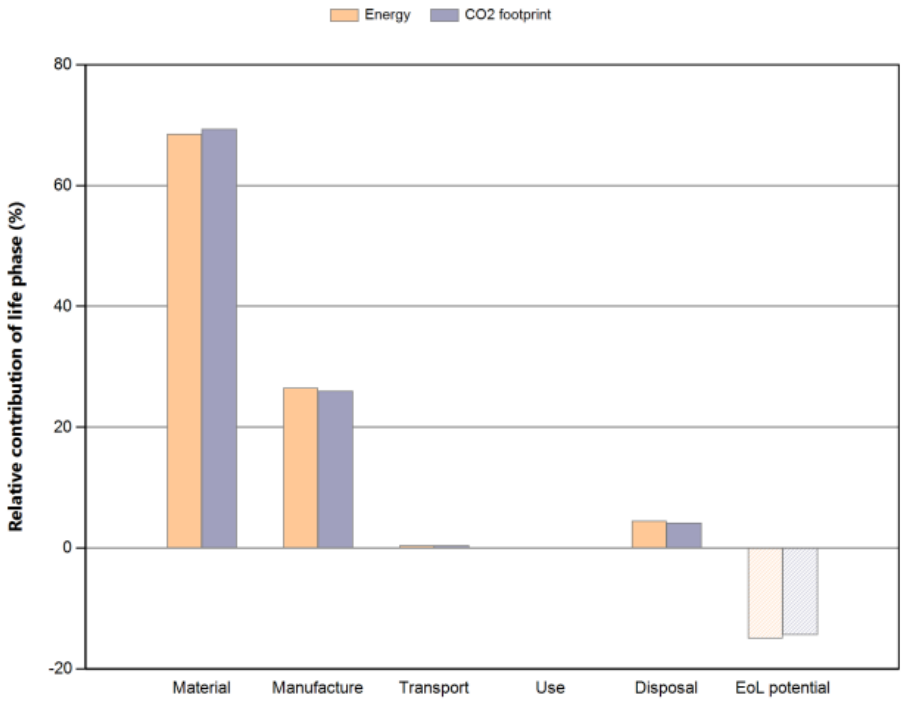

Figure 9.1: *Summary of the contributions of each life cycle phase to the overall environmental impact*

Table 9.2: *Summary table of the contributions of each life cycle phase to the overall environmental impact*

	Energy [MJ]	Energy [%]	CO2 mass [kg]	CO2 mass [%]
Phase				
Material	1.20E+08	68.5	9.64E+06	69.4
Manufacture	4.82E+07	26.5	3.61E+06	26.0
Transport	8.28E+05	0.5	5.69E+04	0.4
Use	7.91E+04	0.0	5.70E+03	0.0
Disposal	8.21E+06	4.5	5.75E+05	4.1
Total (for first life)	1.82E+08	100.0	1.39E+07	100.0
End of life potential	-2.72E+07		-1.99E+06	

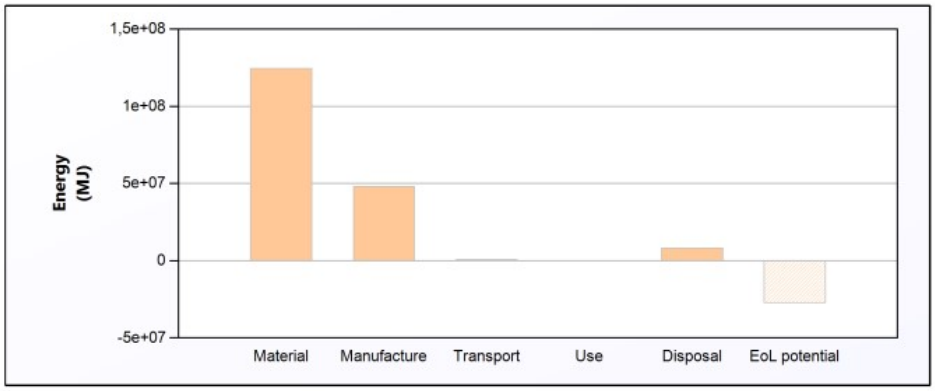

	Energy (MJ/year)
Equivalent annual environmental burden (averaged over 25 year product life):	7,28e+06

Figure 9.2: *Summary of energy consumption of each life cycle phase of the design*

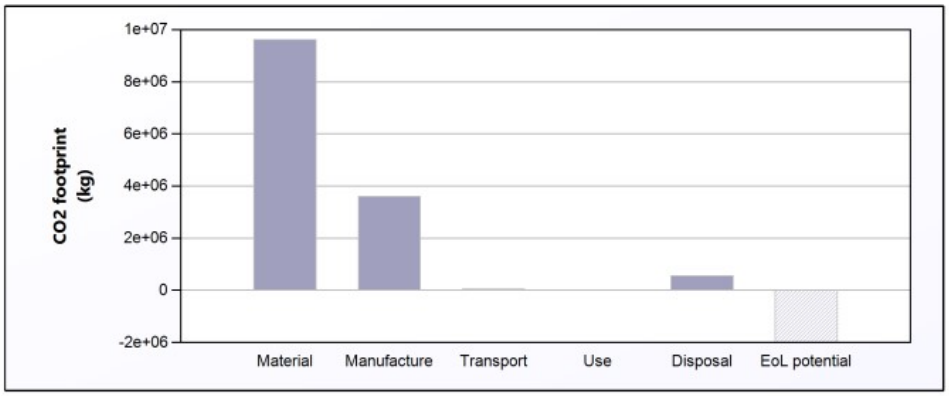

	CO2 (kg/year)
Equivalent annual environmental burden (averaged over 25 year product life):	5,55e+05

Figure 9.3: *Summary of CO_2 of each life cycle phase of the design*

All the numbers that are presented in this chapter come from multiple estimations. The most important one is that the concrete needed to set up the foundations has been neglected. In addition, the routes of the materials and components are also an estimation approximated by Ansys Granta. Finally, smaller complex elements of the structure, such as sensors, PCBs, lubricants, and non-steel metals, have been neglected too to simplify the study. This introduces uncertainties that can only be evaluated, increasing

the level of detail of the study. Being a design synthesis, the scope of this LCA section is not to give precise values but to give the reader an idea of the ecological impact of the project, compared to conventional wind turbines. Based on the results found in Section 7.3 about the annual energy production of the MR-TBD, the total amount of grams of CO_2 per kWh produced by the turbine is 3.73. Several LCA studies have been performed that analyze offshore wind turbines' ecological impacts. Raadal et al., Wang and Sun tried to evaluate the potential for wind energy to mitigate the effects of climate change by reducing CO2 [64, 65]. They did this by performing a comparison between different types of wind turbines, both onshore and offshore. Wang and Sun calculates a CO_2 emission per kWh of 5.23 g. From this, it can be concluded that the MR-TBD is more sustainable in terms of CO_2 emissions due to its very accessible materials and improved life cycle performance, with a CO_2 reduction of 37%. This reduction is mainly due to the high recyclability of the design, by not using composite blades, and short supply lines from manufacturing to assembly and deployment.

9.2. Economic

Economic sustainability refers to the strategy and practices of a business to prioritise long-term economic development over short-term profits. The management of resources, labour protection and safety, encouragement of investments in renewable energy, growth of micro-, small- and medium-sized enterprises, and eliminating waste are all key concepts relating to economic sustainability. As sustainability is a core concept of the proposed system, the engineering team has been making several design choices in order to appeal to the economic sustainability targets established by the UN. By doing so, a number of decisive actions have been formulated to encompass the used economic sustainability strategy:

Restrict the use of REM: A majority of rare Earth metals used in drivetrains in current wind turbine designs are mined in China, with 70% market share of all REM in 2022 according to the U.S. Geological Survey [1]. With rising political and ideological apathy between the Western world and China, it is important to consider the origin of all resources through the lens of possible embargos. Moreover, as the trade restriction imposed by the EU and the US towards Russia, it is becoming apparent that the allocation of resources can become at least a deterrent, or at most an economic weapon. In this spirit, the proposed design has focused on eliminating REM and moving towards locally and readily available materials such as copper and steel alloys. Through this strategy, it is believed that the proposed design can contribute to investment and energy safety.

Promote effective use of natural resources: Perhaps the most used and most essential natural resource in the wind energy department is the wind itself. Yet, current wind farms output, on average, between 35% and 45% capacity factors for the last decade, according to Statista [2]. The proposed design was evaluated to have a capacity factor of 56.7%, as given by the total energy production calculated in Section 7.3 and divided by the annual rated energy production. With the implementation of the wake control subsystem, the capacity factor will not decrease with the size of the wind park. Moreover, by improving on the power density of conventional wind turbines, the proposed design can utilise prime offshore parcels rated for low LCOE more efficiently and effectively. Thus, the energy needs of the country could be met through more sustainable and ecological means without having the negative impact of restricting sea space now allocated for other economic uses.

Minimize waste: All structural materials have been chosen so that they can be recycled upwards to 90%. Additionally, the rotor blades, which are conventionally made out of fibreglass composites and are difficult if not impossible to recycle, have been manufactured out of structural steel. This was possible through the innovation in the rotor concept of using the vertical axis configuration coupled together with low rotor RPM operations. Yet, not only material waste was considered, but also

[1] URL: https://pubs.usgs.gov/periodicals/mcs2023/mcs2023-rare-earths.pdf [cited on 20 June 2023]

[2] URL: https://www.statista.com/statistics/1368679/global-offshore-wind-capacity-factor/#:~:text=Between%202010%20and%202021%2C%20the,wind%20stood%20at%2039%20percent. [cited on 20 June]

time waste during energy production. Through design decisions concerning the drivetrain, rotor and tower, the accessibility, maintainability and repairability were improved when compared to a conventional WT. Moreover, the capability to replace important assemblies, such as gearboxes, and make repairs onshore without having prolonged downtime further minimises wasted time, and in turn, wasted energy

Promote affordable and cheap energy: Investing in the green energy sector through novel and high performing designs improves the detachment from conventional GHG emissive energy sources. Through the development of this system, the engineering team is facilitating the Dutch governmental plan of expanding wind energy production in the North Sea to 380 GW by 2030. This will assure that electricity is not subjected to high volatility caused by external or malicious factors, such as how the price of oil driven by the invasion of Ukraine by Russia caused an increase in spot price of up to 1000% [3]. Moreover, as the wind is a free resource, the design towards long life and high maintainability will reduce the cost of electricity, leading to more affordable energy for the consumer.

9.3. Social

Social sustainability concerns the management of the impact imposed by businesses on people, communities and society in general. The cornerstone of social sustainability is covered by the first six UN Global Compact principles and focuses on labour rights and equity, protecting future generations from avoidable concerns, helping and empowering communities at risk and promoting human rights. The proposed design has been engineered with social sustainability in mind from its inception, as a good relationship with stakeholders can increase the social acceptance of large-scale projects such as this one, facilitating development in the process. In this sense, the further social sustainability aspects were considered:

Improving labour safety: Forbes estimated that in 2011 wind turbines contributed to 163 accidents leading to 14 deaths in England alone [4]. The engineering team was aware of the great health hazard imposed by maintenance procedures and made an objective to create better and safer work conditions for the repair crew. Firstly, all electrical and mechanical drivetrain components have been moved to a much lower height compared to traditional wind turbines to avoid accident risks. Furthermore, these components, which usually have the highest failure rates and downtimes, have been placed on a spacious platform in order to avoid cramped working conditions. Lastly, multiple sensors and a pre-emptive maintenance strategy were employed in order to minimise the number of visits to the turbine altogether.

Avoiding REM: As mentioned in the previous section, a majority of rare Earth metals come from China. This increasing demand for RRM has sparked a multitude of illegal, toxic and unsafe mining sites all around the resource-rich regions of China. The Yale School of the Environment has conducted an investigation into the illegal RRM mining operations in southern Jiangxi and reported on the great environmental impact on the hillside of the region [5]. The two main mining methods include the use of harmful chemicals and acids, and the removal of layers of topsoil, both having a destructive and long-term effect on the region. By not using RRM in the design, the MR-TBD team takes a stance against these practices and acknowledges the vicious cycle of a green future dependent on the hazardous mining of natural resources.

Improving equity in OEM distribution: In the current wind energy market only a handful of businesses are able o manufacture large off-shore wind turbines, such as GE, Gamesa, and Vestas. By employing

[3] URL: https://www.statista.com/statistics/1314549/netherlands-monthly-wholesale-electricity-price/ [cited on 20 June 2023]

[4] URL https://www.forbes.com/sites/jamesconca/2013/09/29/forget-eagle-deaths-wind-turbines-kill-humans/?sh=252f59215467 [cited on 20 June 2023]

[5] URL: https://e360.yale.edu/features/china-wrestles-with-the-toxic-aftermath-of-rare-earth-mining [cited on 20 June 2023]

ordinarily available materials and common manufacturing practices, the MR-TBD team encourages small to medium OEMs to tackle the production of wind turbine parts and assemblies. It is believed that through a bigger manufacturing pool, the smaller and local businesses can thrive and compete against the established manufacturers, leading to more prosperity and innovation.

Protect fisheries and fishermen: The MR-TBD design was specifically conceived in order to yield a higher energy density compared to traditional HAWTs. Through this, the team takes affirmative action to protect the North Sea fishing grounds and the people dependent on them from the ever-expanding plans for the installation of wind energy. By having higher energy density systems, it is possible to obtain more electricity without infringing on fishing and protected grounds, maintaining the health of the natural habitats that reside in the North Sea and protecting the livelihood of the people who depend on them.

10

Technical Risk Assessment

In this chapter, the technical risk assessment of the project mission is performed. This consists of identifying the technical risks that affect the success of the project mission. The risks are quantified according to their perceived probability of occurrence and seriousness of impact. Next, a mitigation plan is devised for the risks that pose the highest impact on the project mission to bring them down to an acceptable level, including contingency for the risks that remain at a high level.

10.1. Risk Identification

Risk categorisation

To identify the technical risks affecting the designed system, risk categories were first identified to break down the aspects of the project where risks might arise. This is broken down into:

Technical performance risks These affect the system during operation, causing it to perform at a lower performance level than required. These risks can be broken down for each subsystem at this design stage.

Cost risks These are risks that can increase the project's costs beyond the allocated cost budget.

Scheduling risks These are risks that can cause a delay in the scheduling of the project mission. This includes the system's design, production, transportation, operation, and decommissioning.

Sustainability risks Since sustainability is a driving factor in the design of this mission, risks related to not meeting the sustainability goals of the system or inadvertently becoming unsustainable are included in this category.

Programmatic risks These are risks that result from events out of the control of the project management. This can include events arising from higher management or international or national directives. This can also include natural disasters and other events that pose a risk to the mission's success.

The likelihood of the risks is categorised into: very unlikely with a chance of occurrence less than five percent (<5%), unlikely (<25%), plausible (<50%), likely (<95%) and very likely (>95%). Furthermore, the consequences were divided into negligible, marginal, critical and catastrophic implications for the project. Negligible risks incur no reductions in technical performance; marginal risks incur a slight reduction in technical performance; critical risks reduce technical performance significantly to a point where system success is questionable; catastrophic risks cause some of the mission requirements not to be achieved, leading to mission failure [1].

A few subsystem risks were added based on a literature review. Hou et al. discuss several risks related to the monopile subsystem [66]. During installation, these include pile sliding due to soil properties, hammer refusal if the monopile is allowed to set while installing, and damage due to crane accidents. The operational risks include scouring and corrosion due to the sea environment, fatigue failure and collisions with ships [66]. For the generators and gearbox, Shafiee and Dinmohammadi present a fault tree diagram that outlines the standard failure modes, including wear of gearbox teeth, over-warming and abnormal vibrations [67]. Additionally, a fault tree diagram describes a few potential modes of failure for rotor blades [67]. Thermal cycling has been described to cause 55% of converter failures, followed by vibration-induced failures at 20% by Sepulveda et al., considering that the power converter shows high failure rates [68].

In the final stage of design, each subsystem's weaknesses presented risks that became more clear while getting further into the design and some previous risks were no longer considered as it became clear that they would not present a threat to the project. For example, as shown in Figure 10.1, the WCT faced some

[1] URL: https://brightspace.tudelft.nl/d2l/le/content/498709/viewContent/2937470/View [cited 19 June 2023]

risks of retraction during higher wind speeds, as it generates much more force on a structure in these conditions. The YCT subsystem showed to be unstable during wind speeds higher than the rated wind speed, this also posed a risk that was only discovered during the final design.

Some risks are present under two different subsystems. For example, the YCT and RTR subsystems have bearings and the same risks under different codes. This is because despite the risks being the same, yaw-bearing risks present more considerable consequences as only one yaw-bearing system supports the whole structure. In contrast, the rotor bearings only support the rotor, making their failure consequence less critical. Due to dividing the risk into multiple smaller subsystems, the rotor and drivetrain subsystems present mostly marginal risks as they only heavily affected the performance of only one rotor assembly. Taking all the above into account, the identified technical risks of the project are laid out in Figure 10.1.

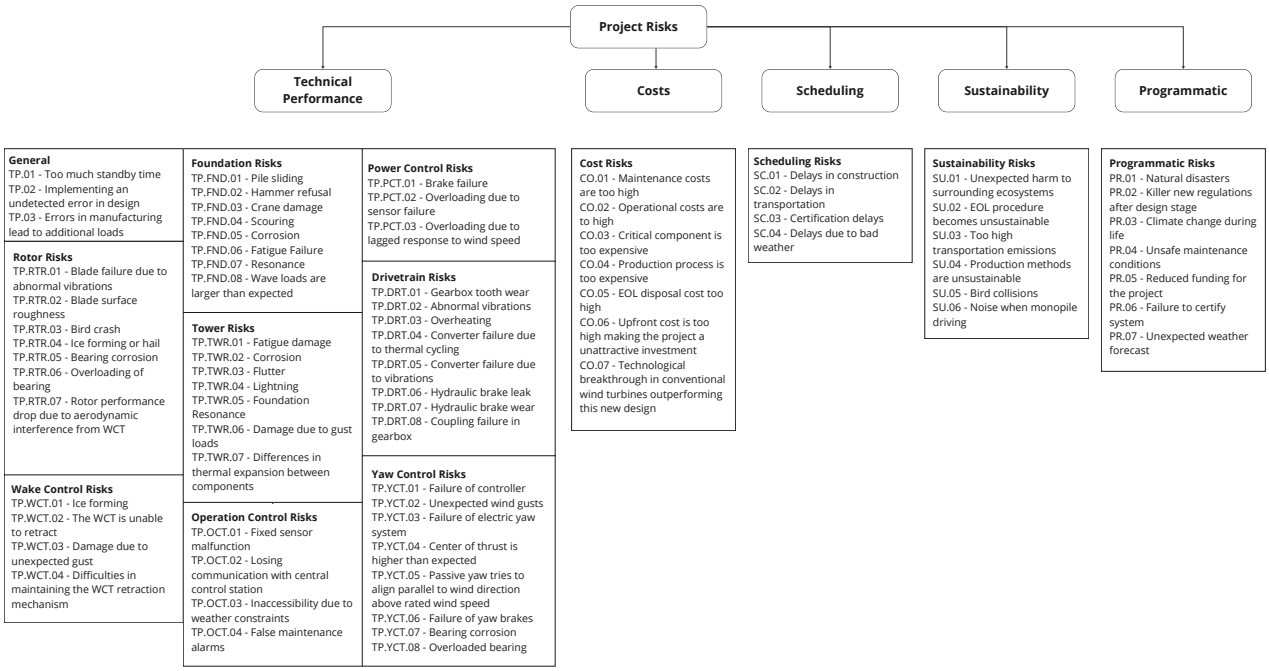

Figure 10.1: *Project Risks*

For each of these risks, the likelihood and consequence are predicted and added to the risk matrix in Figure 10.2. Risks that have been mitigated are highlighted in bold.

10.2. Risk Management

In this section, risk mitigation measures are determined for the risks with the highest combination of likelihood and consequence (risks in the top right corner of Figure 10.2).

Table 10.1: *Reasoning and mitigation for highest risks*

Risk	Reasoning	Mitigation
TP.TWR.05 - The truss structure resonates with the rotor frequency	Structural members may be damaged due to resonance with the rotor frequency.	A more detailed natural frequency analysis should be performed. If natural frequencies are still close to the rotor frequency, dampeners can be installed in the mounting brackets of the shaft bearings.
TP.TWR.07 - Differences in thermal expansion between components	Can cause high additional stresses in structural members leading to buckling, especially in interfaces between different materials.	Thermal expansion should be modelled, and the design should be modified to withstand these loads.
SU.01 - Unexpected harm to surrounding ecosystems	The wind farm may seriously impact the surrounding ecosystems. This would have catastrophic consequences leading to mission failure since institutions will never allow the building of the farm.	Study site ecology. Avoid fragile areas. Minimise system size. Minimise noise emissions
PR.04 - Unsafe maintenance conditions	Maintenance design is a crucial element of a wind turbine design. Therefore, it is a critical risk not to have safe maintenance procedures.	Apply a strict safety procedure for operators. Design for facilitated maintenance. Automate maintenance as much as possible. Minimise maintenance
PR.07 - Unexpected weather forecasts	Unexpected weather conditions might lead to the structure has to withstand higher wind speeds than it is ready for or not standby on time.	Implement emergency procedures to prevent damage. Design for unexpected weather conditions.
SU.05 - Bird collisions	Bird populations can be reduced by wind turbine collisions. This is a big risk to the sustainability of the project.	Minimise the size of wind turbine for power produced. Include sensors/deterrents for bird migrations. Turn off the turbine if bird migrations are detected.
TP.TWR.02 - Corrosion	Corrosion of the tower structure is very likely to occur due to high salinity in offshore conditions. This can negatively affect the material properties of the tower.	Use corrosion-resistant coating. Monitor corrosion of vulnerable components.
TP.YCT.07 - Bearing corrosion	Corrosion of bearings is very likely to occur due to high salinity in offshore conditions. A corroded bearing has lower load capabilities and is more likely to fail. This is a critical risk since the yaw bearing holds the whole tower.	Use corrosion-resistant materials or paints. Monitor corrosion of vulnerable components.
TP.YCT.08 - Overloading of bearing	Overloading the bearing can lead to bearing failure, which not only leads to failure of the YCT but also reduces the bearing capability of withstanding tower loads, leading possibly to catastrophic failure	Oversize the yaw bearing. Add supporting elements to support bearing

TP.OCT.03 - Inaccessibility due to weather constraints	During extreme weather conditions accessing the turbine might be impossible. This is often the time when unscheduled maintenance is most likely to be needed, so a lot of damage can occur due to this risk	Add automatic shutdown algorithms to the turbine. Increase health monitoring cameras/sensors to reduce the need for manual inspections.
TP.TWR.04 - Lightning	Lightning is certain to strike the tower during its lifetime. Lightning can cause damage to material and electrical components of the turbine and is the leading cause of unplanned downtime in wind turbines, leading to a much higher maintenance cost [69].	Include wind turbine grounding system. Construct blades with conductive material to avoid lightning arcs. Add surge protectors to electrical systems [69].
SU.04 - Production methods are unsustainable	Production methods will always have at least a small amount of emissions produced. Therefore production methods will never be 100% green. Consequently, this is very likely to be present but, at the same time, marginal.	Optimise logistics. Use manufacturing methods that minimise waste. Employ lean production. Recycle waste
SU.06 - Noise when monopile driving	Monopile driving emits large amounts of noise, capable of killing marine life in the vicinity [70]. Since the monopile used is large, the noise level will be even greater and have a devastating effect on the sustainability of the project.	Use bubble curtains while monopile driving. Pile driving with vibratory hammers [70].
TP.RTR.04, TP.WCT.01 - Ice forming or hail	Ice forming is almost certain due to the cold of the north sea, it can negatively affect the aerodynamics of the rotor and WCT and cause damage.	employ de-icing systems.
TP.DRT.04 - Converter failure due to thermal cycling	This is a likely failure mode for converters due to the different expansion coefficients of different materials in the converter [68].	Model thermal cycling and predict failure date for scheduled maintenance [68].
TP.YCT.05 - Passive yaw aligns the structure with wind direction above rated wind speed	Might cause significant acceleration on the system. When the system becomes parallel to wind speed, no power can be generated.	Apply brakes when approaching rated wind speed. Control thrusts so that thrust to wind speed gradient is positive and the system is stable.
TP.FND.07 - Foundation Resonance	The natural frequencies of the foundation are below the rotor frequency, and in the realm of wave frequencies.	The natural frequency should be further investigated including potential damping from water inside the monopile. If it turns out to be a problem further damping should be installed.

This mitigation leads to the post-mitigation risk matrix as seen in Figure 10.3:

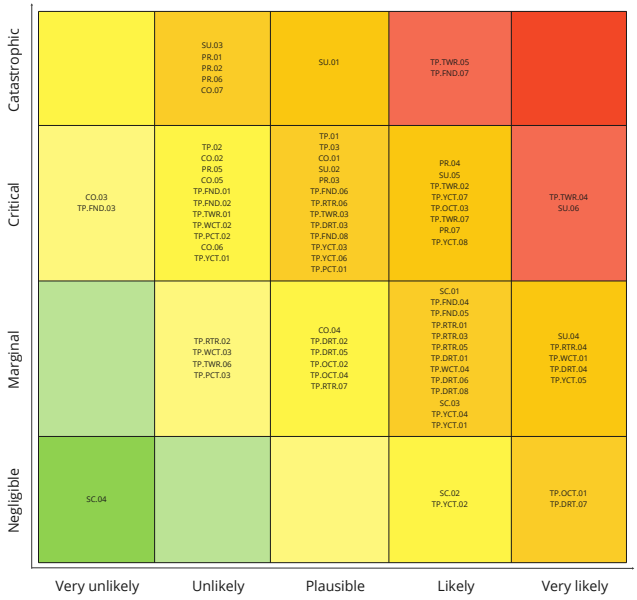

Figure 10.2: *Pre mitigation risk matrix*

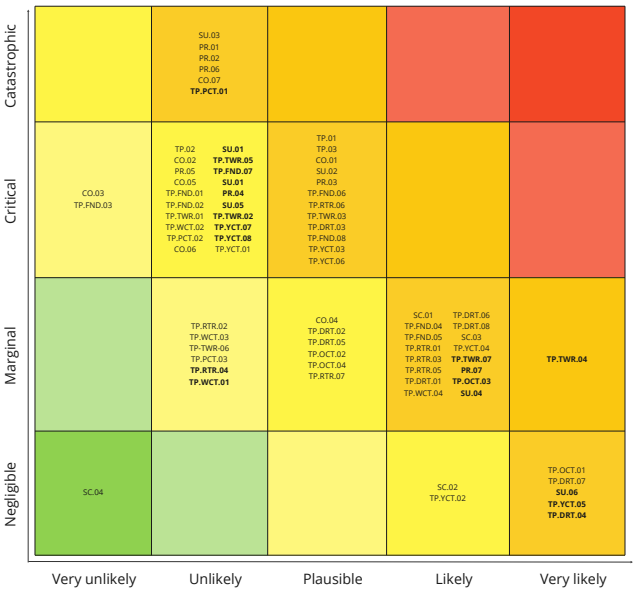

Figure 10.3: *Post mitigation risk matrix*

One risk remains in the high-risk region, **TP.TWR.04**. This is the risk due to lightning. It is very difficult to avoid damage due to lightning in the lifetime of the system. Therefore, a contingency plan was devised in the midterm and implemented in the final design in order to limit the damage caused by this risk. To reduce the maintenance cost needed for this, unmanned inspections and health monitoring sensors can be used to monitor damage caused by lightning strikes since there will be a lot of space to mount these sensors in the wind turbine. Furthermore, manned inspections and repairs can be added to planned maintenance visits to reduce the cost of unplanned maintenance. Since lightning has the potential to cause a surge that prevents the turbine from operating, damaged electrical components need to be replaced promptly to reduce costly downtime.

11

Compliance matrix

This chapter details the compliance of individual subsystems with user, mission, functional, and standard requirements. First, all subsystems are presented, and then the compliance for the entire system is.

11.1. Compliance of the subsystems

This section presents the compliance of the eight separate subsystems defined in the baseline report. Only the requirements deemed as most important and indicative of the design were presented for brevity's sake.

11.1.1. Compliance of TWR

Compliance of the tower to the most critical requirements defined in the preliminary report is listed in Table 11.1. The value for requirement **MR-30-TWR-01** is not finalised yet, because the use of composites was not even considered during the design process, so it was not used at all. With regard to other subsystems, the tower has the most requirements, which could be checked against due to the design having the most detailed models. For this subsystem, most requirements did not need to be changed themselves.

Table 11.1: *Compliance matrix for the tower subsystem*

ID	Requirement	Value	Status
MR-28-TWR-01	The tower height shall not exceed 315 m	Height is 315 m	✓
MR-30-TWR-01	The mass of composites used for the tower shall not exceed **<TBD>** tonnes	No composites are used	✓
MR-32-TWR-01	The tower shall consist of at least 90% of recyclable metals by mass	Tower is 100 % made of steel	✓
MR-34-TWR-01	The tower shall withstand loads due to maximum wind speed of at least $70\,\mathrm{m\,s^{-1}}$	Tower is sized to take winds of $70\,\mathrm{m\,s^{-1}}$	✓
FR-20-TWR-01	The tower shall stay above water	The tower is on the monopile	✓
FR-20-TWR-02	The tower shall transfer all loads to the foundation	The tower transfers all loads to the monopile	✓
FR-27-TWR-01	The tower shall be able to be yawed	The tower is attached to the monopile with a double bearing	✓
SR-01-TWR-01	The tower shall withstand normal wind conditions for its installed location	The tower can withstand load case LDC1, which corresponds to its normal operating condition	✓
SR-02-TWR-01	The tower shall withstand extreme wind conditions for its installed location, occurring every 50 years	The tower can withstand load case LDC3, which corresponds to that condition	✓
SR-12-TWR-01	The tower shall include safety guards and railing to facilitate maintenance	The tower includes safety guards	✓
SR-16-TWR-01	The tower shall have its platform outside of the splash zone	The platform of the tower is 30 m above the surface of the ocean, well out of the splash zone	✓

11.1.2. Compliance of YCT

Compliance of YCT can is presented in Table 11.2. The requirement **MR-28-YCT-01** was updated when analysis in Figure 7.3 was performed. The control system components themselves were designed mostly on a conceptual level, so the requirements presented refer to the functions and operations of the system rather than the specific implementations.

Table 11.2: *Compliance matrix for the yaw control subsystem*

ID	Requirement	Value	Status
MR-08-YCT-01	YCT shall allow to lock the turbine's yaw and prevent it from turning	YCT has a break and emergency break, both of which prevent the structure from turning	✓
MR-28-YCT-01	The yaw control subsystem shall be able to yaw at a rate of $0.2\,^{\circ}\,s^{-1}$ during normal operating conditions	The yaw control subsystem can yaw at a rate of $1\,^{\circ}\,s^{-1}$ during normal operation conditions	✓
SR-12-YCT-01	The yaw control subsystem shall be accessible to inspection and/or maintenance	The yaw control subsystem is designed to be accessible to inspection and maintenance	✓

11.1.3. Compliance of PCT

Table 11.3 shows compliance of the power control system. Requirement **MR-33-PCT-01** was updated based on the rated wind speed and **MR-28-PCT-01** was updated based on the preliminary design presented in the midterm report.

Table 11.3: *Compliance matrix for the power control subsystem*

ID	Requirement	Value	Status
MR-07-PCT-01	The PCT shall allow predictive (condition-based) maintenance	PCT is designed to include sensors, which in combination with DT technology allow for condition-based maintenance strategy	✓
MR-08-PCT-01	The PCT shall be maintained without total operation halt	The modular design allow for maintenance of PCT with only two turbines needing to shut down at once	✓
MR-13-PCT-01	The PCT shall have an energy production density of at least $16\,MW\,km^{-2}$	Energy density of PCT is close to $20\,MW\,km^{-2}$	✓
MR-28-PCT-01	PCT shall not exceed the height of 315 m	PCT reaches until 312 m high	✓
MR-30-PCT-01	PCT shall use less than **<TBD>** % of total mass as composites	PCT does not use composites	✓
MR-33-PCT-01	PCT shall operate with rated wind speed of $11.2\,m\,s^{-1}$	PCT has a rated wind speed of $11.2\,m\,s^{-1}$	✓
FR-10-PCT-01	The system shall be able to adjust the amount of power it produces	The system is stall regulated, in combination with a shaft break and variable loading generator	✓
FR-13-PCT-01	The normal operation of the PCT shall be possible at the platform level	PCT can be operated at platform level	✓

11.1.4. Compliance of DRT

For the compliance of DRT, presented in Table 11.4, most of the requirements presented focus on maintainability and the option to replace it. This is because one of the key parts of the design is modularity and redundancy.

Table 11.4: *Compliance matrix for the power control subsystem*

ID	Requirement	Value	Status
MR-02-DRT-01	The drivetrain shall be produced from common easily sourced metals, limited to non-rare earth metals	drivetrain uses DFIG, which needs no rare earth metals	✓
MR-05-DRT-01	The drive train shall be replaceable	The drive train can be replaced due to modular design	✓
MR-07-DRT-01	The shaft shall be maintainable by predictive maintenance	The shaft incorporates sensors which facilitate predictive maintenance	✓
MR-07-DRT-02	The gearbox shall be maintainable by predictive maintenance	The gearbox incorporates sensors which facilitate predictive maintenance	✓
MR-07-DRT-03	The generators shall be maintainable by predictive maintenance	The generators incorporate sensors which facilitate predictive maintenance	✓
MR-07-DRT-04	The bearings shall be maintainable by predictive maintenance	The bearings incorporate sensors which facilitate predictive maintenance	✓
MR-23-DRT-01	The drive train technology shall be lab tested	Brushless DFIGs have been tested in labs[39]	✓

11.1.5. Compliance of WCT

Wake control system requirements presented are few because the design of the WCT was done mostly on its effects, and not much was done to analyse the structure and mechanisms. As such, the requirements presented are the few ones which refer to things considered so far. Requirement **MR-38-WCT-01** was changed from wetted area to circulation since that was a more relevant quantity at this design stage.

Table 11.5: *Compliance matrix for the wake control subsystem*

ID	Requirement	Value	Status
MR-38-WCT-01	The wake control system shall have circulation of $330\,m^2\,s^{-1}$ at rated wind speed	The wake control system has the circulation of $330\,m^2\,s^{-1}$ at rated wind speed	✓
SR-01-WCT-01	The wake control system shall successfully transfer aerodynamic loads during normal wind conditions to the tower subsystem	WCT transfers all loads to tower structure at all times	✓
SR-03-WCT-01	The wake control subsystem shall successfully transfer aerodynamic loads during extreme wind conditions to the tower substructure	WCT transfers all loads to tower structure at all times	✓

11.1.6. Compliance of OCT

Operations control system compliance matrix Table 11.6 presents requirements related to sensors that the system has to facilitate maintenance. Since other related things were not given much consideration at this design stage, they were not discussed.

Table 11.6: *Compliance matrix for the wake control subsystem*

ID	Requirement	Value	Status
MR-07-OCT-01	The operation control subsystem shall monitor the vibration of the tower subsystem	The operation control subsystem has sensors to monitor the vibration of the tower subsystem	✓
MR-07-OCT-02	The operation control subsystem shall monitor the vibration of the drive train subsystem	The operation control subsystem has sensors to monitor the vibration of the drive train subsystem	✓
MR-07-OCT-03	The operation control subsystem shall monitor the vibration of the rotor subsystem	The operation control subsystem has sensors to monitor the vibration of the rotor subsystem	✓
MR-07-OCT-04	The operation control subsystem shall monitor the strains of the tower subsystem	The operation control subsystem has sensors to monitor the strains of the tower subsystem	✓
MR-07-OCT-05	The operation control subsystem shall monitor the strains of the drive train subsystem	The operation control subsystem has sensors to monitor the strains of the drive train subsystem	✓
MR-07-OCT-06	The operation control subsystem shall monitor the strains of the rotor subsystem	The operation control subsystem has sensors to monitor the strains of the rotor subsystem	✓
FR-18-OCT-01	The OCT shall be able to alert the maintenance department if a failure occurs	The OCT is designed to be able to request maintenance if a failure occurs	✓

11.1.7. Compliance of RTR

Since RTR and DRT share many requirements, only three were presented in Table 11.7. These focus on the operations and logistics of the rotor itself.

Table 11.7: *Compliance matrix for the rotor subsystem*

ID	Requirement	Value	Status
MR-02-RTR-01	The rotor shall be produced from common, easily sourced materials, limited to metals	The rotors are made of steel	✓
MR-05-RTR-01	The rotor shall be replaceable	Rotors and blades can both be replaced separately from the shaft sections	✓
SR-19-RTR-01	The rotor shall be able to stop and be parked	The rotor is designed to be able to stop and be parked	✓

11.1.8. Compliance of FND

The last subsystem compliance matrix Table 11.8, which shows the compliance of the foundation subsystem focuses on its operation and production. These were deemed most indicative of what the focus of the design was, which makes it unique.

Table 11.8: *Compliance matrix for the foundation subsystem*

ID	Requirement	Value	Status
MR-02-FND-01	The foundation shall be produced from common, easily sourced metals, limited to metals and concrete	The monopile is made of marine steel and ocean floor part is encased in concrete	✓
MR-23-FND-01	The foundation technology used shall be lab tested	The monopile technology is in use commonly	✓
FR-21-FND-01	The foundation shall keep all other subsystems above water	Monopile is sized to keep the rest of the turbine above water for load cases LDC1, LDC2, and LDC3	✓
FR-22-FND-01	The foundation shall support a mass of 6628 t	The foundation shall support a mass of 6628 t and environmental loads	✓
SR-20-FND-02	The foundation shall be protected against corrosion	The foundation uses coating and sacrificial plating to prevent corrosion	✓

11.2. System compliance matrix

After subsystem compliance matrices, the overall system compliance matrix is shown in Table 11.9. This is the most important compliance matrix contained in the section. It contains the most important requirements. With requirement **UR-02**, which was deemed the most important of all user requirements, the system is able to meet the needed value and exceeds it by almost 25 %. This is a good margin which allows for a nice safety margin. On the other hand, the second most important of the user requirements **UR-03** was not satisfied. The system can not achieve the full 45 % required for the LCoE. Based on the cost model used in this report and the midterm, this value can not be achieved by the system.

Another important user requirement **UR-06** is satisfied. This one addresses the sustainability of the system, which aims at limiting its environmental impact. At the same time, the system is also more space efficient, since it provides much higher energy density, at 20 $\mathrm{MW\,km^{-2}}$. Combined with **MR-01**, this makes the system sustainable from both the environmental and social perspectives.

Requirements **MR-07**, **MR-37**, **FR-21**, **SR-03**, and **SR-19** were shown to highlight the operational aspects of the entire system. These show the main capabilities which were given the most consideration during these stages of the design. The last requirement **MR-29** was included in order to show that the system is economically feasible.

Table 11.9: *Compliance matrix for the system*

ID	Requirement	Value	Status
UR-01	The system shall have a power rating of at least 30 MW	The system has power rating of 31.3 MW, as stated in Chapter 6	✓
UR-02	The system shall have an energy density of at least 16 $MW km^{-2}$	The system has an energy density close to 20 $MW km^{-2}$	✓
UR-03	The system shall have a 45 % lower levelised cost of energy compared to traditional HAWT	System has 29.6 % reduced LCoE compared to traditional HAWT Section 2.1	×
UR-04	The system shall have multiple rotors	System has 36 rotors	✓
UR-05	The system shall have lower lifetime emissions than traditional horizontal axis offshore wind turbines	Based on LCA, the lifetime emissions are 37 % less polluting Section 9.1	✓
UR-06	The system shall have increased material recyclability than traditional horizontal axis wind turbines	90 % of the structure will be recycled directly as per Subsection 9.1.5	✓
UR-07	The system shall have decreased rare metal use compared to traditional HAWT	System does not use rare earth metals	✓
UR-08	The system shall be installable offshore	the system can be installed offshore	✓
MR-01	The system shall be able to be produced by small Original Equipment Manufacturer(s)	System does need highly complex or specialised components, allowing them all to be produced by small OEM(s)	✓
MR-07	The system shall allow predictive (condition-based) maintenance	System has sensors which allow for use of DT system to implement conditions-based maintenance	✓
MR-29	The system shall be profitable without the intervention of governmental subsidies	Based on the return-on-investment analysis, the system is profitable, with return on investment of between 6.7 and 8.7 %, as per Section 8.3	✓
MR-37	The system shall be able to align to a specified direction	The system has YCT, which allows it to align in any direction	✓
FR-21	The system shall stay above water	The system is on a monopile foundation, which keeps it above the ocean surface	✓
SR-03	The system shall withstand the extreme wind conditions, occurring every 50 years for its installation location	The system is sized to withstand LDC3, which corresponds to worst wind condition in 50 years	✓
SR-19	The system shall allow for parking of the wind turbine	System can park all its rotors and stop operating	✓

12

Future development

This section includes the future development stages for the MR-TBD project, starting from the end of the DSE design stage to the end of the life of the wind farm. Section 12.1 shows the future tasks and Section 12.2 includes a Gantt chart for the tasks to be done.

12.1. Project design and development logic

Figure 12.1 Includes both a flow chart and a breakdown of tasks to be completed after the DSE stage is finished. Blocks that are parallel or staggered in the flow diagram, are performed at the same time.

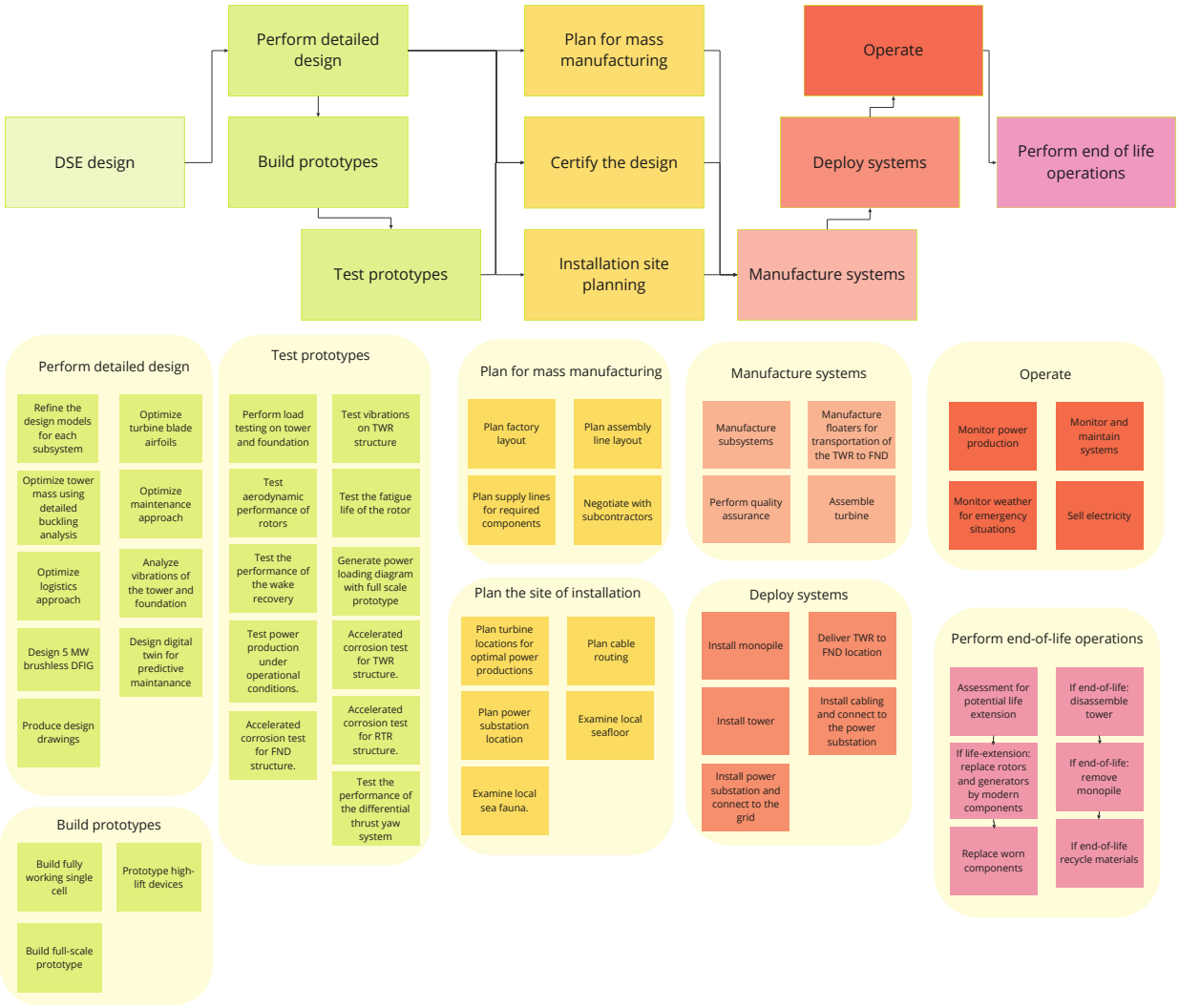

Figure 12.1: *An overview of activities to be performed post-DSE*

12.2. Future design Gantt chart

On the following page, a Gantt chart for the future design is provided.

ID	Unique ID	Task Mode	Task Name	Duration	Start	Finish	Predecessors
0	**0**		**MR-TBD**	**12620 days**	**Mon 4/24/23**	**Fri 9/4/71**	
1	227		DSE design	50 days	Mon 4/24/23	Fri 6/30/23	
2	**228**		**Perform detailed design**	**1145 days**	**Mon 7/3/23**	**Fri 11/19/27**	**1**
3	229		Refine the design models for each subsystem	270 days	Mon 7/3/23	Fri 7/12/24	
4	230		Optimize tower mass using detailed buckling analysis	365 days	Mon 7/15/24	Fri 12/5/25	3
5	231		Optimize logistics approach	365 days	Mon 7/15/24	Fri 12/5/25	3
6	232		Optimize turbine blade airfoils	365 days	Mon 7/15/24	Fri 12/5/25	3
7	233		Design 5 MW brushless DFiG	365 days	Mon 7/15/24	Fri 12/5/25	3
8	234		Optimize Optimise maintenance approach	365 days	Mon 7/15/24	Fri 12/5/25	3
9	235		Analyse vibrations of the tower and foundation	270 days	Mon 12/8/25	Fri 12/18/26	4
10	236		Design digital twin for predictive maintenance	180 days	Mon 12/21/26	Fri 8/27/27	9
11	237		Produce design drawings	60 days	Mon 8/30/27	Fri 11/19/27	10
12	**238**		**Build prototypes**	**485 days**	**Mon 11/22/27**	**Fri 9/28/29**	**2**
13	239		Build fully working single cell	30 days	Mon 11/22/27	Fri 12/31/27	2
14	240		Prototype high-lift devices	30 days	Mon 11/22/27	Fri 12/31/27	2
15	241		Build full-scale prototype	365 days	Mon 1/3/28	Fri 5/25/29	13,14
16	242		Validate the wake recovery	90 days	Mon 5/28/29	Fri 9/28/29	15
17	**243**		**Test prototypes**	**545 days**	**Mon 10/1/29**	**Fri 10/31/31**	**12**
18	244		Perform load testing on tower and foundation	180 days	Mon 10/1/29	Fri 6/7/30	12
19	245		Test aerodynamic performance of rotors	180 days	Mon 10/1/29	Fri 6/7/30	12
20	246		Test the performance of the wake recovery	90 days	Mon 10/1/29	Fri 2/1/30	12
21	247		Test power production under operational conditions	90 days	Mon 10/1/29	Fri 2/1/30	12
22	248		Accelerated corrosion test for FND	365 days	Mon 6/10/30	Fri 10/31/31	18,19,20,21
23	249		Test vibrations on TWR structure	180 days	Mon 6/10/30	Fri 2/14/31	18,19,20,21
24	250		Test the fatigue life of the rotor	365 days	Mon 6/10/30	Fri 10/31/31	18,19,20,21
25	251		Generate power loading diagram	90 days	Mon 6/10/30	Fri 10/11/30	18,19,20,21
26	252		Accelerated corrosion test for TWR	365 days	Mon 6/10/30	Fri 10/31/31	18,19,20,21
27	253		Accelerated corrosion test for RTR	365 days	Mon 6/10/30	Fri 10/31/31	18,19,20,21
28	**254**		**Plan for mass manufacturing**	**730 days**	**Mon 11/3/31**	**Fri 8/18/34**	**17**
29	255		Plan factory	365 days	Mon 11/3/31	Fri 3/25/33	
30	256		Plan supply lines for required components	270 days	Mon 11/3/31	Fri 11/12/32	
31	257		Plan assembly line layout	365 days	Mon 3/28/33	Fri 8/18/34	29
32	258		Negotiate with subcontractors	270 days	Mon 11/15/32	Fri 11/25/33	30
33	259		Certify the design	1100 days	Mon 11/22/27	Fri 2/6/32	2
34	**260**		**Installation site planning**	**720 days**	**Mon 11/3/31**	**Fri 8/4/34**	**17**
35	261		Plan turbine locations for optimal power location	180 days	Mon 11/3/31	Fri 7/9/32	
36	262		Examine local sea fauna	180 days	Mon 7/12/32	Fri 3/18/33	35
37	263		Examine local seafloor	180 days	Mon 7/12/32	Fri 3/18/33	35
38	264		Plan cable routing	180 days	Mon 3/21/33	Fri 11/25/33	37
39	265		Plan power substation location	180 days	Mon 11/28/33	Fri 8/4/34	38
40	**266**		**Manufacture systems**	**220 days**	**Mon 8/21/34**	**Fri 6/22/35**	**33,28,34**
41	267		Manufacture subsystems	180 days	Mon 8/21/34	Fri 4/27/35	
42	268		Perform quality assurance	30 days	Mon 4/30/35	Fri 6/8/35	41
43	269		Manufacture floaters for transportation of the TWR to FND	60 days	Mon 8/21/34	Fri 11/10/34	
44	270		Assemble turbine	10 days	Mon 6/11/35	Fri 6/22/35	42,43
45	**271**		**Deploy systems**	**180 days**	**Mon 8/7/34**	**Fri 4/13/35**	**34**
46	272		Install monopole	2 days	Mon 8/7/34	Tue 8/8/34	
47	273		Deliver TWR to FND location	1 day	Mon 8/7/34	Mon 8/7/34	
48	274		Install tower	5 days	Wed 8/9/34	Tue 8/15/34	46,47
49	275		Install power substation and connect to the grid	180 days	Mon 8/7/34	Fri 4/13/35	
50	276		Install cabling and connect to the power substation	180 days	Mon 8/7/34	Fri 4/13/35	
51	**277**		**Operate**	**9125 days**	**Mon 4/16/35**	**Fri 4/4/70**	**45**
52	278		Monitor power production	9125 days	Mon 4/16/35	Fri 4/4/70	
53	279		Monitor weather for emergency situations	9125 days	Mon 4/16/35	Fri 4/4/70	
54	280		Monitor and maintain systems	9125 days	Mon 4/16/35	Fri 4/4/70	
55	281		Sell electricity	9125 days	Mon 4/16/35	Fri 4/4/70	
56	**282**		**Perform end-of-life operations**	**370 days**	**Mon 4/7/70**	**Fri 9/4/71**	**51**
57	283		Assessment for potential life extension and potential repowerin	270 days	Mon 4/7/70	Fri 4/17/71	
58	284		Disassemble tower	10 days	Mon 4/20/71	Fri 5/1/71	57
59	285		Remove monopile	30 days	Mon 5/4/71	Fri 6/12/71	58
60	286		Recycle materials	60 days	Mon 6/15/71	Fri 9/4/71	59,58

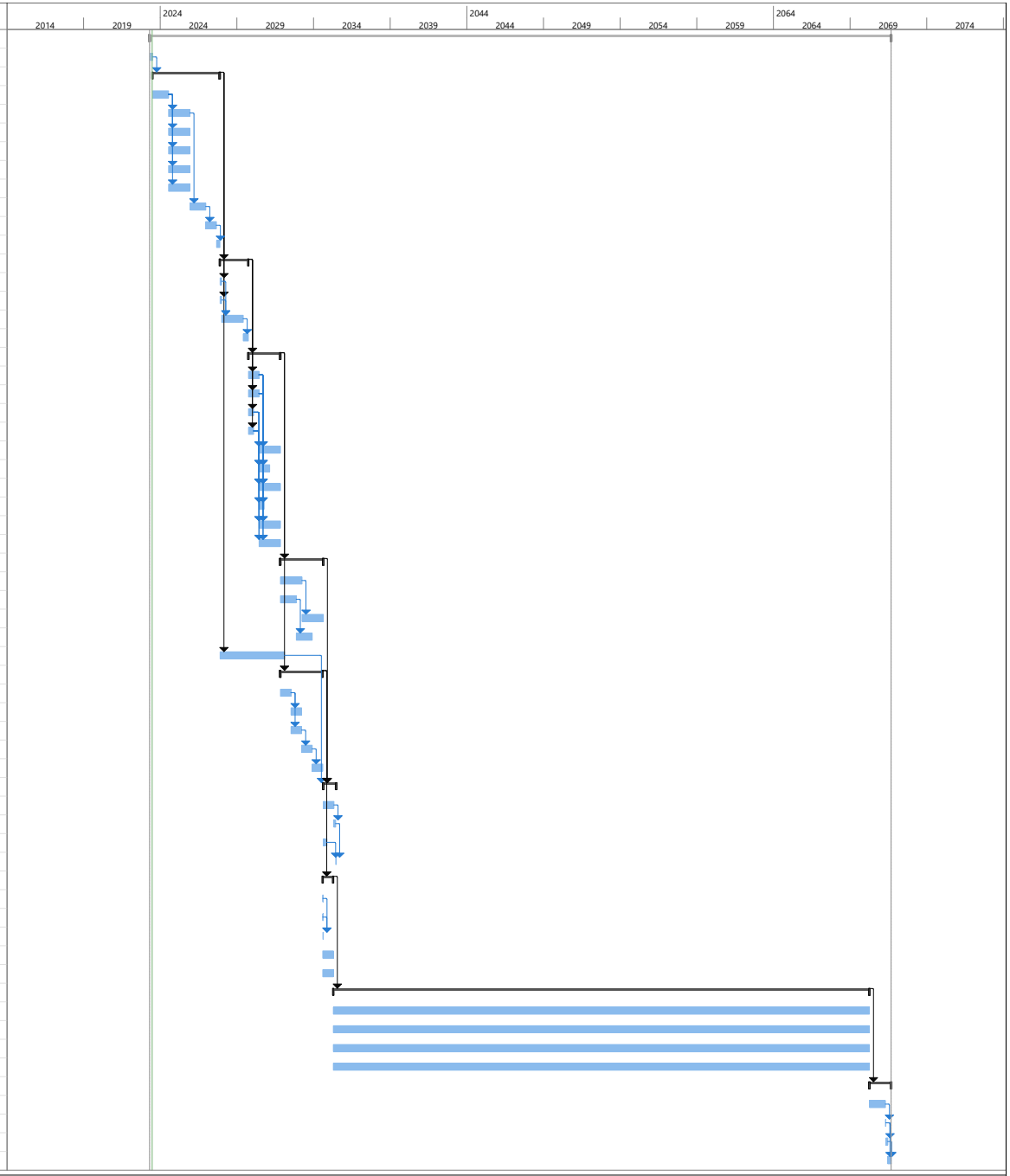

Project: MR-TBD
Date: Wed 6/21/23

Task
Split
Milestone
Summary
Project Summary
Inactive Task
Inactive Milestone
Inactive Summary
Manual Task
Duration-only
Manual Summary Rollup
Manual Summary
Start-only
Finish-only
External Tasks
External Milestone
Deadline
Progress
Manual Progress

13

Conclusion

The project's main objective was to design a multi-rotor VAWT system that has increased power density, is more democratically producible, has better material and emission sustainability, and decreases energy costs compared to conventional wind turbines.

The system was designed to meet the user requirements shown below:

UR-01: The system shall have a power rating of at least 30 MW
UR-02: The system shall have a power density of at least 16 $MW km^{-2}$
UR-03: The system shall have a 45 % lower levelized cost of energy compared to traditional horizontal axis offshore wind turbines
UR-04: The system shall have multiple rotors
UR-05: The system shall have lower lifetime emissions than traditional horizontal axis offshore wind turbines
UR-06: The system shall have increased material recyclability than traditional horizontal axis wind turbines
UR-07: The system shall have decreased rare metal use compared to traditional horizontal axis wind turbine
UR-08: The system shall be installable offshore

The final design is a large truss structure consisting of repeating cubical cells. Inside each cell is a vertical-axis turbine with a triple H-blade rotor. Six rotors are vertically connected to a single shaft, which is connected to the front of the structure. Each shaft is connected to a gearbox with a doubly fed induction generator (DFIG) and a partial converter. The yaw system alters rotors' rotational speed to generate differential thrust in order to yaw. An electrical yaw system is used as a backup. The system uses a high lift device (HLD) to increase the power density to recover the wake domain. The design's critical parameters and resulting components masses are shown in Table 13.1 and Table 13.2 below.

As shown in Table 13.1, the rated power is 31.3 MW, and the power density is 20 $MW km^{-2}$, so **UR-01** and **UR-02** are satisfied. In addition, the turbine was designed as an offshore multi-rotor system, so **UR-04** and **UR-08** are also satisfied. The system uses DFIGs, which do not use rare-earth metals. This means **UR-07** is also satisfied.

To investigate **UR-03**, a cost analysis was performed. After analysis of the current predictions for the wind turbine market, it has been established that MR-TBD is significantly cheaper than current turbines on the market. Using a cost analysis based on modifying the cost for a reference 10 MW wind turbine, it was calculated that the LCoE should drop by 30%. This does not satisfy user requirements, which were to drop the LCoE by 45%, but it is still an attractive investment opportunity. The cost analysis was performed in a conservative manner, leaving the possibility that a more detailed analysis gives way to a lower LCoE. The design also showed a 30% shorter time to break even and profitability at doubled the weighted average cost of capital. The largest cost reductions were obtained on the increase in power density, the cost of the generators, gearboxes, rotors, and the cost of maintenance.

Metal rotors are used instead of composite ones to make the system more sustainable. This accounts for the major majority of non-recyclable components in regular wind turbines. This satisfies **UR-06**.

A life cycle analysis was performed to investigate the emissions for **UR-05**. The analysis aims to evaluate the environmental impact (energy consumed and CO_2 emissions of the turbine's design throughout its entire life cycle. The analysis considers various phases, including material extraction, manufacturing, transportation, operations, decommissioning, and recycling. The MaterialUniverse database of Ansys Granta

Table 13.1: *Key parameters for the MR-TBD design*

Parameter	Unit	Value
Power rating	MW	31.3
Power density	$MW km^{-2}$	20
Turbine class	—	IEC class I
Control	—	Variable speed
Cut-in wind speed	m/s	3
Rated wind speed	m/s	11.2
Cut-out wind speed	m/s	25
Design TSR	—	4.5
Rotor diameter	m	46.7
Rotor height	m	45
Airfoil series	—	DU17DBD25
Number of rotors	—	36
Number of shafts	—	6
Turbine height	m	310
Turbine width	m	295
Cell dimensions	m	46.67 X 46.67 X 33.6
truss thickness ratio	—	0.01
Drivetrain	—	Geared
Gearbox	—	Angular & Planetary
Generator	—	Brushless DFIG
Wake control	—	Adjustable HLD
Wing chord	m	20
Wing span	m	280

Table 13.2: *Weights of all sized subsystems*

Element	Mass [tn]
Rotor	1717
Main shaft	260 X6
Blades	3.2 X6
Bearings	1 X42
Tower	2767
Truss	2455
Bedplate	52 X6
Yaw control	100
Bearings	54
Drivetrain	46
Wake control	648
Wing	81 X4
HLD	81 X4
Drivetrain	150
Gearbox	4 X6
Break	0.6 X6
Generator	16 X6
Converter	4 X6
Miscellaneous	0.4 X6
Monopile	6200
Total	11582

and the EcoAudit function was used to obtain the necessary data for assessing the impact of each phase. The results indicate that the life cycle phases account for 68.5%, 26.5%, 0.5%, 0.00%, and 4% of the overall emissions of the project (energy consumed and CO_2 footprint), respectively. After evaluating the individual phases, the estimated energy consumption is 151000 GJ and the CO2 emissions amount to 11900 ton. This is considering a 15% EOL reduction from the overall emissions due to recycling. Comparing this to conventional wind turbines, the MR-TBD turbine is found to be 37% less polluting. This means that the final user requirement **UR-05** is also satisfied.

Recommendations

A few aspects of the structural design should be further considered. More detailed vibration analysis is required for both the tower and foundation. Based on these results, vibration damping of the shafts and waves should be considered and further researched. In addition, the truss structure's weight may be further reduced by making the elements thinner. A more detailed sheet buckling analysis should be performed to do so safely. Truss or cable components similar to suspension bridges may be added. It should be investigated whether it would result in cost savings. Another aspect of the structural design that requires further attention is thermal expansion. Part of the structure is in the water, which could lead to a thermal gradient in the structure, inducing forces in the members due to shrinking and expansion.

As the design allows relatively easy switching of generators and rotors, fatigue life analysis should be made. Considerably more work will need to be done to determine the potential to extend the service life of the structure cell and change out the generators and rotors to save on costs and increase sustainability. Rotor cycle life should also be investigated as an individual airfoil on a rotor experiences many cycles with a large difference between minimums and maximums.

The shafts in the current design are very heavy, at 260 t per shaft. These should be further researched to decrease the mass. One possibility would be to have generators placed at two levels, at the bottom, and halfway up the tower. This would reduce the load on the shafts, allowing them to be smaller. However, this would make maintenance on the generator and gearbox more difficult. Another approach could be to use the rotors to carry part of the torque. Using this approach, only the parts of the shaft at the bearings would need to be as large as they are now.

Integration of the HLD as a structural element has the potential to reduce the mass of the structure. There is also potential to use the HLDs to assist in yawing of the structure using differential drag. Another interesting area for future analysis would be examining the effects of how HLDs of several turbines interact with each other since it is expected that they would aid wake recovery with their upwash.

A detailed CFD analysis using actuator cylinder theory can be done to better understand interference between two turbines as previous work shows that this increases the pressure coefficient. The study should be repeated using scaled models or industry-level software in order to better inspect the wind farm behaviour since the current method only assumes circulation due to HLDs.

Table 9.1 presents the elements used for manufacturing most of wind turbine's elements. Those decisions have raised many questions in need of further investigation. Particularly, the attention should be focused on rotors since they experience the most water droplet corrosion. This risk of failure can be diminished by the coating. Currently, it was assumed that multiple layers of white organic solvent-based paint will be applied. However, future studies are suggested to find the best combination of materials that will minimise the impact of salt water.

Further design should analyse the soil composition of the sea bed where the turbine will be installed. Analysis of the dynamic loading of the system, together with more insight into the ground properties, will provide an accurate estimate for the monopile driving length. Currently, no estimates were provided for this foundation element as using historical data and extrapolating would yield an inaccurate length.

For maintenance and availability, more detailed analysis and testing should be conducted. An important part of being able to implement a predictive maintenance strategy is knowing the lifetimes and failure modes of all important components. Therefore, elements necessitating predictive maintenance will need to be properly examined.

With respect to the bearings, a greater focus on their position could produce interesting findings that account for the foundation's mass optimisation. As the first bearing is located at 30 m and the second one at 170 m above the level, one particular intriguing scenario would be to place the second one below the first one. This design decision will reduce the monopile's length as it is 140 m into the tower while inducing further loads on the bearings, which will be reflected in larger such elements. More broadly, research is needed to determine which options are more feasible.

Lastly, for the yaw control with differential thrust, a simple on-off controller was used, which resulted in a fast correction rate. However, it was not investigated whether this was the most power-efficient method of yawing. Investigation of other types of control, such as partial power control for each rotor or the use of a PID (proportional integral derivative) controller, is recommended to optimize the system's reaction to wind direction changes. Furthermore, the yaw control of the system should be subjected to a simulation of the usual wind direction behaviour in the region to determine the average power loss due to yaw response time.

Bibliography

[1] Pleshivtsev, V. G., Filippov, G. A., Pak, Y. A., and Livanova, O. V., "EFFECT OF CARBON CONTENT AND STRESSED STATE ON THE CORROSION RATE OF PIPE STEEL IN HEATING SYSTEMS," *Metallurgist*, Vol. 53, 2009, pp. 62–64.

[2] Jamieson, P., Ferreira, C. S., Dalhoff, P., Störtenbecker, S., Collu, M., Salo, E., McMillan, D., McMorland, J., Morgan, L., and Buck, A., "Development of a multi rotor floating offshore system based on vertical axis wind turbines," *Journal of Physics: Conference Series*, Vol. 2257, No. 1, 2022. doi:10.1088/1742-6596/2257/1/012002.

[3] Carroll, J., McDonald, A., and McMillan, D., "Failure rate, repair time and unscheduled O&M cost analysis of offshore wind turbines," *Wind Energy*, Vol. 19, No. 6, 2016, pp. 1107–1119. doi:https://doi.org/10.1002/we.1887.

[4] Carroll, J., McDonald, A., Dinwoodie, I., McMillan, D., Revie, M., and Lazakis, I., "Availability, operation and maintenance costs of offshore wind turbines with different drive train configurations," *Wind Energy*, Vol. 20, No. 2, 2017, pp. 361–378. doi:https://doi.org/10.1002/we.2011.

[5] Freeman, K., Frost, C., Hundleby, G., Roberts, A., Valpy, B., Holttinen, H., Ramírez, L., and Pineda, I., "Our energy, our future. How offshore wind will help Europe go carbon-neutral." , 2019.

[6] "Guide to an offshore wind farm," , January 2019.

[7] Distelbrink, L., Fetecau, M., Gonzalez, L., Jemioł, B., Rizk, M. K., Peralta Tapia, M., Porcescu, I., Pudāns, J., Roth, J., and Tuğtekin, M., "60MW Multi-Rotor Vertical Axis Wind Turbine Baseline techreport," , 2023.

[8] Distelbrink, L., Fetecau, M., Gonzalez, L., Jemioł, B., Rizk, M. K., Peralta Tapia, M., Porcescu, I., Pudāns, J., Roth, J., and Tuğtekin, M., "60MW Multi-Rotor Vertical Axis Wind Turbine Midterm techreport," , 2023.

[9] Cox, K., and Echtermeyer, A., "Structural Design and Analysis of a 10MW Wind Turbine Blade," *Energy Procedia*, Vol. 24, 2012, pp. 194–201. doi:https://doi.org/10.1016/j.egypro.2012.06.101, selected papers from Deep Sea Offshore Wind R&D Conference, Trondheim, Norway, 19-20 January 2012.

[10] Bayati, I., Belloli, M., Bernini, L., Mikkelsen, R., and Zasso, A., "On the aero-elastic design of the DTU 10MW wind turbine blade for the LIFES50+ wind tunnel scale model," *Journal of Physics: Conference Series*, Vol. 753, No. 2, 2016, p. 022028. doi:10.1088/1742-6596/753/2/022028.

[11] Tüfekci, M., Genel, E., Tatar, A., and Tüfekci, E., "Dynamic Analysis of Composite Wind Turbine Blades as Beams: An Analytical and Numerical Study," *Vibration*, Vol. 4, No. 1, 2021, pp. 1–15. doi:10.3390/vibration4010001.

[12] Macquart, T., Kucukbahar, D., and Prinsen, B., "Dutch Offshore Wind Market techreport 2023," , April 2023.

[13] Witha, B., Hahmann, A., Sile, T., Dörenkämper, M., Ezber, Y., García-Bustamante, E., González-Rouco, J. F., Leroy, G., and Navarro, J., "WRF model sensitivity studies and specifications for the NEWA mesoscale wind atlas production runs," Tech. rep., NEWA, May 2019. doi:10.5281/zenodo.2682604.

[14] Coelingh, J., van Wijk, A., and Holtslag, A., "Analysis of wind speed observations over the North Sea," *Journal of Wind Engineering and Industrial Aerodynamics*, Vol. 61, No. 1, 1996, pp. 51–69. doi:https://doi.org/10.1016/0167-6105(96)00043-8.

[15] Coelingh, J., van Wijk, A., and Holtslag, A., "Analysis of wind speed observations over the North Sea," *Journal of Wind Engineering and Industrial Aerodynamics*, Vol. 61, No. 1, 1996, pp. 51–69. doi:https://doi.org/10.1016/0167-6105(96)00043-8.

[16] Hasager, C. B., Barthelmie, R. J., Christiansen, M. B., Nielsen, M., and Pryor, S. C., "Quantifying offshore wind resources from satellite wind maps: study area the North Sea," *Wind Energy*, Vol. 9, No. 1-2, 2006, pp. 63–74. doi:https://doi.org/10.1002/we.190.

[17] Pryor, S., and Barthelmie, R., "Climate change impacts on wind energy: A re-

view," *Renewable and Sustainable Energy Reviews*, Vol. 14, No. 1, 2010, pp. 430–437. doi:https://doi.org/10.1016/j.rser.2009.07.028.

[18] Siegismund, F., and Schrum, C., "Decadal changes in the wind forcing over the North Sea," , October 2018.

[19] Fischer, T., De Vries, W. E., and Schmidt, B., "Upwind design basis (WP4: Offshore foundations and support structures)," Tech. rep., TU Delft, 2010.

[20] Ottermo, F., Eriksson, S., and Bernhoff, H., "Parking strategies for vertical axis wind turbines," *ISRN Renewable Energy*, Vol. 2012, 2012, p. 1–5. doi:10.5402/2012/904269.

[21] Vire, A., "Fundamentals of Wind Energy I - Lecture 2," , 2023.

[22] K.W Hermans, J. W. P., "Future XL monopile foundation design for a 10 MW wind turbine in deep water," Tech. Rep. ECN-E–16-069, Energieonderzoek Centrum Nederland, Den Haag, NL, Dec 2016.

[23] Çetin, N., Yurdusev, M., Ata, R., and Özdamar, A., "ASSESSMENT OF OPTIMUM TIP SPEED RATIO OF WIND TURBINES," *Mathematical and Computational Applications*, Vol. 10, No. 1, 2005, pp. 147–154.

[24] Kallehave, D., Byrne, B. W., LeBlanc Thilsted, C., and Mikkelsen, K. K., "Optimization of monopiles for offshore wind turbines," *Philosophical Transactions of the Royal Society A: Mathematical, Physical and Engineering Sciences*, Vol. 373, No. 2035, 2015, p. 20140100. doi:10.1098/rsta.2014.0100.

[25] Sánchez, S., López-Gutiérrez, J.-S., Negro, V., and Esteban, M. D., "Foundations in Offshore Wind Farms: Evolution, Characteristics and Range of Use. Analysis of Main Dimensional Parameters in Monopile Foundations," *Journal of Marine science and Engineering*, 2019. doi:10.3390/jmse7120441.

[26] Negro, V., López-Gutiérrez, J.-S., Esteban, M. D., Alberdi, P., Imaz, M., and Serraclara, J.-M., "Monopiles in offshore wind: Preliminary estimate of main dimensions," *Ocean Engineering*, Vol. 133, 2017, pp. 253–261. doi:doi.org/10.1016/j.oceaneng.2017.02.011.

[27] Carroll, J., McDonald, A., Dinwoodie, I., McMillan, D., Revie, M., and Lazakis, I., "Availability, operation and maintenance costs of offshore wind turbines with different drive train configurations," *Wind Energy*, Vol. 20, No. 2, 2016, p. 361–378. doi:10.1002/we.2011.

[28] Li, C., Mogollón, J. M., Tukker, A., Dong, J., von Terzi, D., Zhang, C., and Steubing, B., "Future material requirements for global sustainable offshore wind energy development," *Renewable and Sustainable Energy Reviews*, Vol. 164, 2022. doi:10.1016/j.rser.2022.112603.

[29] Pavel, C. C., Lacal-Arántegui, R., Marmier, A., Schüler, D., Tzimas, E., Buchert, M., Jenseit, W., and Blagoeva, D., "Substitution strategies for reducing the use of rare earths in wind turbines," *Resources Policy*, Vol. 52, 2017, pp. 349–357. doi:10.1016/j.resourpol.2017.04.010.

[30] Balaram, V., "Rare Earth Element Deposits: Sources, and Exploration Strategies," *Journal of the Geological Society of India*, Vol. 98, 2022, pp. 1210–1216. doi:10.1007/s12594-022-2154-3.

[31] Kharade, V., and Jagtap, K., "A Review Study on Vertical axis Wind Turbines (lift and drag type) for Optimizing the Aerodynamic and Structural Performance," *Recent Developments in Mechanical Engineering*, 2019, pp. 61–65.

[32] Castellani, F., Astolfi, D., Peppoloni, M., Natili, F., Buttà, D., and Hirschl, A., "Experimental Vibration Analysis of a Small Scale Vertical Wind Energy System for Residential Use," *Machines*, Vol. 7, No. 2, 2019. doi:10.3390/machines7020035.

[33] Battisti, L., Brighenti, A., Benini, E., and Castelli, M. R., "Analysis of Different Blade Architectures on small VAWT Performance," *Journal of Physics*, Vol. 753, No. 6, 2016. doi:10.1088/1742-6596/753/6/062009.

[34] International Electrotechnical Commission, "IEC 61400-1: Wind turbine generator systems Part 1: Design requirements," Tech. rep., IEC, 2005. IEC 61400-1:2005(E).

[35] Gaertner, E., Rinker, J., Sethuraman, L., Zahle, F., Anderson, B., Barter, G., Abbas, N., Meng, F., Bortolotti, P., Skrzypinski, W., Scott, G., Feil, R., Bredmose, H., Dykes, K., Shields, M., Allen, C., and Viselli,

A., "Definition of the IEA Wind 15-Megawatt Offshore Reference Wind Turbine," Tech. rep., NREL, 2020. NREL/TP-5000-75698.

[36] Bortolli, P., Tarres, H. C., Dykes, K., Merz, K., Sethuraman, L., Verelst, D., and Zahle, F., "Systems Engineering in Wind Energy - WP2.1 Reference Wind Turbines," Tech. rep., NREL, May 2019.

[37] Lee, Y.-L., and Barkey, M. E., "Chapter 4 - Stress-Based Uniaxial Fatigue Analysis," *Metal Fatigue Analysis Handbook*, edited by Y.-L. Lee, M. E. Barkey, and H.-T. Kang, Butterworth-Heinemann, Boston, 2012, pp. 115–160. doi:https://doi.org/10.1016/B978-0-12-385204-5.00004-5.

[38] Li, S., Lamei, A., Wong, C., and Hayatdavoodi, M., "Concept design and analysis of wind-tracing floating offshore wind turbines," *ASME 2019 2nd International Offshore Wind Technical Conference*, American Society of Mechanical Engineers (ASME), 2019, pp. 1–9. doi:10.1115/IOWTC2019-7580.

[39] Abdi, E., McMahon, R., Malliband, P., Shao, S., Mathekga, M. E., Tavner, P., Abdi, S., Oraee, A., Long, T., and Tatlow, M., "Performance analysis and testing of a 250 kW medium-speed brushless doubly-fed induction generator," *IET Renewable Power Generation*, Vol. 7, No. 6, 2013, pp. 631–638. doi:https://doi.org/10.1049/iet-rpg.2012.0234.

[40] Sethuraman, L., Xing, Y., Gao, Z., Venugopal, V., Mueller, M., and Moan, T., "A 5MW direct-drive generator for floating spar-buoy wind turbine: Development and analysis of a fully coupled Mechanical model," *Proceedings of the Institution of Mechanical Engineers, Part A: Journal of Power and Energy*, Vol. 228, 2014, pp. 718–741. doi:10.1177/0957650914537262.

[41] de Haan, T., "Buckling monopiles: Stability of a monopile based offshore wind turbine," Master's thesis, TU Delft, Delft, NL, Jan 2020.

[42] Bakhti, R., Benahmed, B., and Laib, A., "Finite Element Investigation of Offshore Wind Turbines Natural Frequency with Monopile Foundations System," *Journal of Vibration Engineering and Technologies*, 2023. doi:10.1007/s42417-023-00989-3.

[43] Jalbi, S., Shadlou, M., and Bhattacharya, S., "Chapter 16 - Practical Method to Estimate Foundation Stiffness for Design of Offshore Wind Turbines," *Wind Energy Engineering*, edited by T. M. Letcher, Academic Press, 2017, pp. 329–352. doi:https://doi.org/10.1016/B978-0-12-809451-8.00016-3.

[44] Schløer, S., Castillo, L. G., Fejerskov, M., Stroescu, E., and Bredmose, H., "A model for Quick Load Analysis for monopile-type offshore wind turbine substructures," *Journal of Physics: Conference Series*, Vol. 753, No. 9, 2016, p. 092008. doi:10.1088/1742-6596/753/9/092008.

[45] Anandavijayan, S., and Brennan, A. M. F., "A numerical analysis of the effects of manufacturing processes on material pre-strain in offshore wind monopiles," *Procedia Structural Integrity*, Vol. 13, 2018, pp. 953–958. doi:https://doi.org/10.1016/j.prostr.2018.12.178.

[46] Xia, T., Ding, Y., Dong, Y., Chen, Z., Zheng, M., Pan, E., and Xi, L., "Collaborative production and predictive maintenance scheduling for flexible flow shop with stochastic interruptions and monitoring data," *Journal of Manufacturing Systems*, Vol. 65, 2022, pp. 640–652. doi:https://doi.org/10.1016/j.jmsy.2022.10.016.

[47] Zhong, D., Xia, Z., Zhu, Y., and Duan, J., "Overview of predictive maintenance based on digital twin technology," *Heliyon*, Vol. 9, No. 4, 2023, p. e14534. doi:https://doi.org/10.1016/j.heliyon.2023.e14534.

[48] Mwaniki, J., Lin, H., and Dai, Z., "A Condensed Introduction to the Doubly Fed Induction Generator Wind Energy Conversion Systems," *Journal of Engineering (United Kingdom)*, Vol. 2017, 2017. doi:10.1155/2017/2918281.

[49] Abdullah, M., Yatim, A. H., and Tan, C. W., "A study of maximum power point tracking algorithms for wind energy system," *2011 IEEE 1st Conference on Clean Energy and Technology, CET 2011*, 2011. doi:10.1109/CET.2011.6041484.

[50] De Tavernier, D., Ferreira, C., and Goude, A., "Vertical-axis wind turbine aerodynamics," *Handbook of*

Wind Energy Aerodynamics, Springer, 2022, pp. 1317–1361.

[51] T. Harris, C. B., J.H. Rumbarger, "Wind Turbine Design Guideline DG03: Yaw and Pitch Rolling Bearing Life," *Innovation for our energy future*, 2009.

[52] MacMahon, E. N., Stock, A., Leithead, W., and Jamieson, P., "Yaw control for 20MW offshore multi rotor system," *European Wind Energy Association Annual Event (EWEA 2015)*, 2015.

[53] Teunis, M., Collier, M. P., Bakker, E. G. R., Didderen, K., Gyimesi, A., and Lengkeek, W., "Ecological impact of decommissioning offshore wind farms Overview of potential impacts and their importance," Tech. rep., Bureau Waardenburg Ecology Landscape, 1 2020.

[54] Lindqvist, M., and Lundin, J., "Spare Part Logistics and Optimization for Wind Turbines-Methods for Cost-Effective Supply and Storage," , 2010.

[55] E.C.M. Ruijgrok, B. B., E.J. van Druten, "Cost Evaluation of North Sea Offshore Wind Post 2030," Tech. rep., North Sea Wind Power Hub Consortium, 2019.

[56] B.H. Bulder, E. B., and Bedon, G., "Optimal wind farm power density analysis for future offshore wind farms," *ECN*, 2018.

[57] Stehly, T., and Duffy, P., "Cost of Wind Energy Review," *NREL Transforming energy*, 2022.

[58] Ferreira, C. S., "60 MW VAWT MultiRotor Wind Energy System," , 2023.

[59] Smith, E. B., "Design of Nacelle for a 10 MW Wind turbine," Tech. rep., NTNU, 2012.

[60] Wang, S., Nejad, A. R., and Moan, T., "On design, modelling, and analysis of a 10-MW medium-speed drivetrain for offshore wind turbines," *Wind Energy*, Vol. 23, 2020, pp. 1099–1117. doi:10.1002/we.2476.

[61] Bortolotti, P., Tarres, H. C., K. Dykes, K. M., Sethuraman, L., Verelst, D., and Zahle, F., "IEA Wind Task 37 on Systems Engineering in Wind Energy WP2.1 Reference Wind Turbines," Tech. rep., IEA, May 2019.

[62] Ozoemena, M., Cheung, W., and Hasan, R., "Comparative LCA of technology improvement opportunities for a 1.5 MW wind turbine in the context of an onshore wind farm," *Clean Technologies and Environmental Policy*, Vol. 20, 2018, p. 173–190. doi:10.1007/s10098-017-1466-2.

[63] Schleisner, L., "Life cycle assessment of a wind farm and related externalities," *Renewable Energy*, Vol. 20, No. 3, 2000, pp. 279–288. doi:https://doi.org/10.1016/S0960-1481(99)00123-8.

[64] Raadal, H. L., Vold, B. I., Myhr, A., and Nygaard, T. A., "GHG emissions and energy performance of offshore wind power," *Renewable Energy*, Vol. 66, 2014, pp. 314–324. doi:https://doi.org/10.1016/j.renene.2013.11.075.

[65] Wang, Y., and Sun, T., "Life cycle assessment of CO2 emissions from wind power plants: Methodology and case studies," *Renewable Energy*, Vol. 43, 2012, pp. 30–36. doi:https://doi.org/10.1016/j.renene.2011.12.017.

[66] Hou, G., Xu, K., and Lian, J., "A review on recent risk assessment methodologies of offshore wind turbine foundations," *Ocean Engineering*, Vol. 264, 2022, p. 112469. doi:https://doi.org/10.1016/j.oceaneng.2022.112469.

[67] Shafiee, M., and Dinmohammadi, F., "An FMEA-based risk assessment approach for wind turbine systems: a comparative study of onshore and offshore," *Energies*, Vol. 7, No. 2, 2014, pp. 619–642. doi:https://doi.org/10.3390/en7020619.

[68] Sepulveda, M., Davies, P., Spring, M., Shek, J., Thies, P., and Oterkus, E., "Risk assessment of an offshore wind turbine and remaining useful life estimation of the power converter. Improving availability by prioritising failures with higher risk to operation," *Open Research Exeter*, 2016.

[69] Glushakow, B., "Effective lightning protection for wind turbine generators," *IEEE Transactions on Energy Conversion*, Vol. 22, No. 1, 2007, pp. 214–222. doi:doi.org/10.1109/TEC.2006.889622.

[70] Saleem, Z., “Alternatives and modifications of Monopile foundation or its installation technique for noise mitigation,” Tech. rep., Technical University of Delft, 2011.

A

Vibration analysis

In this section, several tables and figures have been used in order to calculate the natural frequency of the system combining the foundation of the wind turbine and soil. Soil characteristics have been computed based on its profile, flexibility and stiffness coefficients.

Table A.1: *Formulas for stiffness of monopiles exhibiting rigid behavior [43]*

TABLE 16.1 Formulas for Stiffness of Monopiles Exhibiting Rigid Behavior

Ground Profile (See Fig. 16.4)	K_L	K_{LR}	K_R
Homogeneous	$3.2\left(\frac{L}{D_P}\right)^{0.62} f_{(vs)} E_{SO} D_P$	$-1.8\left(\frac{L}{D_P}\right)^{1.56} f_{(vs)} E_{SO} D_P{}^2$	$1.65\left(\frac{L}{D_P}\right)^{2.5} f_{(vs)} E_{SO} D_P{}^3$
Parabolic	$2.65\left(\frac{L}{D_P}\right)^{1.07} f_{(vs)} E_{SO} D_P$	$-1.8\left(\frac{L}{D_P}\right)^{2} f_{(vs)} E_{SO} D_P{}^2$	$1.63\left(\frac{L}{D_P}\right)^{3} f_{(vs)} E_{SO} D_P{}^3$
Linear	$2.35\left(\frac{L}{D_P}\right)^{1.53} f_{(vs)} E_{SO} D_P$	$-1.8\left(\frac{L}{D_P}\right)^{2.5} f_{(vs)} E_{SO} D_P{}^2$	$1.59\left(\frac{L}{D_P}\right)^{3.45} f_{(vs)} E_{SO} D_P{}^3$

*$f_{(vs)} = 1 + 0.6|v_s - 0.25|$

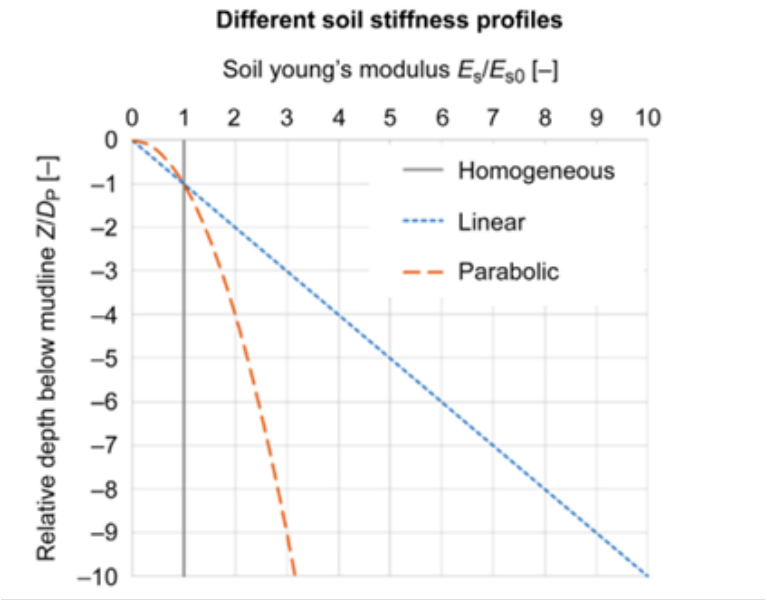

Figure A.1: *Homogeneous, linear, and parabolic soil stiffness profiles [43]*

Table A.2: *The wind speeds(W) and H_S for normal weather scenario [44]*

W (m/s)	P_{rel} (-)	I (-)	H_S (m)	T_p (s)
4.16	0.11	0.29	1.10	5.88
6.23	0.14	0.23	1.18	5.76
8.31	0.16	0.20	1.31	5.67
10.39	0.15	0.18	1.48	5.74
12.47	0.13	0.17	1.70	5.88
14.55	0.11	0.16	1.91	6.07
16.62	0.08	0.15	2.19	6.37
18.70	0.05	0.15	2.47	6.71
20.78	0.03	0.14	2.76	6.99
22.56	0.02	0.14	3.09	7.40
24.94	0.01	0.14	3.42	7.80

Table A.3: *The wind speeds(W) and H_S for extreme weather conditions [44]*

W (m/s)	I (-)	H_S (-)	$T_{p,min}$ (m)	$T_{p,max}$ (s)	T_p for $f_1 = 1/Tp$ (s)	T_p for $f_1 = 2/Tp$ (s)
4.16	0.82	5.88	4	11	+	+
6.23	0.90	5.76	4	11.5	+	+
8.31	1.05	5.67	4	11.5	+	+
10.39	1.23	5.74	4	11.	+	+
12.47	1.46	5.88	5	9	-	-
14.55	1.72	6.07	5	8	-	-
16.62	2.07	6.37	5	9	-	-
18.70	2.38	6.71	5	10	-	+
20.78	2.80	6.90	5	8	-	-
22.56	3.13	7.40	7	9	-	-
24.94	3.58	7.80	7	10	-	+

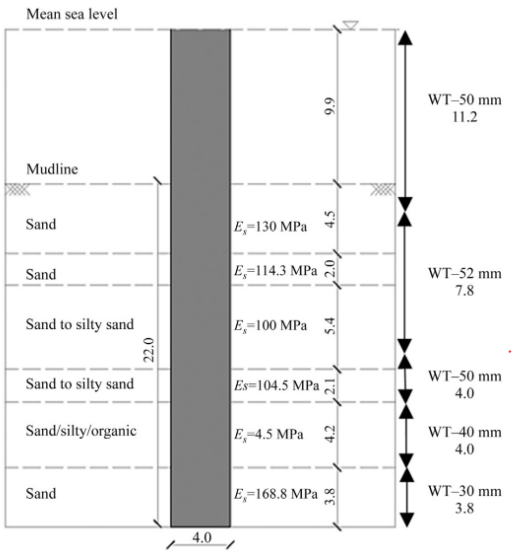

Figure A.2: *Young Modulus of the soil depending on the depth [43]*

B

LCA detailed results

Table B.1: *Material extraction detailed analysis*

Component	Material	Recycled content* (%)	Part mass (kg)	Qty.	Total mass (kg)	Energy (MJ)	CO2 footprint (kg)
Structure	Medium carbon steel	90,0%	6e+03	404	2,4e+06	2,6e+07	2e+06
Shafts	Medium carbon steel	90,0%	2,4e+05	6	1,5e+06	1,6e+07	1,2e+06
Base plate	High carbon steel	90,0%	3,1e+05	1	3,1e+05	3,4e+06	2,6e+05
Blades	Low carbon steel	90,0%	1,1e+03	108	1,1e+05	1,2e+06	9,3e+04
Bearings	Low alloy steel	90,0%	1e+03	42	4,2e+04	4,7e+05	3,5e+04
Monopile	Low carbon steel	90,0%	6,1e+06	1	6,1e+06	6,4e+07	4,9e+06
HLD	Medium carbon steel	90,0%	2,7e+05	4	1,1e+06	1,2e+07	9,1e+05
Bearings	Low alloy steel	90,0%	5e+04	2	1e+05	1,1e+06	8,3e+04
Cables	Copper	90,0%	1,8e+04	1	1,8e+04	3,2e+05	2,4e+04
Gearbox	Medium carbon steel	90,0%	4e+03	6	2,4e+04	2,6e+05	2e+04
Brakes	Low alloy steel	90,0%	6e+02	6	3,6e+03	4e+04	3e+03
Total				**581**	**1,2e+07**	**1,2e+08**	**9,6e+06**

Table B.2: *Manufacturing process detailed analysis*

Component	Process	Amount processed	Energy (MJ)	CO2 footprint (kg)
Structure	Roll forming	2,4e+06 kg	1,3e+07	9,5e+05
Shafts	Roll forming	1,5e+06 kg	7,6e+06	5,7e+05
Base plate	Roll forming	3,1e+05 kg	2e+06	1,5e+05
Blades	Extrusion, foil rolling	1,1e+05 kg	6,3e+05	4,7e+04
Bearings	Casting	4,2e+04 kg	4,7e+05	3,5e+04
Monopile	Roll forming	6,1e+06 kg	1,8e+07	1,3e+06
HLD	Roll forming	1,1e+06 kg	5,7e+06	4,2e+05
Bearings	Casting	1e+05 kg	1,1e+06	8,3e+04
Cables	Wire drawing	1,8e+04 kg	9e+04	6,7e+03
Gearbox	Casting	2,4e+04 kg	2,7e+05	2e+04
Brakes	Casting	3,6e+03 kg	4e+04	3e+03
Total			**4,8e+07**	**3,6e+06**

Table B.3: *Transportation detailed analysis*

Stage name	Transport type	Distance (km)	Energy (MJ)	CO2 footprint (kg)
Factory - Drydock	Rail freight	1,1e+02	4,6e+05	3,3e+04
Drydock - Wind site	Coastal freight	1,2e+02	3,6e+05	2,6e+04
Total		**2,3e+02**	**8,3e+05**	**6e+04**

Table B.4: *Decommissioning detailed analysis*

Component	End of life option	Energy (MJ)	CO2 footprint (kg)
Structure	Recycle	1,7e+06	1,2e+05
Shafts	Recycle	1e+06	7,1e+04
Base plate	Recycle	2,2e+05	1,5e+04
Blades	Recycle	8e+04	5,6e+03
Bearings	Recycle	2,9e+04	2,1e+03
Monopile	Recycle	4,3e+06	3e+05
HLD	Recycle	7,6e+05	5,3e+04
Bearings	Recycle	7e+04	4,9e+03
Cables	Recycle	1,3e+04	8,8e+02
Gearbox	Recycle	1,7e+04	1,2e+03
Brakes	Recycle	2,5e+03	1,8e+02
Total		**8,2e+06**	**5,7e+05**

Table B.5: *Recycling detailed analysis*

Component	End of life option	Energy (MJ)	CO2 footprint (kg)
Structure	Recycle	-5,8e+06	-4,1e+05
Shafts	Recycle	-3,5e+06	-2,5e+05
Base plate	Recycle	-7,4e+05	-5,3e+04
Blades	Recycle	-2,6e+05	-1,9e+04
Bearings	Recycle	-9,3e+04	-7,7e+03
Monopile	Recycle	-1,4e+07	-1e+06
HLD	Recycle	-2,6e+06	-1,9e+05
Bearings	Recycle	-2,2e+05	-1,8e+04
Cables	Recycle	-8,2e+04	-4,6e+03
Gearbox	Recycle	-5,7e+04	-4,1e+03
Brakes	Recycle	-7,9e+03	-6,6e+02
Total		**-2,7e+07**	**-2e+06**

C

Whole Cost Model

Table C.1 is based on data from Catapult [6].

Table C.1: *The entire cost model based on data from Catapult [6]*

Reference turbine cost breakdown from Catapult	Rounded Cost (£/MW)	LCoE [EUR/MWh]	Assumption 1 (area with lower LCoE) Percentage change	New cost	LCoE [EUR/MWh]	Assumption 2 (denser wind farm O&M) Percentage change	New cost	LCoE [EUR/MWh]	Assumption 3 (Wake losses) Percentage change	New cost	LCoE [EUR/MWh]	Assumption 4 (Conventional design -->MR-TBD) Percentage change	New cost	LCoE [EUR/MWh]	Assumption 5 (Wake regeneration) Percentage change	New cost	LCoE [EUR/MWh]
Turbine [3]																	
Nacelle	**£398.000,00**	**€ 5,84**		**£398.000,00**	**€ 5,84**		**£398.000,00**	**€ 5,84**		**£398.000,00**	**€ 8,35**		**£327.534,75**	**€ 6,87**		**£327.534,75**	**€ 4,81**
Bedplate	£20.000,00	**€ 0,29**	0,00%	£20.000,00	**€ 0,29**	0,00%	£20.000,00	**€ 0,29**	0,00%	£20.000,00	**€ 0,42**	26,21%	£25.242,72	**€ 0,53**	0,00%	£25.242,72	**€ 0,37**
Main bearing	£20.000,00	**€ 0,29**	0,00%	£20.000,00	**€ 0,29**	0,00%	£20.000,00	**€ 0,29**	0,00%	£20.000,00	**€ 0,42**	-50,00%	£10.000,00	**€ 0,21**	0,00%	£10.000,00	**€ 0,15**
Main shaft	£20.000,00	**€ 0,29**	0,00%	£20.000,00	**€ 0,29**	0,00%	£20.000,00	**€ 0,29**	0,00%	£20.000,00	**€ 0,42**	28,71%	£25.741,53	**€ 0,54**	0,00%	£25.741,53	**€ 0,38**
Gearbox	£70.000,00	**€ 1,03**	0,00%	£70.000,00	**€ 1,03**	0,00%	£70.000,00	**€ 1,03**	0,00%	£70.000,00	**€ 1,47**	-54,55%	£31.818,18	**€ 0,67**	0,00%	£31.818,18	**€ 0,47**
Generator	£100.000,00	**€ 1,47**	0,00%	£100.000,00	**€ 1,47**	0,00%	£100.000,00	**€ 1,47**	0,00%	£100.000,00	**€ 2,10**	-54,55%	£45.454,55	**€ 0,95**	0,00%	£45.454,55	**€ 0,67**
Power take-off	£70.000,00	**€ 1,03**	0,00%	£70.000,00	**€ 1,03**	0,00%	£70.000,00	**€ 1,03**	0,00%	£70.000,00	**€ 1,47**	-10,00%	£63.000,00	**€ 1,32**	0,00%	£63.000,00	**€ 0,92**
Control system	£25.000,00	**€ 0,37**	0,00%	£25.000,00	**€ 0,37**	0,00%	£25.000,00	**€ 0,37**	0,00%	£25.000,00	**€ 0,52**	0,00%	£25.000,00	**€ 0,52**	0,00%	£25.000,00	**€ 0,37**
Yaw system	£17.000,00	**€ 0,25**	0,00%	£17.000,00	**€ 0,25**	0,00%	£17.000,00	**€ 0,25**	0,00%	£17.000,00	**€ 0,36**	-11,11%	£15.111,11	**€ 0,32**	0,00%	£15.111,11	**€ 0,22**
Yaw bearing	£7.000,00	**€ 0,10**	0,00%	£7.000,00	**€ 0,10**	0,00%	£7.000,00	**€ 0,10**	0,00%	£7.000,00	**€ 0,15**	466,67%	£39.666,67	**€ 0,83**	0,00%	£39.666,67	**€ 0,58**
Nacelle auxiliary systems	£7.000,00	**€ 0,10**	0,00%	£7.000,00	**€ 0,10**	0,00%	£7.000,00	**€ 0,10**	0,00%	£7.000,00	**€ 0,15**	-50,00%	£3.500,00	**€ 0,07**	0,00%	£3.500,00	**€ 0,05**
Nacelle cover	£10.000,00	**€ 0,15**	0,00%	£10.000,00	**€ 0,15**	0,00%	£10.000,00	**€ 0,15**	0,00%	£10.000,00	**€ 0,21**	-50,00%	£5.000,00	**€ 0,10**	0,00%	£5.000,00	**€ 0,07**
Small engineering components	£25.000,00	**€ 0,37**	0,00%	£25.000,00	**€ 0,37**	0,00%	£25.000,00	**€ 0,37**	0,00%	£25.000,00	**€ 0,52**	10,00%	£27.500,00	**€ 0,58**	0,00%	£27.500,00	**€ 0,40**
Structural fasteners	£7.000,00	**€ 0,10**	0,00%	£7.000,00	**€ 0,10**	0,00%	£7.000,00	**€ 0,10**	0,00%	£7.000,00	**€ 0,15**	50,00%	£10.500,00	**€ 0,22**	0,00%	£10.500,00	**€ 0,15**
Rotor	**£196.000,00**	**€ 2,88**		**£196.000,00**	**€ 2,88**		**£196.000,00**	**€ 2,88**		**£193.360,00**	**€ 4,06**		**£21.641,20**	**€ 0,45**		**£21.641,20**	**€ 0,32**
Blades	£130.000,00	**€ 1,91**	0,00%	£130.000,00	**€ 1,91**	0,00%	£130.000,00	**€ 1,91**	0,00%	£130.000,00	**€ 2,73**	-99,00%	£1.300,00	**€ 0,03**	0,00%	£1.300,00	**€ 0,02**
Hub casting	£15.000,00	**€ 0,22**	0,00%	£15.000,00	**€ 0,22**	0,00%	£15.000,00	**€ 0,22**	0,00%	£15.000,00	**€ 0,31**	-75,00%	£3.750,00	**€ 0,08**	0,00%	£3.750,00	**€ 0,06**
Blade bearings	£20.000,00	**€ 0,29**	0,00%	£20.000,00	**€ 0,29**	0,00%	£20.000,00	**€ 0,29**	0,00%	£20.000,00	**€ 0,42**	-100,00%	£-	**€ -**	0,00%	£-	**€ -**
Pitch system	£10.000,00	**€ 0,15**	0,00%	£10.000,00	**€ 0,15**	0,00%	£10.000,00	**€ 0,15**	0,00%	£10.000,00	**€ 0,21**	-100,00%	£-	**€ -**	0,00%	£-	**€ -**
Spinner	£2.000,00	**€ 0,03**	0,00%	£2.000,00	**€ 0,03**	0,00%	£2.000,00	**€ 0,03**	0,00%	£2.000,00	**€ 0,04**	0,00%	£2.000,00	**€ 0,04**	0,00%	£2.000,00	**€ 0,03**
Rotor auxiliary systems	£4.000,00	**€ 0,06**	0,00%	£4.000,00	**€ 0,06**	0,00%	£4.000,00	**€ 0,06**	0,00%	£4.000,00	**€ 0,08**	0,00%	£4.000,00	**€ 0,08**	0,00%	£4.000,00	**€ 0,06**
Fabricated steel components	£8.000,00	**€ 0,12**	0,00%	£8.000,00	**€ 0,12**	0,00%	£8.000,00	**€ 0,12**	0%	£5.360,00	**€ 0,11**	-33,00%	£3.591,20	**€ 0,08**	0,00%	£3.591,20	**€ 0,05**
Structural fasteners	£7.000,00	**€ 0,10**	0,00%	£7.000,00	**€ 0,10**	0,00%	£7.000,00	**€ 0,10**	0,00%	£7.000,00	**€ 0,15**	0,00%	£7.000,00	**€ 0,15**	0,00%	£7.000,00	**€ 0,10**
Tower	£67.000,00	**€ 0,98**		£67.000,00	**€ 0,98**		£67.000,00	**€ 0,98**		£67.000,00	**€ 1,41**		£114.282,35	**€ 2,40**		£114.282,35	**€ 1,68**
Steel	£60.000,00	**€ 0,88**	0,00%	£60.000,00	**€ 0,88**	0,00%	£60.000,00	**€ 0,88**	0,00%	£60.000,00	**€ 1,26**	76,47%	£105.882,35	**€ 2,22**	0,00%	£105.882,35	**€ 1,55**
Tower internals	£7.000,00	**€ 0,10**	0,00%	£7.000,00	**€ 0,10**	0,00%	£7.000,00	**€ 0,10**	0,00%	£7.000,00	**€ 0,15**	20,00%	£8.400,00	**€ 0,18**	0,00%	£8.400,00	**€ 0,12**
Other (includes assembly, wind turbine supplier aspects of installation and commissioning, profit and warranty)	£340.000,00	**€ 4,99**	0,00%	£340.000,00	**€ 4,99**	0,00%	£340.000,00	**€ 4,99**	0,00%	£340.000,00	**€ 7,13**	20,00%	£408.000,00	**€ 8,56**	0,00%	£408.000,00	**€ 5,99**
Balance of Plant [3]											**€ -**			**€ -**	0,00%		
Cables	£170.000,00	**€ 2,50**		£102.000,00	**€ 1,50**		£84.500,00	**€ 1,24**		£84.500,00	**€ 1,77**		£80.125,00	**€ 1,68**		£80.125,00	**€ 1,18**
Export cable	£130.000,00	**€ 1,91**	-50,00%	£65.000,00	**€ 0,95**	0,00%	£65.000,00	**€ 0,95**	0,00%	£65.000,00	**€ 1,36**	0,00%	£65.000,00	**€ 1,36**	0,00%	£65.000,00	**€ 0,95**
Array cable	£35.000,00	**€ 0,51**	0,00%	£35.000,00	**€ 0,51**	-50,00%	£17.500,00	**€ 0,26**	0,00%	£17.500,00	**€ 0,37**	-25,00%	£13.125,00	**€ 0,28**	0,00%	£13.125,00	**€ 0,19**
Cable protection	£2.000,00	**€ 0,03**	0,00%	£2.000,00	**€ 0,03**	0,00%	£2.000,00	**€ 0,03**	0,00%	£2.000,00	**€ 0,04**	0,00%	£2.000,00	**€ 0,04**	0,00%	£2.000,00	**€ 0,03**
Turbine foundation	£280.000,00	**€ 4,11**		£181.000,00	**€ 2,66**		£181.000,00	**€ 2,66**		£181.000,00	**€ 3,80**		£235.507,25	**€ 4,94**		£235.507,25	**€ 3,46**
Transition piece	£100.000,00	**€ 1,47**	0,00%	£100.000,00	**€ 1,47**	0,00%	£100.000,00	**€ 1,47**	0,00%	£100.000,00	**€ 2,10**	50,00%	£150.000,00	**€ 3,15**	0,00%	£150.000,00	**€ 2,20**
Corrosion protection	£20.000,00	**€ 0,29**	0,00%	£20.000,00	**€ 0,29**	0,00%	£20.000,00	**€ 0,29**	0,00%	£20.000,00	**€ 0,42**	25,00%	£25.000,00	**€ 0,52**	0,00%	£25.000,00	**€ 0,37**
Scour protection	£10.000,00	**€ 0,15**	0,00%	£10.000,00	**€ 0,15**	0,00%	£10.000,00	**€ 0,15**	0,00%	£10.000,00	**€ 0,21**	0,00%	£10.000,00	**€ 0,21**	0,00%	£10.000,00	**€ 0,15**
Foundation cost	£150.000,00	**€ 2,20**	-66,00%	£51.000,00	**€ 0,75**	0,00%	£51.000,00	**€ 0,75**	0,00%	£51.000,00	**€ 1,07**	-0,97%	£50.507,25	**€ 1,06**	0,00%	£50.507,25	**€ 0,74**
Offshore substation	£125.000,00	**€ 1,84**		£105.209,00	**€ 1,54**		£95.450,00	**€ 1,40**		£95.450,00	**€ 2,00**		£95.450,00	**€ 2,00**		£95.450,00	**€ 1,40**
Electrical system	£45.000,00	**€ 0,66**	0,00%	£45.000,00	**€ 0,66**	-15,00%	£38.250,00	**€ 0,56**	0,00%	£38.250,00	**€ 0,80**	0,00%	£38.250,00	**€ 0,80**	0,00%	£38.250,00	**€ 0,56**
Facilities	£20.000,00	**€ 0,29**	0,00%	£20.000,00	**€ 0,29**	-15,00%	£17.000,00	**€ 0,25**	0,00%	£17.000,00	**€ 0,36**	0,00%	£17.000,00	**€ 0,36**	0,00%	£17.000,00	**€ 0,25**
Structure	£60.000,00	**€ 0,88**	-33,00%	£40.200,00	**€ 0,59**	0,00%	£40.200,00	**€ 0,59**	0,00%	£40.200,00	**€ 0,84**	0,00%	£40.200,00	**€ 0,84**	0,00%	£40.200,00	**€ 0,59**
Onshore substation	£30.000,00	**€ 0,44**		£30.000,00	**€ 0,44**		£30.000,00	**€ 0,44**		£30.000,00	**€ 0,63**		£30.000,00	**€ 0,63**		£30.000,00	**€ 0,44**
Buildings, access and security	£8.000,00	**€ 0,12**	0,00%	£8.000,00	**€ 0,12**	0,00%	£8.000,00	**€ 0,12**	0,00%	£8.000,00	**€ 0,17**	0,00%	£8.000,00	**€ 0,17**	0,00%	£8.000,00	**€ 0,12**
Other (includes electrical equipment and systems)	£22.000,00	**€ 0,32**	0,00%	£22.000,00	**€ 0,32**	0,00%	£22.000,00	**€ 0,32**	0,00%	£22.000,00	**€ 0,46**	0,00%	£22.000,00	**€ 0,46**	0,00%	£22.000,00	**€ 0,32**
Operations base	£3.000,00	**€ 0,04**	0,00%	£3.000,00	**€ 0,04**	0,00%	£3.000,00	**€ 0,04**	0,00%	£3.000,00	**€ 0,06**	0,00%	£3.000,00	**€ 0,06**	0,00%	£3.000,00	**€ 0,04**
Total										£2.043.620,00	**€ 42,86**		£1.892.546,35	**€ 39,69**			
Development and project management [3]											**€ -**			**€ -**			
Part	Original Price										**€ -**			**€ -**			
Development and consenting services	£50.000,00	**€ 0,73**	-33,00%	£33.500,00	**€ 0,49**	0,00%	£33.500,00	**€ 0,49**	0,00%	£33.500,00	**€ 0,70**	25,00%	£41.875,00	**€ 0,88**	0,00%	£41.875,00	**€ 0,61**
Environmental surveys	£4.000,00	**€ 0,06**	0,00%	£4.000,00	**€ 0,06**	-20,00%	£3.200,00	**€ 0,05**		£3.200,00	**€ 0,07**	0,00%	£3.200,00	**€ 0,07**	0,00%	£3.200,00	**€ 0,05**
Resource and metocean assessment	£4.000,00	**€ 0,06**	0,00%	£4.000,00	**€ 0,06**	-20,00%	£3.200,00	**€ 0,05**	0,00%	£3.200,00	**€ 0,07**	0,00%	£3.200,00	**€ 0,07**	0,00%	£3.200,00	**€ 0,05**
Geological and hydrographical surveys	£4.000,00	**€ 0,06**	0,00%	£4.000,00	**€ 0,06**	0,00%	£4.000,00	**€ 0,06**	0,00%	£4.000,00	**€ 0,08**	0,00%	£4.000,00	**€ 0,08**	0,00%	£4.000,00	**€ 0,06**
Engineering and consultancy	£4.000,00	**€ 0,06**	0,00%	£4.000,00	**€ 0,06**	0,00%	£4.000,00	**€ 0,06**	0,00%	£4.000,00	**€ 0,08**	-25,00%	£3.000,00	**€ 0,10**	0,00%	£5.000,00	**€ 0,07**
Development expenditure incurred by lost projects	£54.000,00	**€ 0,79**	0,00%	£54.000,00	**€ 0,79**	0,00%	£54.000,00	**€ 0,79**	0,00%	£54.000,00	**€ 1,13**	0,00%	£54.000,00	**€ 1,13**	0,00%	£54.000,00	**€ 0,79**
Total	£120.000,00	**€ 1,76**		£103.500,00	**€ 1,52**		£101.900,00	**€ 1,50**		£101.900,00	**€ 2,14**		£111.275,00	**€ 2,33**		£111.275,00	**€ 1,63**
											€ -			**€ -**			
Installation and comissioning [3]											**€ -**			**€ -**			
Part	Original Price										**€ -**			**€ -**			
Foundation Installation	£100.000,00	**€ 1,47**	-50,00%	£50.000,00	**€ 0,73**	0,00%	£50.000,00	**€ 0,73**	0,00%	£50.000,00	**€ 1,05**	-33,00%	£33.500,00	**€ 0,70**	0,00%	£33.500,00	**€ 0,49**
Offshore substation installation	£35.000,00	**€ 0,51**	-50,00%	£17.500,00	**€ 0,26**	0,00%	£17.500,00	**€ 0,26**	0,00%	£17.500,00	**€ 0,37**	0,00%	£17.500,00	**€ 0,37**	0,00%	£17.500,00	**€ 0,26**
Onshore substation construction	£25.000,00	**€ 0,37**	0,00%	£25.000,00	**€ 0,37**	0,00%	£25.000,00	**€ 0,37**	0,00%	£25.000,00	**€ 0,52**	0,00%	£25.000,00	**€ 0,52**	0,00%	£25.000,00	**€ 0,37**
Onshore export cable installation	£5.000,00	**€ 0,07**	0,00%	£5.000,00	**€ 0,07**	0,00%	£5.000,00	**€ 0,07**	0,00%	£5.000,00	**€ 0,10**	0,00%	£5.000,00	**€ 0,10**	0,00%	£5.000,00	**€ 0,07**
Offshore cable installation	£220.000,00	**€ 3,23**		£113.250,00	**€ 1,66**		£90.600,00	**€ 1,33**		£90.600,00	**€ 1,90**		£77.340,00	**€ 1,62**		£77.340,00	**€ 1,14**
Cable burial	£20.000,00	**€ 0,29**	-50,00%	£10.000,00	**€ 0,15**	-20,00%	£8.000,00	**€ 0,12**	0,00%	£8.000,00	**€ 0,17**	-15,00%	£6.800,00	**€ 0,14**	0,00%	£6.800,00	**€ 0,10**
Cable pull-in	£7.500,00	**€ 0,11**	-50,00%	£3.750,00	**€ 0,06**	-20,00%	£3.000,00	**€ 0,04**	0,00%	£3.000,00	**€ 0,06**	-30,00%	£2.100,00	**€ 0,04**	0,00%	£2.100,00	**€ 0,03**
Electrical testing and termination	£6.500,00	**€ 0,10**	0,00%	£6.500,00	**€ 0,10**	-20,00%	£5.200,00	**€ 0,08**	0,00%	£5.200,00	**€ 0,11**	0,00%	£5.200,00	**€ 0,11**	0,00%	£5.200,00	**€ 0,08**
Other (cable-laying vessel, seruvey works, route clearnace, cable protection)	£186.000,00	**€ 2,73**	-50,00%	£93.000,00	**€ 1,37**	-20,00%	£74.400,00	**€ 1,09**	0,00%	£74.400,00	**€ 1,56**	-15,00%	£63.240,00	**€ 1,33**	0,00%	£63.240,00	**€ 0,93**
Turbine installation	£50.000,00	**€ 0,73**	-25,00%	£37.500,00	**€ 0,55**	-15,00%	£31.875,00	**€ 0,47**	0,00%	£31.875,00	**€ 0,67**	-20,00%	£25.500,00	**€ 0,53**	0,00%	£25.500,00	**€ 0,37**
offshore logistics	£3.650,00	**€ 0,05**		£2.850,00	**€ 0,04**		£2.350,00	**€ 0,03**		£2.350,00	**€ 0,05**		£2.350,00	**€ 0,05**		£2.350,00	**€ 0,03**
Sea-based support	£2.500,00	**€ 0,04**	-40,00%	£1.500,00	**€ 0,02**	-20,00%	£1.200,00	**€ 0,02**	0,00%	£1.200,00	**€ 0,03**	0,00%	£1.200,00	**€ 0,03**	0,00%	£1.200,00	**€ 0,02**
Marine coordination	£850,00	**€ 0,01**	0,00%	£850,00	**€ 0,01**	0,00%	£850,00	**€ 0,01**	0,00%	£850,00	**€ 0,02**	0,00%	£850,00	**€ 0,02**	0,00%	£850,00	**€ 0,01**
Weather forecasting and metocean data	£300,00	**€ 0,00**	0,00%	£300,00	**€ 0,00**	0,00%	£300,00	**€ 0,00**	0,00%	£300,00	**€ 0,01**	0,00%	£300,00	**€ 0,01**	0,00%	£300,00	**€ 0,00**
Insurance, project management & contingency	£212.000,00	**€ 3,11**	0,00%	£212.000,00	**€ 3,11**	0,00%	£212.000,00	**€ 3,11**	0,00%	£212.000,00	**€ 4,45**	0,00%	£212.000,00	**€ 4,45**	0,00%	£212.000,00	**€ 3,11**
Total	£650.650,00	**€ 9,55**		£462.900,00	**€ 6,80**		£434.325,00	**€ 6,38**		£434.325,00	**€ 9,11**	0,00%	£398.190,00	**€ 8,35**		£398.190,00	**€ 5,85**
Maintenance and service [3]																	
Part	Original Price Per Year																
Turbine	£33.000,00	€ 8,56	-50,00%	£16.500,00	€ 4,28	0,00%	£16.500,00	€ 4,28	0,00%	£16.500,00	€ 6,12	-60,00%	£6.600,00	€ 2,45	0,00%	£6.600,00	€ 1,71
Balance of plant	£18.000,00	€ 4,67	-40,00%	£10.800,00	€ 2,80	0,00%	£10.800,00	€ 2,80	0,00%	£10.800,00	€ 4,00	-15,00%	£9.180,00	€ 3,40	0,00%	£9.180,00	€ 2,38
Total per Year	£51.000,00	€ 13,23		£27.300,00	€ 7,08		£27.300,00	€ 7,08		£27.300,00	€ 10,12		£15.780,00	€ 5,85		£15.780,00	€ 4,09
											€ -			€ -			
Operations [3]											€ -			€ -			
Part	Original Price Per Year										€ -			€ -			
Staff training	£500,00	€ 0,13	0,00%	£500,00	€ 0,13	0,00%	£500,00	€ 0,13	0,00%	£500,00	€ 0,19	-50,00%	£250,00	€ 0,09	0,00%	£250,00	€ 0,06
Onshore logistics	£450,00	€ 0,12	0,00%	£450,00	€ 0,12	-15,00%	£382,50	€ 0,10	0,00%	£382,50	€ 0,14	0,00%	£382,50	€ 0,14	0,00%	£382,50	€ 0,10
Offshore logistics	£1.600,00	€ 0,42	-30,00%	£1.120,00	€ 0,29	-15,00%	£952,00	€ 0,25	0,00%	£952,00	€ 0,35	-25,00%	£714,00	€ 0,26	0,00%	£714,00	€ 0,19
Health and safety inspections	£400,00	€ 0,10	0,00%	£400,00	€ 0,10	0,00%	£400,00	€ 0,10	0,00%	£400,00	€ 0,15	-33,00%	£268,00	€ 0,10	0,00%	£268,00	€ 0,07
Other (insurance, environmental studies and compensation payments)	£22.000,00	€ 5,71	0,00%	£22.000,00	€ 5,71	0,00%	£22.000,00	€ 5,71	0,00%	£22.000,00	€ 8,15	0,00%	£22.000,00	€ 8,15	0,00%	£22.000,00	€ 5,71
Total per Year	£24.950,00	€ 6,47		£24.470,00	€ 6,35		£24.234,50	€ 6,29		£24.234,50	€ 8,98		£23.614,50	€ 8,75		£23.614,50	€ 6,13
Decommissioning [3]																	
Part	Original Price																
Turbine decommissioning	£45.000,00	€ 0,27	-30,00%	£31.500,00	€ 0,19	-15,00%	£26.775,00	€ 0,16	0,00%	£26.775,00	€ 0,23	-30,00%	£18.742,50	€ 0,16	0,00%	£18.742,50	€ 0,11
Foundation decommissioning	£75.000,00	€ 0,45	-33,00%	£50.250,00	€ 0,30	-15,00%	£42.712,50	€ 0,26	0,00%	£42.712,50	€ 0,37	-33,00%	£28.617,38	€ 0,25	0,00%	£28.617,38	€ 0,17
Cable decommissioning	£140.000,00	€ 0,85	-50,00%	£70.000,00	€ 0,42	-20,00%	£56.000,00	€ 0,34	0,00%	£56.000,00	€ 0,48	-20,00%	£44.800,00	€ 0,39	0,00%	£44.800,00	€ 0,27
Substation decommissioning	£65.000,00	€ 0,39	-30,00%	£45.500,00	€ 0,27	0,00%	£45.500,00	€ 0,27	0,00%	£45.500,00	€ 0,39	0,00%	£45.500,00	€ 0,39	0,00%	£45.500,00	€ 0,27
Total	£325.000,00	€ 1,96		£197.250,00	€ 1,19		£170.987,50	€ 1,03		£170.987,50	€ 1,48		£137.659,88	€ 1,19		£137.659,88	€ 0,83
Development and project management		€ 1,76			€ 1,52			€ 1,50			€ 2,14			€ 2,33			€ 1,63
Turbine		€ 14,70			€ 14,70			€ 14,70			€ 20,94			€ 18,28			€ 12,79
Balance of plant		€ 8,93			€ 6,18			€ 5,78			€ 8,26			€ 9,31			€ 6,52
Installation and commissioning		€ 9,55			€ 6,80			€ 6,38			€ 9,11			€ 8,35			€ 5,85
Operation, maintenance, and service		€ 19,71			€ 13,43			€ 13,37			€ 19,10			€ 14,60			€ 10,22
Decommissioning		€ 1,96			€ 1,19			€ 1,03			€ 1,48			€ 1,19			€ 0,83
TOTAL		€ 56,61			€ 43,82			€ 42,76			€ 61,03			€ 54,07			€ 37,85
Development and project management		3%			3%			3%			4%			4%			3%
Turbine		26%			26%			26%			37%			32%			23%
Balance of plant		16%			11%			10%			15%			16%			12%
Installation and commissioning		17%			12%			11%			16%			15%			10%
Operation, maintenance, and service		35%			24%			24%			34%			26%			18%
Decommissioning		3%			2%			2%			3%			2%			1%
Capex [EUR/MW]	£2.379.650,00	€ 34,94		£1.988.600,00	€ 29,20		£1.931.175,00	€ 28,35		£1.928.535,00	€ 40,45		£1.825.005,55	€ 38,28		£1.825.005,55	€ 26,79
Opex [EUR/MW/year]	£75.950,00	€ 19,71		£51.770,00	€ 13,43		£51.534,50	€ 13,37		£51.534,50	€ 19,10		£39.394,50	€ 14,60		£39.394,50	€ 10,22
Decommissioning [GBP/MW]	£325.000,00	€ 1,96		£197.250,00	€ 1,19		£170.987,50	€ 1,03		£170.987,50	€ 1,48		£137.659,88	€ 1,19		£137.659,88	€ 0,83
LCoE [EUR/MWh]	€ 56,61	€ 56,61		€ 43,82	€ 43,82		€ 42,76	€ 42,76		€ 61,03	€ 61,03		€ 54,07	€ 54,07		€ 37,85	€ 37,85
Annual energy produciton (per MW installed)	4471		0%	4471		0%	4471		-30,00%	3129,7		0%	3129,7		42,86%	4471	